PERFORMANCE SIMULATION AND CONTROL DESIGN FOR DIESEL ENGINE NO_X EMISSION REDUCTION TECHNOLOGIES

BY

HAI WU

DISSERTATION

Submitted in partial fulfillment of the requirements
for the degree of Doctor of Philosophy in Agricultural and Biological Engineering
in the Graduate College of the
University of Illinois at Urbana-Champaign, 2011

Urbana, Illinois

Doctoral Committee:

Associate Professor Xinlei Wang, Chair
Professor Alan C. Hansen
Professor Chia-fon Lee
Professor K.C. Ting

ABSTRACT

Fuel efficiency and emission reductions are the two consistent drivers for internal combustion engine development for both on-highway and off-road vehicles. Advanced combustion technologies are proposed for the improvement of fuel consumption and reduction of harmful gas production inside the cylinder in laboratory engines. Outside cylinder technologies and after-treatment are the alternatives for a production engine to meet the stringent emission standards. Advanced control technologies play important roles in the realization of new technologies. This research was aimed at investigating possible techniques and feasible methods of implementation to reduce diesel engine emissions to meet the more stringent Tier 4 standards. In this study, two technologies are studied for off-road diesel engine NO_x emission reductions: stoichiometric combustion ignition (SCI) and lean NO_x trap (LNT).

The concept of the stoichiometric compression ignition (SCI) engine was investigated for implementation in a turbocharged diesel engine through co-simulation. At first, an integrated environment for 1D engine modeling with control function was proposed for a SCI performance evaluation and control implementation. The SCI engine has been evaluated by Constant Speed Load Acceptance tests under steady-state and transient conditions. For SCI implementations, basic controls have been designed including air-fuel ratio (AFR) control, torque limiting control and idle speed control. The proposed control strategies have been verified with 1D detail models in the integrated environments. Further, the Mean Value Engine Model (MVEM) is proposed for advanced model based control design. The SCI engine subsystems are modeled using an orifice constrain model for throttle, turbine, and wastegate; filling and emptying model for intake and exhaust manifolds; rotational dynamic for engine camshaft and turbocharger shift, air-charging model and exhaust properties regressed by the data from integrated simulation at different engine operating conditions. The MVEM was implemented in Matlab/Simulink for verification. Modular and system verification was conducted for steady-state and transient state consistency with the 1D detail model. The results are promising, but the whole system needs further tuning for dynamic control design.

The lean-NO_x trap, as an alternative after-treatment for NO_x control, has been studied for generic diesel engine emission control. Based on experimental data, an improved NO_x adsorption model is proposed for integrated engine control and optimization.

ACKNOWLEGEMENTS

This work would not have been possible without the help from many faculty members from the University of Illinois at Urbana-Champaign and engineers from the John Deere Company. At first, I would like to extend my appreciation to Professor Xinlei Wang, my PhD program advisor, who opened a gate and led me into the engine and emission control area. I am grateful to him for giving me the opportunities to write project proposals and manage research plans, the freedom to investigate different technical ideas, and to participate in professional conferences in the Agricultural engineering and automotive engineering area. His continuing financial support in the stages of coursework, project research, and after-project research is a substantial reason for the success of this thesis research. The author and his family would like take this opportunity to thank him for caring about our life in Urbana. This study and the work here built my friendship with him and other faculty members, my knowledge in the engine area and my experience in the industry, which are very important for my future career and life.

I am grateful for the help and support from engineers at the John Deere Company and John Deere Technology Innovation Center on campus. I appreciate their trust and guidance in the research stage. Their project topics made this research practical and meaningful to both industry and academia. The basis of this research is relative to their innovation to challenge the new difficulties while facing market and governmental standards. I am indebted to Dr. Richard Windsor, Dr. Xinqun Gui, Dr. Kirby Baumgard and Dr. Budhadeb Mahakul, for every question in the project, every visit to their group, for their kindness and support for me. The most important aspect I learned from them is their solid and earnest working style throughout the process of new technology development. They are very diligent in their work, at the same time they have been very kind and patient with me. The spirit and knowledge I learned from the time I worked at their company will forever stay with me and encourage me in my future work.

I would like to express my earnest thanks to my committee members: Professor Alan C. Hansen, Professor Chia-fon Lee, and Professor K. C. Ting for their effort and time, especially their valuable suggestions to my research and encouraging comments about my work. What I learned from Dr. Lee and Dr. Hansen’s classes built the basis of my research, which was a brand new area to me.

Many thanks also go to the Department of Agricultural and Biological Engineering, to Dr. Ting's leadership and the hardworking faculty that make this department a No. 1 program. I would also like to thank the department staff for all their help, especially Ms. Ronda Sullivan for her time spent processing inches of paper work and kindness in helping me. I want to thank Ms. Mary Beth Munhall, Mr. Randy Fonner and Prof. Richard Cooke for all their efforts in correcting and formatting my thesis.

During my study and research period, I got help from many people and shared many memorable times with officemates and classmates. I really enjoyed the time with members of the BEE group; their different research topics enriched my knowledge in the bioengineering and environmental engineering.

Last but not least, I feel grateful to my wife, Xiao Chen, for her love and support, to my parents for their understanding and encouragement, to my daughter and son for their love. Together with my friends, they all make me real, and vivid in life.

TABLE OF CONTENTS

NOMENCLATURE vii
ABBREVIATIONS AND ACRONYMS ix

1 INTRODUCTION 1
1.1 Motivation 1
1.2 Objectives and Approaches 2

2 APPROACHES 4
2.1 SCI Engine Performance Simulation and Governor Design 4
2.2 Mean Value Model of SCI Engine 6
2.3 After-treatment Control for Diesel Engine NO_x Reduction 7

3 LITERATURE REVIEW 8
3.1 Diesel Engine NO_x Emission and Related Technologies 8
3.2 Control Design for Diesel Engines 15

4 INTEGRATED 1D ENGINE AND CONTROL SIMULATION ENVIRONMENT 19
4.1 Engine Simulation Environment Structure 19
4.2 Constant Speed Load Acceptance Performance Simulation for SCI Engine 20

5 CONTROL DESIGN FOR SCI ENGINE IMPLEMENTATION 33
5.1 AFR Feed-forward Control 33
5.2 All Season and Altitude Torque Limiting 39
5.3 Idle Speed Control 54

6 MEAN VALUE MODEL OF SCI ENGINE 63
6.1 Introduction 63
6.2 Engine Module for MVEM 67
6.3 MVEM Implementation in Simulink 101
6.4 MVEM Verification 101
6.5 Conclusions 115

7 LEAN NO_X TRAP STORAGE MODEL 118
7.1 Model Development 118
7.2 Model Validation and Analysis 126
7.3 Conclusions 128

8 CONCLUSIONS AND RECOMMENDATIONS 131
8.1 Conclusions 131
8.2 Recommendations 133

9 REFERENCES 134

APPENDIX A 138
A.1 Regression Models of Fueling 138

APPENDIX B 140
B.1 Simulation Verification of Fueling Control 140
B.2 Simulation Verification of Torque Limiting Control 150

APPENDIX C 167
C.1 Engine Geometry 167
BIOGRAPHY 168

NOMENCLATURE

A_{th}	(mm^2)	Throttle wide open area
A_{wg}	(mm^2)	Wastegate opening
CD_f		Forward discharge coefficient
$\dot{m}_{comp}$	(kg/s)	Compressor mass flow rate
$\dot{m}_{cyl}$	(kg/s)	Air mass flow rate into the cylinder
$\dot{m}_{ex}$	(kg/s)	Exhaust gas mass flow rate through exhaust manifold
$\dot{m}_f$	(kg/s)	Fuel mass flow rate
$\dot{m}_{im}$	(kg/s)	Air mass flow rate into the intake manifold
$\dot{m}_t$	(kg/s)	Exhaust gas mass flow rate through turbine
$\dot{m}_{th}$	(kg/s)	Air mass flow rate through throttle
$\dot{m}_{wg}$	(kg/s)	Exhaust gas mass flow rate through wastegate
N_e	(rpm)	Engine speed
p_{amb}	(bar)	Ambient pressure
p_b	(bar)	Boost pressure
p_{em}	(bar)	Exhaust manifold pressure
p_{ex}	(bar)	Exhaust manifold pressure
p_{cmp}	(bar)	Compressor pressure
p_{im}	(bar)	Intake manifold pressure
P_T	(W)	Power of turbine
P_C	(W)	Power of compressor
V_b	(m^3)	Intercooler boost volume
R	(kJ/kg×°K)	Gas constant of the air
T_{amb}	(°K)	Atmospheric temperature

T_b	($^\circ$K)	Intercooler temperature
T_{comp}	($^\circ$K)	Compressor outlet temperature
T_{ex}	($^\circ$K)	Exhaust manifold temperature
T_{im}	($^\circ$K)	Intake manifold temperature
T_t	($^\circ$K)	Turbine outlet temperature
TQ_b	$(\mathrm{N}\cdot\mathrm{m})$	Engine brake torque
V_d	(m^3)	Cylinder displacement volume
V_{em}	(m^3)	Exhaust manifold volume
V_{im}	(m^3)	Intake manifold volume
θ_{th}	(degree)	Throttle opening
λ		Relative air/fuel ratio
ε		Heat transfer effectiveness

ABBREVIATIONS AND ACRONYMS

AFR	Air Fuel Ratio
CI	Compression Ignition
DPF	Diesel Particulate Filter
EGR	Exhaust Gas Recirculation
EMP	Exhaust Manifold Pressure
EPA	Environmental Protection Agency
FFV	Fully Flexible Valve
HCCI	Homogeneous Charge Compression Ignition
IC	Internal Combustion
ISE	Integrated engine and control Simulation Environment
IMP	Intake Manifold Pressure
LNT	Lean NO_x Trap
LTC	Low Temperature Combustion
MVEM	Mean Value Engine Model
PCCI	Premixed Charge Compression Ignition
PID	Proportional-Integral-Derivative
SCI	Stoichiometric Compression Ignition
SCR	Selective Catalytic Reduction
SI	Spark Ignition
SISO	Single Input Single Output
TWC	Three Way Catalyst

1 INTRODUCTION

1.1 Motivation

Since 1876 when Nikolaus Otto first developed the spark-ignition engine and 1892 when Rudolf Diesel invented the compression-ignition engine, the internal combustion (IC) engine has been providing power for people in many areas from electricity generation to daily transportation, from field harvesting combines to lawn mowers. It also has been changing our life depending on the environment of air, water and soil day after day. It has already been shown that the carbon exhaust and harmful gas emissions from the IC engine have contributed to the issue of global warming, and diseases of the respiration system of the human body, et al.

Representing the United States government, the Environmental Protection Agency (EPA) has put strict regulations on highway and off-road vehicle emissions to reduce the impact of IC engine emissions on our environment. As shown in Figure 1.1, off-road vehicles PM and NO_x emission

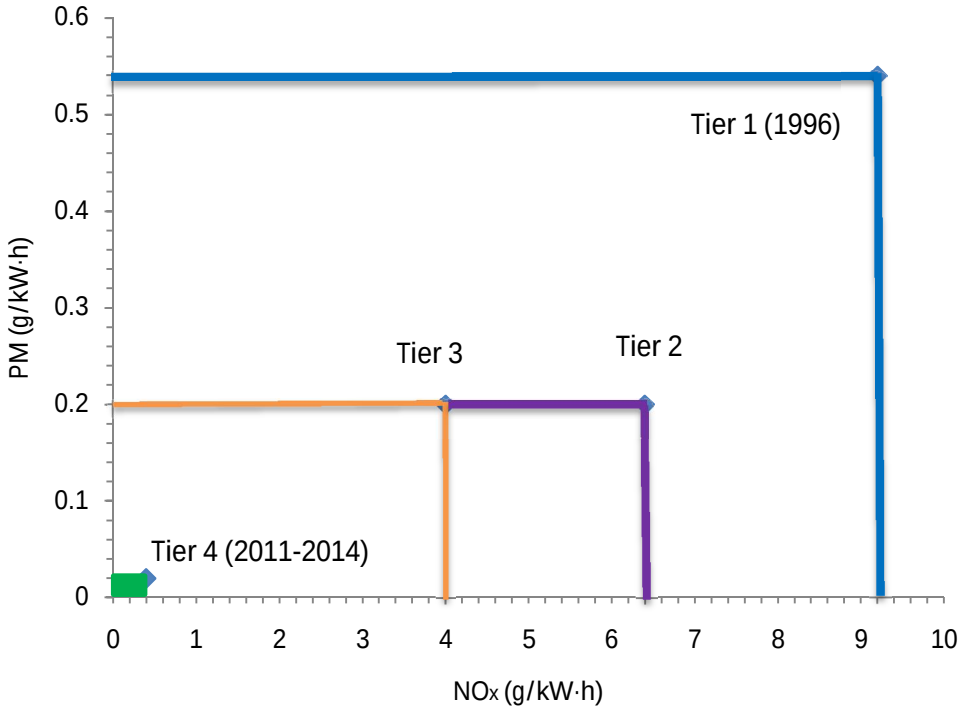

Figure 1.1. Tier 4 emission standards for off-road vehicles.

were regulated to reduced more than 90% in last decades. In response, scientists and engineers have made contributions that dramatically reduce engine emissions. New technologies are also being investigated continuously to make further improvements. Some have been used to adjust the in-cylinder combustion to improve the emissions. These technologies include advanced combustion, such as homogeneous charge compression ignition (HCCI), low temperature combustion (LTC) and Premixed Charge Compression Ignition (PCCI). Some are aimed at reducing the emissions by changing outside cylinder pressure, temperature, mixture composition, like exhaust gas recirculation (EGR), Fully Flexible Valve (FFV) for cam-less engines and Stoichiometric Compression Ignition for using a three way catalyst (TWC) in CI engines. Mainly, these methods are to change engine operation without changing the combustion. After-treatment technologies, such as, Lean NO_x Trap (LNT), selective catalytic reduction (SCR), and Three Way Catalyst (TWC), are to adsorb and convert the produced harmful gas into a green gas.

The Stoichiometric Compression Ignition (SCI) engine is a promising approach to allow the integration of a diesel engine and the reliable three-way catalyst (TWC) technology for HC, CO, and NO_x control. To implement the SCI technology on a generic diesel engine, some related technologies need to be investigated to verify the feasibility of a SCI engine on a different scale of horse power engine. Those technologies include the air fuel ratio (AFR) control for steady-state and transient state, and electrical control governor of engine systems.

The SCI technically has limitations on high load conditions because of the high exhaust temperature issue. For a heavy duty engine, the lean NO_x trap is an alternative way to reduce NO_x emissions. To implement the LNT in diesel engines, a lean/rich shift control needs to be designed based on a control oriented model of LNT. So modeling and controls are the interest in this emission reduction study.

1.2 Objectives and Approaches

The overall objective of this research was to investigate two alternative diesel engine NO_x emission reduction technologies. One is stoichiometric compression ignition and another is lean NO_x trap after-treatment. These are two options to could meet Tier 4 EPA regulations for off-road diesel engines.

The feasibility study of stoichiometric compression ignition was conducted on a John Deere diesel engine. Since the SCI technology has never been applied to a diesel engine before and to investigate the SCI performance and control feasibility before the engine test design, an integrated detail engine simulation, control design and verification environment was proposed. The research processes and specific objectives were:

1. Model John Deere 6090H diesel engine in 1D detail GT-Power simulation environment
2. Design control integrated Matlab/Simulink model for simulation condition automatic search.
3. Conduct performance simulation of constant speed load acceptance test for SCI diesel engine based on John Deer 6090H engine.
4. Design control design and implement it in the integrated engine and control simulation environment (ISE).
    a. Feed-forward air-fuel ratio design and verification for SCI engine.
    b. Torque limiting control design and verification for SCI engine.
    c. Over-speed control design and verification for SCI engine.
    d. Idle speed control design and verification for SCI engine.
5. Develop mean value engine model for SCI engine.
6. Develop lean NO_x trap model for general diesel after-treatment control.

2 APPROACHES

In this emission reduction research, the feasibility of implementation of SCI to a turbocharged diesel engine from the aspects of performance, AFR control strategy, and the governor design were investigated. Since the SCI concept has limitations in its application of heavy duty engines, the after-treatment system model for a generic diesel engine was also discussed.

2.1 SCI Engine Performance Simulation and Governor Design

2.1.1 SCI Engine Performance Simulation

Performance simulation aims to verify the engine system configuration, investigate the dynamic of the engine power output under steady-state and transient process, fuel economy under different operation, turbocharged operation condition, efficiency over the whole range of operating conditions.

To investigate SCI engine performance, the engine detail model was developed in a GT-Power environment. The model has been validated through engine experiments. The simulation results will be capable of prediction for both steady-state and transient process with the agreement of 95% or higher against experiments (He and Lin, 2007). To facilitate the performance simulation, an engine model in GT-Power and a control module in Simulink integrated simulation environment need to be developed. Then the steady-state and transient state could be simulated under various conditions.

2.1.2 SCI Engine Fuel Injection Modeling

AFR control is an important part of SCI implementation, which affects after-treatment system performance and vehicle drivability. The AFR accuracy in both steady-state and transient conditions are needed to be considered. As a first stage, the feed forward control model is being investigated in order to have simple structure of control.

There are some candidate AFR control strategies that can be used for SCI AFR control, which are different in control structure, sensor types and locations. Among these methods, intake manifold pressure (IMP) based feed forward control was selected for its advantages in the uniform value within the intake manifold and no time delay compared with other methods. To keep the AFR at the stoichiometric rate, a fueling function based on engine perimeters was

studied. Before conducting an engine test, steady-state and transient data of engine operation were collected from the performance simulation, which covers torque transients under different engine speed and load conditions. Since the AFR was limited to stoichiometric condition in performance simulation, the simulation data were valid for fuel injection modeling. A multiple regression was adopted based on different engine parameters and their interaction. The fueling models were verified in the GT-Power and Simulink integrated simulation environment. Engine tests are used for further validation.

2.1.3 Torque Limiting Control

To maintain the engine operation within safe conditions, the torque and turbocharger speed limiting control needed to be investigated. For the SCI engine, these two requirements were closely related by the stoichiometric fueling strategy. Therefore, they were being studied together. Tentative control criteria were designed to meet the steady-state and transient requirements under different ambient conditions.

Since direct torque measurement was not available in real time engine operation, indirect intake manifold pressure (IMP) based PID control was adopted because the SCI engine torque mainly depends on the air-charge into cylinders. While the mass of cylinder charge also depended on the temperature of intake air, a wide range of ambient conditions were considered for torque limiting control design. The torque limiting control needed to be effective under all ambient conditions for different temperatures and altitudes, so a steady-state IMP requirement function was defined first. This function was obtained by conducting a linear regression of 72 combinations of different engine speeds, torque levels, temperatures, and pressures. Then IMP based PI control was investigated to meet the steady-state and dynamic criteria, such as steady-state error, the limit of overshoot, and the settling time. The wastegate opening was controlled to adjust the air-flow rate for manipulating the torque output and turbocharger speed. The parameter interactions were also studied. Further parameter tuning was done for extreme conditions of engine speed and ambient temperature.

The torque and turbocharger speed limiting controls were validated in GT-power and Simulink integrated environment at this stage to save engine development time and to reduce the engine test risk. Engine tests are needed for validation and verification.

2.1.4 Idle Speed Control

After the engine is started, it is required to be stabilized at the idle speed of 850 rpm. But there always exits disturbances, for instance, the air-conditioning on and off, load change from shift gear, et al. The idle speed should be kept within the 10 rpm range of 850 rpm. Idle speed control challenges the throttle control of the air path. If control is not sensitive enough, the engine will stall once there is a small load added on; or the engine speed would run away after the load is taken off, for example, when the air-conditioner is turned off.

It is necessary to test the SCI engine scheme under the idle speed condition with load disturbance. This will verify the throttle configuration, the minimum opening, and the controller sensitivity.

2.2 Mean Value Model of SCI Engine

The engine and control integrated simulation environment is only suitable for classical control design, no model based method and verification. Because there is no engine model available for further system dynamic analysis. The 1D detail engine model based simulation is designed for engine performance analysis. It takes a longer time for repeating control design and simulation verification. So the control oriented model is necessary for further control development, for example, all speed governor design, and SCI Engine air path control design.

As the air path system gets complicated after adding throttle to a turbocharged diesel engine, there will be two control variables, throttle and wastegate opening, for the air path systems. The advanced control design is necessary for SCI engine implementation. One way is to use multi loops to stabilize the control unit one by one. Multivariable control is an alternative vs. SISO control for speed control over idle speed and all speeds. MVEM facilitates the control strategy design. Once the various controllers are designed with the MVEM, all the control can be verified in the Integrated Simulation Environment (ISE). This design and verification process would reduce the cost of an engine test dramatically. As for the modeling error produced during the model simplification, i.e., heat transfer and loss, robust control design would be used to consider the model error and un-modeled dynamics.

2.3 After-treatment Control for Diesel Engine NO_x Reduction

SCI is a very promising technology for diesel engine emission reduction, but it will be limited to the heavy duty diesel engine. Alternative technologies for emission control should also be investigated. Some available after-treatment technologies are lean NO_x trap, selective catalyst reducer, diesel particulate filter, et al. They have similar operation models: First, the after-treatment device adsorbs specific emission from the exhaust gases; while the trap or reactor reaches its full capacity, the engine must run a special operation to regenerate the device. But how do we estimate the adsorbing rate, at different temperatures, different flow rates, and pressure condition? How long should the regeneration be? Those control strategies are going to be investigated in this research.

For LNT operation, it needs to run the engine under lean and rich conditions alternately. During lean operation, NO_x in the feedgas passes through the LNT and is stored as barium nitrate. When the quantity of stored NO_x reaches a certain threshold, the trap must be purged by switching to rich operation for a short period of time to regenerate the storage sites and recover efficiency. The released NO_x is then catalytically reduced by reductants, such as, CO and HC in the feedgas. The lean rich switch control is critical to achieve the best tradeoff among competing requirements such as fuel economy, emissions, and drivability.

To best control the Lean/Rich operation for LNT, a control oriented model needs to be developed for control and optimization design. The chemical reaction is too complicated to know exactly based on reaction rate and chemical compounds in the catalyst. But chemical and physical phenomenon is a good base for model development, which is the key in following control and diagnosis design.

3 LITERATURE REVIEW

The diesel engine has a notorious reputation as a noisy, smoky, and sluggish power plant. This reputation has been improved by applying advanced combustion technologies, such as direct injection, lean combustion, EGR, and after-treatment systems, for example, DPF. The higher fuel efficiency and power density of diesel engines are their advantages over gasoline engines. Diesel emissions are carbon dioxide (CO_2), carbon monoxide (CO), hydrocarbon (HC), Nitrogen Oxides (NO_x) and Particulate Matter (PM). After carbon dioxide was identified as a green gas contributing to global warming, diesel engines emerged as an alternative to gasoline engines, due to their low fuel consumption. The diesel engine also has lower CO_2 emissions compared to gasoline engines, after lean burn combustion is applied to highway vehicles. For off-road vehicles for agricultural and construction machinery, the diesel engine has a dominant position in the market because of its higher power density.

To further decrease diesel emissions to meet ever stringent environment regulations, research on emission reduction methods have been investigated on in-cylinder combustion aspects, i.e. premixed charge compression ignition (PCCI), homogeneous charge compression ignition (HCCI), engine operation aspect, i.e., EGR, SCI, and after-treatment aspect, i.e., Lean NO_x Trap (LNT), Diesel Particulate Filter (DPF), Selective Catalytic Reduction (SCR).

3.1 Diesel Engine NO_x Emission and Related Technologies

3.1.1 Nitrogen Oxides Emission

While nitric oxide (NO) and nitrogen dioxide (NO_2) are usually grouped together as an NO_x emission, nitric oxide is the predominant (90% or more) oxide of nitrogen produced inside the engine cylinder. The principle source of NO is the oxidation of atmospheric nitrogen. The mechanism of NO has been extensively studied in the literature. Heywood (Heywood, 1988) summarized the generally accepted formation of NO. In the combustion of near-stoichiometric fuel-air mixtures, the principle reactions governing the formation of NO from molecular nitrogen (and its destruction) are:

$$\begin{aligned} O + N_2 &= NO + N \\ N + O_2 &= NO + O \\ N + OH &= NO + H \end{aligned} \tag{3-1}$$

The NO formation rate of the above reactions is given by:

$$\frac{d[NO]}{dt} = k_1^+[O][N_2] + k_2^+[N][O_2] + k_3^+[N][OH] - k_1^-[NO][N] - k_2^-[NO][O] - k_3^-[NO][H] \tag{3-2}$$

where [ ] denote species concentration when k_i are the value of 3forward and reverse rate.

It is appropriate to assume that the combustion and NO formation processes are decoupled (Heywood, 1988). In engines, combustion occurs at high pressures so the flame reaction zone is extremely thin (0.1 mm) and residence time within this zone is short. The burned gases during the early combustion process are compressed to a higher temperature. So the post-flame gases dominate the NO_x formation. It is logical to assume that the combustion and NO formation processes should be decoupled.

The NO_x formation rate is affected by the availability of oxygen, nitrogen, and the temperature. The strong temperature dependence of the NO formation rate can be evident in the initial NO formation rate:

$$\frac{d[NO]}{dt} = \frac{6\times10^{16}}{T^{1/2}} \exp\left(\frac{-69090}{T}\right)[O_2]_e^{1/2}[N_2]_e \tag{3-3}$$

Where $[\ ]_e$ denotes equilibrium concentration.

This is fundamental to the EGR technology for reducing NO_x by introducing exhaust gas recirculation into the intake manifold. The recirculated burned gases can be used to dilute the oxygen concentration, which will reduce the combustion temperature and slow down the NO_x formation.

3.1.2 Exhaust Gas Recirculation and Control Design

The Exhaust Gas Recirculation (EGR) has been introduced as an essential NO_x reducing technology for heavy duty diesel engines. In engines, the NO_x formation is the result of reaction

between N_2 and O_2 at temperatures above 2000K. The NO_x formation rate increases exponentially with temperature. Hence, in diesel engines most NO_x forms in both the flame front and the post-flame gases of the diesel spray, because the highest temperatures are located there. The EGR reduces these temperatures and, therefore, the amount of NO_x emissions (Heywood, 1988). Some experimental results have illustrated the trend and relationship between the burned gas fraction, AFR, NO_x and smoke (Stefanopoulou et al., 2000). From Figure 3.1and Figure 3.2, both the burned gas fraction and the AFR need to be controlled accurately in implementing the EGR technology. In turbocharged diesel engines, the Variable Geometry Turbocharger (VGT)

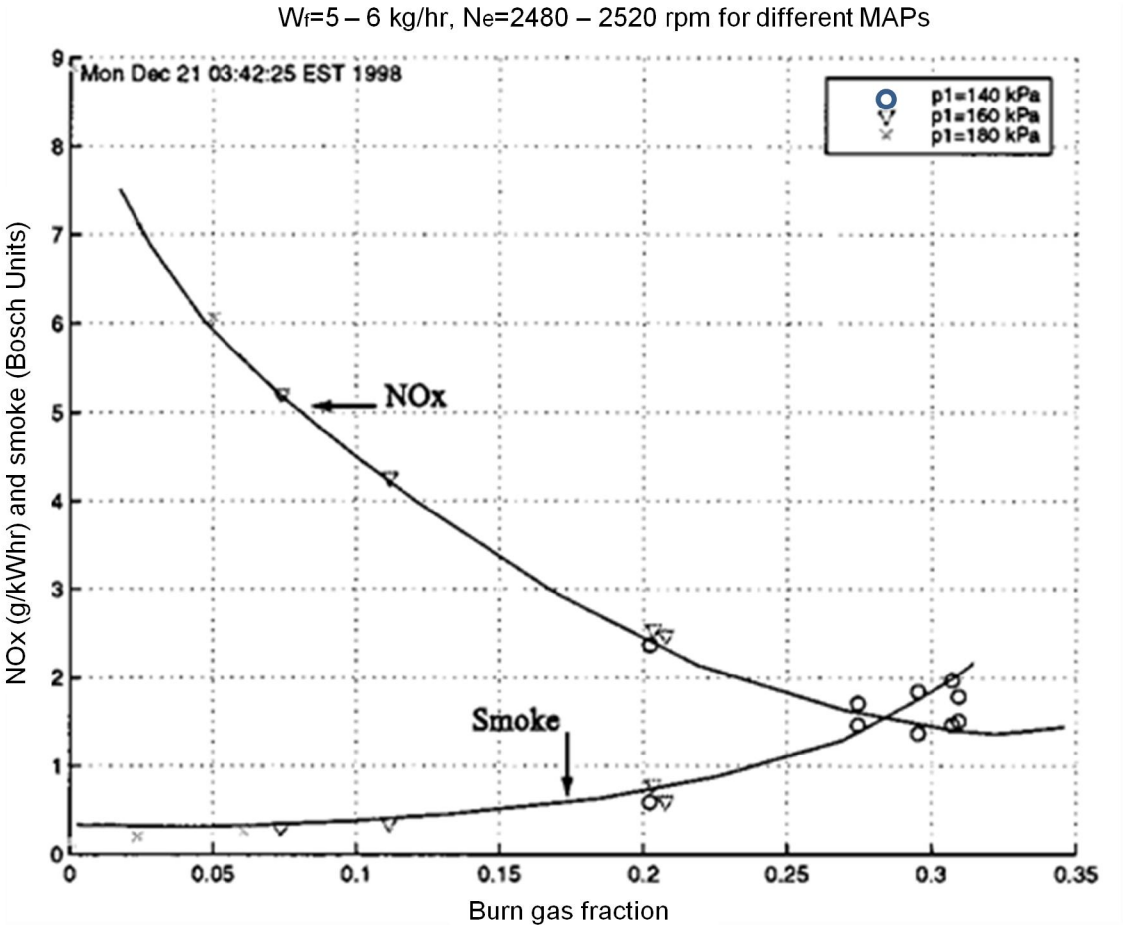

Figure 3.1. Relationship between the NO_x and smoke, burned gas fraction (Stefanopoulou et al., 2000).

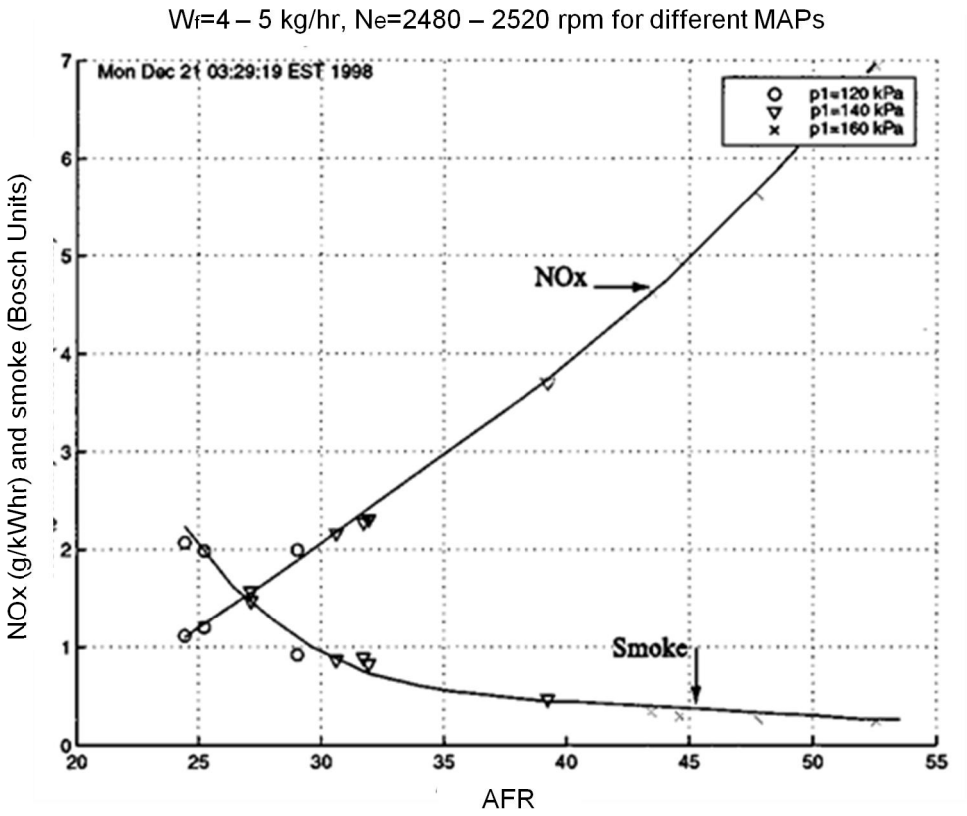

Figure 3.2. Relationship between the NO_x and smoke, AFR, (Stefanopoulou et al., 2000).

is another system input for system management. The three control variables will affect the drivability, fuel economy and NO_x emissions.

Several literature references have discussed the control design for this situation. Stefanopoulou et al. (2000) demonstrated that at the optimal operation points, the performance variable that most directly affects the emissions becomes closely dependent. Specifically, the performance variables cannot be controlled independently using EGR and VGT actuators. This plant singularity at the optimal condition does not allow the application of integral control and leads to a difficult tracking problem. Authors designed a nonlinear feed-forward and a gain scheduled multivariable controller. The controller makes it possible to run the engine at optimal conditions by coordinating the EGR and VGT. Shu (2001) developed a nonlinear dynamical model of a diesel engine, including EGR and VGT, in the formation of control and state observation. The Model MIMO predictive control strategy was investigated for coordinating EGR and VGT. Compared to the decentralized/centralized feedback PI control schemes, the author demonstrated that the

closed loop response is robust to strategy error and achieves stable tacking of the performance set points, thereby reducing NO_x and smoke emissions.

3.1.3 Stoichiometric Compression Ignition (SCI) Combustion

The ever stringent future emission regulations will not be met by improving diesel combustion alone, but will require the use of after-treatment devices with an improved engine system. Besides LNT and SCR, the three-way catalyst and four-way catalyst which were used in gasoline engines, are also promising candidates for diesel engines. Though the three-way catalyst is a well-established technology in gasoline engines, there are still many questions about applying the stoichiometric combustion condition to diesel engines. Some of them are fuel economy, soot emissions, and high exhaust temperatures for heavy duty diesel. The intrinsic character of compression combustion is the stratified mixing-controlled combustion. The locally rich spots of the flame front are the sources of soot, unburned hydrocarbons, and carbon monoxide emissions.

Many tests have been conducted to investigate the obstacles of SCI engines (Chase et al., 2007). The combustion character of rich diesel combustion near the stoichiometric operating condition was evaluated (Lee et al., 2006) in order to use the three-way catalyst in exhaust systems. The results indicate the stoichiometric operation can reduce NO_x emissions to around 0.1 g/kW-hr, sacrificing fuel economy by 28%, compared with the best standard diesel operation, and 8% more than by lean operation. The 80% fuel economy lost in the low combustion efficiency also has high carbon monoxide and hydrocarbon emissions. The poor fuel-air mixing is the main reason for the low combustion efficiency. Engine combustion design is the way to face those issues in the SCI engine. High fuel injection pressures, utilizing optimally targeted sprays and group-nozzles are used to improve mixing (Kim et al., 2009), but this method is restricted to light load operation. For higher load conditions, using throttled intake pressure without EGR to avoid excessive soot, it was found that the soot could be reduced to target levels by means of a DPF (Chase et al., 2007).

So far, the stoichiometric compression ignition engine is still in the research and development stage. To face the requirements of emissions and fuel economy, some concrete detail technologies need to be re-considered, especially for the stoichiometric diesel. Among them are the air fuel ratio control, EGR control, DPF regeneration control, and electronic governor for

engine operation. For specific diesel engines, engine performance is also of interest for design and production considerations.

The AFR control is critical for the operation of the SCI engine. The requirement for the air fuel ratio is to be controlled at $\lambda = 1$ during steady-state and transient state. One way to control fueling is to control air flow. Another way to achieve stoichiometric combustion is to increase EGR (Lee et al., 2006). Since the three-way catalyst operation window is very narrow, accurate AFR control during transients is necessary to minimize the volume and cost of the TWC. AFR control has been well discussed for gasoline engines, but most of them are feedback based approaches. The disadvantage of the feedback control is that there is always a delay between when the combustion and exhaust reaches the sensor location. Feed forward control, which has not had much attention, is necessary for AFR control during the transient process.

3.1.4 After-treatment System for NO_x Emission Reduction

The oxides of nitrogen (NO_x) are a major contributor to the formation of ground-level ozone. The increase of NO_x is a great concern to the environment. One major NO_x emission source is from off-road and highway vehicles powered with diesel engines. Increasingly stringent diesel engine emission regulations in Europe and the U.S. have stimulated intense interest in after-treatment technologies for engine exhaust control. For example, in the U.S., the Tier 4 regulation for non-road vehicles (130–560kW), requires that the particulate matter (PM) emissions must be reduced by more than 90%, from the Tier 3 level of 0.20 g/kW-h to 0.02 g/kW-h by the end of 2011. The NO_x emissions reduction will be phased in through two stages: one from the Tier 3 level of 4.0 g/kW-h to 2.2 g/kW-h in the year 2011, and in the second phase down to 0.4 g/kW-h in 2014 (U.S. EPA, 2004). In order to meet the EPA emission regulations, some after-treatment devices, such as oxygen catalytic converters, diesel particulate filters and Lean NO_x Traps (LNT) will be required. The LNT is one of the promising technologies to control NO_x. It can be used in two modes (Kabin et al., 2004). One is a lean-rich switching mode, in which exhausted NO_x is adsorbed when the engine runs under normal lean conditions, and is released in the form of nitrogen, when the engine runs under rich conditions (Bailey, 1997). The stoichiometric ratio is the ratio of air for which there is complete combustion, yielding only CO_2, H_2O, and N_2. The second mode is an active lean NO_x trap technology, in which engine fuel, i.e. hydrocarbons (HC) are injected upstream of the catalyst to provide a reducing agent for the nitrate regeneration

(Lueders and Stommel, 1999). One advantage of LNTs is that the NO_x emissions can be reduced without dramatic changes in the design of the engine, even though there is a need for moderate ECU modification to fulfill control and diagnosis functions.

There are two challenges associated with the LNT technology: one is the control of the shift between lean and rich operations. During lean operation, the NO_x in the feedgas passes through the LNT and is stored as barium nitrate. When the quantity of stored NO_x reaches a certain threshold, the trap must be purged by switching to rich operation for a short period of time to regenerate the storage sites and recover efficiency. The released NO_x is then catalytically reduced by reductants, such as CO and HC in the feedgas. The lean rich switch control is critical to achieving the best tradeoff among competing requirements such as fuel economy, emissions, and drivability. Another challenge is the detection of any malfunction in the LNT. The LNT can experience deterioration and malfunctions that can go unnoticed, by both the driver and repair technician. Those types of malfunctions could result in high emissions without a corresponding adverse drivability or impact on fuel economy. This problem could be avoided by incorporating a well-designed OBD-II (expanded On-Board Diagnostics standard) system to detect malfunctions of emission after-treatment systems.

A great deal of research, including experiments and modeling, is under way to investigate ways to solve the problems and improve control and monitoring of those devices. A system model can simulate the NO_x storage, release and conversion inside LNT. Current models fall into three main categories based on development strategies. These include 3-dimensional computational fluid dynamics (CFD) based models; 1-dimensional CFD based models; and 0-dimensional mean value based models. The 3D and 1D CFD models contain more detailed physics and chemical kinetics and have a high spatial resolution, but require intensive computational time, which limit their integration into real-time control. The 0D model focuses on engine, vehicle, and after-treatment control strategies. This model is not as accurate as the 1D and 3D models, but pursues real-time analysis goals and can be used in model based control (Bolton et al., 2002)

Several researchers have tried to develop control-oriented models. A pseudo-equilibrium model was proposed by Daw et al. (2003) to simulate the lean-phase operation of LNTs. Aswani et al. (2005) developed control-oriented, gray-box mathematical models for diesel active lean NO_x catalysts to predict NO_x reduction and catalyst chemical reactions. Shamim et al. (2002)

investigated the physiochemical processes of the NO_x trap systems and developed a quantitative prediction model for diesel and lean burn engines. Wang et al. (1999, 2000) developed control oriented dynamic models based on the trapping efficiency as a function of trap temperature, catalyst loading, space velocity and feedgas concentration. The model was parameterized at one operating condition and validated against the experimental results at other conditions. These models did not include changes in engine operating conditions and unit-to-unit variability, which will lead to uncertainty in a model that is developed off-line.

3.2 Control Design for Diesel Engines

To implement all the advanced diesel engine technologies, the engine control unit has to become more functional in managing all the aspects of the engine operation. This includes the intake process, valve timing, fuel amount control, injection timing, multiple injection, gas recirculation rate, wastegate opening or VGT angle, AFR control for engine operation and after-treatment operation. The overall control system has become more complicated as the subsystems are correlated and need to be integrated for the control design, optimization for fuel economy and drivability concerns.

3.2.1 Map Based vs. Model Based Design Method

Engine control has become an important technology in engine innovation over the last two decades. In order to meet the enhanced requirements for better fuel efficiency and lower exhaust emissions, controls had to be applied to both steady-state and transient states.

In the industrial area, the map based classical method is the most widely adopted because of its simplicity and stable performance. But as the engine system becomes more and more complicated, model based design becomes necessary. For some applications, like EGR and HCCI engines, advanced control strategies must be applied for the engine operation. In consideration of maintenance cost and reusability, model based design will be overshadowed by the classical methods. In these applications, control design is an interplay between physical reality, modeling and design methods. Even though classical control design, it can solve problems, and modern control theory will play a more and more important role in engine and automotive application.

In modern control applications, it begins with mathematical modeling. An effective engine model will facilitate the process of control and diagnosis design. They will also be the base for sensor fusion, adaptive control, and supervision. Computational software becomes a very necessary part of the engineering design. As a result, co-design and co-simulation of mechanics and control will bring the engine design and verification process into a new era.

3.2.2 Mean Value Engine Model

3.2.2.1 Three Categories of Engine Models

Engine models can be classified into three categories: detail model, 1D model, and the simplified physical model.

(1) Partial differential based detail model. This model is used to analyze the fluid field inside the engine, like the cylinder, manifold, for mechanical part design. This model is used by production engineers and engine researchers. Some software applications used for this model are Fluid, KIVA, among others.

(2) One dimensional model for performance analysis. The other two dimensions are not as important for the overall system operation and performance analysis. The commercial software used in this area are GT-Power and Wave, among others.

(3) The physically based dynamic model, which uses ordinary differential equations with time variables, is interested in the system transient and steady state. The objective in control design is to guarantee the engine system working within the designated conditions (torque limiting, idle speed control) and stabilize the system under un-expected disturbances (load, temperature, manual change of gear, AC). This model is used by control engineers and is mostly implemented in Matlab with a fitting model and ordinary differential equation models.

The engine itself, is modeled by a model in (1) – (3) for analysis and implementation, and only represents the body of the engine system. Another important part of the engine is the “head” of the system, which manages the whole system of the engine. It resides in the ECU, and is implemented by embedded software and hardware. The controller is modeled with ordinary differential equation and logics.

The work done in this thesis has mainly focused on the third type of model, and the combination of model (2) with model (3), which is given a name “Integrated Simulation Environment.”

3.2.2.2 Mean Value Engine Model (MVEM)

The Mean Value Engine Model is physically based and is intended mainly for control applications. It consists of algebraic equations of the flow constraints of the compressor, throttle, EGR valve, et al., and the differential equations of the dynamic descriptions of engine speed, turbine speed, and manifold pressures. In this form, it is easy to fit into different engines and requires relatively less engine data compared with other detail models.

Hendricks (1997) summarized the engine modeling for control application in a paper. The idea of the engine model can be traced back to the 1970s (Monk and Comfort, 1970), in which an analog electric circuit model was developed to represent the dynamic behavior of an IC engine and their eddy current dynamometer system. In the paper (Powell, 1979), an engine acceleration dynamic alone with regression of the engine torque, throttle flow rate map, and fuel injection dynamic were proposed. Dobner and Fruechte (1983) pointed out that linear models cannot accurately represent the engine’s operation during the large transients that are associated with most drivability problems. Then a detail dynamic model for the carbureted spark-ignition engine was developed, this model is based on describing the physical processes that occur in the engine. The use of normalized parameters readily allows simulating different engines, and the modular structure accommodates changing component performance characteristics and adding new model features. This model is very close to the mean value model, which was later introduced by Hendricks and Sorenson (1990) for a SI engine. This model has been used in real-time engine control applications, because it is compact enough to run in real-time and can be used as an embedded model, within a control algorithm or as an observer (Moskwa and Hedrick, 1987). Del Re et al. (2010) built up the Mean Value Engine Model by basic blocks (the volume block, gas exchange block, heat exchange models, combustion model, environment models, et al.,) and the interface definition. The model was especially used to investigate the robustness against the parameter variation in a series production. The robustness of the control strategy is easily accessed for all functional parameters of the engine. Not only can the usual parameters be considered, but all simulated components. So the system quality isn’t unusual and rarely considered situations can be verified. This MVEM was successfully applied to the Homogenous

Charge Compression Ignition Engine (HCCI) (Rausen et al., 2005). The EGR valve, the exhaust re-breathing lift, and the fueling rate on the cylinder charging were modeled. A set of simplified algebraic equations was used to describe the states after the HCCI combustion. After validation from experiments, the simple model can capture the temperature, pressure, A/F ratio, and inert gas fraction. Through modeling these variables, the thermodynamic state (pressure, temperature) and concentration (oxygen and inert gas) of the exhausted mass flow were controlled for the next combustion event.

The requirements of MVEM development:

- Represents the key system thermodynamics and fluid dynamics, and be able to predict the system variables in steady-state and transient in response to internal (valve, throttle, wastegate opening, fueling rate) and external disturbances (load, temperature).
- Has modular structure or is object oriented for reuse and iterative learning capability.
- Provide more functions in simulation to fit tight schedules and shrinking budgets.
- Provides a simulation environment for not only control, but also for diagnosis design.
- Meets the engine system control with expendability to emission control design.
- Is a validation platform for more and more complex control strategies.

In response to these requirements, engine model and simulation have to evolve. A rising topic is validation, with its need for a model to stimulate control units for testing purposes.

The importance of modeling and simulation in power-train and combustion engine development becomes undisputed as the automotive and engine systems are getting more complex. At the same time, market competition and legislation promote higher requirements for the development of performance, fuel economy and emissions. One of the biggest advantages of modeling and simulation is that they can be used to study different concepts in air loop architecture in the early stage of the project. The design deficiency and adjustment can be found and done early to reduce the experimental cost. While the available computing power and the number of tools are increasing, the choice of the right tool has significant impact on the development process.

4 INTEGRATED 1D ENGINE AND CONTROL SIMULATION ENVIRONMENT

4.1 Engine Simulation Environment Structure

To simulate the engine performance and control design for the SCI engine operation, the GT-Power and Matlab simulation software are integrated to implement the 1-D thermodynamic and combustion model and the control algorithm analysis, as shown in Figure 4.1. This simulation environment facilitates the performance simulation with virtual ECU functions, meanwhile it provides more detail engine information for control performance analysis than a simplified model. Further, ODB-II function can also be investigated with the same comprehensive model.

GT-Power and Simulink communicates through the S-function. Simulation data can be collected on both sides: GT-Power and Simulink. Simulink observes engine data from the sensor block and GT-Power obtains control signals from Simulink to control fuel injection, throttle, wastegate, et al. The advantage of integrating the two simulations is that GT-Power provides high fidelity for both engine performance simulation for engine design and the engine dynamics for control system synthesis. At the same time, Simulink simulates the ECU functions and then makes the simulation of engine operation close to the engine test. Both the steady-state conditions and transient dynamic can be verified qualitatively and quantitatively.

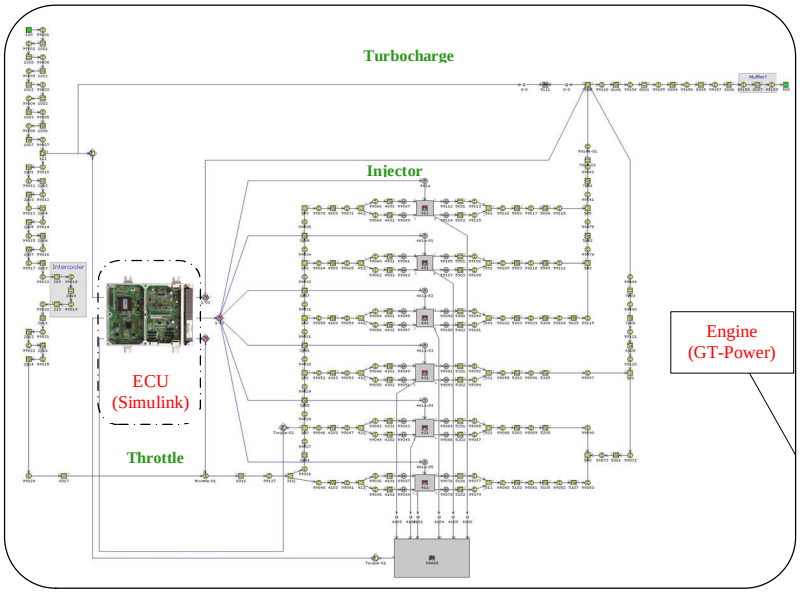

Figure 4.1. Layout of integrated simulation environment.

4.2 Constant Speed Load Acceptance Performance Simulation for SCI Engine

Constant speed load acceptance (CSLA) tests simulate the load increase in non-road mobile (eg. agricultural or excavator). In engine applications, the governor will adjust air charge and fueling to overcome the load change in order to keep the engine speed constant. For turbocharged diesel engines, this transient process tests the engine capability, transient time, and turbocharger dynamic. For the SCI engine, there are a series of events that happen during the process. First, the wastegate opening will be adjusted to absorb more kinetic energy from the exhaust gases. The turbine speeds up from one equilibrium condition to another equilibrium condition according to the wastegate opening. To obtain a quick response, the engine governor could fully close the wastegate and fully open the throttle to have a maximum amount of air supply, while keeping constant the AFR. Then the governor adjusts the wastegate or throttle opening to corresponding level. Leaving the throttle open and adjusting the wastegate will improve fuel economy. The John Deere 6090H Engine model was used for a SCI CSLA performance simulation. Engine geometry parameters are shown in Table C.1. in Appendix C. The engine layout in GT-Power is shown in Figure 4.2.

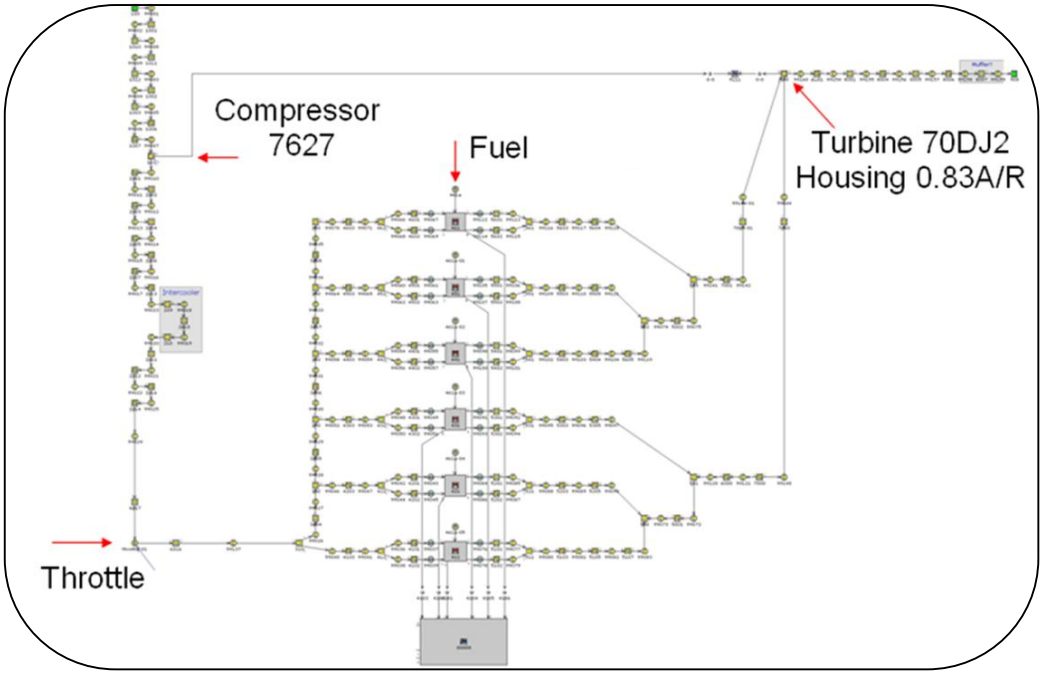

Figure 4.2. 6090H SCI engine model in GT-Power.

The engine specifications are attached in Appendix C. One example is shown in Figure 4.3, to demonstrate how Matlab controls the detailed engine model in the Simulink environment. One advantage of the integrated simulation is that the feedback control can be applied to search operating conditions. In Figure 4.3, torque control is used to find the full load fueling condition at different engine speeds.

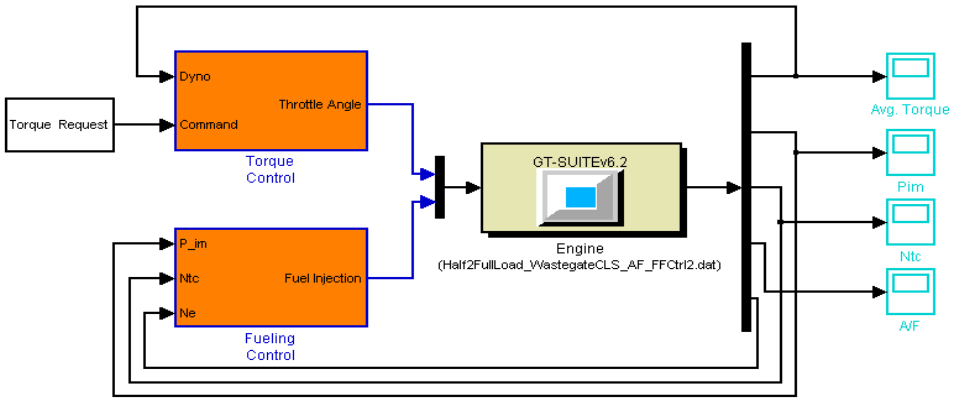

Figure 4.3. Integrated 1D detail model with Simulink for torque control.

4.2.1 Feedback Control for Performance Conditions Search

Constant Speed Load Acceptance tests were investigated at engine speeds of 900 rpm, 1100 rpm, 1500 rpm, 1800 rpm, and 2100 rpm. Engine torque curve is defined in Figure 4.4. Since the brake power, pumping loss and friction power are different at different engine conditions, to simulate CSLA, the corresponding throttle and wastegate conditions need to be defined for each simulation run. The engine torque feed-back control was defined with the integrated simulation

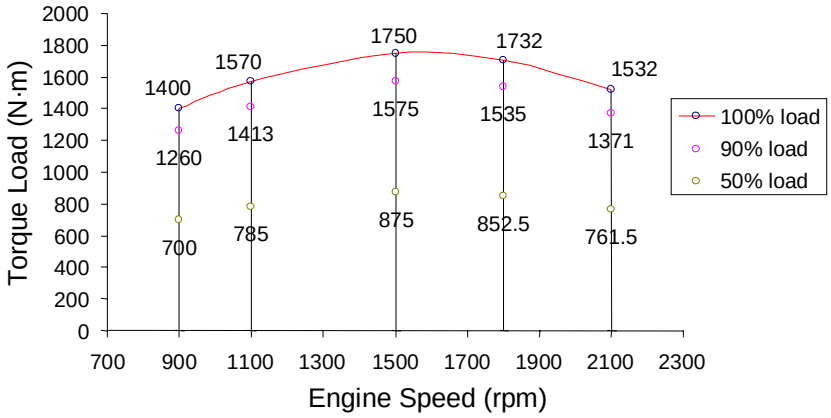

Figure 4.4. Engine torque curve, CSLA 90%, 50% torque level.

environment. To search throttle angle under closed wastegate condition, for example, the throttle was closed at a given time while the throttle was controlled to follow the reference input of torque level, as shown in Figure 4.5. Figure 4.6 demonstrates the two control variables of throttle and wastegate are controlled. During the process, the air fuel ratio was controlled by the AFR

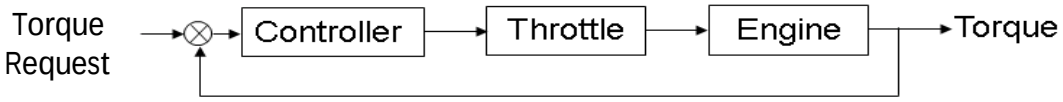

Figure 4.5. Feedback control for simulation condition search.

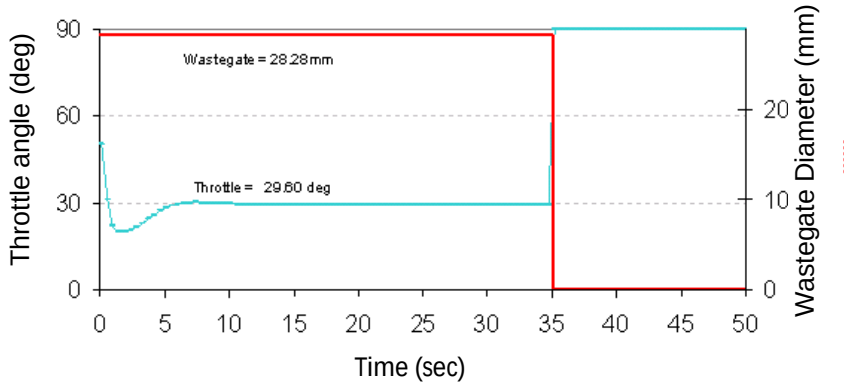

Figure 4.6. Throttle and wastegate change during the CSLA condition searching.

limit in the block of GT-Power at 14.4. For the John Deere 6090H engine, all the necessary steady-state conditions are searched and listed in Table 4.1, and Table 4.2.

Table 4.1. CLSA conditions for John Deere 6090H engine.

Wastegate Open Initially		Initial Conditions		Results
Engine Speed (rpm)	50% to Full Torque (N-m)	Throttle Angle 0-90/Open (deg)	TC Speed (rpm)	CSLA Time (sec)
900	700 – 1400	23.46	20,629	2.75
1100	785 – 1570	33.12	27,553	1.88
1500	875 – 1750	47.80	37,713	1.13
1800	852 – 1705	32.66	45,845	0.83
2100	761 – 1432	29.60	47,172	0.67

Table 4.2. Conditions of 50% load for wastegate initially open or closed cases.

Cases		50% Load Initial: Wastegate Open				50% Load Initial: Wastegate Closed			
Engine Speed (rpm)	Torque 50% (N-m)	Throttle Angle (deg)	TC Speed (rpm)	CSLA Time (sec)	Fuel (mg/ cycle)	Throttle Angle (deg)	TC Speed (rpm)	CSLA Time (sec)	Fuel (mg/cycle)
900	700	23.46	20629	2.77	96.3	11.72	50277	1.45	96.9
1100	785	33.12	27525	1.8	102.9	11.28	70765	0.33	104.4
1500	875	47.80	37712	1.1	111.1	13.02	82674	0.18	113.7
1800	853	32.66	45845	0.8	109.8	13.63	91106	0.19	113.1
2100	762	29.60	47172	0.9	101.4	13.87	94594	0.11	105.8

4.2.2 CSLA Simulation Results and Analysis

The CLSA simulation results are summarized in Table 4.3. One of the CSLA Performance

Table 4.3. Conditions and simulation results under full-load steady states.

Engine Speed (rpm)	Wastegate Opening (mm)	Total Fuel (mg /cycle)	BSFC (g/kW-h)	Air Mass Flow-rate (Kg/s)	Compressor P2/P1	IMP (bar)	EMP (bar)	Turbine Inlet Temp. (°C)	Turbine Speed (rpm)
900	21.07	180	216	0.116	1.76	1.68	1.74	916	73069
1100	22.72	195	209	0.153	1.90	1.79	1.90	918	78289
1500	23.03	211	205	0.227	2.10	1.93	2.11	915	88129
1800	24.78	208	207	0.268	2.11	1.90	2.21	944	91952
2100	26.59	190	211	0.284	1.97	1.73	2.17	963	90259

simulation results at 2100 rpm is shown in Figure 4.7, for which torque request was changed from the 50% to 100% level. The engine response illustrates the dynamic of the engine during

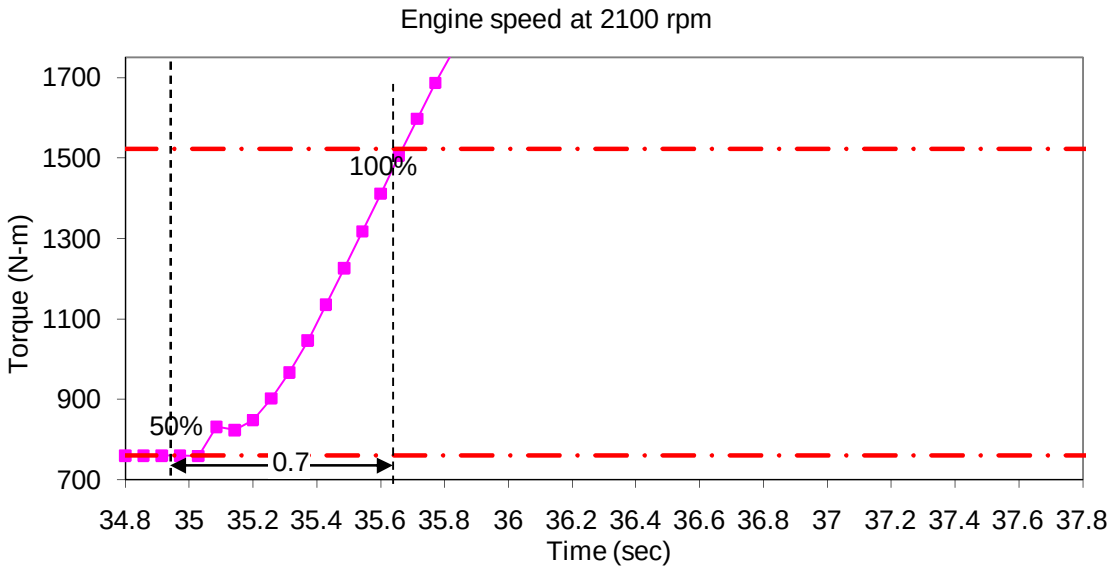

Figure 4.7. Example of CSLA test at 2100 rpm.

the process. The engine wastegate was initially opened, then was closed after 35 seconds. It takes about 0.6 s to transfer from half load of 761 N·m to full load of 1432 N·m. The engine speed was maintained, by connecting to a dynamometer, the load level was adjusted to balance the engine torque output. As shown in the Figure 4.7, engine torque jumps up initially, levels out for a while, before climbing up smoothly to the full level. The transient process demonstrates the turbocharger dynamic, that air mass flow can only increase after the wastegate changes. After the throttle was opened, a certain amount of air was sucked into the cylinder, which produced the torque jump. But before the turbocharger began speeding up, there was not enough air available. After the turbocharger sped up, the boost pressure increased while the compressor was powered up. Compared with the engine torque response at 900 rpm in Figure 4.8, the engine takes a longer transient process to climb from half load of 700 N·m to full load of 1400 N·m for about 2.8 seconds. The turbocharger lag was not significant compared with the case at 2100 rpm.

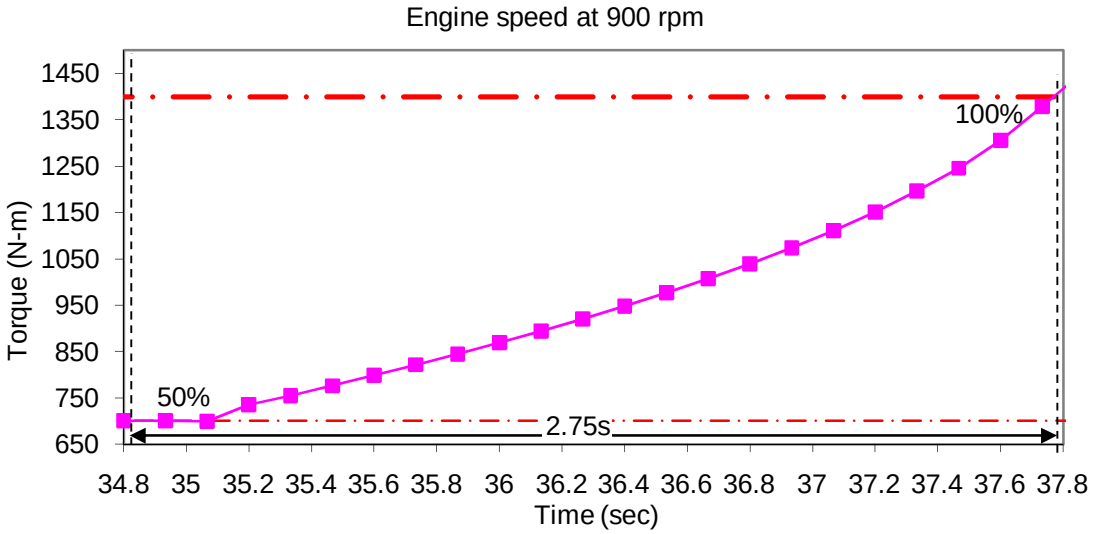

Figure 4.8. CSLA test at 900 rpm.

The comparison of the CSLA simulation results, between the condition of 0% to 90% load level and 50% to 100% load, is shown in Figure 4.9. The response times of 50% -100% load are about the half of that for 0 – 90% level. The simulation results of the initial condition differences is shown in Figure 4.10. The wastegate closed condition has less response time than that of the wastegate initially open case, because the turbocharger speed is higher for the wastegate closed case, shown in Figure 4.10. In the wastegate initially closed case, the turbocharger is easily sped up to the desired value. Figure 4.11 indicates that the throttle angle is different corresponding to the wastegate opening condition, to reach the same 50% load condition. Therefore, the wastegate open cases have better fuel efficiency compared to the wastegate closed cases, as shown in Figure 4.13. Brake specific fuel consumption at full load condition is shown in Figure 4.14. The turbocharger speed over engine speeds under full load condition is indicated in Figure 4.15. Intake and exhaust manifold pressure, which is useful for control design, is shown in Figure 4.16. Information about the compressor and turbine are show from Figure 4.17 to Figure 4.21, which is useful for configuration verification. Figure 4.18 shows the compressor steady-state operation line. The transient process of the compressor is illustrated in Figure 4.19 and Figure 4.20 for 50% to 100% load under wastegate initially closed and open conditions separately.

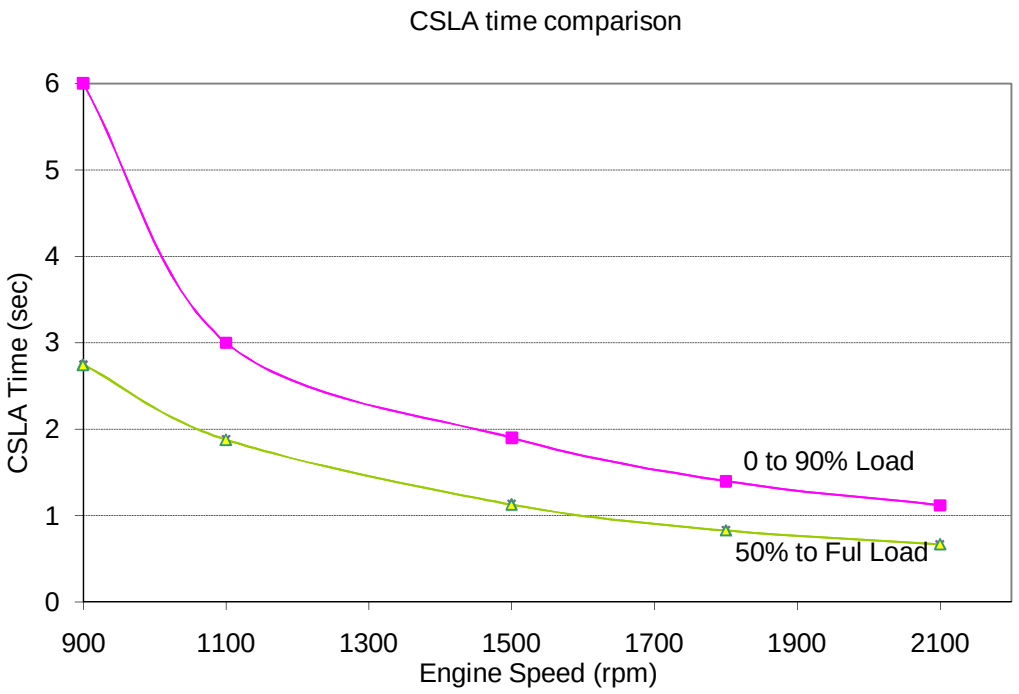

Figure 4.9. CSLA results wastegate initially open.

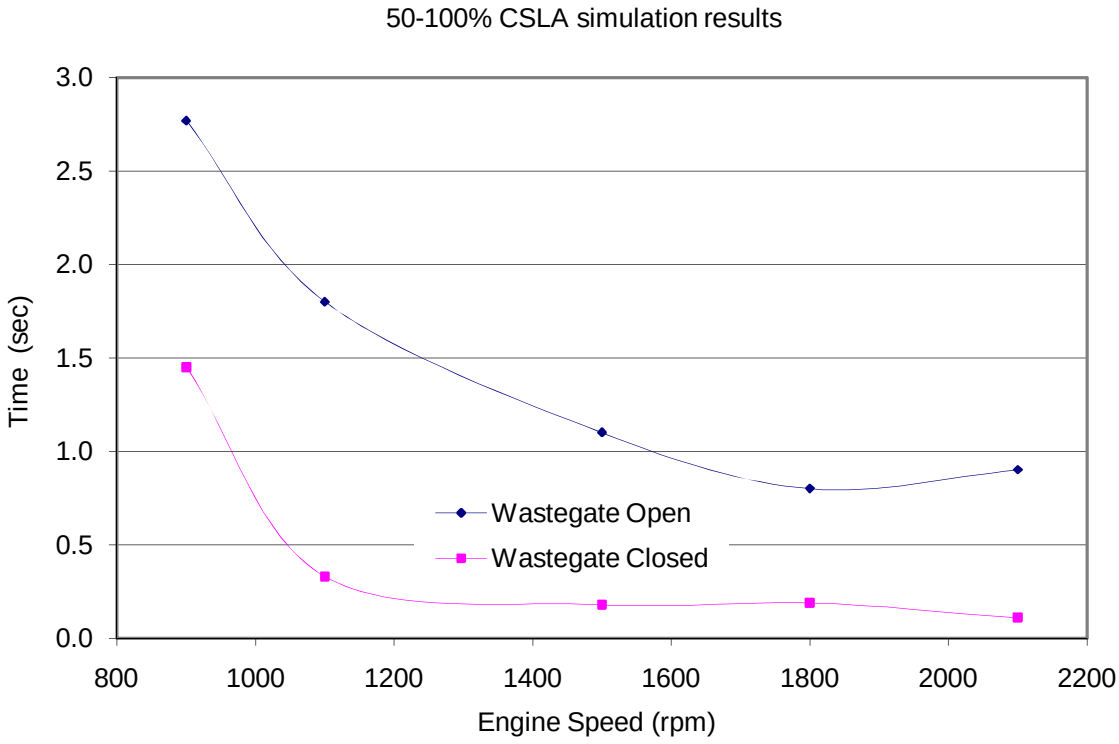

Figure 4.10. Comparison of CSLA time with wastegate initially open or closed.

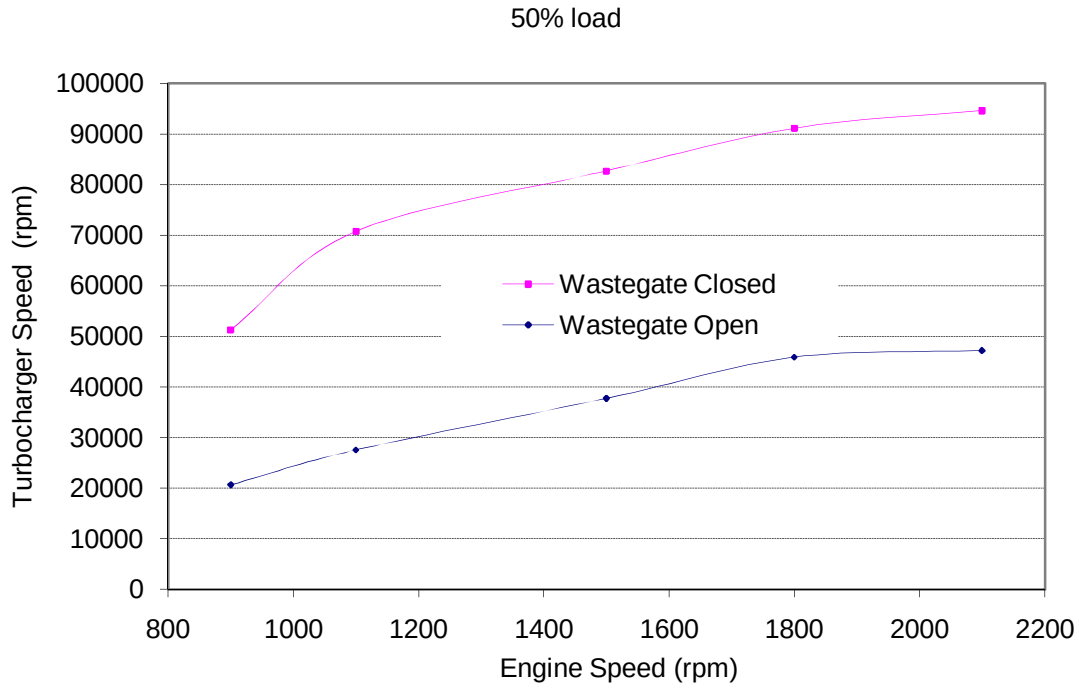

Figure 4.11. Comparison of turbocharger speed with wastegate initially open or closed.

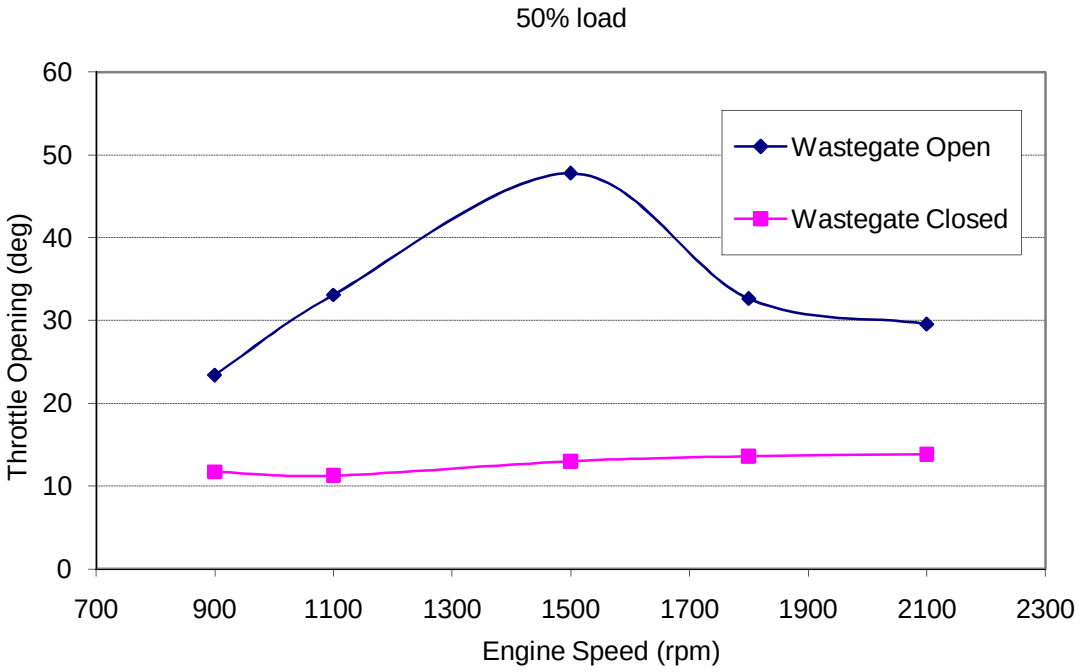

Figure 4.12. Comparison of throttle opening with wastegate initially open or closed.

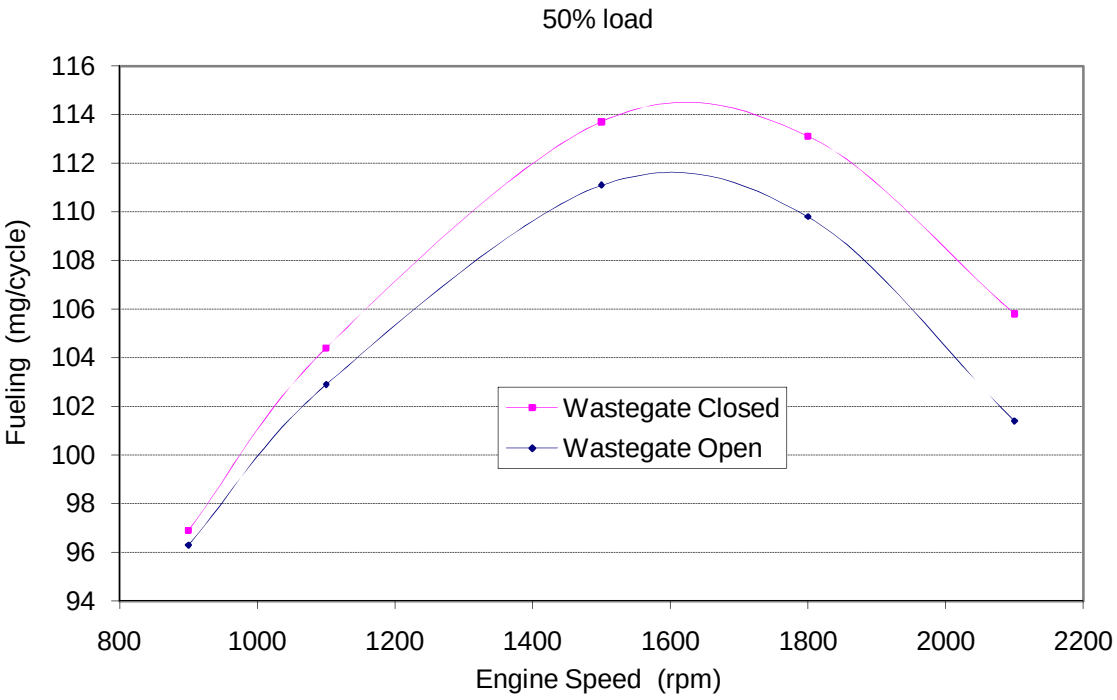

Figure 4.13. Comparison of fuel efficiency with wastegate initially open or closed.

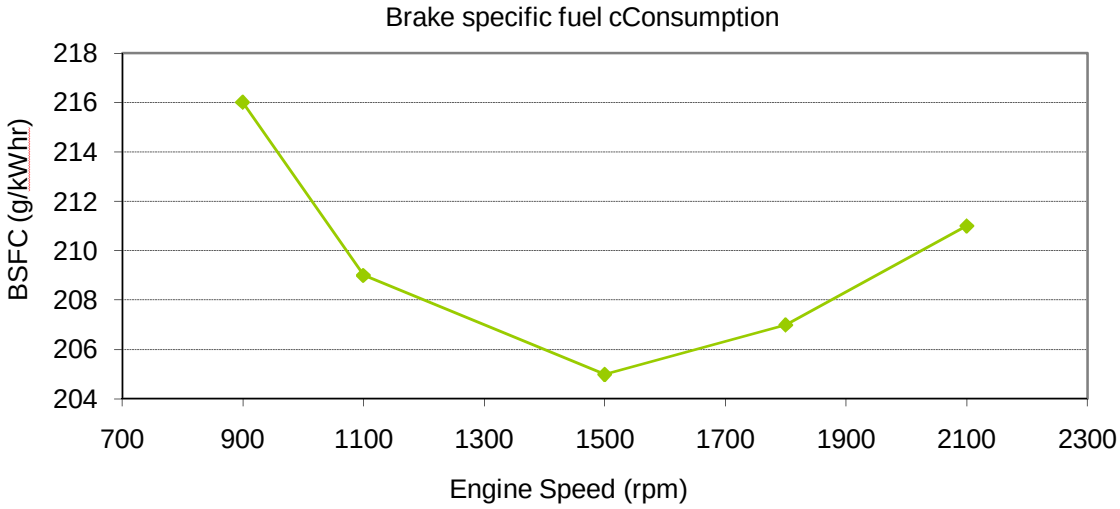

Figure 4.14. Engine brake specific fuel consumption.

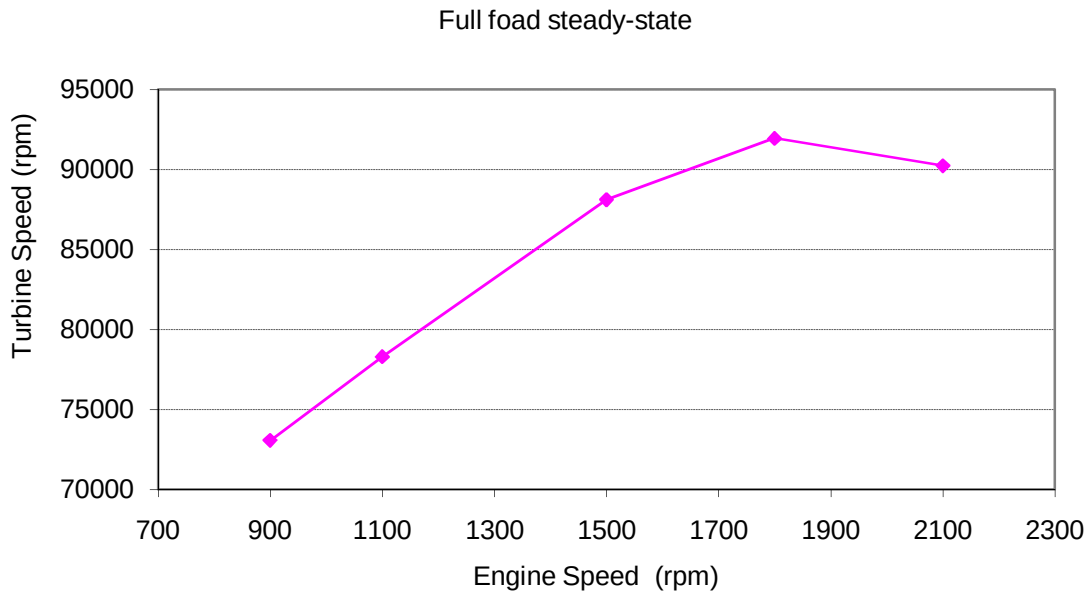

Figure 4.15. Turbocharger speed over engine speeds under full load condition.

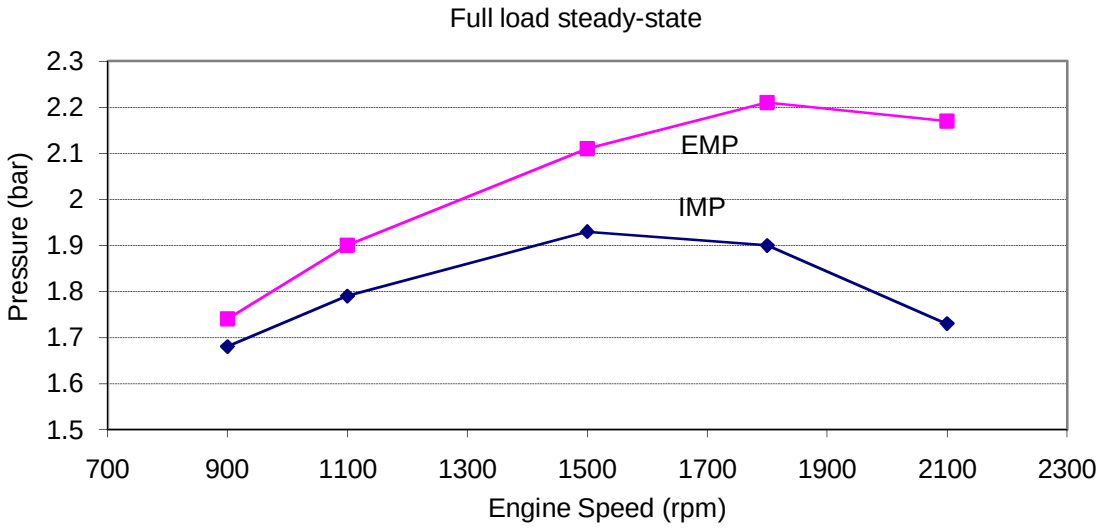

Figure 4.16. Comparison of intake manifold pressures and exhaust manifold pressure.

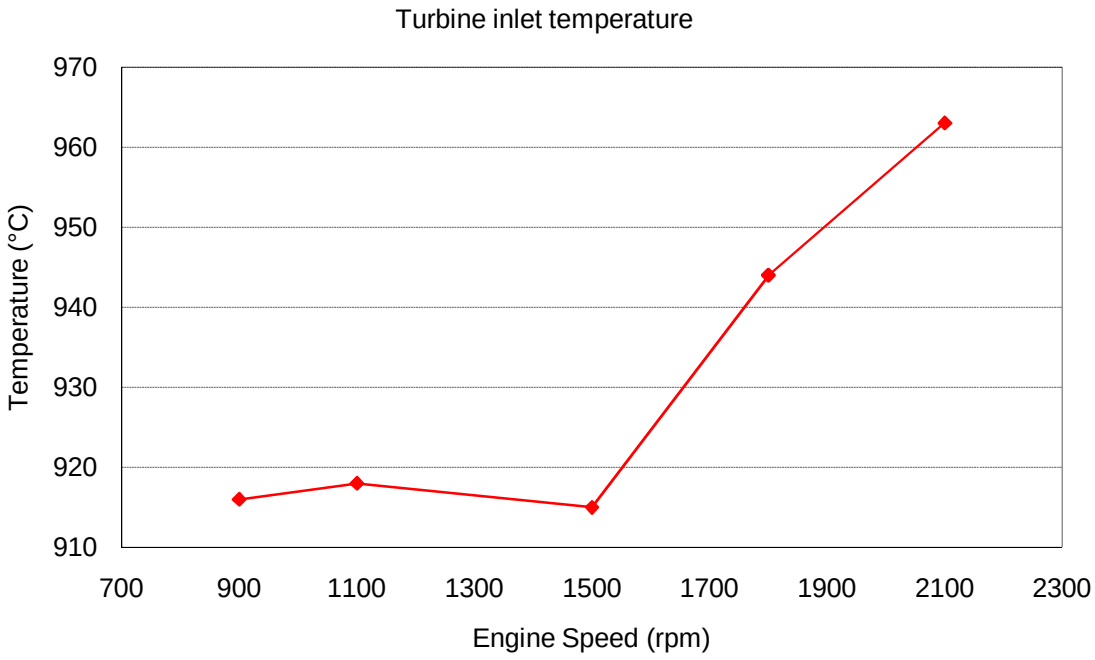

Figure 4.17. Turbine inlet temperature under full load conditions.

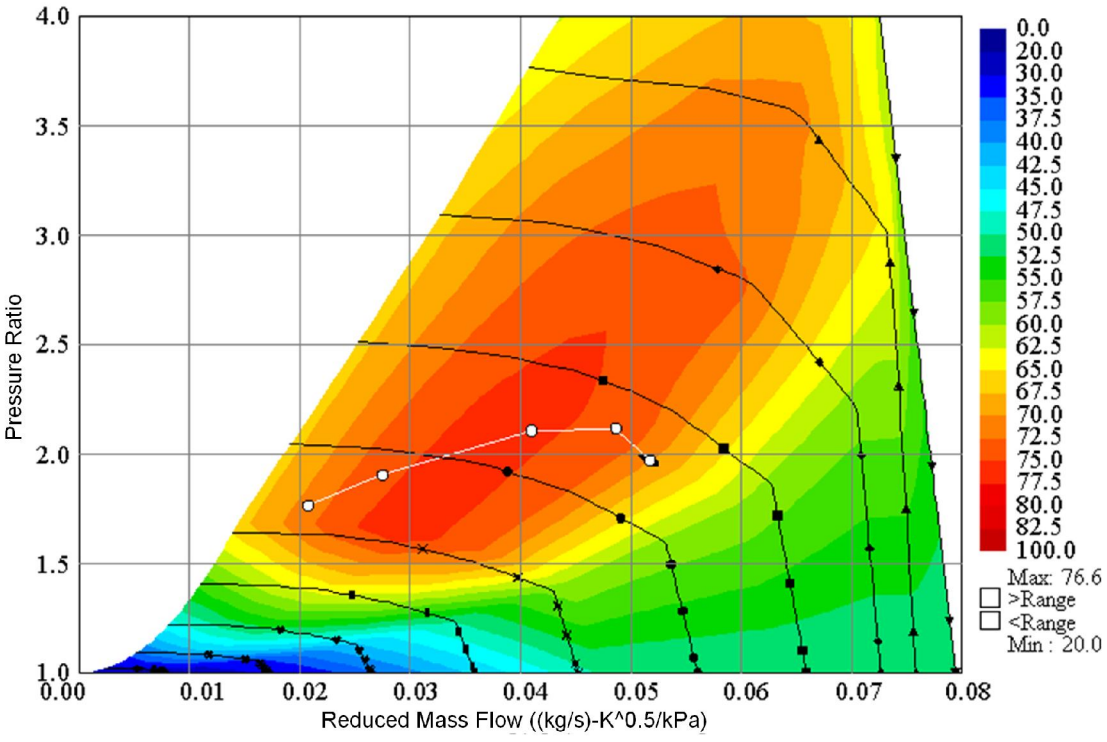

Figure 4.18. Full load steady-state compressor operating line.

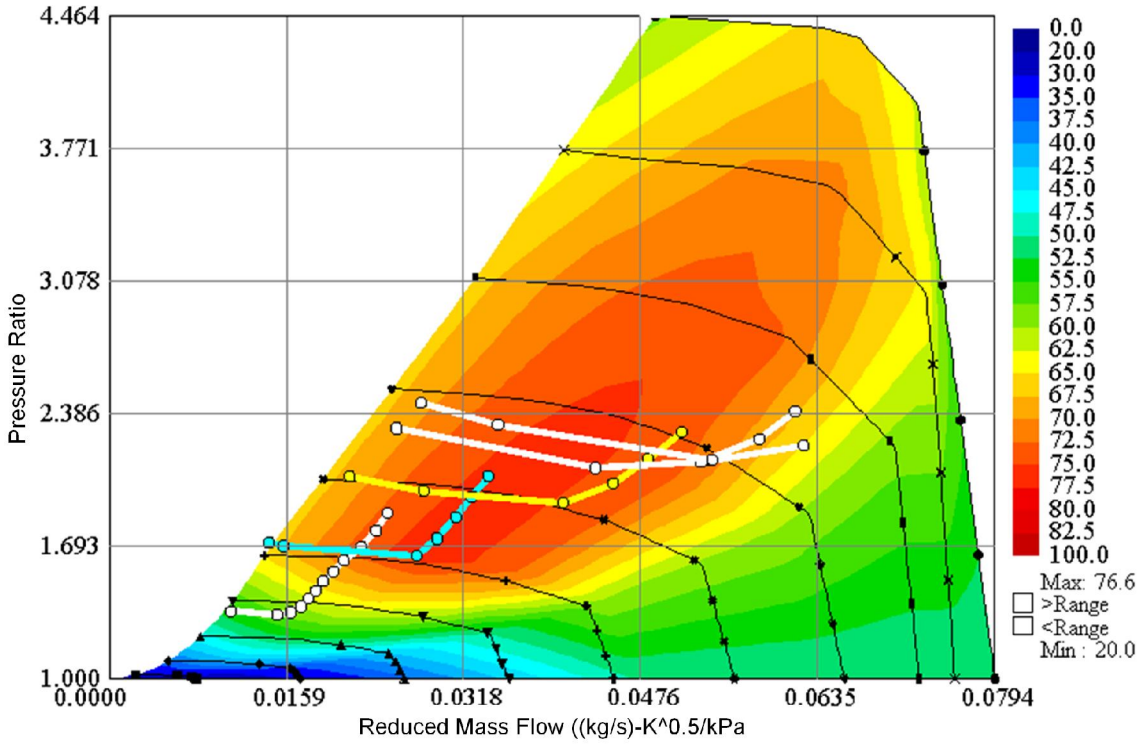

Figure 4.19. Compressor transient lines from 50% to 100% load with wastegate initially closed.

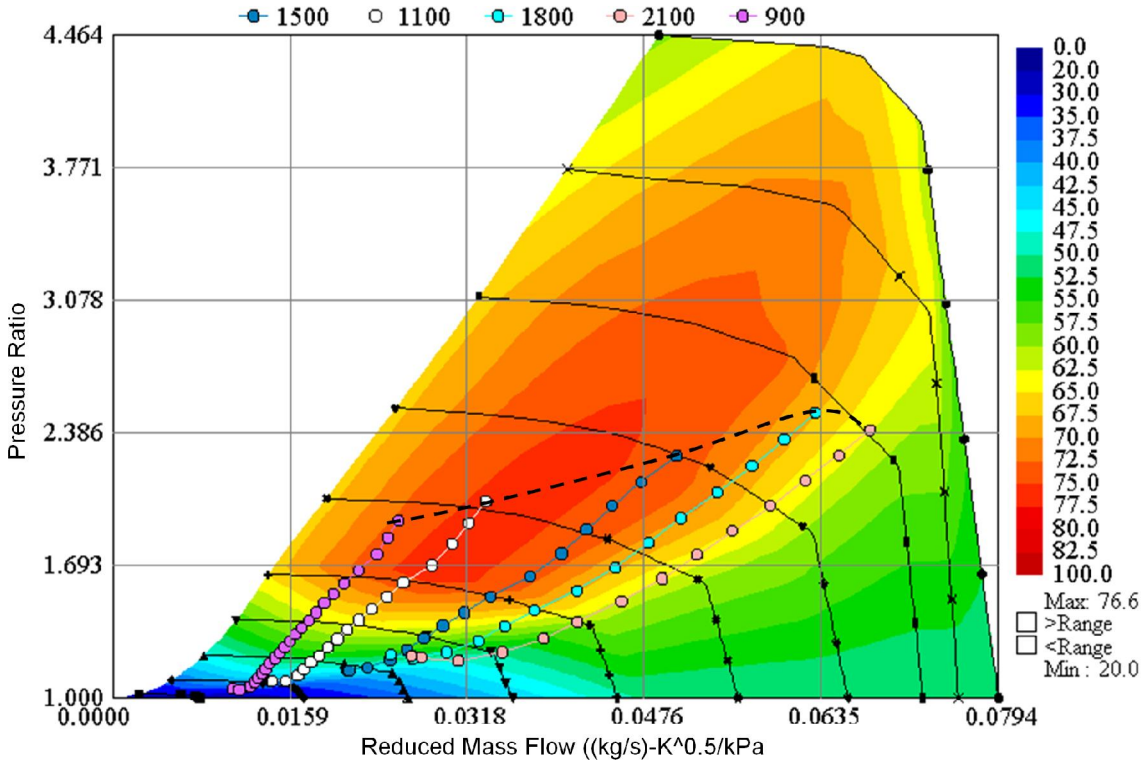

Figure 4.20. Compressor transient lines from 50% to 100% load with wastegate initially open.

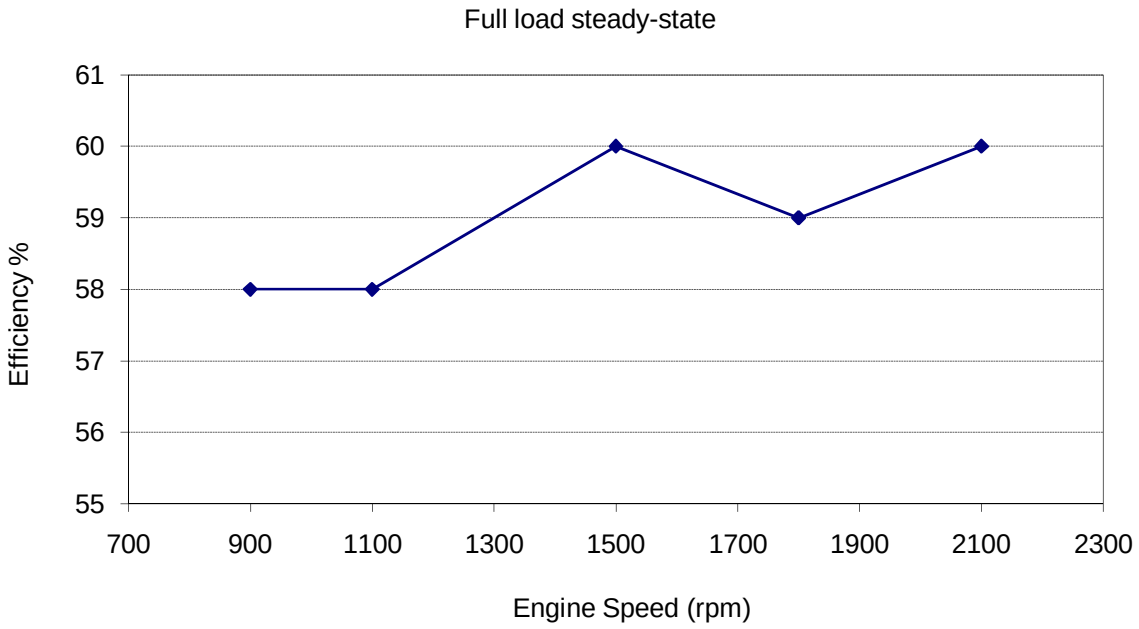

Figure 4.21. Compressor efficiency under full load conditions.

5 CONTROL DESIGN FOR SCI ENGINE IMPLEMENTATION

5.1 AFR Feed-forward Control

5.1.1 Introduction

The AFR control is essential for implementing stoichiometric combustion in a SCI engine in both steady-state and transient conditions, which affects the engine out emissions and the performance of the TWC. The oxygen sensor based feedback control is generally used in gasoline engines. The drawback of this method is the time delay of sensing and the reliability of the sensor, especially as SCI has a high exhaust temperature. The exponential dependence of soot on the equivalence ratio is a great challenge for the general oxygen sensor based feedback control system used to regulate an engine's air fuel ratio. An air-flow sensor based feed-forward control is an alternative method. But this method also has the drawback of signal discrepancy, which can not reflect the air-charging into the cylinder. To eliminate the time delay associated with feedback control, feed-forward fueling control needs to be investigated for stoichiometric AFR control. Therefore, a method based on intake manifold pressure (IMP) is selected for AFR control in SCI engines as the IMP is uniform inside the intake manifold. The feed-forward control was investigated by using GT-Power to simulate the engine operation under steady-state and transient conditions.

With an ideal AFR control method, a torque limiting control was considered as one important part of the engine operation to make sure that the engine provides enough torque under different ambient situations while preventing overshooting. As the torque is hard to measure in real-time, a feed-forward method based on the IMP sensor was adopted. This study includes the condition searching for IMP under different ambient conditions and the PID controller tuning to meet the certain criterion. The results of the simulation study will provide qualitative analysis and useful information for the future engine design and test.

For stoichiometric combustion, the fuel and air proportions is defined as (Heywood, 1988)

$$C_a H_b + \left(a + \frac{b}{4}\right)\left(O_2 + 3.773 N_2\right) = aCO_2 + \frac{b}{2} H_2O + 3.773\left(a + \frac{b}{4}\right) N_2 \qquad (5\text{-}1)$$

The diesel fuel used in this research has carbon and hydrogen atom numbers per molecule of $a = 13.5, b = 23.6$. The air-fuel ratio for this SCI engine is:

$$\left(\frac{A}{F}\right)_s = \frac{34.56(4+y)}{12.011+1.008} = 14.42 \tag{5-2}$$

where $y = b/a$.

5.1.2 Data Collection for Fueling Function Regression

To simulate the SCI operating condition, the Air-to-Fuel Ratio Limit of "InjProfile" connection (in GT-Power, shown in Figure 5.1) is set to 14.4. While the engine performance simulations were conducted under different speeds and load conditions, engine data, such as fuel injection quantity, intake manifold pressure, intake and exhaust air temperature, engine speed, turbocharger speed, et al., were collected. Both the steady-state and transient data are used to model the feed-forward fueling control based on the available sensor signals.

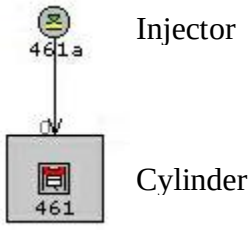

Figure 5.1. Stoichiometric AFR for SCI engine in GT-Power.

5.1.3 Fueling Model for Stoichiometric AFR Control

The fueling control was designed based on the available sensor parameters, such as, intake manifold pressure (P_{im}), engine speed (N_e), and turbocharger speed (N_{tc}). To consider the dynamic effects of air-charging, the intake manifold pressure change (ΔP_{im}) was also included. Multivariable linear regressions were used to obtain the prediction function of fueling from linear term, quadratic term and interaction term of parameters. Relatively few parameters were used to keep the function succinct for further implementation consideration. The regression data was obtained from the performance simulation under perfect stoichiometric conditions.

Several combinations of interaction terms were used to predict the fueling. Improvement was made through a series of regression models (see Appendix A). A simulation based on method (A9), the initial steady-state prediction was not good enough. The initial state predictions were improved after more initial steady data were added for the linear regressions. The updated equation is:

$$M_{fuel}7 = 127.8P_{im} - 0.011P_{im}N_e - 16.1dP_{im} - 0.03dP_{im}N_e - 0.00015N_{tc} + 6.5\text{E}-8N_{tc}N_e - 0.0014N_e - 25.86 \quad (5\text{-}3)$$

Based on the statistical analysis in Figure A.1. Variance analysis of model 8 in Appendix A, the dP_{im} had a low *p* value and was excluded. The equation was named as Method 8.

$$M_{fuel}8 = 127.8P_{im} - 0.011P_{im}N_e - 0.043dP_{im}N_e - 0.00016N_{tc} + 6.8\text{E}-8N_{tc}N_e - 0.0014N_e - 25.69 \quad (5\text{-}4)$$

To compare the perditions for different throttle and turbocharger speed conditions, method 8 was also applied to the wastegate initially opened condition. The fueling predictions matched the simulation data.

5.1.4 Comparison of Fueling Model Prediction with Simulation Data

To evaluate the regression model, a comparison was made for conditions with different throttle angles and turbocharger speeds from 50% to 100% load simulations.

Case 1

- Wastegate initially Closed

Case 2

- Wastegate initially Open

The comparisons of 10 cases are attached in Appendix A. The results show that both steady-state and transient fueling control match the “online fueling” data from the former ideal Stoichiometric AFR limit methodology with the Injection Profile Connection. However, the fueling prediction presented in Figure 5.2 is based on the offline simulation data. More engine testing is needed for verification of this model.

Table 5.1. Condition of fueling control.

Cases		Initial: 50% Load Wastegate Open				Initial: 50% Load Wastegate Closed			
Engine Speed (rpm)	Torque 50% (N·m)	Throttle Angle (deg)	TC Speed (rpm)	CSLA Time (sec)	Fuel (mg/ cycle)	Throttle Angle (deg)	TC Speed (rpm)	CSLA Time (sec)	Fuel (mg/cycle)
900	700	23.46	20629	2.8	96.3	11.72	50277	1.45	96.9
1100	785	33.12	27525	1.8	102.9	11.28	70765	0.33	104.4
1500	875	47.80	37712	1.1	111.1	13.02	82674	0.18	113.7
1800	852	32.66	45845	0.8	109.8	13.63	91106	0.19	113.1
2100	761	29.60	47172	0.9	101.4	13.87	94594	0.11	105.8

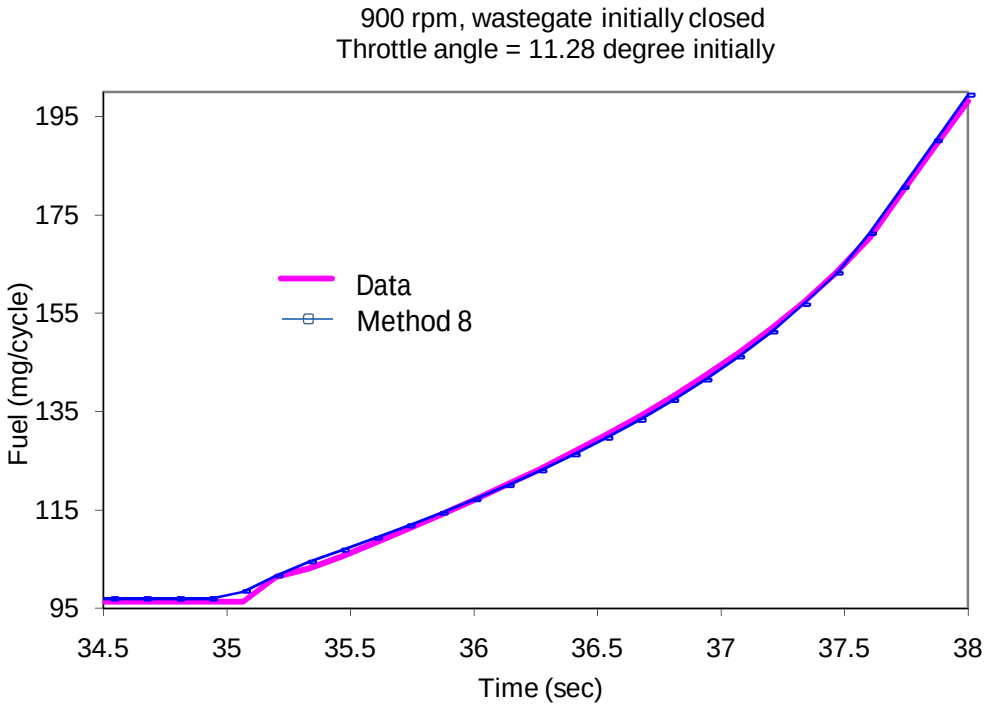

(a)

Figure 5.2. Comparison between fueling model prediction and simulation data.

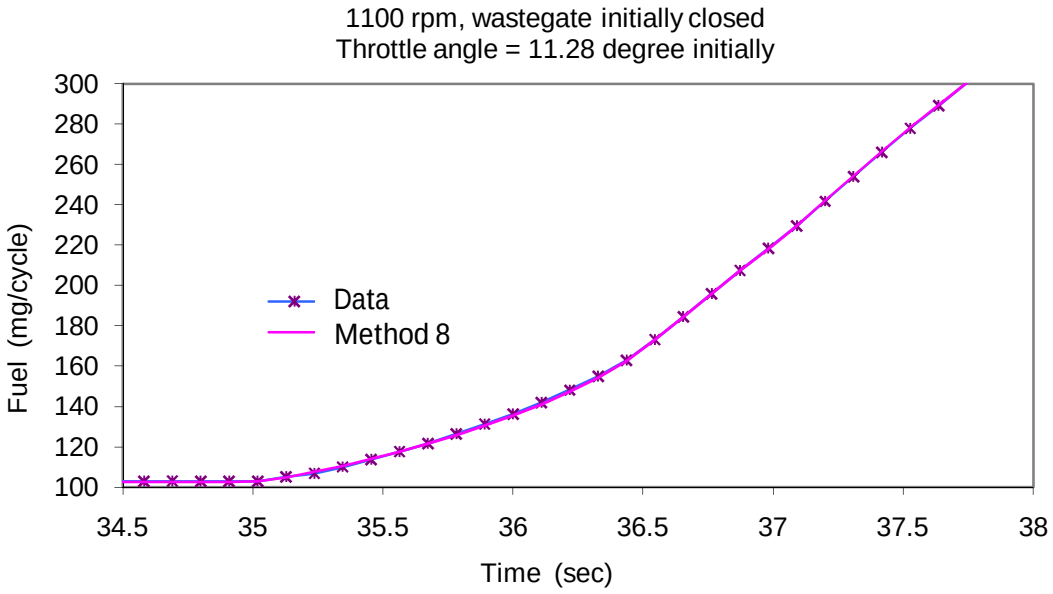

(b)

Figure 5.2 (cont.). Comparison between fueling model prediction and simulation data.

5.1.5 Verification of Fueling Model

To further verify the fueling control, method (5-4) was applied as the feed-forward controller for the AFR control. The integrated simulation was used to verify the AFR control, as shown in Figure 5.3. In the figure, the fueling control algorithm was implemented in Simulink. The engine data of IMP, engine speed and turbocharger speed were sent from GT-Power. The control signals were sent back to GT-Power after the calculations.

The simulations of transient tests from 50% to 100% torque level were carried out. The simulation results are shown in Figure 5.4 for engine speeds from 900 rpm to 2100 rpm. The air-fuel ratios were maintained at almost the same as for the steady-state at the same speed, but at different torque levels. During the transience, there were little jumps in the AFR. Further investigation on the transient fueling control is needed if the AFR criterion is very strict, especially for the smaller capacity of TWC.

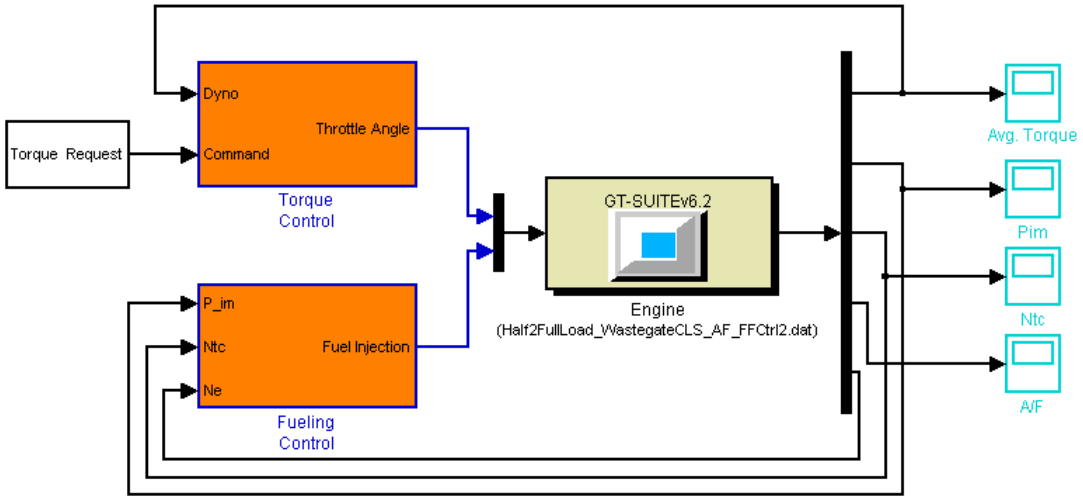

Figure 5.3. Schematics of AFR control for SCI engine.

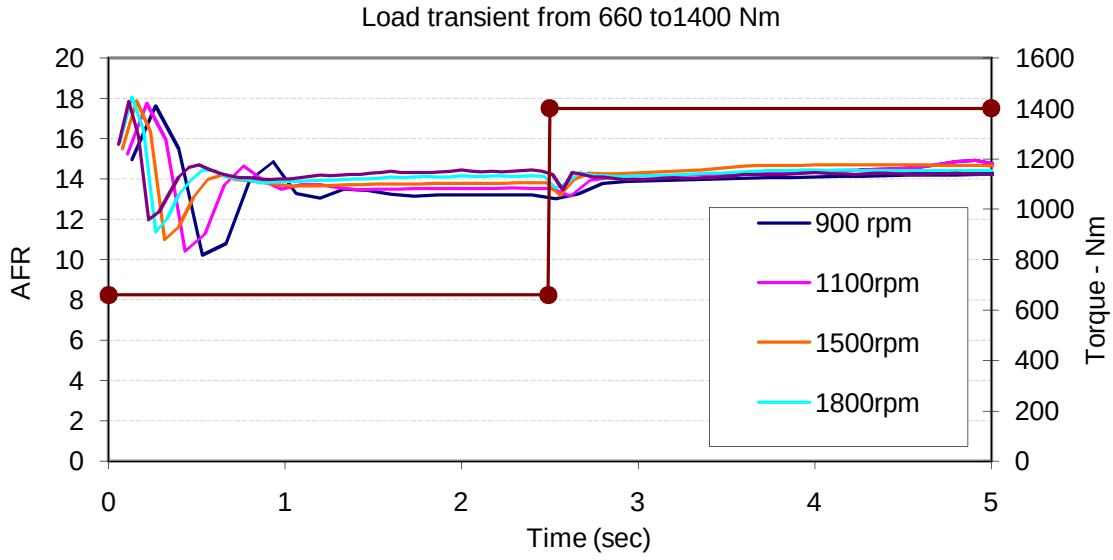

Figure 5.4. Simulation results of transient operation of engine from 660 to 1400 N·m under different engine speeds.

5.2 All Season and Altitude Torque Limiting

The torque limiting control is an important part of engine operation management to avoid the engine running into dangerous conditions. It is necessary to have both steady-state accuracy and avoid excessive torque overshoot. Both transient and steady-state operations need to control the throttle and wastegate. The coordination of the wastegate and the throttle could be controlled at lighter loads for engine economy or responsiveness. In economy mode, the engine operates at steady-state with the wastegate open and slightly throttled; while in responsive mode, the engine operates at steady-state with the wastegate closed and an open throttle. Upon request, the throttle is fully opened and the wastegate fully closed to reach the targeted torque level. In torque limiting control, the target is for full load level, with a limited overshoot for quick torque response and output. The ambient conditions are important factors in engine torque output and the control must operate at a wide range of altitudes and temperatures. The command function and PID control were designed to meet this requirement, and engine torque limiting performance was investigated and verified.

5.2.1 IMP Function Model

The IMP based torque control is a direct method to manipulate the engine power output. But it is affected by ambient conditions, such as temperature and pressure. Before designing a power limit control, the IMP under different altitude and temperature conditions needs to be defined. Then it can be used for later limiting of the torque.

The engine operating conditions are defined for ambient conditions ranging from 0 – 40^{o}C in temperature and 0-1950m in altitude. The ambient pressure varies with altitude as shown in Figure 5.5 based on the data from Table B.1 in Appendix B. To design and verify the torque limiting control, simulations were carried out at different ambient conditions indicated in Table 5.2, at five different engine speeds of 900, 1100, 1500, 1800, 2100 rpm. To find the relationship between intake manifold pressure, engine condition, and ambient conditions, the IMP search is carried out and results are shown in Table 5.3. The results are shown in Figure 5.6.

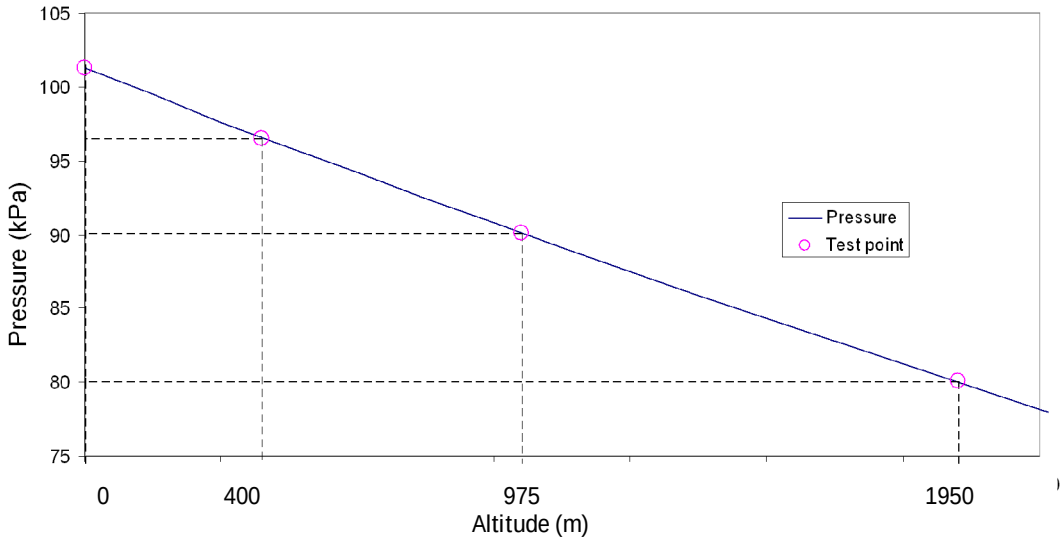

Figure 5.5. Ambient pressure varies with altitude.

Table 5.2. Ambient conditions.

Altitude (m)	Pressure (bar)	Temperature		
		0 (ºC) 273.15 (K)	25 (ºC) 298.15 (K)	40 (ºC) 313.15 (K)
0	1.0133	Condition 1	Condition 4	Condition 7
975	0.9013	Condition 2	Condition 5	Condition 8
1950	0.8010	Condition 3	Condition 6	Condition 9

Table 5.3. 100% load intake manifold pressure.

Case	Ambient Temp (ºC)	Altitude (m)	Ambient Temp (K)	Ambient Pressure (bar)	Engine Speed (rpm)	Torque Request (N·m)	IMP (bar)	Torque Output (N·m)	Torque Error (N·m)
1	0	0	273.15	1.0133	900	1400	1.58	1400	0
2	0	0	273.15	1.0133	1100	1570	1.68	1570	0
3	0	0	273.15	1.0133	1200	1643	1.74	1643	0
4	0	0	273.15	1.0133	1300	1682	1.78	1682	0
5	0	0	273.15	1.0133	1400	1715	1.81	1716	1
6	0	0	273.15	1.0133	1500	1750	1.80	1750	0
7	0	0	273.15	1.0133	1800	1705	1.77	1706	1
8	0	0	273.15	1.0133	2100	1523	1.62	1523	0
9	0	975	273.15	0.9013	900	1400	1.52	1400	0
10	0	975	273.15	0.9013	1100	1570	1.65	1570	0
11	0	975	273.15	0.9013	1200	1643	1.71	1643	0
12	0	975	273.15	0.9013	1300	1682	1.74	1682	0
13	0	975	273.15	0.9013	1400	1715	1.77	1715	0
14	0	975	273.15	0.9013	1500	1750	1.80	1750	0
15	0	975	273.15	0.9013	1800	1705	1.77	1705	0
16	0	975	273.15	0.9013	2100	1523	1.62	1523	0
17	0	1950	273.15	0.801	900	1400	1.52	1400	0
18	0	1950	273.15	0.801	1100	1570	1.65	1570	0
19	0	1950	273.15	0.801	1200	1643	1.71	1643	0
20	0	1950	273.15	0.801	1300	1682	1.74	1682	0
21	0	1950	273.15	0.801	1400	1715	1.77	1715	0

Table 5.3 (cont. 1). 100% load intake manifold pressure.

Case	Ambient Temp (ºC)	Altitude (m)	Ambient Temp (K)	Ambient Pressure (bar)	Engine Speed (rpm)	Torque Request (N·m)	IMP (bar)	Torque Output (N·m)	Torque Error (N·m)
22	0	1950	273.15	0.801	1500	1750	1.81	1750	0
23	0	1950	273.15	0.801	1800	1705	1.79	1705	0
24	0	1950	273.15	0.801	2100	1523	1.64	1523	0
25	25	0	298.15	1.0133	900	1400	1.63	1400	0
26	25	0	298.15	1.0133	1100	1570	1.77	1570	0
27	25	0	298.15	1.0133	1200	1643	1.83	1643	0
28	25	0	298.15	1.0133	1300	1682	1.87	1682	0
29	25	0	298.15	1.0133	1400	1715	1.89	1715	0
30	25	0	298.15	1.0133	1500	1750	1.93	1750	0
31	25	0	298.15	1.0133	1800	1705	1.90	1705	0
32	25	0	298.15	1.0133	2100	1523	1.73	1523	0
33	25	975	298.15	0.9013	900	1400	1.62	1400	0
34	25	975	298.15	0.9013	1100	1570	1.76	1570	0
35	25	975	298.15	0.9013	1200	1643	1.83	1643	0
36	25	975	298.15	0.9013	1300	1682	1.87	1682	0
37	25	975	298.15	0.9013	1400	1715	1.90	1715	0
38	25	975	298.15	0.9013	1500	1750	1.93	1750	0
39	25	975	298.15	0.9013	1800	1705	1.91	1705	0
40	25	975	298.15	0.9013	2100	1523	1.74	1523	0
41	25	1950	298.15	0.801	900	1400	1.61	1400	0
42	25	1950	298.15	0.801	1100	1570	1.76	1570	0
43	25	1950	298.15	0.801	1200	1643	1.83	1643	0

Table 5.3 (cont. 2). 100% load intake manifold pressure.

Case	Ambient Temp (ºC)	Altitude (m)	Ambient Temp (K)	Ambient Pressure (bar)	Engine Speed (rpm)	Torque Request (N·m)	IMP (bar)	Torque Output (N·m)	Torque Error (N·m)
44	25	1950	298.15	0.801	1300	1682	1.87	1682	0
45	25	1950	298.15	0.801	1400	1715	1.90	1715	0
46	25	1950	298.15	0.801	1500	1750	1.94	1750	0
47	25	1950	298.15	0.801	1800	1705	1.92	1705	0
48	25	1950	298.15	0.801	2100	1523	1.76	1523	0
49	40	0	313.15	1.0133	900	1400	1.68	1400	0
50	40	0	313.15	1.0133	1100	1570	1.83	1570	0
51	40	0	313.15	1.0133	1200	1643	1.90	1643	0
52	40	0	313.15	1.0133	1300	1682	1.94	1682	0
53	40	0	313.15	1.0133	1400	1715	1.97	1715	0
54	40	0	313.15	1.0133	1500	1750	2.01	1750	0
55	40	0	313.15	1.0133	1800	1705	1.98	1705	0
56	40	0	313.15	1.0133	2100	1523	1.80	1523	0
57	40	975	313.15	0.9013	900	1400	1.68	1400	0
58	40	975	313.15	0.9013	1100	1570	1.83	1570	0
59	40	975	313.15	0.9013	1200	1643	1.90	1643	0
60	40	975	313.15	0.9013	1300	1682	1.94	1682	0
61	40	975	313.15	0.9013	1400	1715	1.97	1715	0
62	40	975	313.15	0.9013	1500	1750	2.01	1750	0
63	40	975	313.15	0.9013	1800	1705	1.99	1705	0
64	40	975	313.15	0.9013	2100	1523	1.82	1523	0
65	40	1950	313.15	0.801	900	1400	1.67	1400	0

Table 5.3 (cont. 3). 100% load intake manifold pressure.

Case	Ambient Temp (ºC)	Altitude (m)	Ambient Temp (K)	Ambient Pressure (bar)	Engine Speed (rpm)	Torque Request (N-m)	IMP (bar)	Torque Output (N-m)	Torque Error (N-m)
66	40	1950	313.15	0.801	1100	1570	1.83	1570	0
67	40	1950	313.15	0.801	1200	1643	1.90	1643	0
68	40	1950	313.15	0.801	1300	1682	1.94	1682	0
69	40	1950	313.15	0.801	1400	1715	1.98	1715	0
70	40	1950	313.15	0.801	1500	1750	2.02	1750	0
71	40	1950	313.15	0.801	1800	1705	2.00	1705	0
72	40	1950	313.15	0.801	2100	1523	1.84	1523	0

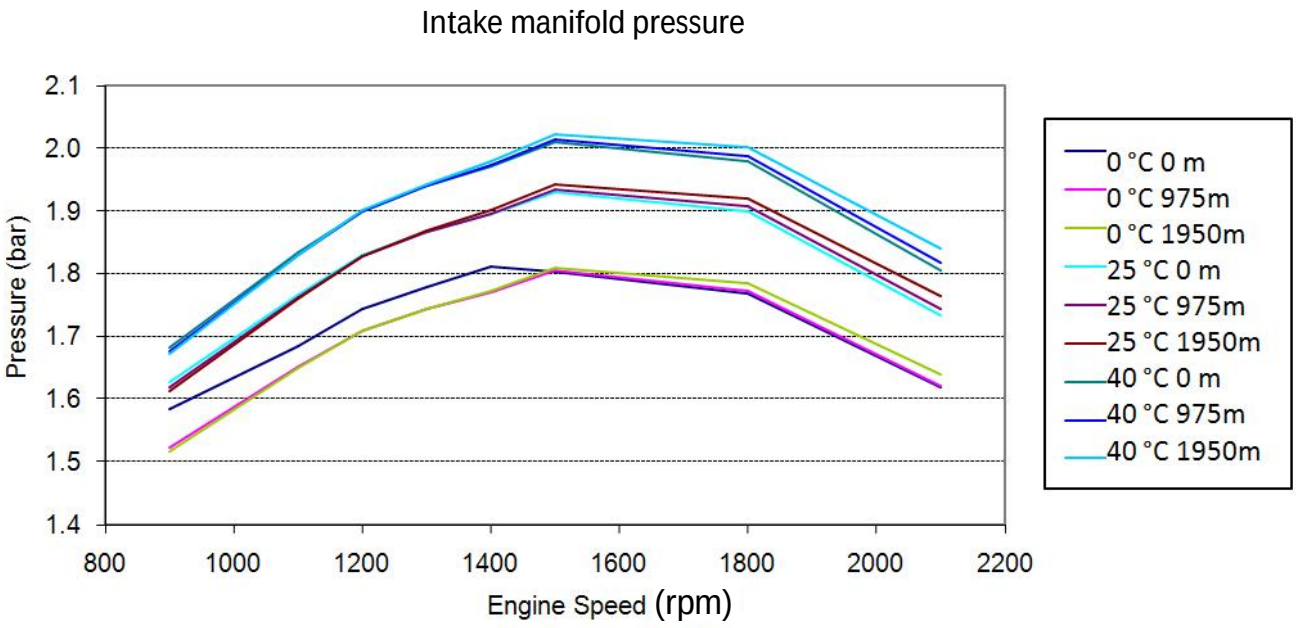

Figure 5.6. Intake manifold pressure at different engine speeds.

For each engine speed condition, the IMP and ambient temperature relationship can be defined by the following functions. Their linear functions are shown in Figure 5.7

900 rpm: $$P_{im} = 0.0034\,T_{amb} + 0.6118 \quad (5\text{-}5)$$

1100 rpm: $$P_{im} = 0.0042\,T_{amb} + 0.5067 \quad (5\text{-}6)$$

1200 rpm: $$P_{im} = 0.0045\,T_{amb} + 0.5029 \quad (5\text{-}7)$$

1300 rpm: $$P_{im} = 0.0046\,T_{amb} + 0.4982 \quad (5\text{-}8)$$

1400 rpm: $$P_{im} = 0.0047\,T_{amb} + 0.4924 \quad (5\text{-}9)$$

1500 rpm: $$P_{im} = 0.0052\,T_{amb} + 0.3749 \quad (5\text{-}10)$$

1800 rpm: $$P_{im} = 0.0053\,T_{amb} + 0.3169 \quad (5\text{-}11)$$

2100 rpm: $$P_{im} = 0.0049\,T_{amb} + 0.2949 \quad (5\text{-}12)$$

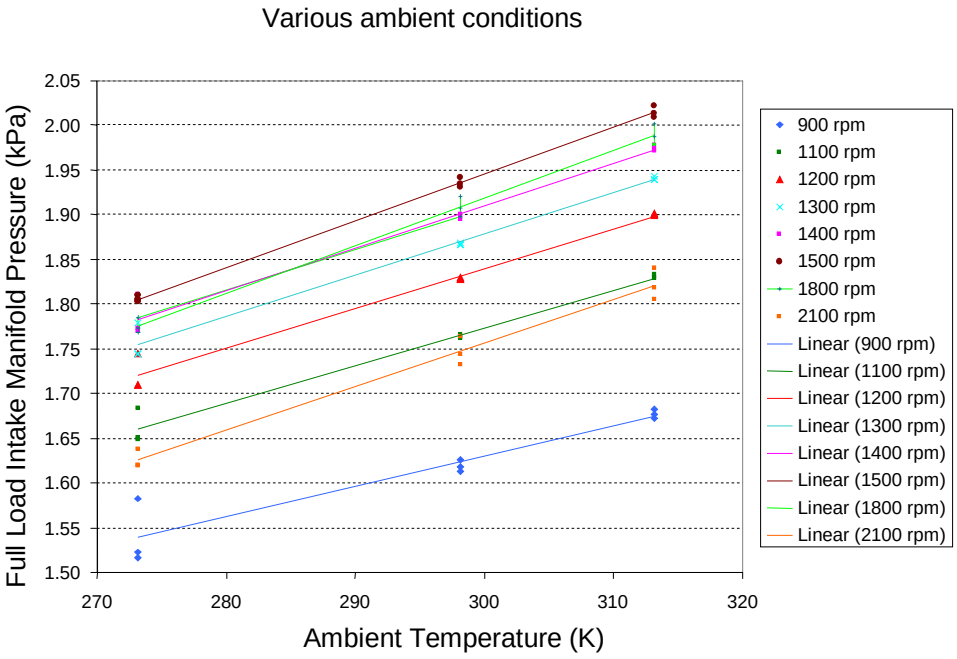

Figure 5.7. Linear function of IMP with engine speed and ambient condition.

A more complete regression for the intake manifold pressure (P_{im}) was defined based on the ambient temperature (T_{amb}), engine speed (N_e), square of engine speed (N_e^2), and their interaction term ($N_e \cdot T_{amb}$) for various altitudes and seasons:

$$P_{im} = -0.59 + 0.0028 \cdot T_{amb} + 0.0017 \cdot N_e + 1.23\text{E}-06 \cdot N_e \cdot T_{amb} - 6.628\text{E-}07 \cdot N_e^2 \quad (5\text{-}13)$$

The prediction based on function (5-13) and simulation data compare well as shown in Figure 5.8.

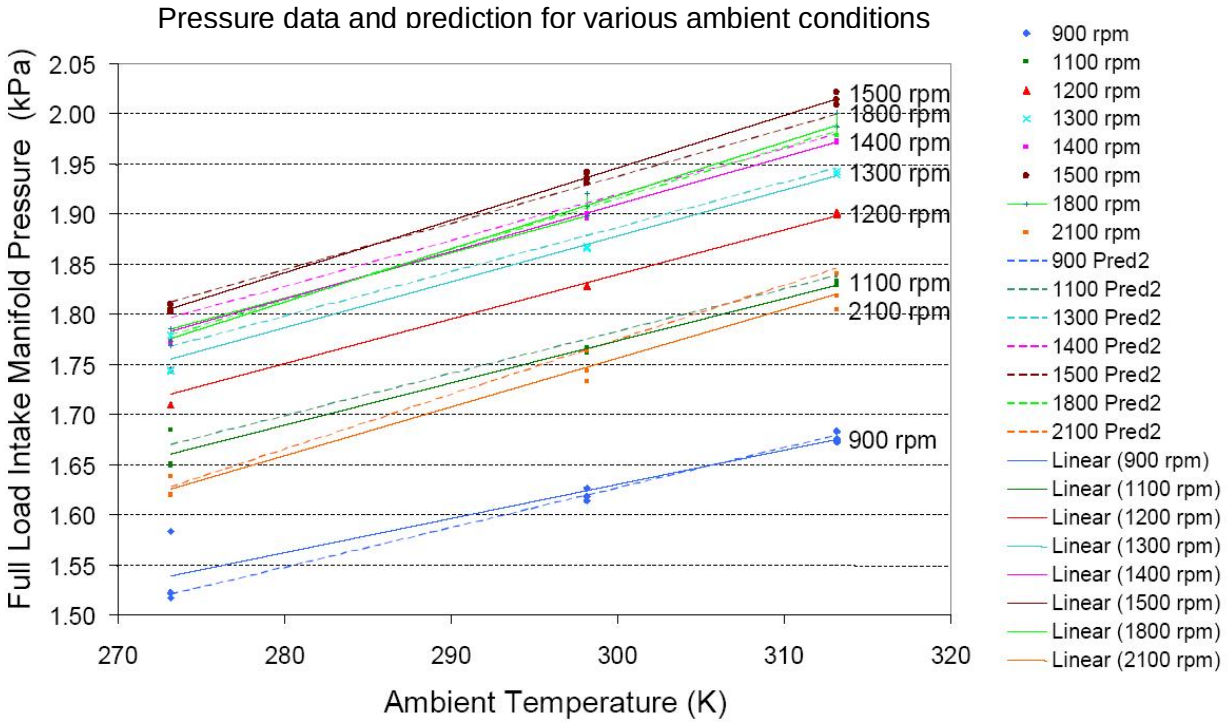

Figure 5.8. Comparison of intake manifold pressure prediction with data.

5.2.2 PID Controller Design for Torque Limiting

5.2.2.1 Torque Limiting Performance Criterion

Tentative torque limiting performance criteria as shown in Figure 5.9 (step responses are from the 50% to 100% level) are defined as follows:

Rise time (difference corresponding to torque without limiting):

$$\Delta t_r < 0.2\text{s} \tag{5-14}$$

Overshoot level: $$M_p < 7\% \tag{5-15}$$

Deviation band: $$\delta < \pm 3\% \tag{5-16}$$

Settling time: $$t_s < 1s \tag{5-17}$$

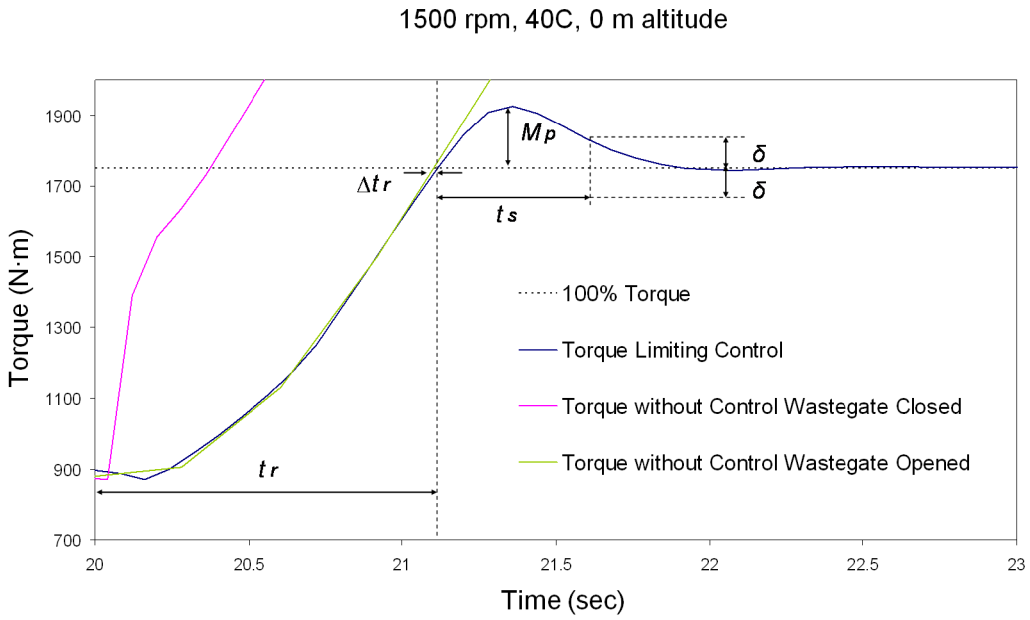

Figure 5.9. Control performance criteria.

5.2.2.2 Parameter Tuning

Several parameter sets were used to investigate the transient dynamics of torque response. These parameters are:

$$K_{p_1} = -50,\ K_{i1} = -100 \tag{5-18}$$

$$K_{p_2} = -50,\ K_{i2} = -150 \tag{5-19}$$

$$K_{p_3} = -70,\ K_{i3} = -150 \tag{5-20}$$

As the results show in Figure 5.10, the integral term K_i can adjust the setting time; and the proportional term K_p can be used to adjust the overshoot, according to performance settings.

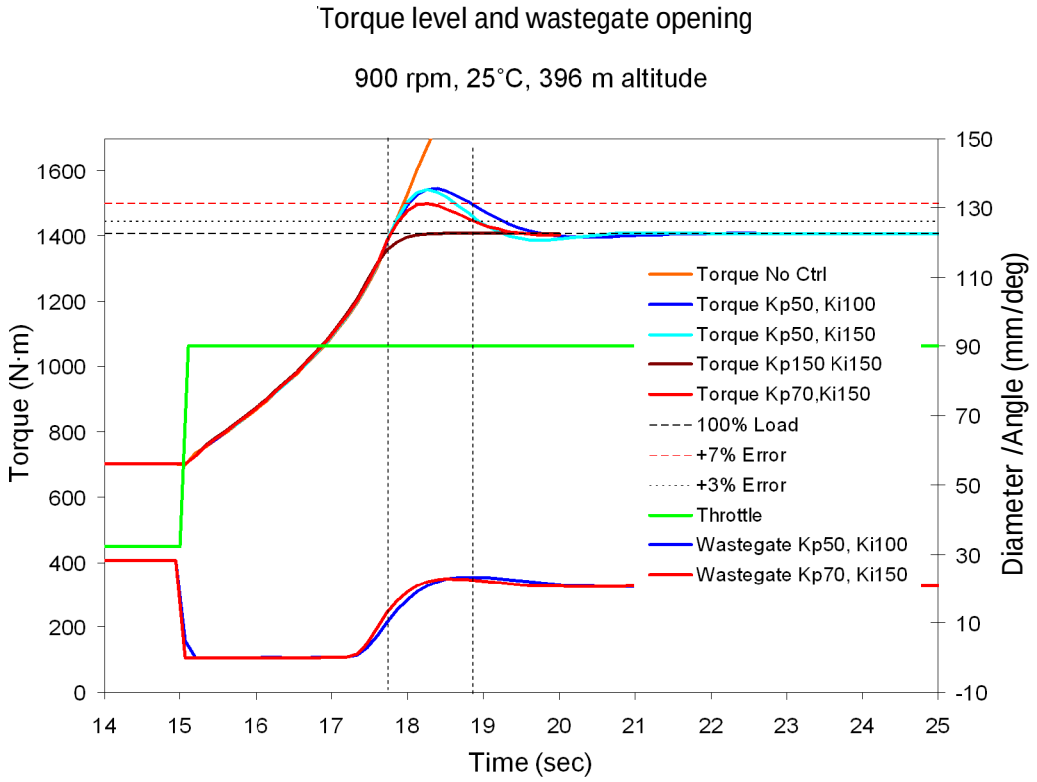

Figure 5.10. PID tuning for torque limiting.

After a performance comparison of parameters, the parameter set of (5-20) was chosen for torque limiting.

The input of wastegate control consists of proportional term (red line), and integral term (pink line), as shown in Figure 5.11. The control input is limited for the wastegate angle range 0-28.28 mm (corresponding to 0-90º). The input to wastegate (green line) shows the certain predicting function before IMP reaches the target value. This is because of the initial wastegate condition.

5.2.3 Simulation Verification of Torque Limiting

5.2.3.1 Simulation Verification under 50% - 100% Torque Level

The control performance was verified under normal operation conditions with two extreme conditions of 0 m, 40ºC and 1220 m, 0ºC within engine speed of 900–2100rpm. Integrated simulation conditions are shown in Table 5.4. The results of one case are shown in Figure 5.12. The torque output without limiting control is shown in the Figure 5.12 for comparison. The rising time is about same. The limited torque output overshot at around 7% of the target level.

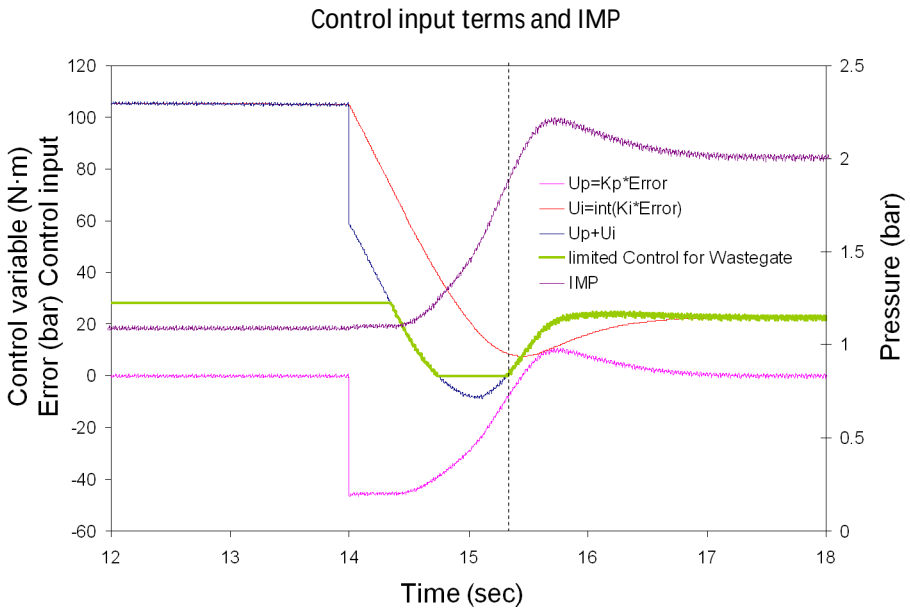

Figure 5.11. Control input analysis of PID with saturation.

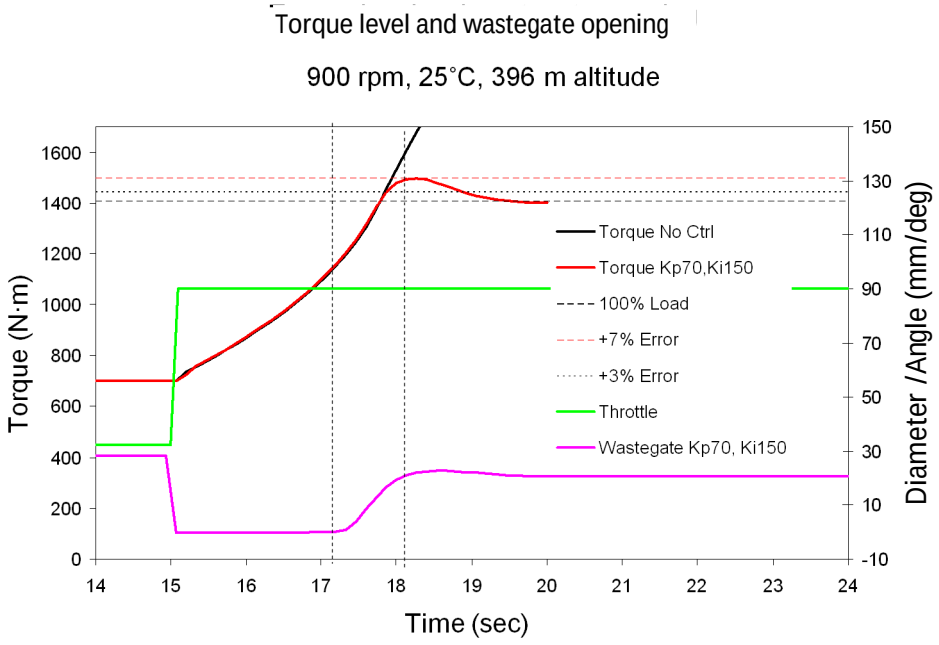

Figure 5.12. Torque limiting PID control - with Kp(-75), Ki(-150).

It also drops rapidly to the steady-state level without further fluctuation. Figure 5.13 indicates that the turbocharger speed is well controlled as well. All results of the 15 cases are shown in Appendix B.2. The results of the simulation verify that the PID controller with parameters $K_p = -70, K_i = -150$ can meet the design criterion.

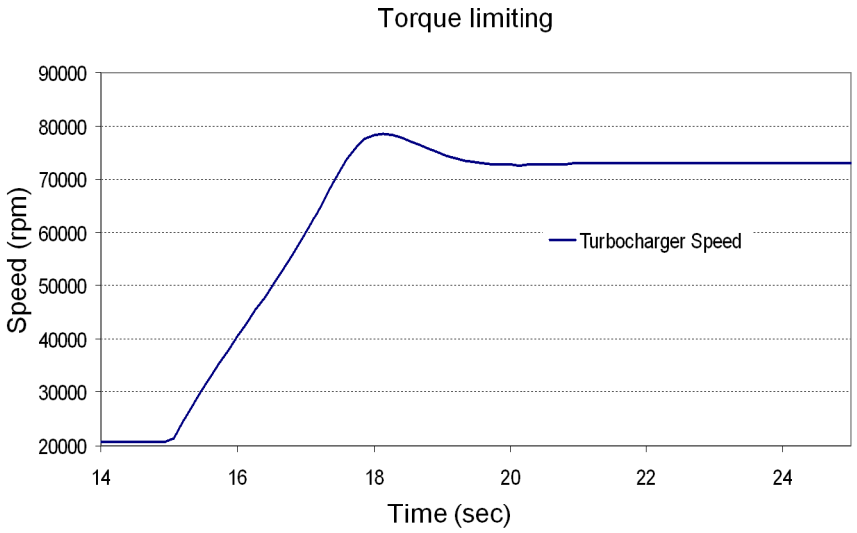

Figure 5.13. Torque limiting PID control - with Kp(-75), Ki(-150).

Table 5.4. Torque limiting control verification conditions – economic mode (wastegate initially open).

	Ambient			50% Load Initial Condition					100% Load Steady State				
	Temperature (K)	Pressure (bar)	Engine Speed (rpm)	IMP (bar)	Wastegate Dia (mm)	Throttle Angle (deg)	Torque Target (N·m)	Torque Output (N·m)	IMP (bar)	Throttle Angle (deg)	Wastegate Dia. (mm)	Torque Level (N·m)	Torque Output (N·m)
Normal Condition	298.15	0.966	900	0.949	23.29	90	700	700	1.683	90	20.82	1400	1407
	298.15	0.966	1100	0.996	32.89	90	785	787	1.792	90	22.72	1570	1570
	298.15	0.966	1500	1.047	47.87	90	875	879	1.932	90	23.03	1750	1750
	298.15	0.966	1800	1.039	33.16	90	866	880	1.902	90	24.79	1705	1705
	298.15	0.966	2100	0.953	29.78	90	766	786	1.767	90	25.94	1523	1550
0 ºC 1950 m	273.15	0.801	900	0.843	69.62	90	672	679	1.516	90	20.71	1400	1350
	273.15	0.801	1100	0.876	90.00	90	739	740	1.648	90	21.77	1570	1542
	273.15	0.801	1500	0.940	90.00	90	844	884	1.810	90	21.52	1750	1750
	273.15	0.801	1800	0.962	30.25	90	865	1024	1.785	90	22.74	1705	1704
	273.15	0.801	2100	0.882	26.97	90	767	880	1.638	90	23.60	1523	1522
40 ºC 0 m	313.15	1.013	900	0.987	22.31	90	700	701	1.683	90	20.76	1400	1350
	313.15	1.013	1100	1.035	32.10	90	785	786	1.833	90	21.80	1570	1543
	313.15	1.013	1500	1.086	51.22	90	874	876	2.009	90	22.09	1750	1749
	313.15	1.013	1800	1.081	35.80	90	866	874	1.978	90	23.99	1705	1704
	313.15	1.013	2100	0.991	30.92	90	766	778	1.805	90	26.00	1523	1522

5.2.3.2 Simulation Verification under Different Torque Levels

The 50%-85% and 60%-100% torque level simulations in several conditions were used to verify the torque limiting control for other general conditions. The conditions are shown in Table 5.5. Results of the torque output can also meet the design criterion, as shown in Figure 5.14 and Figure 5.15.

Table 5.5. Two different conditions for verification simulations.

Condition	Ambient and Engine			Initial Load Condition				Target Steady-State Load			
	Temp (K)	Pressure (bar)	Engine Speed (rpm)	IMP_Ini (bar)	Throttle Angle (deg)	Wastegate Dia (mm)	Torque Output (N·m)	IMP_Ini (bar)	Throttle Angle (deg)	Wastegate Dia (mm)	Torque Output (N·m)
25ºC 396m	298	0.97	1500	1.05	47.9	90	879	1.631	90	25.9	1461
0ºC 1950m	273	0.80	1800	0.96	30.3	90	1024	1.785	90	22.7	1704

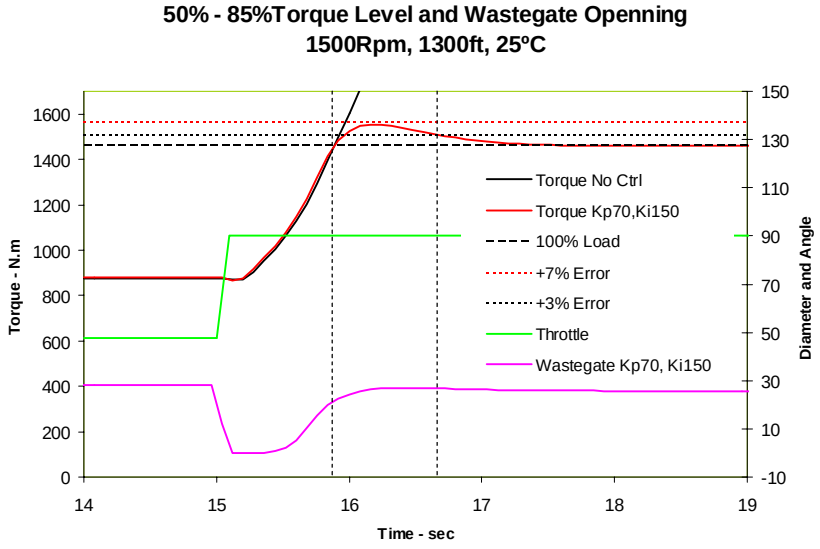

Figure 5.14. Simulation verification at torque level 50%-85%, engine speed of 1500 rpm, ambient condition of 298k, 0.97 bar.

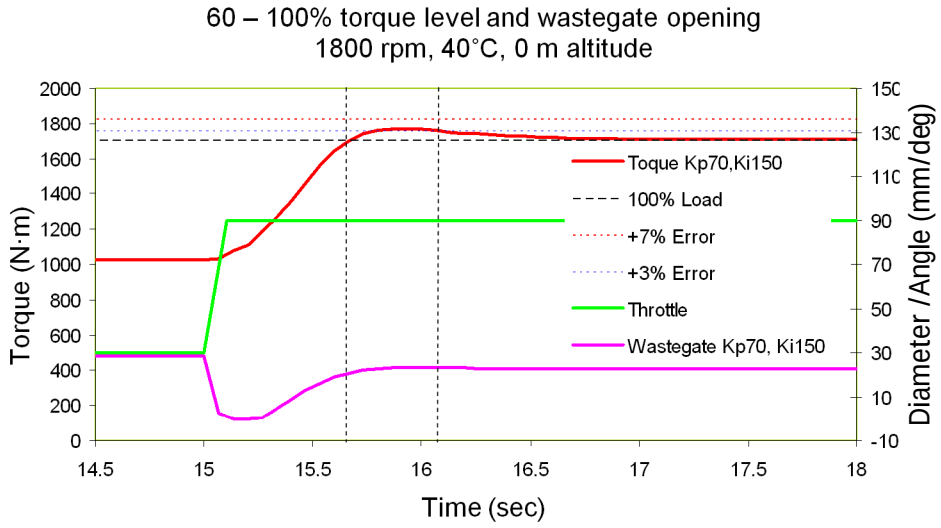

Figure 5.15. Simulation verification at torque level 60%-100%, engine speed of 1800 rpm, ambient condition of 273k, 0.80 bar.

5.2.3.3 Summary

Feed-forward fueling control based on IMP was investigated for the SCI engine AFR control. A linear regression was used to generalize the mass of fuel injection based on the available sensor information. The simulation shows that the prediction of the fueling model gives an agreement with data under different engine speeds and loads for both transient and steady-state conditions. Further engine testing is needed to validate the model parameters and structures.

For torque limiting control, the IMP based feed-forward method was investigated. To meet the wide changes of the application environment, the IMP function for feed-forward input was obtained through linear regression based on available sensor data. The prediction was compared with data sets (from performance simulations) and the results show good agreement between them. The PI control was developed as a torque limiting function. To tune the PID control for torque control, different parameters were tested for the PID method. The PI control with $K_p = -70, K_i = -150$ was verified in Simulink with the engine model in GT-Power. The simulation shows that the PI control provides enough accuracy margins for tentative performance criterion.

5.3 Idle Speed Control

One of the most important operating modes for SCI engine is in the idle speed region. This is because off-road engines spend a large part of their running time in this mode. Once the engine is started, engine speed jumps from zero into idle mode. Then engine control is turned to governor to stabilize the engine at idle speed. At anytime in idle mode, the engine is subjected to any load change. If there is no control, engine speed tends to stall when the load is increased, or tends to "run away" when it loses load instantaneously. Moreover, a large measure of operator satisfaction is dependent on the engine operating smoothly and reliably in and around idles.

The objective of idle speed control is to overcome the disturbance from load and maintain the engine speed within a specified range. The typical load disturbances during idle condition are from air conditioning compressors, power steering pumps, battery charging and other accessories. Idle speed control is designated into two cases: (1) anti-disturbance capability; and (2) engine is blipped with or without load. Besides, there are slow changes in the condition under which an engine operates, like ambient temperature and pressure, fuel quality, lubricant temperature, et al. This condition was not considered in this research.

Methodology of idle speed control involves PID control (Nishimura and Ishii, 1986), Linear quadratic control (Powell and Powers, 1981), discrete adaptive sliding mode control (Li and Yurkovich, 1999, 2000); for unknown disturbance, disturbance observers can be used (Gibson et al., 2006); Feed forward and feedback method can be used to improve the stability of idle control (Butts et al., 1999; Butts et al., 1995; Li and Yurkovich, 2000); advanced control of nonlinear method (Kjergaard et al., 1994), H-infinity technique (Carnevale and Moschetti, 1993), besides, some artificial intelligent methods (Abate and Dosio, 1990) are investigated to increase the robustness of idle speed control

Because advanced control designs are dependent on the more complex models, PID control is used for integrated simulation environment for simplification and rapid verification of this SCI engine control design.

5.3.1 Case 1: Idle Speed Control with Load Disturbance

The idle governor will control the throttle to maintain the SCI engine (8000S) at 850 rpm with 10 (N-m) torque output. A 3KW load disturbance will be applied to test the robustness of the governor. Based on the relation between power P and torque T,

$$P = T \cdot \omega \tag{5-21}$$

3KW load disturbance is equivalent to 33.7 N·m at 850 rpm. The disturbance is applied and removed in 0.5 second. One example of the torque request and expected speed performance is shown in Figure 5.16 and Figure 5.17.

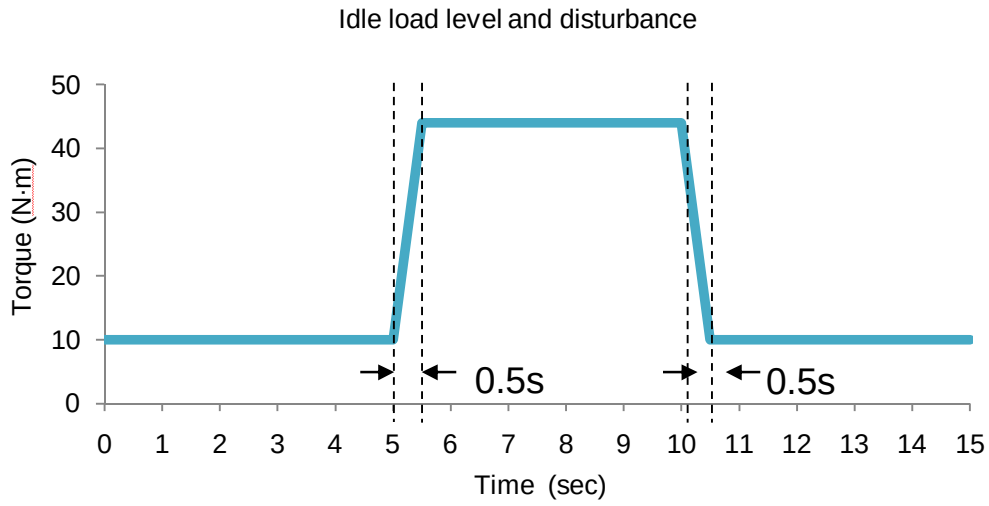

Figure 5.16. Idle speed control load disturbance simulating engine accessory consumption.

5.3.2 Control Method

Based on the literature review, PID control can be the first candidate for control design and simulation. First, the PI control is tested. After parameters tuning, gains is defined as:

$$\begin{aligned} K_P &= 0.1 \\ K_i &= 0.01 \end{aligned} \tag{5-22}$$

From the results shown above, PI control can be a tentative method for further testing. Model based methods can also be investigated to compare the performance.

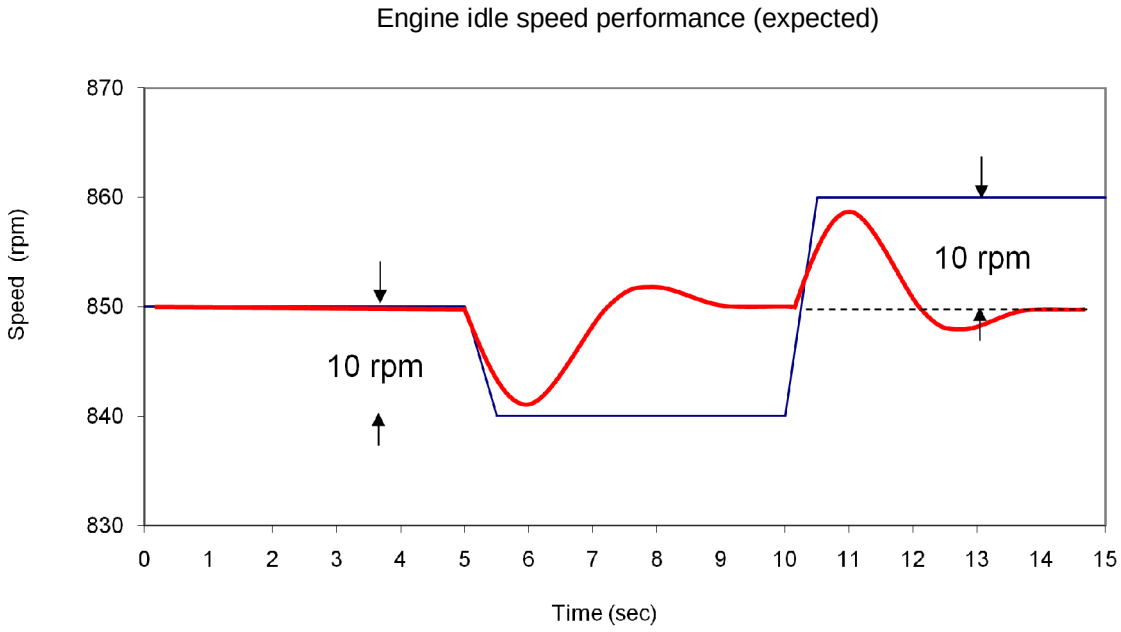

Figure 5.17. Engine idle speed control performance cretiria.

5.3.3 Simulation Results

Idle speed control is designed and verified with the 1D detail model based on speed feedback in load model of GT-Power. The PI control is implemented in Matlab/Simulink. After parameter tuning, the feasible results are shown as follows from Figure 5.18 to Figure 5.22.

The load of 30 N·m is applied at 70s within 0.5s, in Figure 5.20, and withdrew at 120s within 0.5s, in Figure 5.21 to test the PI control performance of idle speed change. The detail of engine speed changes are shown in Figure 5.21, in which the amplitude of speed fluctuation is ± 10 rpm is much less than 30 rpm requirement. The control variable, throttle angle, is shown in Figure 5.22. Once the disturbance was applied, the throttle response went quickly from 2.2 to 3 degree, then stabilized around 3.4 degree with a time of 20s. The situation is vice versa for the disturbance withdrawal condition.

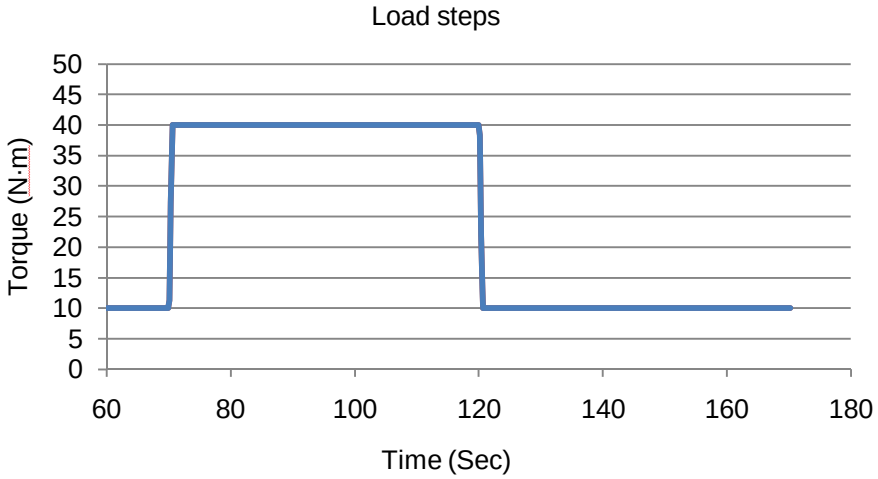

Figure 5.18. Load disturbance used for integrated simulation verification.

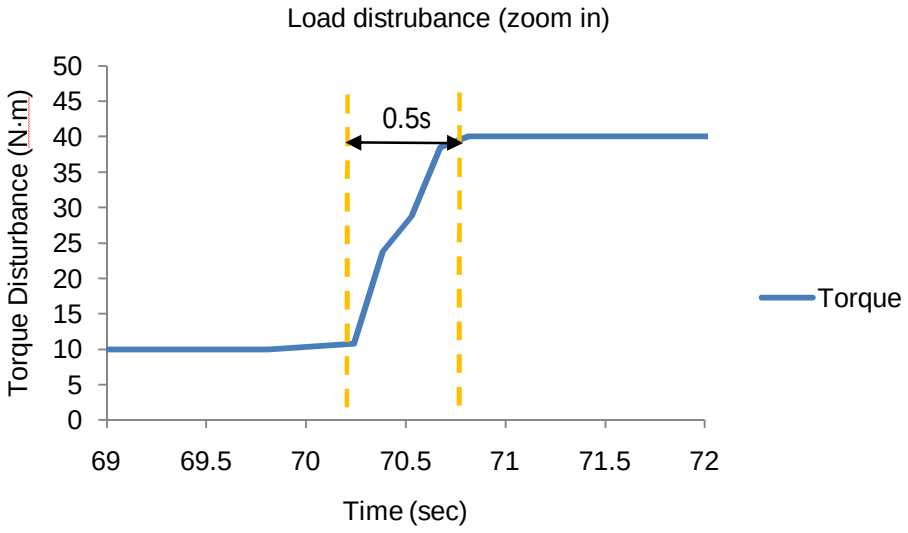

Figure 5.19. Load disturbance zoomed in for jumping up edge.

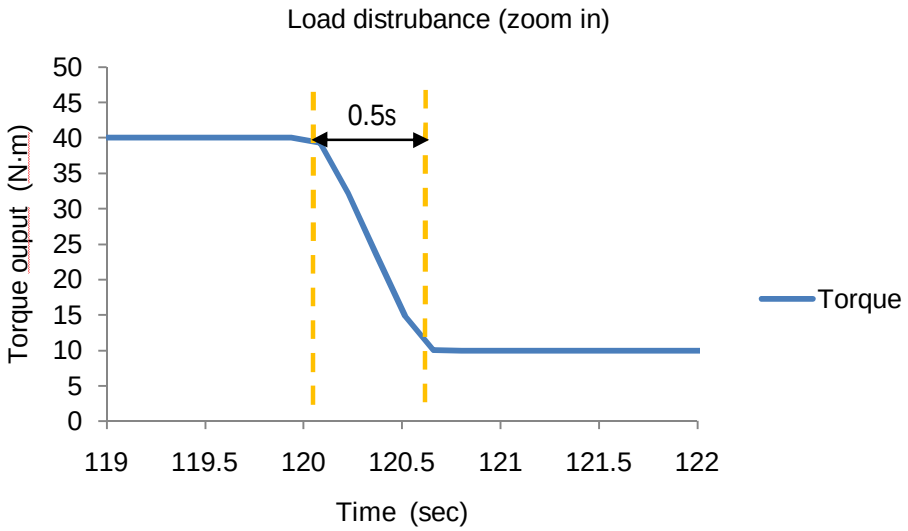

Figure 5.20. Load disturbance zoomed in for jumping down edge.

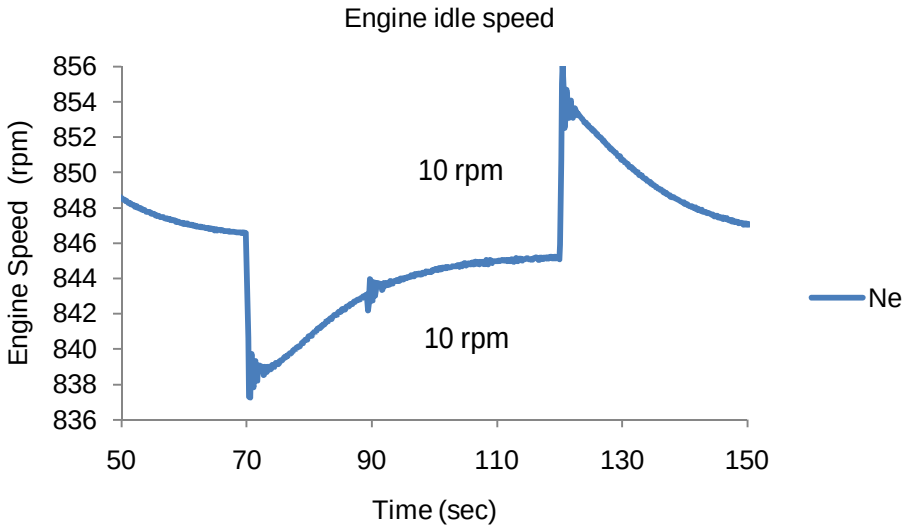

Figure 5.21. Integrated simulation verification results.

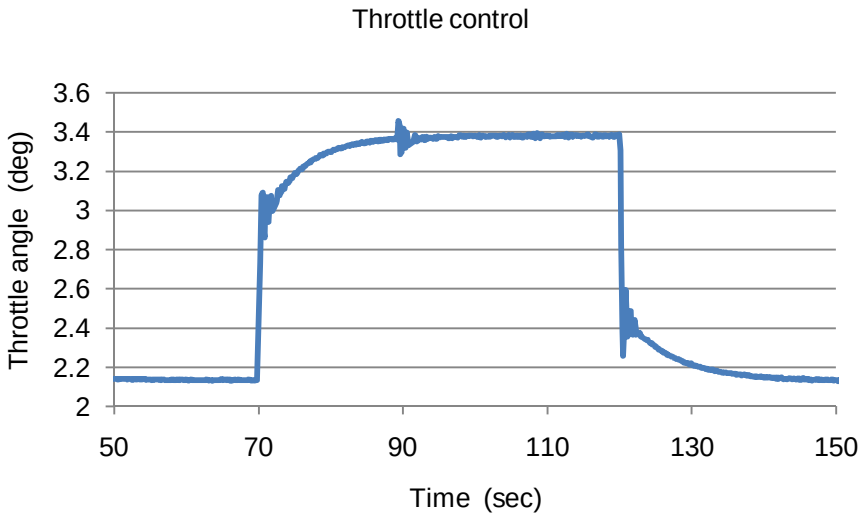

Figure 5.22. Throttle control during the idle speed control for load disturbance.

5.3.4 Case 2: Idle Speed Control while Engine is Blipped with or without Load.

The idle governor is used to take control of the throttle to switch the engine speed between 1500 rpm and 850 rpm as commanded, while there is 10 (N-m) load on-off applied to the engine. The action of the throttle switch needs to be done within 0.3 second, shown in Figure 5.23, and the transient response of the engine speed is expected to settle down to 30 rpm band within 3 bounces in Figure 5.24. The PI controller for engine blip is tested in the integrated simulation environments, the simulation results are listed from Figure 5.25 to Figure 5.28.

Figure 5.25 indicates the throttle action during the idle speed control for instantaneous load change; throttle angle was controlled around 5.3degrees, once the disturbance happened, it was stabilized after several fluctuations about 2.3degrees. During the process, the engine output torque was maintained at the same level at 10 N·m, shown in Figure 5.26. The control results of engine speeds were maintained within 850 ± 30 rpm, the speed came back to the 30 rpm band within only one bounce, shown in Figure 5.27 (zoomed in Figure 5.28).

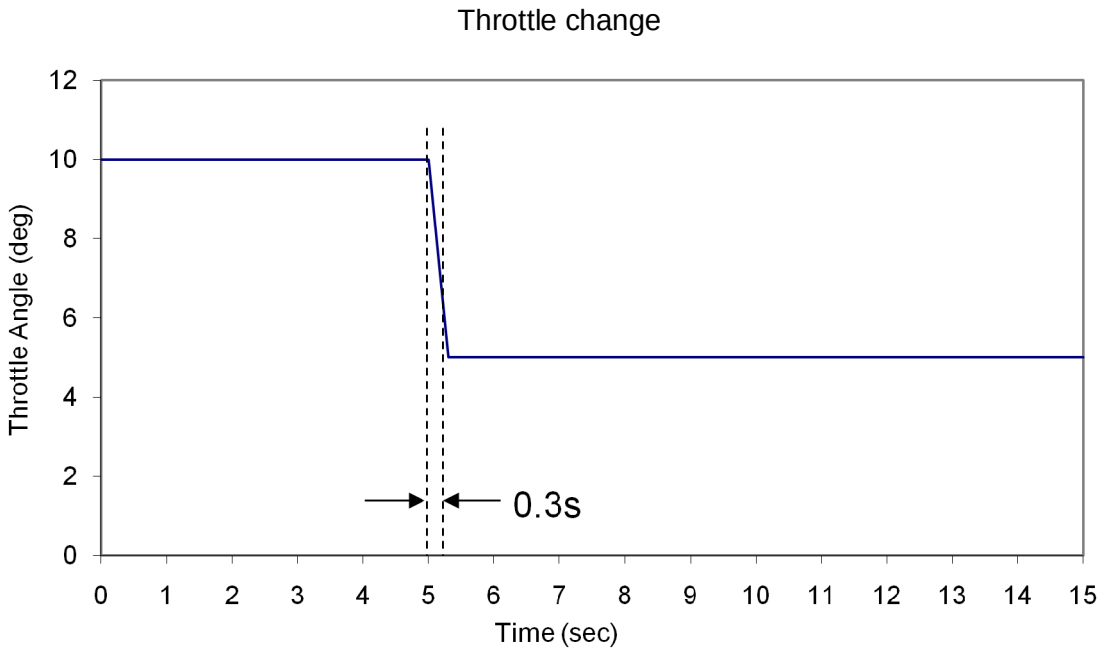

Figure 5.23. Throttle change in 0.3s for engine blipping.

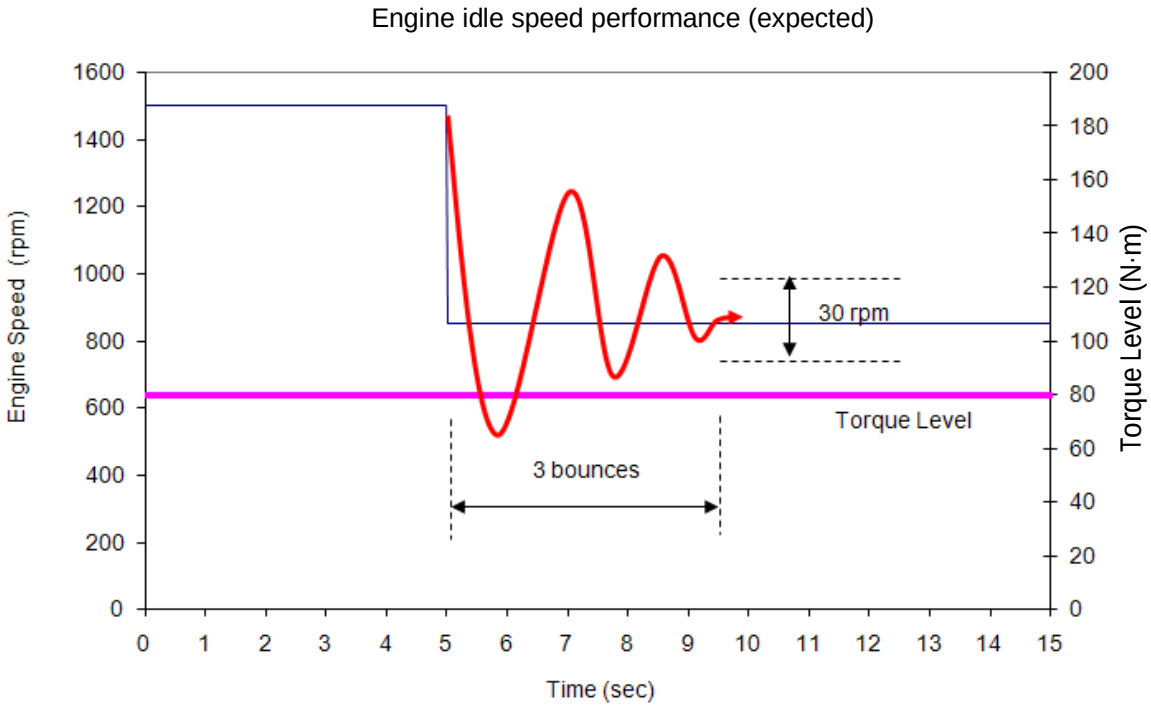

Figure 5.24. Engine idle speed control performance requirement.

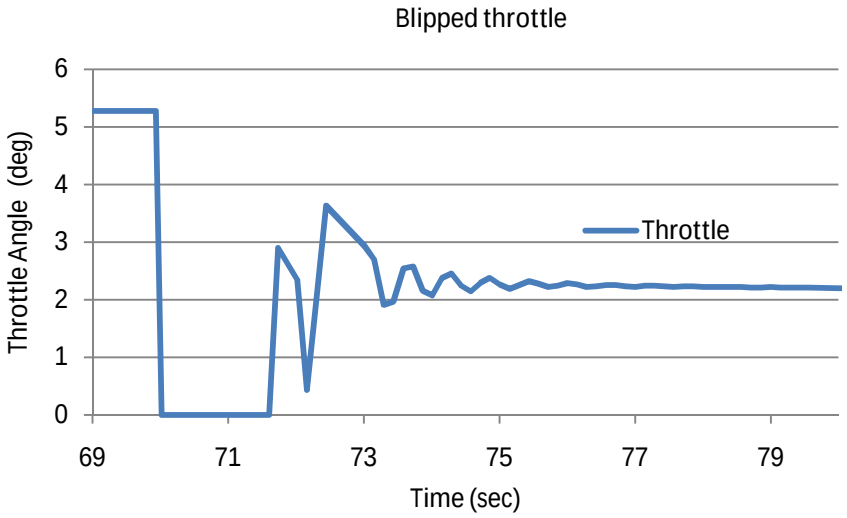

Figure 5.25. Integrated detail model verification for idle speed control: throttle change during the blipping.

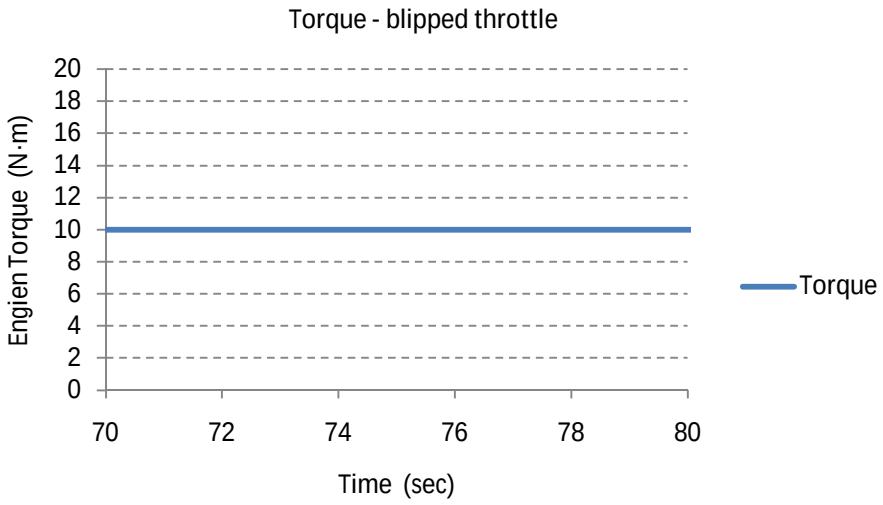

Figure 5.26. Integrated detail model verification for idle speed control: torque response.

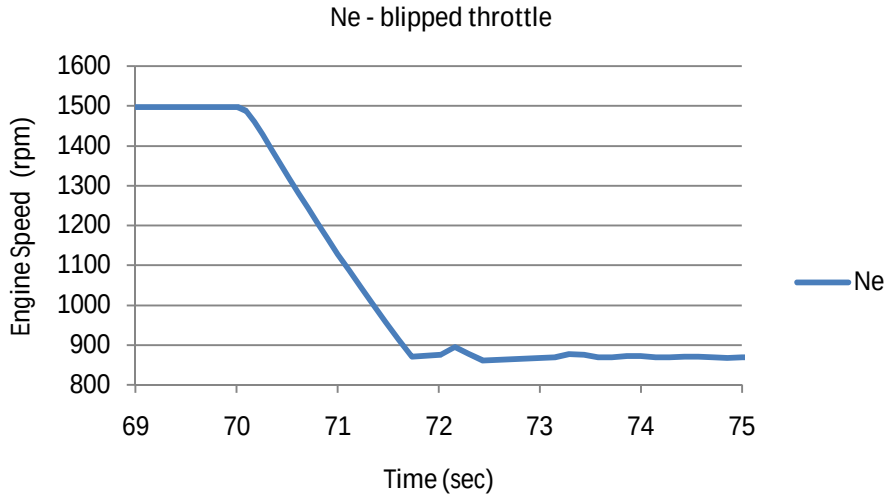

Figure 5.27. Integrated detail model verification for idle speed control: engine speed response.

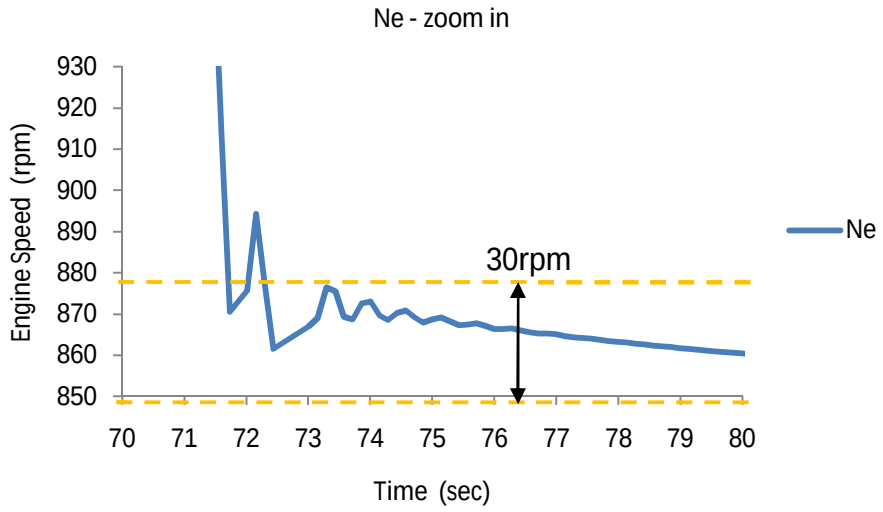

Figure 5.28. Integrated detail model verification for idle speed control: Engine response (Zoom in).

6 MEAN VALUE MODEL OF SCI ENGINE

Mean value engine model (MVEM) is the basis of control design for advanced internal combustion engines. The engine performance transient process usually takes a few cycles. The MVEM provides an adequate accurate description of the engine dynamics with reasonable approximation by ignoring the heat loss and sub-cycle events. MVEM is very important for engine system control development, especially when the modern engine becomes more and more complicated when equipped with throttle, turbocharger and after-treatment systems. Usually the MVEM is developed based on data from engine tests, which is a costly and time consuming process. In this chapter, the air path MVEM modeling method based on the 1D detail model is discussed for a turbocharged diesel engine. Simulation is applied to demonstrate the effectiveness of this new method. This approach could be used to get the MVEM for control design even before the prototype engine is available. It reduces the cost, risk and labor compared with the test data based approach. This MVEM model can be built in modules and the parameters can be validated for a specific engine. These advantages make it applicable to a wide range of engines.

6.1 Introduction

The ever increasing EPA regulations on vehicle emissions and the fuel economy demands from markets promotes the innovation for advanced engine technology. In past decades electronic control has made a big contribution to the development of some new technologies. For example, to improve the engine performance and drivability, the electronic throttle control and turbocharger were applied in spark ignition (SI) engines, while the cruise control was implemented and power density was improved. To balance the turbine at both low speed and high speed conditions, wastegate or variable geometry turbocharger (VGT) control became necessary. Exhaust gas recirculation (EGR) technology and after-treatment systems were the main methods to reduce NO_x emission from inside and outside the cylinders. Besides, the overlap vale, internal exhaust gas recirculation (EGR), high pressure fuel injection, and multiple fuel injection technology may be necessary for the promising homogeneous charged compression ignition (HCCI) engines. Furthermore, combustion model switching, multistage turbochargers

have been discussed more and more for high performance in recent articles (Bengtsson et al., 2007; Canova et al., 2007; Chauvin et al., 2007). The implementation of these new technologies depends on the control system to cooperate with the sub-systems, like the air system, fuel system, combustion in chambers, and exhaust system.

Modern control theory depends on the system model much more than classic control, like proportional-integrative-derivative (PID) control and frequency domain regulation. While modern control theory provides more advanced properties including robustness, optimization, multivariable control, learning ability, and adaptivity. Nowadays, engine modeling technology plays an important role in the engine design and brings more challenges to control engineers. Different control oriented modeling methods have been used for different purposes in the implementation of advanced engine technology, such as a simple input-output block model and the MVEM which consists of detail sub-systems. In addition, the crank angle based combustion model and fluid dynamics based air charge model are needed for in-cylinder control.

In the modern diesel engine, the turbocharger is widely used to increase power density. The turbocharger increases the complexity for the engine to deliver the expected torque to the crankshaft, while satisfying demands for drivability and fuel economy, subject to emission constraints. However, an improper choice of controller and parameters can lead to an undesirable torque response. A large amount of simulation and testing is necessary for control design and verification (Pettiti et al., 2007). To eliminate the testing time, an accurate and simple engine model is expected to analyze engine dynamics in order to design stable and robust control. The fact is that control engineers have to trade off the model accuracy and the model computation time.

In the area of engine design and control design, different engine models at different detail levels are available for different applications. The combustion chamber design needs to investigate the atomization property of fuel injection, the fluid turbulence, and the combustion characteristics, etc. The KIVA (Los-Alamos-National-Laboratory, 1989) model is designed to describe three dimensional fluid dynamics and chemical reactions in the cylinder with simulation time in the order of 10-100 hours. To study the performance of an engine system including cylinder,

turbocharger, intercooler, wastegate or variable nozzle turbine (VNT), EGR, intake and exhaust manifolds, the 1D detail simulation model can be developed using commercial software tools such as Gamma Technology's GT-Power or Ricardo's WAVE. The simulation time scale is in hours, approximately 100 engine cycles. The GT-Power simulation tool also provides control design modules, but they are limited in flexibility and functionality.

As the modern internal combustion engine becomes more and more complex to meet increasing demands for lower emissions and higher fuel economy, the development of an engine controller for such systems can be time-consuming and labor-intensive. Usually, this process includes many iterations and extensive calibrations. As a result, control engineers prefer an accurate and simplified control oriented model to design and verify their algorithm, before applying the results into on-line testing and calibration. The simplified model should also capture the dynamics of interested variables accurately enough. Meanwhile, most control engineers prefer Matlab and Simulink for their control design. Several mean value engine models were proposed to meet such requirements. In (He and Lin, 2007), hybrid radial basis functions was used to approximate the simulation results of the detailed model for cylinder quantities. Pettiti et al. (2007) developed a Mean value model from standard experimental measurements (BMEP, VSFC, etc.) at partial and full load conditions at different engine speeds. It was used to investigate the turbocharger lag in order to predict vehicle performance during the transient conditions. The advantage and disadvantage of empirical and analytical models were discussed in (Schulten and Stapersoma, 2003). Then a mean value model of the gas exchange was developed for use in power train applications.

In engine performance control, the most interested variables are engine and turbocharger torque, speed, fluid dynamics at throttle and manifold temperature, pressure, and mass flow rate. The fast sub-cycle events like combustion and valve timing may be ignored according to specific application. Then the simulation can be carried out in a short time, on the seconds or minutes level.

The rapid development of computer technology provides increasingly powerful capability for control engineering. So far, a personal computer (PC) can afford for the integrated simulation

interacting between the 1D detail model and the Simulink control model at the same time. Even though the computing speed is still very slow for control design purposes, but it is fast enough for control verification for both steady and transient performance simulations. Compared with experimental data, the validated GT-Power model is capable of predicting the engine performance with an error generally less than 3% (He, 2005). The advantage of the integrated simulation is that it simultaneously simulates the engine performance and control function. It can be utilized for control algorithm verification and fault detection and diagnosis algorithm verification. In this paper, the integrated simulation is used to represent the test engine and is compared with the MVEM results.

Control design always takes several steps: modeling, simulation, HIL verification, and calibrations with a real plant. A general engine control design process is illustrated in Figure 6.1. First, the 1D detail model can be started from the prototype engine, or from the original model with adjustment of the sub-systems. Second, performance simulation, like the constant speed load acceptance (CSLA) test, the federal test procedure (FTP) test, can be conducted to verify the design, emission requirement and subsystem configuration. During this phase, the controller can be included for operation point searching. The controller can be designed in GT-Power or Simulink. During the second stage, the mean value model can be obtained based on the integrated simulation environment. More simulations need to be conducted to cover the wide range of engine operation conditions. Third, based on the mass conservation and energy conservation, each sub-system module is modeled based on the simulation data regression or identification such as manifold volume, volumetric efficiency, etc. Then the sub- systems are integrated together to form the MVEM. Fourth, the entire MVEM is verified with the 1D detail model in GT-Power. The MVEM captures the main dynamics of engine variables while there is error compared to the variables from the physical engine. Fifth, advanced control, such as robust control, is designed to cover the model error and un-modeled dynamics. After stabilized control is obtained with the MVEM, a further verification is necessary to check the control with the 1D detail model again. Sixth, before testing the control on the prototype engine, the hardware-in-loop simulations need to be carried out. The design control can be downloaded to dSPACE or Xpc, control system by interacting with GT-Power through signal interface. Finally, the

controller is connected to the real test engine to verify the real-time capability, stability and performance.

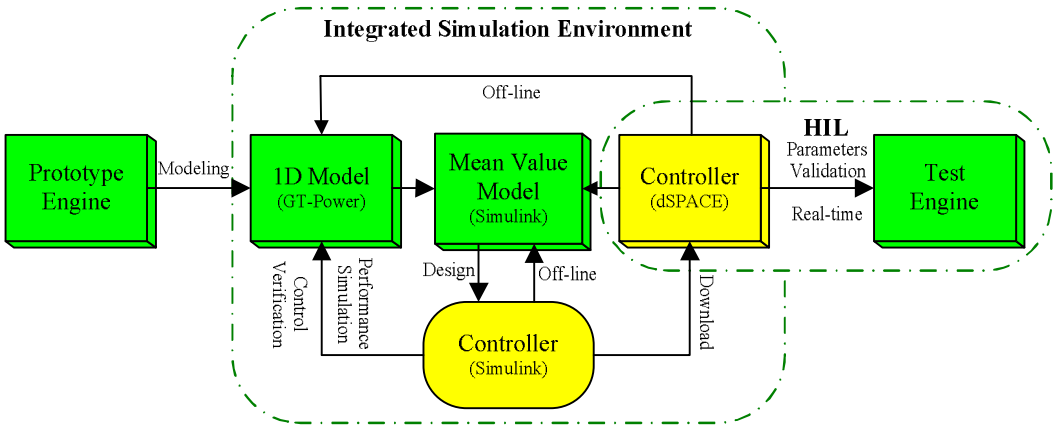

Figure 6.1. Engine control system development procedure.

The accuracy and computation speeds always are in conflict. Because the 1D model is simplified for MVEM development, the errors will occur. In fact, no model is perfect. The model error and un-modeled dynamic will be considered in the control design along with robustness and adaptivity. Integrated engine and control simulation environments, which was introduced in chapter 2, was use to facilitate the performance simulation for MVEM development purposes.

6.2 Engine Module for MVEM

6.2.1 Mean Value Engine Module

The control oriented sub-system models of a turbocharged diesel engine system are presented in this section. The system layout is shown in Figure 6.2. These sub-system models include compressor, intercooler, intake manifold, engine combustion, exhaust manifold, turbine, wastegate, engine crank shaft dynamic, and turbocharger dynamic. The detail process of modeling and verification of each module are introduced. The model parameters are identified using regression techniques. Each model was verified with simulation data from the 1D detail GT-Power model. With the implementation of models in Simulink, each MVEM sub-system is verified with the entire GT-Power engine model for steady and transient state.

For the mean values model, it was assumed that the air obeys the ideal gas law, the pressure is uniform in the intake and exhaust manifold, and there is not any heat losses to the walls. In combustion, heat is released in the whole combustion chamber at homogeneous conditions, and the gases can be regarded as ideal gases.

6.2.2 Compressor

The turbine and compressor are connected through a shaft to utilize the kinetic energy from the exhaust to increase air density in the intake manifold. The mass flow rate through them depends on the pressure ratio between the outlet and inlet, and the corrected speed. They are modeled based on map data from the manufacturer.

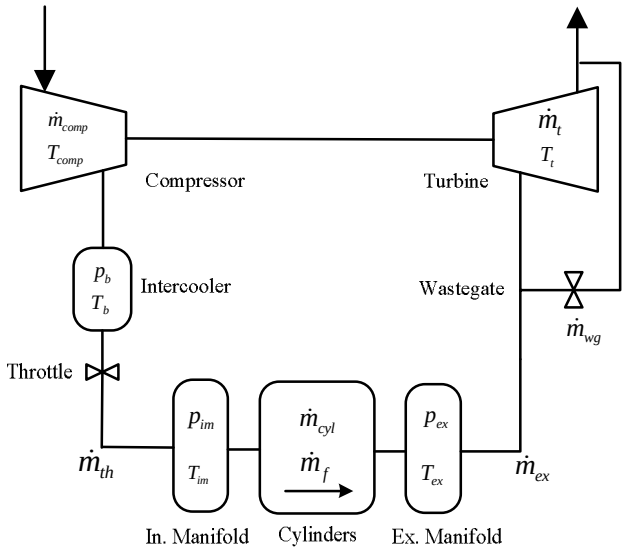

Figure 6.2. Engine structure and main variables of MVEM.

As described in (Heywood, 1988), the compressor's corrected mass flow rate, efficiency and the temperature change are modeled as a function of the pressure ratio and the corrected turbine speed.

$$\frac{m\sqrt{T_{in}}}{p_{in}}, \eta, \frac{\Delta T}{T_{in}} = f\left(\frac{N_{tc}}{\sqrt{T_{in}}}, \frac{p_{out}}{p_{in}}\right) \tag{6-1}$$

The inlet of the compressor is assumed at ambient conditions.

$$p_{in} = p_{amb}$$
$$T_{in} = T_{amb} \tag{6-2}$$

To avoid using complex function and regression, look-up tables are used for the flow rate and efficiency prediction. The compressor map is extracted from the table defined by operation data from the manufacturer. For other operation points in between, the interpolation is applied as shown in Figure 6.3 and Figure 6.4 for both flow rate and efficiency.

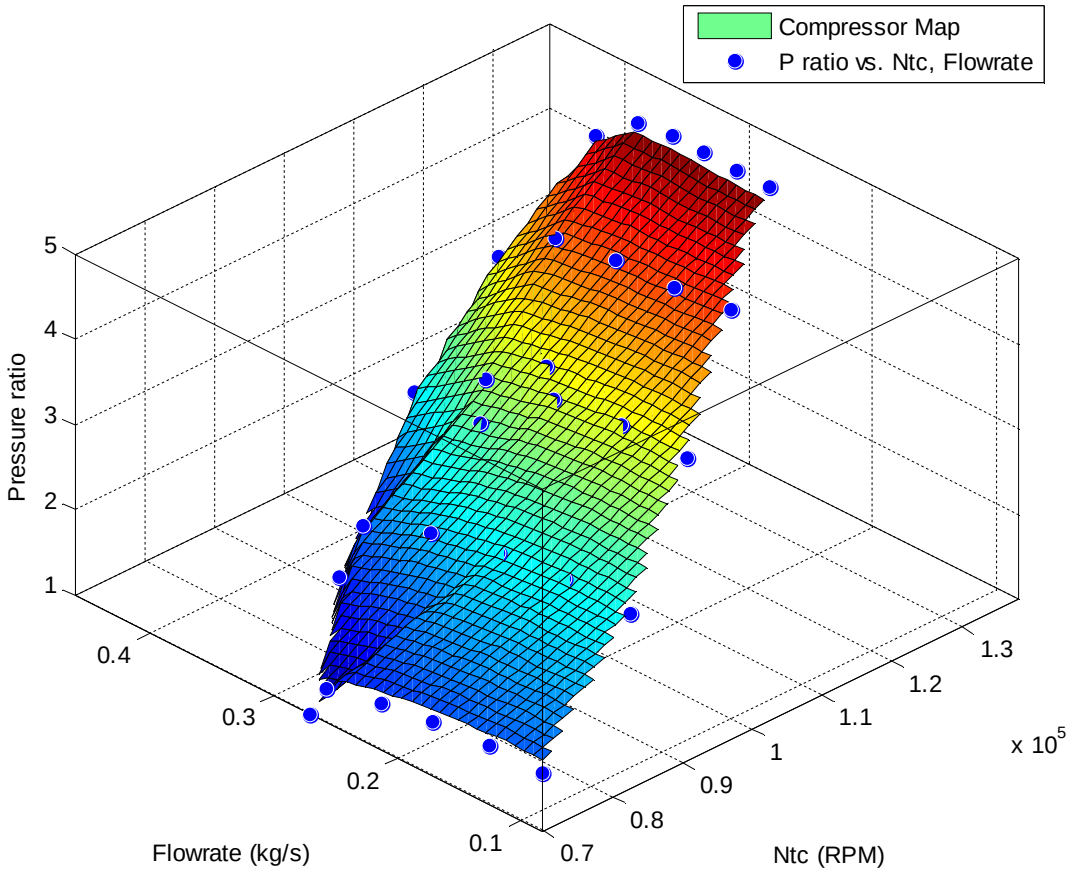

Figure 6.3. Compressor performance map and interpolation.

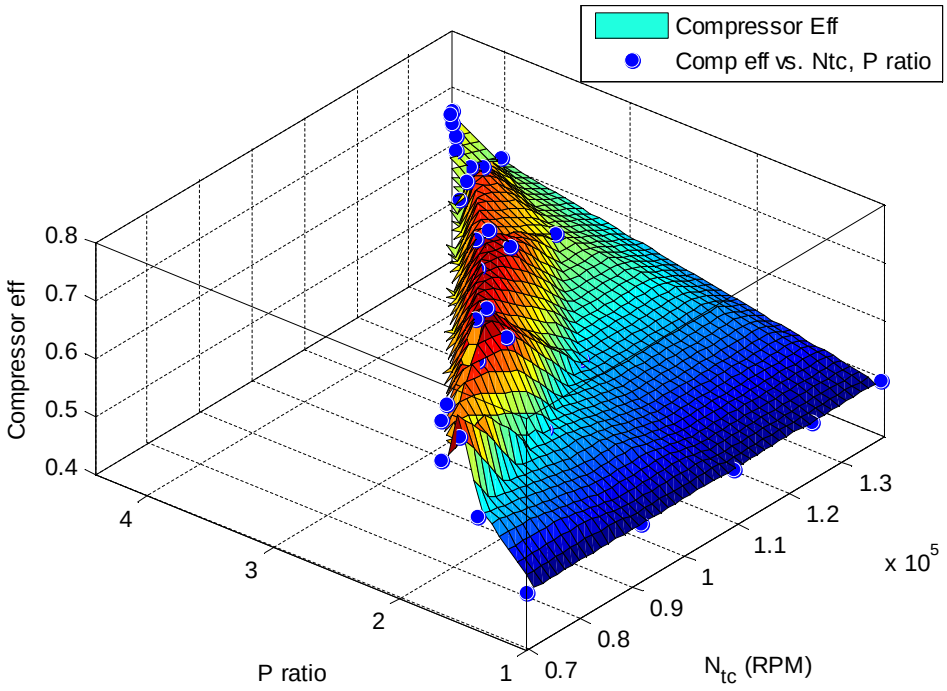

Figure 6.4. Compressor efficiency map and interpolation.

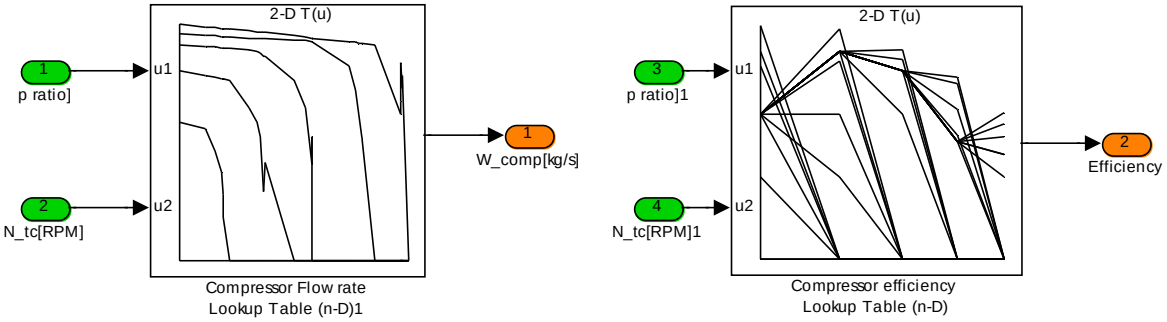

Figure 6.5. Compressor lookup table implementation in Matlab/Simulink.

The compressor exit temperature can be calculated by

$$T_c = T_{amb}\left[1+\frac{1}{\eta_c}\left(\left(\frac{p_b}{P_{amb}}\right)^{\frac{\gamma-1}{\gamma}}-1\right)\right] \qquad (6\text{-}3)$$

where η_c is the isentropic efficiency of the compressor, which was obtained from the look up table. The γ is the specific heat ratio, which is 1.401 at the intake air path.

6.2.3 Intercooler

The air temperature T_c increases after the compression, so the intercooler was used to cool it down. The gas temperature at the exit of the intercooler T_b is given by

$$T_b = T_c - \varepsilon\left(T_c - T_{coolant}\right) \tag{6-4}$$

where T_{cool} is assumed to be same with T_{amb} for simplicity, ε is the effectiveness of the intercooler. The pressure drop, filling and emptying effect of the intercooler volume is considered together with the intake manifold. The heat transfer effectiveness was identified by the simulation data. The value of $\varepsilon = 0.9845$ is used in this model.

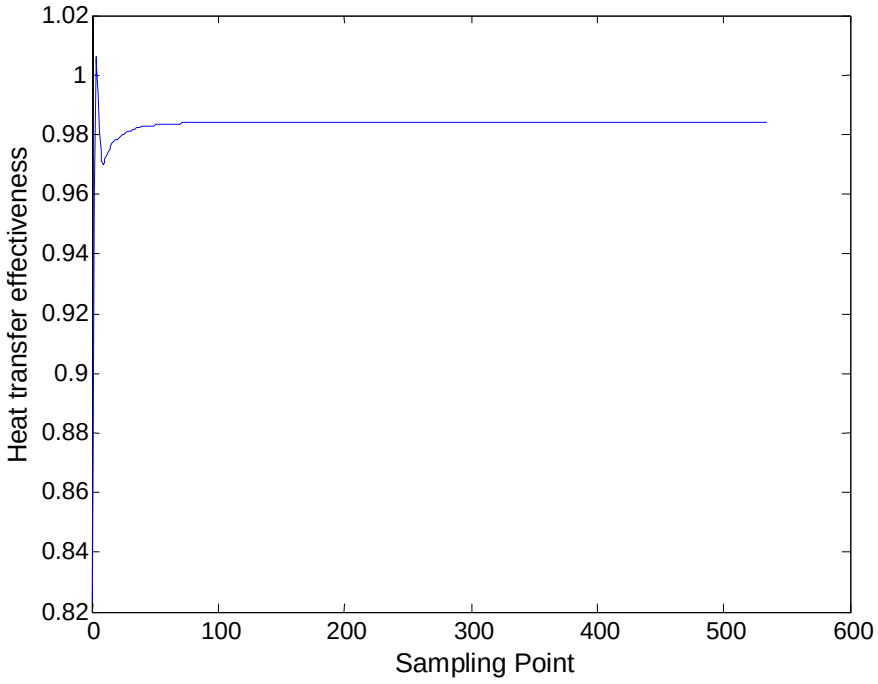

Figure 6.6. Heat transfer effectiveness of intercooler.

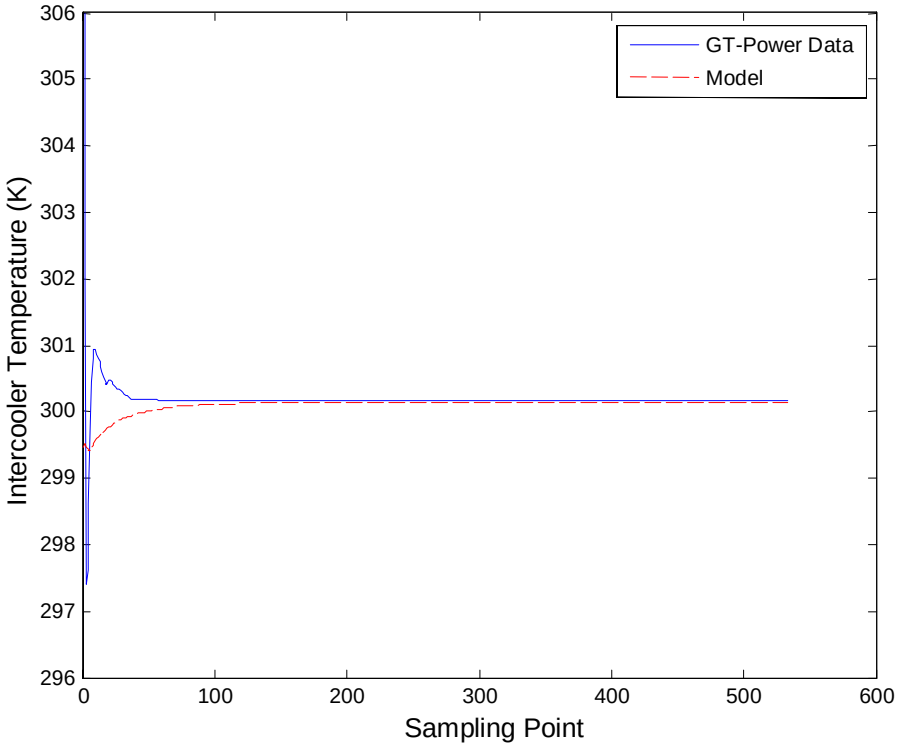

Figure 6.7. Intercooler temperature comparison between GT-Power and model data.

6.2.4 Intercooler pressure dynamic

6.2.4.1 Inter-cooler Volume Estimation

The inter-cooler pressure dynamic is model by a control volume filled with ideal gas, with assumption of the constant temperature. Based on ideal gas queation

$$p_b V_b = mRT_b \tag{6-5}$$

The pressure dynamic can be expressed as

$$\frac{dp_b}{dt} V_b = \frac{dm}{dt} RT_b = \dot{m}RT_b + mR\dot{T}_b \tag{6-6}$$

The temperature was assumed constant; the second term of the model was ignored for simplicity. So the intercooler pressure dynamic model becomes

$$\frac{dp_b}{dt} = \frac{R}{V_{ic}} \dot{m} T_b = k\left(\dot{m}_{comp} - \dot{m}_{th}\right) T_b \tag{6-7}$$

Constant k is estimated by the pressure dynamic during process of opening wastegate gradually under 900, 1100, 1500, 1800 and 2100 rpm. Then the control volume of intercooler is calculated by,

$$V_b = R/k \tag{6-8}$$

where the gas constant is $268.9 \frac{\text{J}}{\text{kg} \cdot {}^{\circ}\text{K}}$.

6.2.4.2 Simulation and Volume Estimation Results

The intercooler volume estimation is based on the pressure dynamic as shown in Figure 6.8. For the engine speed from 900 rpm to 2100 rpm, the corresponding temperature change and air

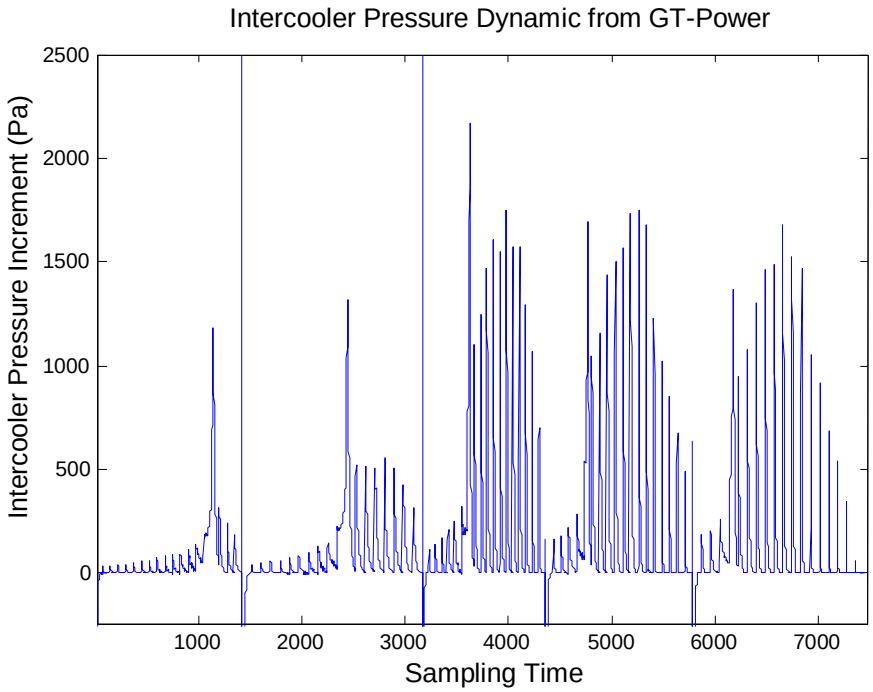

Figure 6.8. Intercooler pressure increscent of a transient under different engine condition from 900 rpm to 2100 rpm.

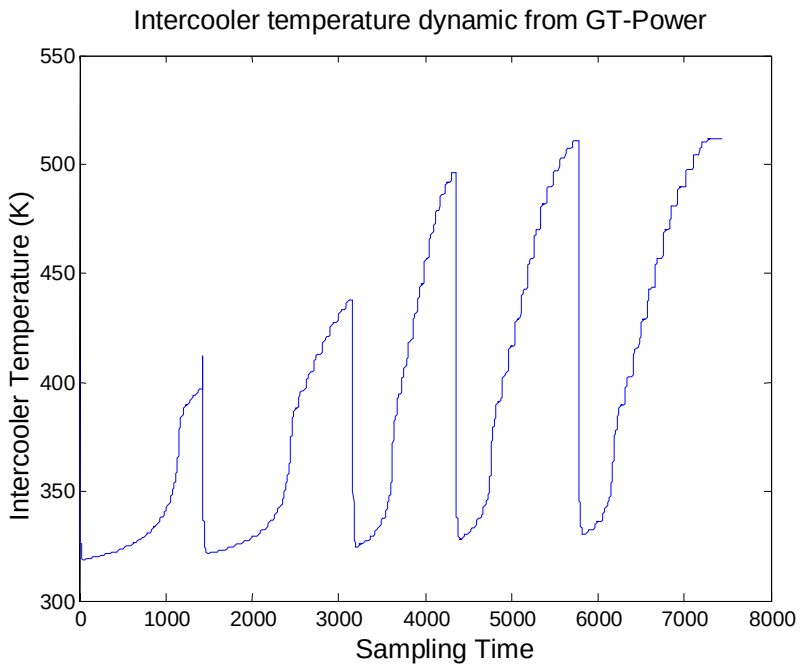

Figure 6.9. Intercooler temperature of a transient under different engine condition from 900 to 2100 rpm.

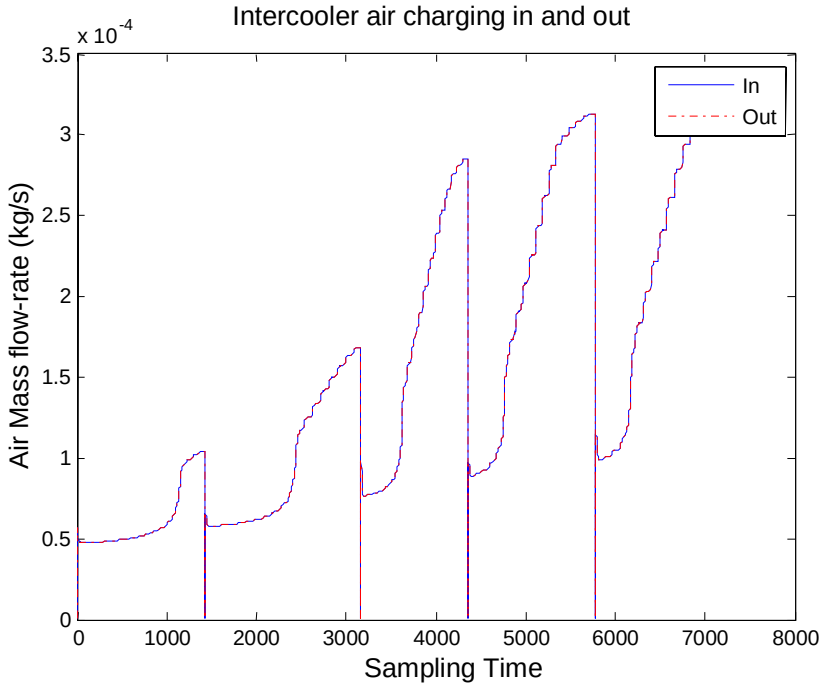

Figure 6.10. Intercooler inlet and outlet mass rate flow of a transient under different engine condition from 900 rpm to 2100 rpm.

flow-rates are listed in Figure 6.9 and Figure 6.10. From equation (6-7) and (6-8), the boost volume of intercooler was estimated and values are shown in Figure 6.11. The average value is used for this sub-system model.

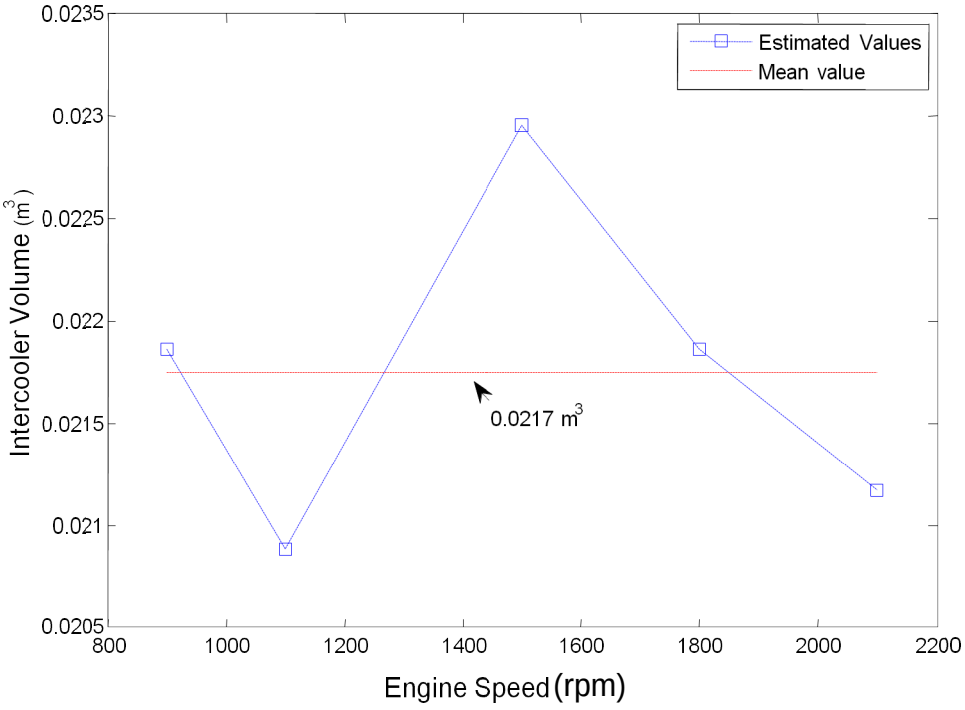

Figure 6.11. Estimated intake manifold volume and mean value.

6.2.4.3 Physical Inter-cooler Volume

To verify the physical inter-cooler volume, the actual volume between compressor and throttle was calculated by adding all the parts' volume, as shown in Figure 6.12. The geometry and parameters were from GT-Power part structure and data. The volumes are listed in Table 6.1, and the total volume is 0.02 m^3. Intercooler control volume estimation is 0.0217 m^3, which is close to the geometric volume of total volme, 0.02007 m^3. The volume estimation error is about 8% with 6% variation.

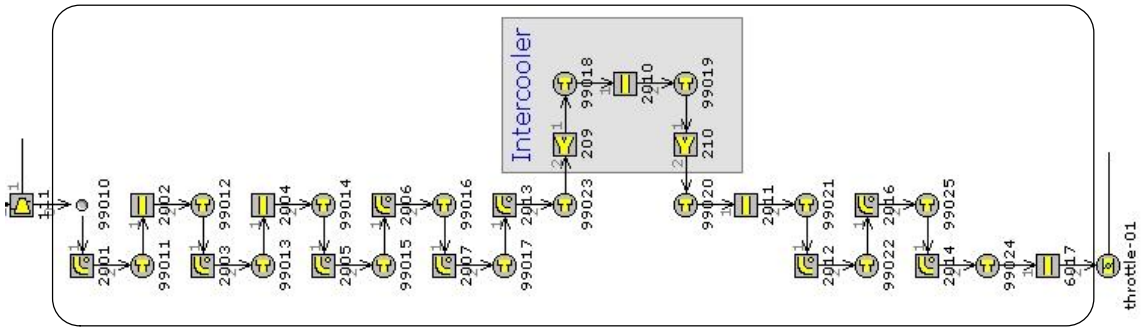

Figure 6.12. Control volume of intercooler.

Table 6.1. Approximate intercooler volume calculated by parts.

Part Number	Length (mm)	Diameter (mm)	Area (mm^2)	Volume (mm^3)
2001	243.4	72.7	4149	0.00101
2002	194	72.7	4149	0.00080
2003	72.7	72.7	4149	0.00030
2004	557.9	72.7	4149	0.00231
2005	179.6	72.7	4149	0.00075
2006	188.7	72.7	4149	0.00078
2007	168.9	72.7	4149	0.00070
2009	343.4	72.7	4149	0.00142
2010	620	72.7	4149	0.00257
2011	286.9	72.7	4149	0.00119
2012	72.7	72.7	4149	0.00030
2016	223.3	72.7	4149	0.00093
2014	120	66	3419	0.00041
2017	53	66.55	3477	0.00018
209				0.00320
210				0.00320
Total Volume				0.02007

6.2.5 Intercooler Module Implementation

The intercooler module is implemented in Simulink/Matlab. The block inputs and outputs are shown in Figure 6.13. The detail implementation is shown in Figure 6.14.

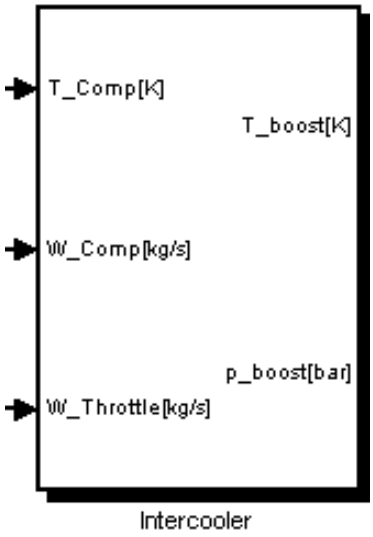

Figure 6.13. Intercooler block in Simulink.

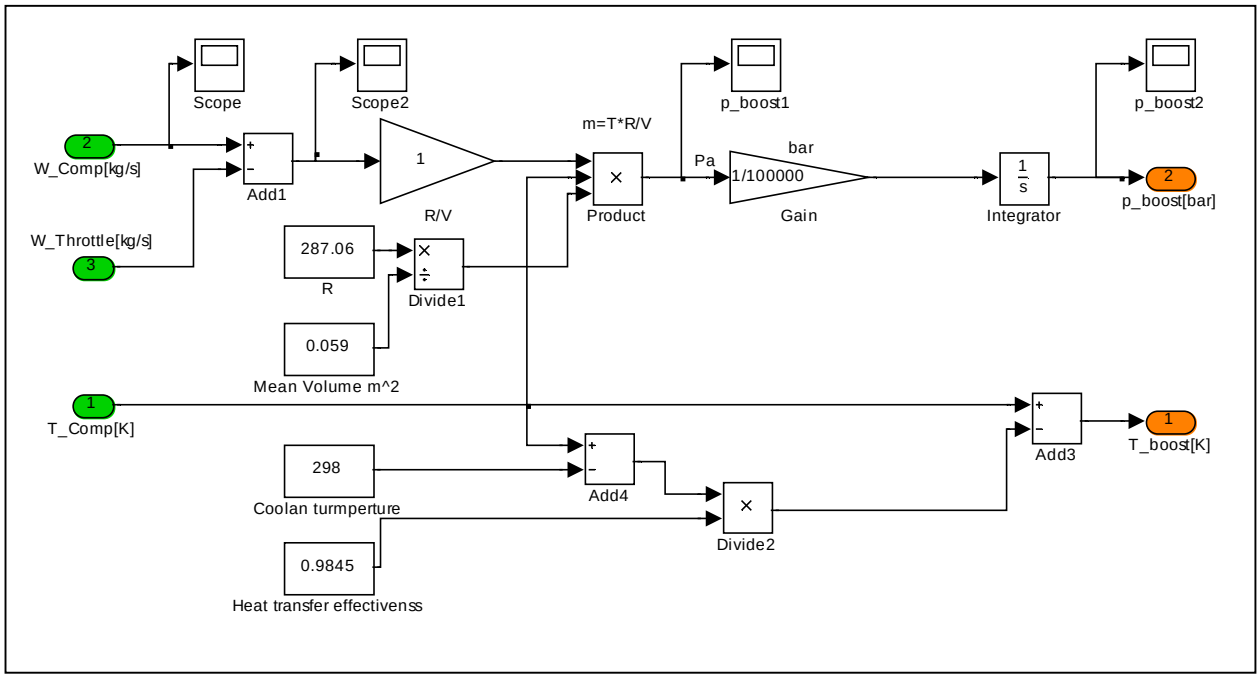

Figure 6.14. Intercooler implementation in Simulink.

6.2.6 Throttle

The flow through the throttle can be modeled using the standard orifice according to Heywood (Heywood, 1988).

$$\dot{m}_{th} = \begin{cases} \dfrac{CD_f A_T p_b}{\sqrt{RT_b}} \left(\dfrac{p_{IM}}{p_b}\right)^{1/\gamma} \left\{ \dfrac{2\gamma}{\gamma - 1} \left[1 - \left(\dfrac{p_{IM}}{p_b}\right)^{\frac{\gamma-1}{\gamma}} \right] \right\}^{\frac{1}{2}}, & \dfrac{p_{IM}}{p_b} > 0.528 \\ \dfrac{CD_f A_T p_b}{\sqrt{RT_b}} \sqrt{\gamma} \left(\dfrac{2}{\gamma+1}\right)^{\frac{\gamma+1}{2(\gamma-1)}}, & \dfrac{p_{IM}}{p_b} \le 0.528 \end{cases} \tag{6-9}$$

Where p_{IM} is the intake manifold pressure, p_b is the boost pressure after intercooler. A_T is the area of throttle at full opening, while CD_f is the discharge coefficient corresponding to the throttle opening degree. The T_b is the temperature after intercooler. The specific heat ratio, γ, is chosen as 1.401 for intake manifold. Throttle discharge coefficient was estimated by the date from performance simulation.

$$CD_f = 0.002458 + 3.566\text{e-}4\theta_{th} + 5.353\text{e-}4\theta_{th}^2 - 2.322\text{e-}5\theta_{th}^3 + 5.191\text{e-}7\theta_{th}^4 - 5.147\text{e-}9\theta_{th}^5 + 1.811\text{e-}11\theta_{th}^6 \tag{6-10}$$

The fitting function and the data comparison is shown in Figure 6.15. As a part of MVEM, it is implemented in Matlab/Simulink in Figure 6.18. The model prediction and simulation data are compared in Figure 6.16, in which shows the good consistence during low pressure ration and small throttle opening. For model (6-9), gas constant is 287.68 J/(kg K) in unit conversion.

$$\begin{aligned} \frac{kg}{s} &= \frac{m^2 \frac{N}{m^2}}{\sqrt{8.314 \frac{J}{mol \cdot K} K}} = \frac{m^2 \frac{kg \cdot \frac{m}{s^2}}{m^2}}{\sqrt{8.314 \frac{N \cdot m}{mol \cdot K} K}} = \frac{m^2 \frac{kg \cdot \frac{m}{s^2}}{m^2}}{\sqrt{8.314 \frac{kg \frac{m}{s^2} \cdot m}{0.029 kg \cdot K} K}} \\ &= \frac{1 \cdot \frac{kg \cdot \frac{m}{s^2}}{1}}{\sqrt{8.314 \frac{1 \cdot \frac{m^2}{s^2}}{0.029 \cdot 1 \cdot 1} \cdot 1}} = \frac{1 \cdot \frac{kg \cdot \frac{m}{s^2}}{1}}{\sqrt{\frac{8.314}{29}} \cdot \frac{m}{s}} = \sqrt{\frac{0.029}{8.314}} \frac{kg}{s} = \sqrt{\frac{1}{287.68}} \frac{kg}{s} \end{aligned} \tag{6-11}$$

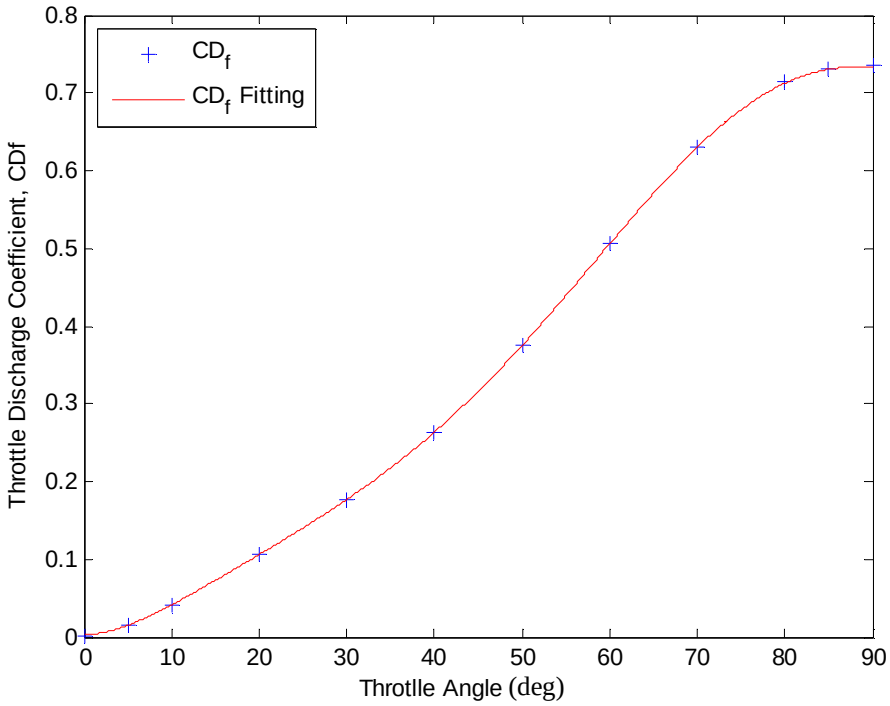

Figure 6.15. Throttle discharge coefficient and the fitting.

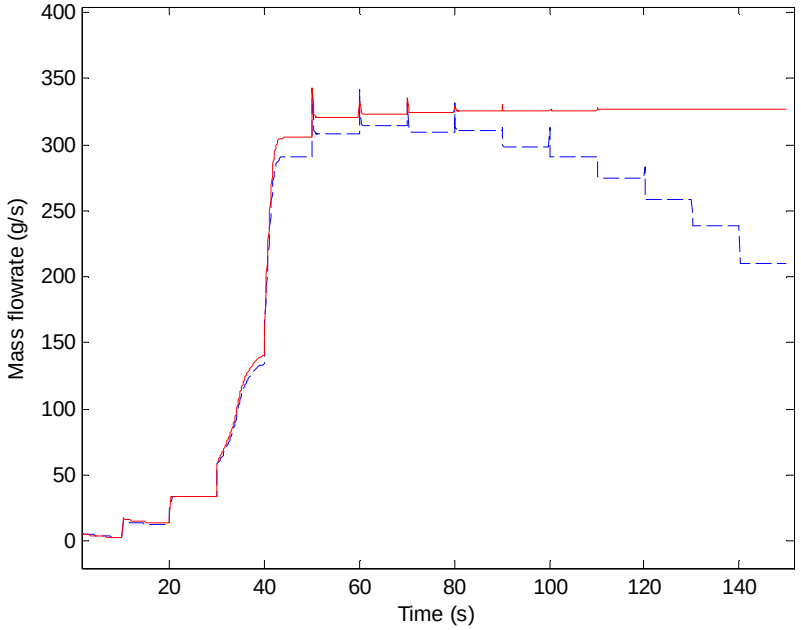

Figure 6.16. Comparison between the simulation data (red solid line) and model prediction (blue dash line).

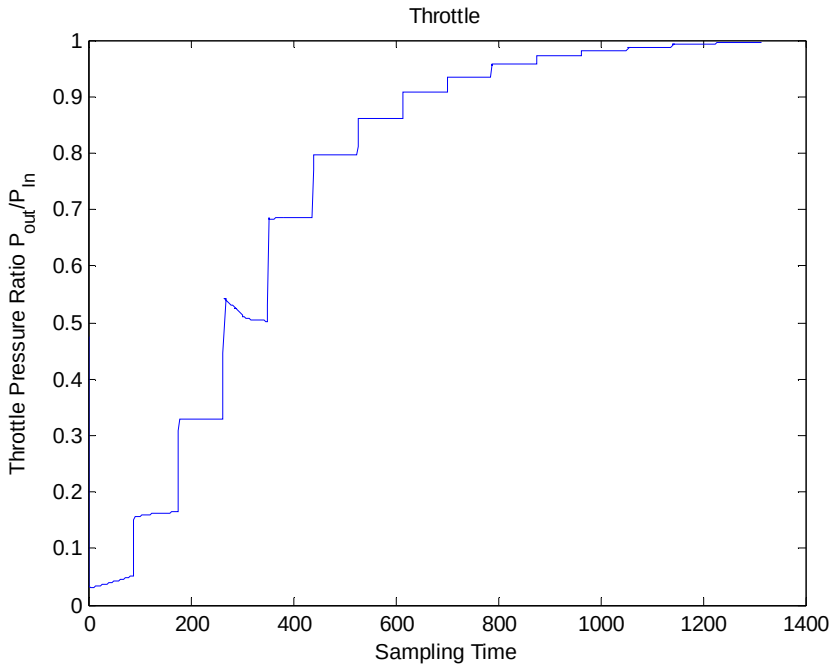

Figure 6.17. Pressure ratio at throttle during the flow rate verification.

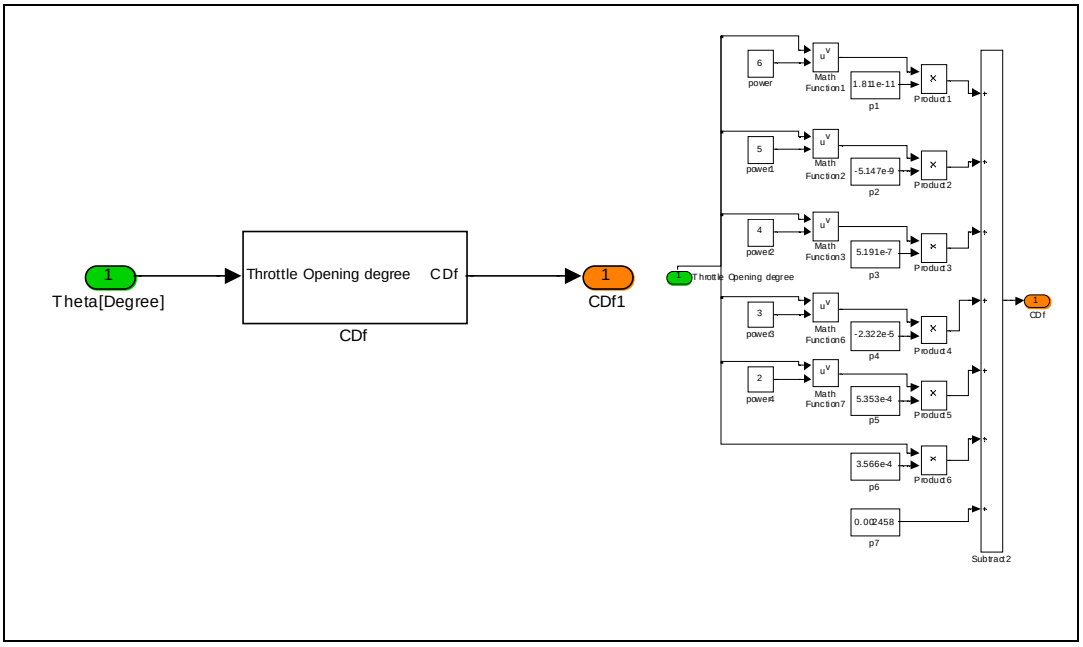

Figure 6.18. Throttle discharge implementation in Matlab/Simulink.

6.2.7 Intake Manifold

Intake manifold is modeled as open thermodynamic volume, filling and emptying with ideal gas by compressor and engine air charging process. Neglecting heat losses through walls and assuming an ideal gas with constant specific heat, intake manifold pressure is modeled as (Hendricks et al., 1996)

$$\dot{p}_{im} = \left(\dot{m}_{th} - \dot{m}_{cyl}\right)\frac{RT_{im}}{V_{im}} \tag{6-12}$$

where p_{IM} and T_{IM} are the pressure and temperature of intake manifold; R is the ideal gas constant. The thermodynamic state $\dot{p}_{IM}$ is used to describe the results from the filling process of the compressor flow and emptying process of air sucking/changing into the cylinders. The manifold volume is the key parameter in the model. Based on the simulation data obtained over an operating range from 900-2100 rpm, Figure 6.19 shows the volumes and the mean value. Intake manifold pressure dynamic model prediction is compared with GT-Power model in Figure 6.19.

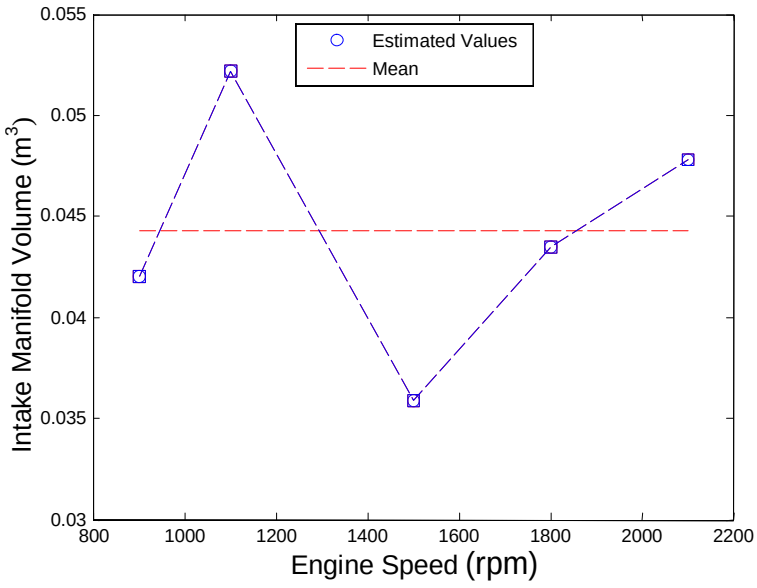

Figure 6.19. Estimated intake manifold volume and the mean value.

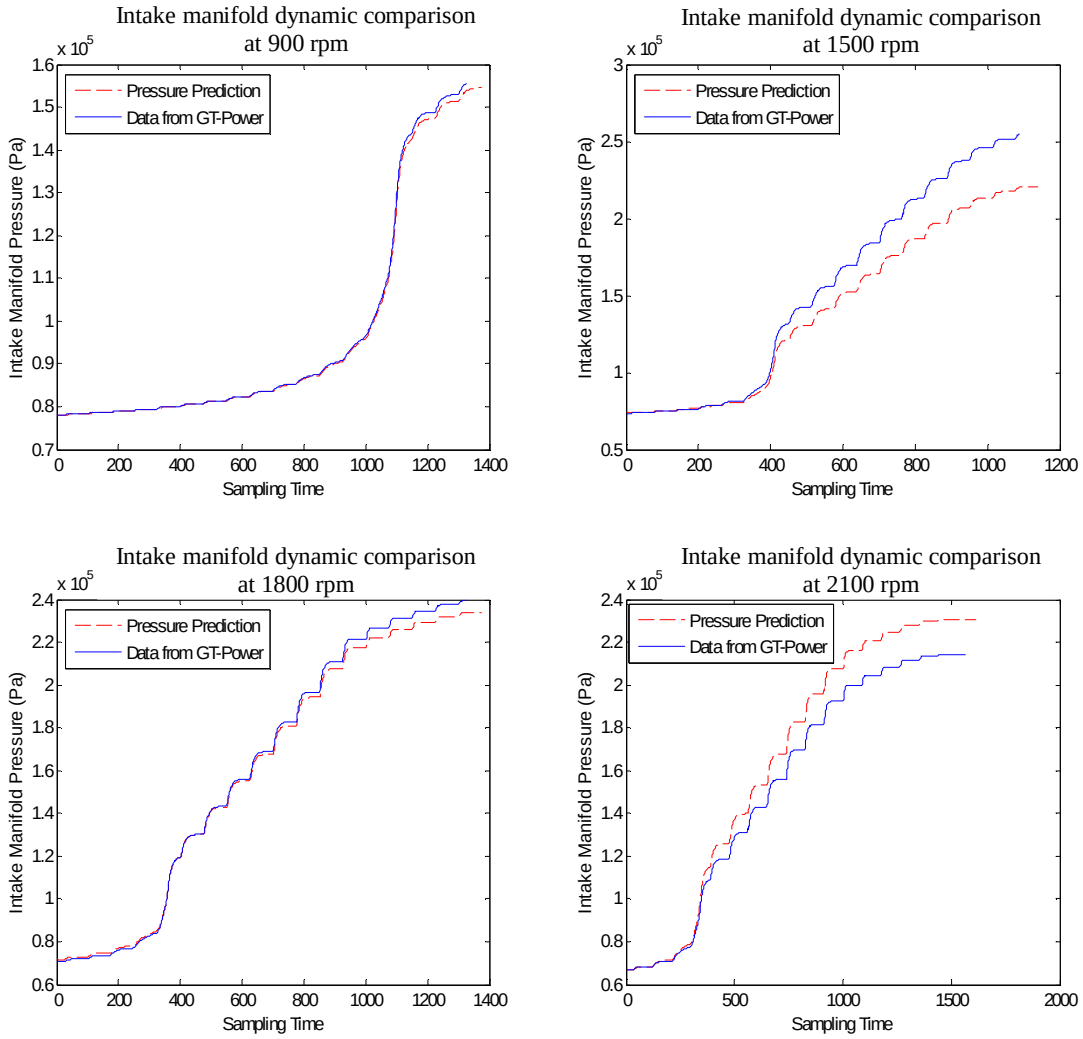

Figure 6.20. Comparison of intake manifold dynamic model prediction and GT-Power data.

6.2.8 Engine

6.2.8.1 Air-charging Model

Air charging into the cylinder is a highly nonlinear process depending on the volumetric efficiency η_{vol}, engine speed N_e and intake manifold states of T_{im}, p_{im}, which describes the engine pumping process as

$$\dot{m}_{cyl} = \eta_{vol} \frac{p_{im}}{T_{im} R_{im}} \frac{N_e}{60} \frac{V_d}{2} \tag{6-13}$$

where V_d is the displacement volume. The volumetric efficiency is mainly a function of engine speed, intake manifold pressure. The intake manifold change Δp_{im} is included to consider the dynamic effects of the air-charging process. The back pressure effect is taken into account in terms of $p_{ex} - p_{im}$. Then the air-charging process is modeled as

$$\dot{m}_{cyl} = f\left(p_{im}, p_{im} N_e, \Delta p_{im} N_e, N_{tc}, N_e N_{tc}, N_e, (p_{ex} - p_{im}) \right) \tag{6-14}$$

The comparison between model prediction and GT-Power data is shown in Figure 6.21. Both steady-state and transient processes are well predicted by the model.

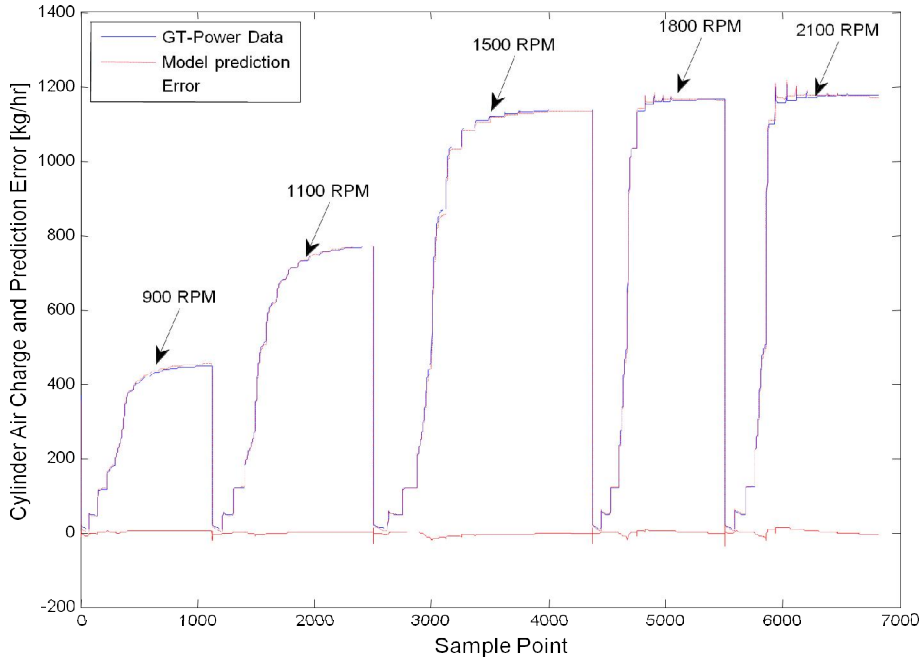

Figure 6.21. Air-charging model prediction, GT-power data and prediction error.

6.2.8.2 Engine Shaft Dynamics

Four different instantaneous torque quantities are used in engine torque computation: Indicated, Crank Pin, Shaft, and Brake torques. The instantaneous Indicated torque, $TQ_i(t)$, represents the

thermodynamic work transferred from the gas to the piston (converted via geometry to a torque applied to the crankshaft). After accelerating the engine, the crank-sliders overcome the friction between the mechanical parts, and shaft torque is produced. The shaft torque is the quantity to overcome the crank shaft inertia to produce the engine speed, designated as $N_e(t)$ in the model. Brake torque is the quantity available at flywheel, which is the final torque net of all cranktrain inertia. Its value is exactly equal and opposite of the value for the sum of all external loads.

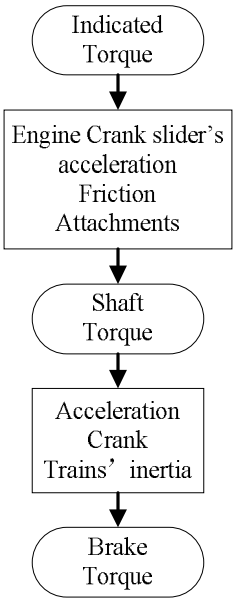

Figure 6.22. Engine Torque and their relation.

The indicated torque and friction torque need to be modeled to evaluate shaft torque and engine speed dynamics.

From Newtonian Mechanics, the engine crankshaft dynamics can be derived as in (6-8), where I_e is the engine inertia. TQ_{shaft} is the break torque load and TQ_{load} is the torque load

$$\dot{N}_e = \frac{60}{2\pi}\frac{TQ_{shaft} - TQ_{load}}{I_e} \tag{6-15}$$

Shaft torque $TQ_{shaft} = TQ_{ind} - T_{friction}$ is the difference between the indicated torque and the friction torque.

As the air charging is proportional to intake manifold pressure (6-9), the simplified shaft torque is modeled as

$$TQ_{Ind} = k_0 + k_1 m_f + k_2 N_e + k_3 N_e m_f \tag{6-16}$$

Fuel rate m_f and engine speed N_e are obtained from offline simulation. The linear regression results are:

$$TQ_{Ind} = -110.43 + 9.0455 m_f - 0.0103 N_e - 0.0004 N_e m_f \tag{6-17}$$

The model prediction and GP-Power data are compared in Figure 6.23.

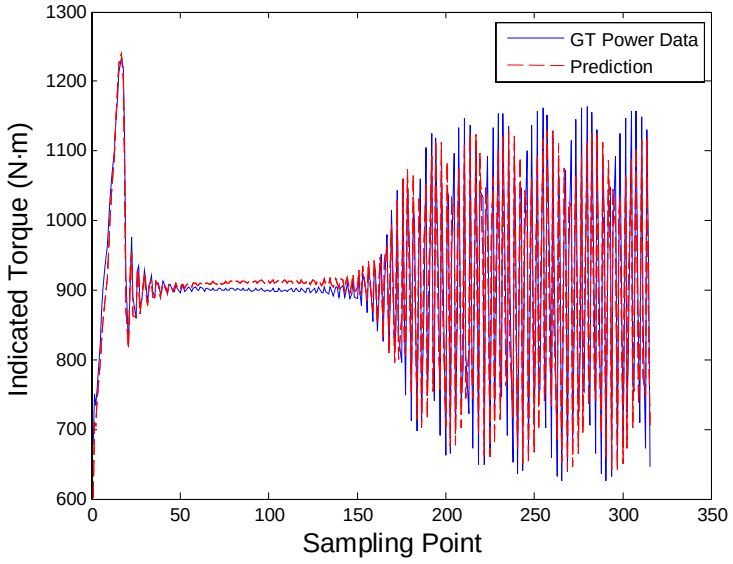

Figure 6.23. Engine torque model prediction and GT-Power data.

Friction and pumping losses are considered in one term as $TQ_{friction}$. It represents the hydrodynamic and pumping friction torque. The fluid-film friction is the principal mechanical losses during the engine operation. Both pumping and friction are the function of engine speed as stated:

$$TQ_{friction} = 0.7302 + 29.2581 m_f + 42.35 N_e + 0.0078 N_e m_f \tag{6-18}$$

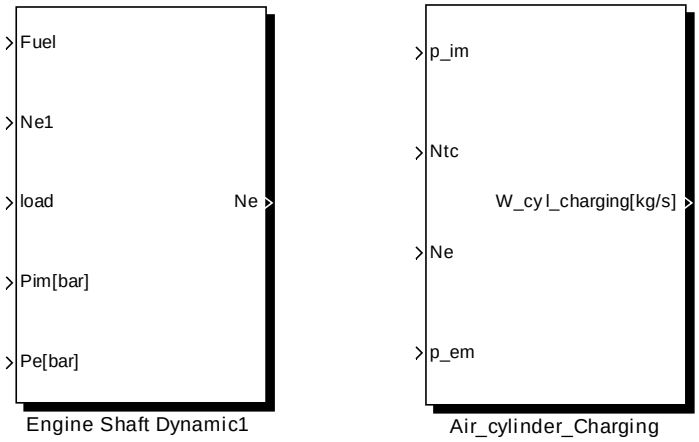

Figure 6.24. Engine shaft and air charging block in Matlab/Simulink.

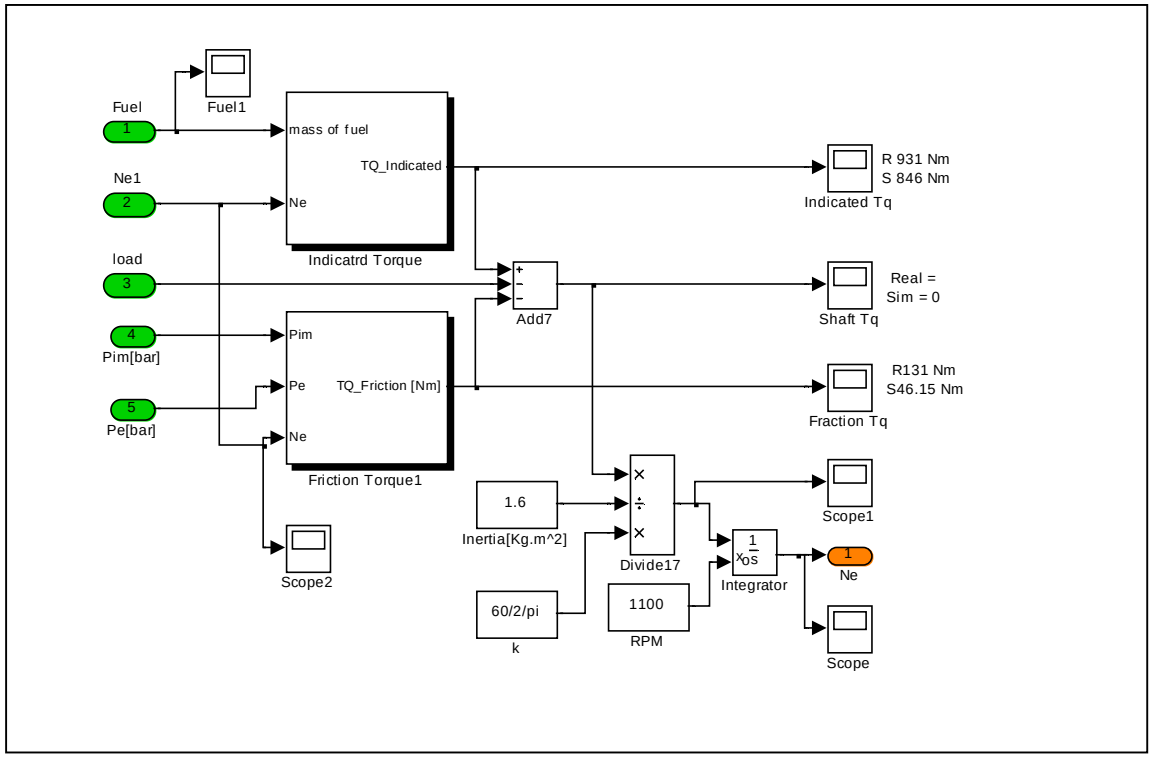

Figure 6.25. Engine shaft dynamic implementation in Matlab/Simulink.

6.2.9 Exhaust Manifold

To model the conditions in the exhaust manifold, the temperature of the mass flow from the cylinder into the exhaust manifold is necessary. It is a function of fuel flow, air flow into the cylinders, and engine speed.

$$T_{ex} = f(m_f, m_{air}, N_e)$$

$$T_{ex} = 984.34 + 0.3049 m_f + 0.057 N_e + 0.0004 m_f N_e \tag{6-19}$$

Model prediction and GT-Power data are compared in Figure 6.26.

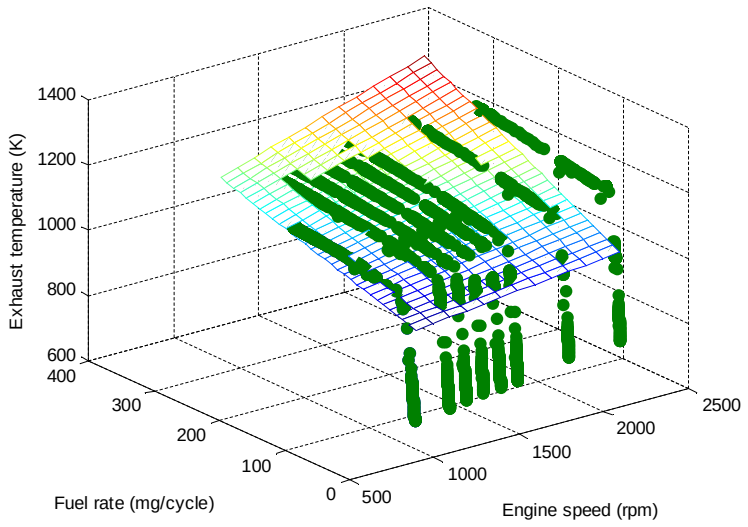

Figure 6.26. Exhaust temperature model prediction (net) and GT-Power data (dots) comparison.

The exhaust pressure dynamics are modeled as in the intake manifold.

$$\dot{p}_{em} = \left(\dot{m}_{ex} - \dot{m}_{turb} - \dot{m}_{wg}\right)\frac{RT_{em}}{V_{em}} \tag{6-20}$$

where $\dot{m}_{ex}$ is exhaust mass flow rate, which consist of fuel and air flow rate into the cylinder; $\dot{m}_{turb}$ and $\dot{m}_{wg}$ are turbine flow rates and wastegate flow rates respectively. The wastegate opening is used to adjust the bypass flow as $\dot{m}_{wg}$, in order to control the exhaust manifold pressure. The engine air density is indirectly adjusted through the turbocharger power by the exhaust manifold pressure. The estimated Equivalent exhaust manifold volume and the mean values are shown in

Figure 6.27. One of the model predictions at 1100 rpm is illustrated in Figure 6.28 and the comparison with GT-Power data.

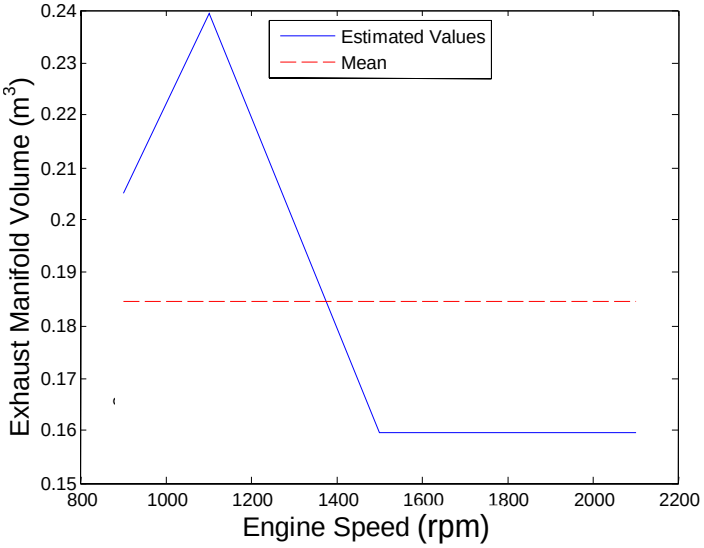

Figure 6.27. Exhaust manifold volume and mean value.

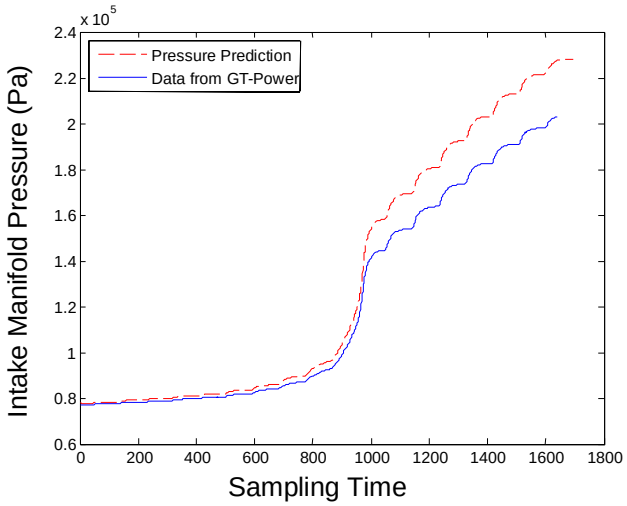

Figure 6.28. Model prediction of exhaust manifold pressure dynamic (1100 rpm) and GT-Power data.

6.2.10 Turbine and Wastegate

6.2.10.1 Turbine

Turbine performance is important for engine control. The easy model, look-up table, is usually used for the turbine flow model. Manufacturer provided flow map data and efficiency data were used in the look-up table model first, and implemented in the Matlab 2D look-up table. The accuracy is not enough in the steady-state and transient state verification. Then the turbine was modeled as an orifice. According to orifice model stated in throttle modeling; the mass flow through it can be described as follows, with supersonic and chocked flows.

$$\dot{m}_{turbine} = \begin{cases} \dfrac{\left(CD_f A_{orifice}\right) p_1}{\sqrt{RT_0}} \left(\dfrac{p_2}{p_1}\right)^{1/\gamma} \left\{ \dfrac{2\gamma}{\gamma - 1} \left[1 - \left(\dfrac{p_2}{p_1}\right)^{\frac{\gamma-1}{\gamma}} \right] \right\}^{\frac{1}{2}} & \dfrac{p_2}{p_1} > 0.546 \\ \dfrac{\left(CD_f A_{orifice}\right) p_1}{\sqrt{RT_0}} \sqrt{\gamma} \left(\dfrac{2}{\gamma + 1}\right)^{\frac{\gamma+1}{2(\gamma-1)}} & \dfrac{p_2}{p_1} \le 0.546 \end{cases} \tag{6-21}$$

where CD_f is the discharge coefficient of the orifice opening of max area $A_{orifice}$; p_1 and p_2 are inlet and out pressure.

For model identification and later verification purposes, a GT-Power model was run at the throttle angle of 14.3 degree, with the wastegate in closed condition. A transient process of turbine was obtained. The transient is from the initial turbine speed of 90,000 rpm, slowing down to 80,000 rpm because of the latency of intake manifold pressure. Not much air is available for combustion, as the stoichiometry is maintained for the SCI scheme. Then gradually, as the density of the intake manifold increases, the fuel injection model is then increased, more exhaust power is available to speed up the turbine. In this simulation, the turbine speed reaches stabilization around 100,000 rpm. In the control analysis, this non-minimum phase characteristic cause's difficulty in the dynamic control and stability. The special phase latency needs to be taken into account for the engine control deign, in which the system control is more complex than the control in conventional diesel engines.

The unknown parameter of model (6-13), $CD_f A_{orifice}$ is treated as one parameter in the model identification. The combine effect of turbine dynamic change in speed and mass flow rate is embedded in the integrated parameter. Notice that the specific heat capacity ratio at the exhaust pipe is about 1.3, and the critical pressure ratio is 0.546. As shown in Figure 6.29, the turbine exhaust flow runs through the equivalent orifice under both subcritical chocked flow conditions. The separate models need to be considered.

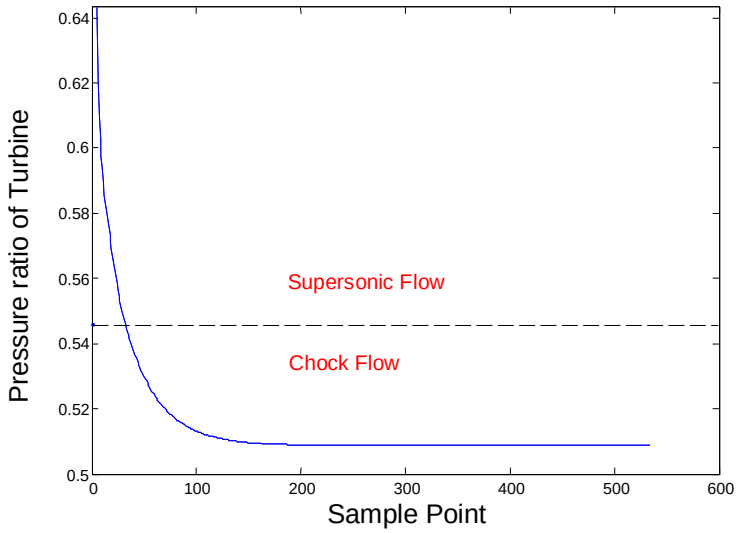

Figure 6.29. Turbine fluid dynamic under subcritical and chocked flow conditions.

The detail simulation data are shown in for correlation analysis among the flow rate, turbine speed, and discharge coefficient and opening pressure ratio. From (a) and (c), the equivalent turbine discharge coefficients have different stages under supersonic and chock flow condition. The correlation between the discharge coefficient and turbine speed is obvious. For the supersonic flow, the discharge coefficient has little oscillation, but the trend is for good development as turbine speed decreases and then increases. For chock flow, the mass flow rate will only depend on the upstream pressure and temperature. But in this case, the down stream pressure and temperature do not change dramatically; the ambient pressure and temperature are adopted for simplification. From Figure 6.30(a) and (b), the discharge coefficient follows the turbine speed in a consistent relationship.

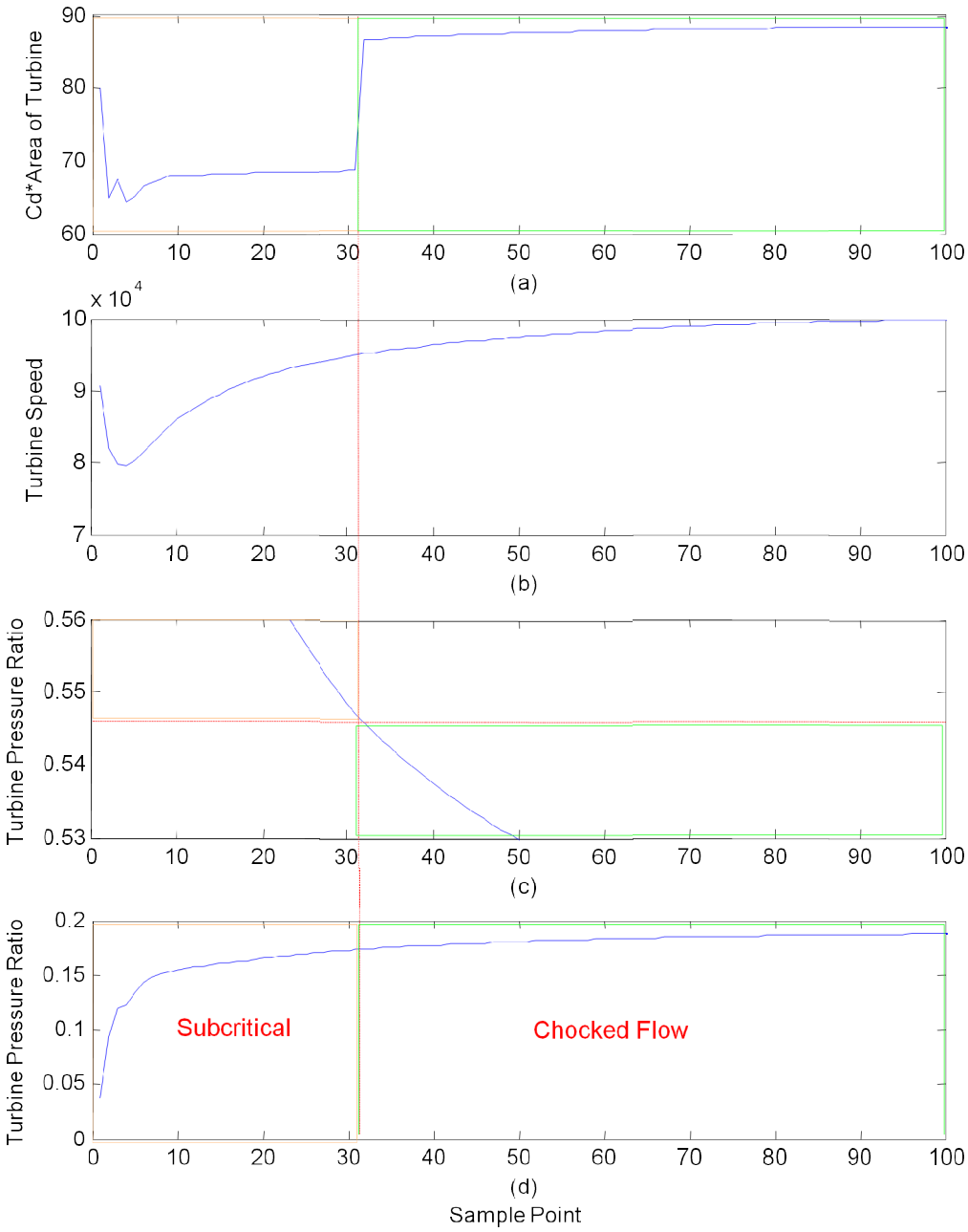

Figure 6.30. Correlation between the discharge coefficient of turbine and the turbine speed under $p_r > 0.546$ and chock flow conditions $p_r < 0.546$.

According to the correlation between the discharge coefficient and engine speed, two separate models are created. The model of the product of discharge coefficient and equivalent opening of the turbine is obtained from the GT-Power simulation data as a function of turbine speed as

$$CD_f A_{turb\_sub} = 51.3049 + 1.8617\text{e-}004 \cdot N_{tc} \quad (6\text{-}22)$$

$$CD_f A_{turb\_chocked} = 52.1474 + 3.6403\text{e-}004 \cdot N_{tc} \quad (6\text{-}23)$$

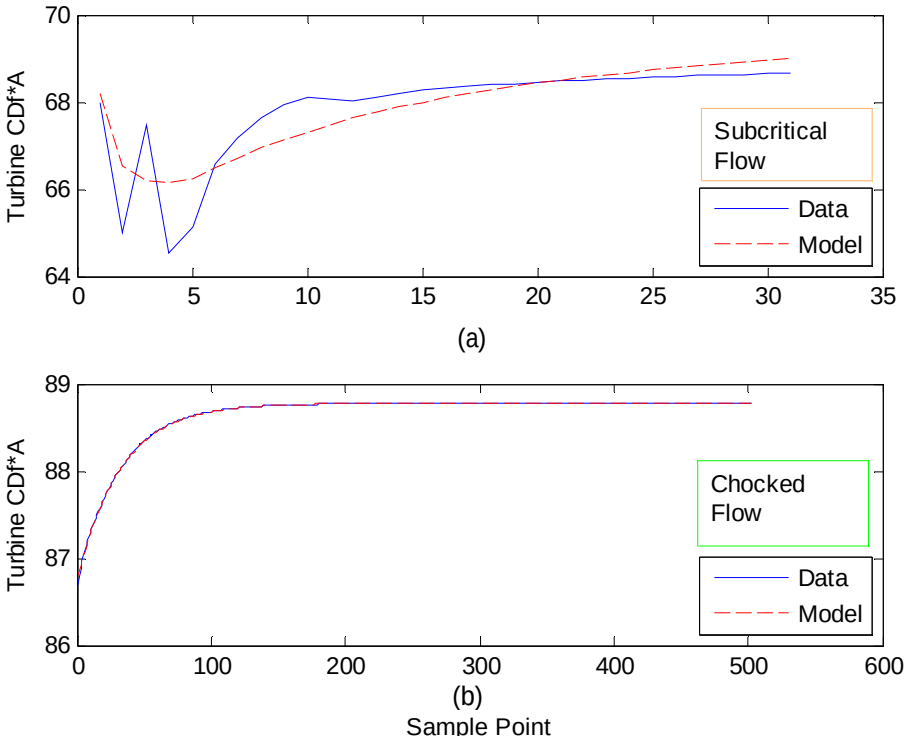

Figure 6.31. Turbine discharge coefficient time equivalent opening fitting model and comparisons with GT-Power data.

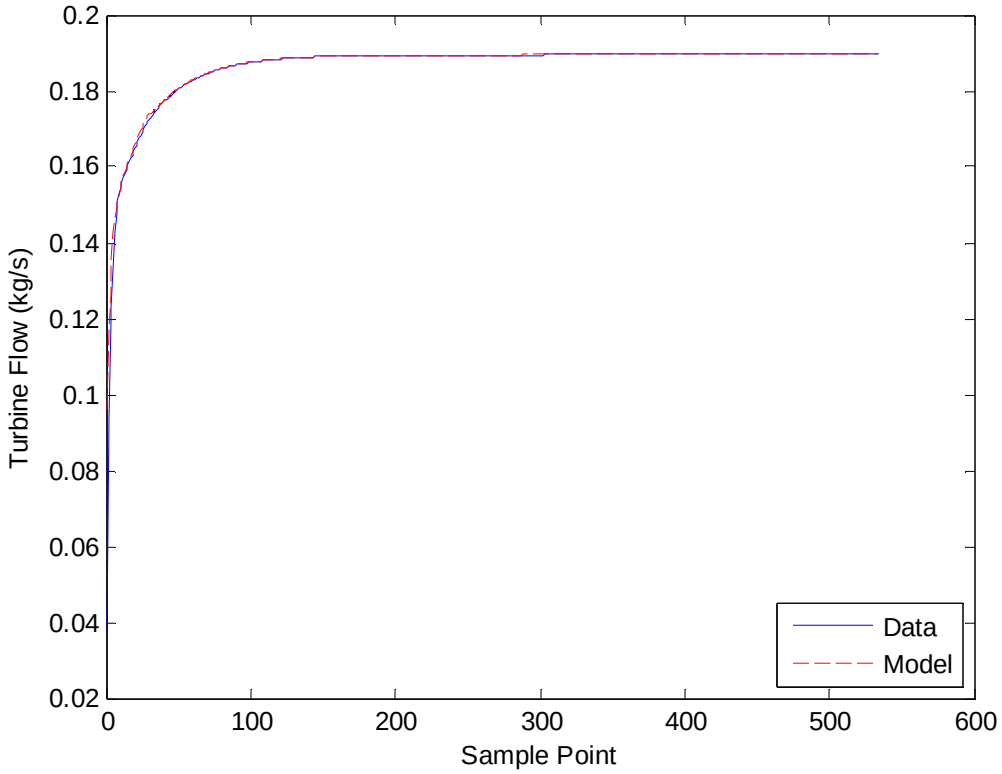

Figure 6.32. Turbine flow comparison between GT-Power data and model prediction.

Based on model (6-14) and (6-15), the orifice model based turbine flow estimation was compared with the GT-Power data in Figure 6.30 (d). The comparison is shown in Figure 6.32, which has good consistency for both the subsonic and chock flow conditions during the whole GT-Power process.

In another set of simulation data, the turbine dynamic is shown in Figure 6.33. For the first three cases of 900 rpm, 1100 rpm and 1500 rpm, shows the good agreement of $CD_f A_{turb}$ with GT-Power data. For 1800 rpm and 2100 rpm cases, the turbine runs out of map without control. It also implies that the control design is important for the engine to run within safe system operating conditions.

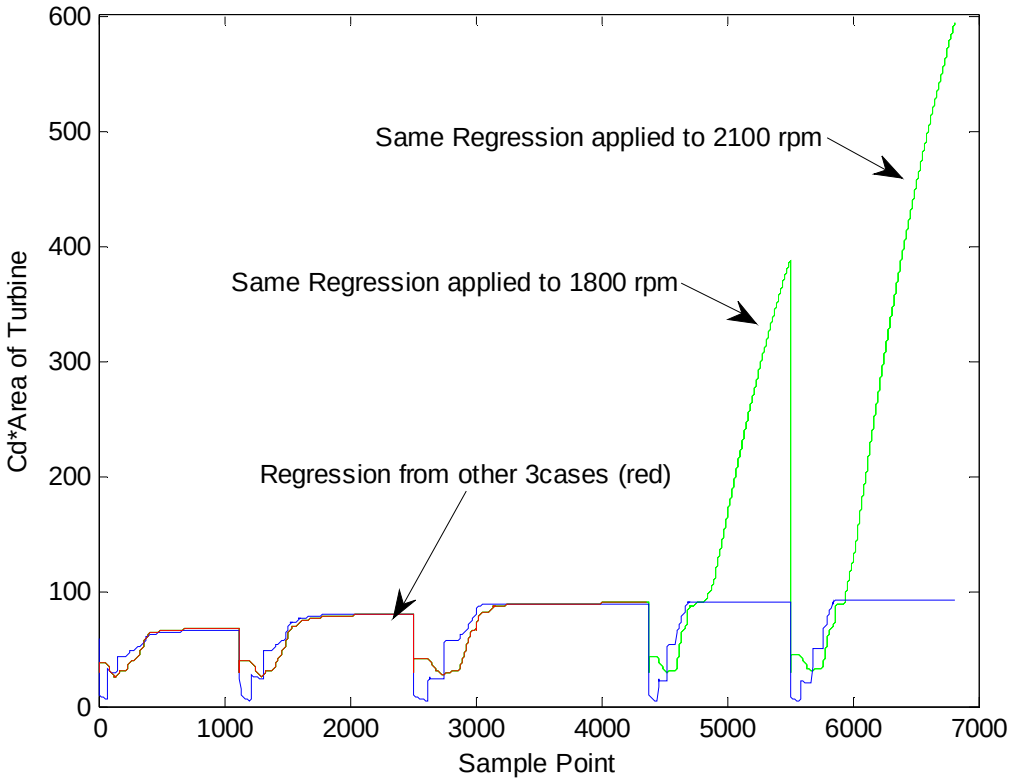

Figure 6.33. Comparison of equivalent turbine opening and GT-Power data.

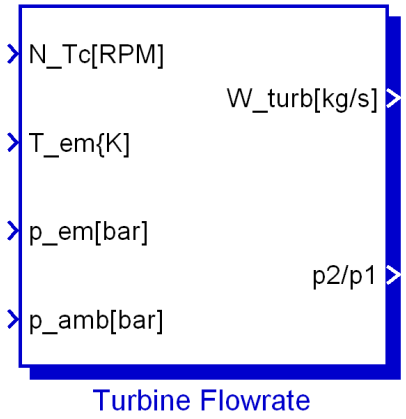

Figure 6.34. Turbine flow rate model in Simulink.

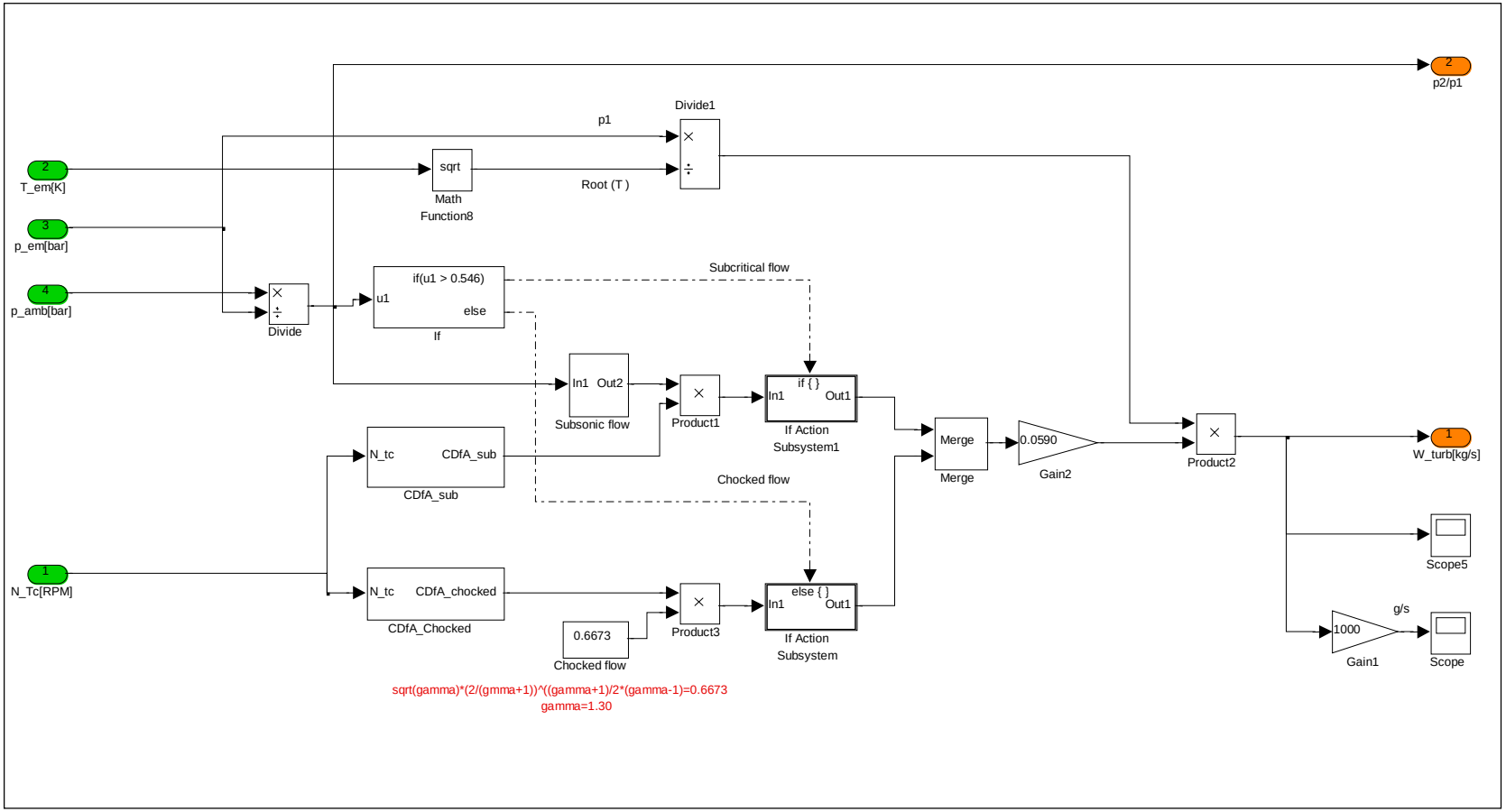

Figure 6.35. Turbine flow rate model implementation in Matlab/Simulink.

6.2.10.2 Wastegate

To simplify the wastegate flow-rate modeling, it was modeled as an orifice as described in equation (6-15). The discharge coefficient CD_{f_wg} is estimated based on linear model of the wastegate opening A_{wg}, and engine speed N_e,

$$CD_{f\_wg} = 0.4518A_{wg} + 303.87A_{wg} \times N_e + 0.039 \tag{6-24}$$

A comparison of discharge coefficient and flow rates from the models and GT-Power simulation are shown in Figure 6.36 and Figure 6.37.

The turbine exit temperature, T_t, is given by

$$T_t = \left[1 - \left[1 - \left(\frac{P_{amb}}{P_{ex}}\right)^{\frac{\gamma-1}{\gamma}}\right]\eta_t\right] T_{ex} \tag{6-25}$$

where the turbine efficiency is determined by a lookup table based on map data as a function of

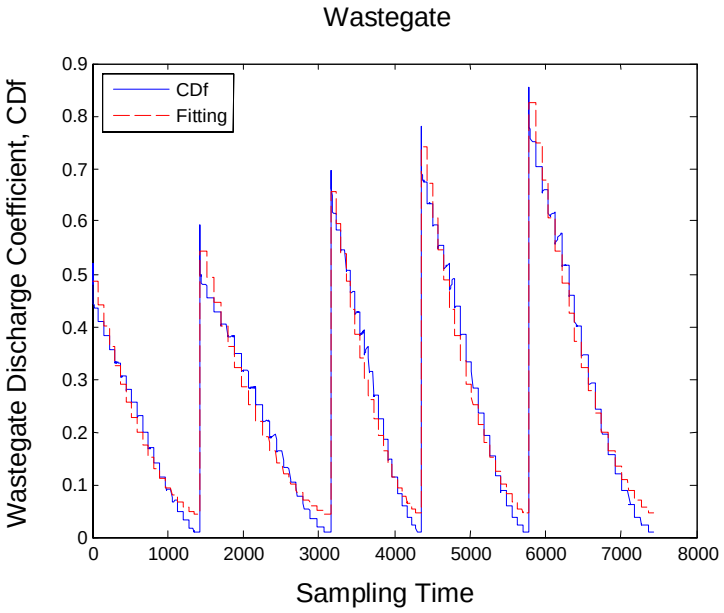

Figure 6.36. Discharge coefficient of wastegate as orifice.

corrected turbine speed and pressure ratio.

$$\eta_t = f\left(\frac{P_{amb}}{P_{ex}}, \frac{N_{tc}}{\sqrt{T_{ex}}}\right) \tag{6-26}$$

The turbine outlet pressure is assumed as an ambient condition for simplification.

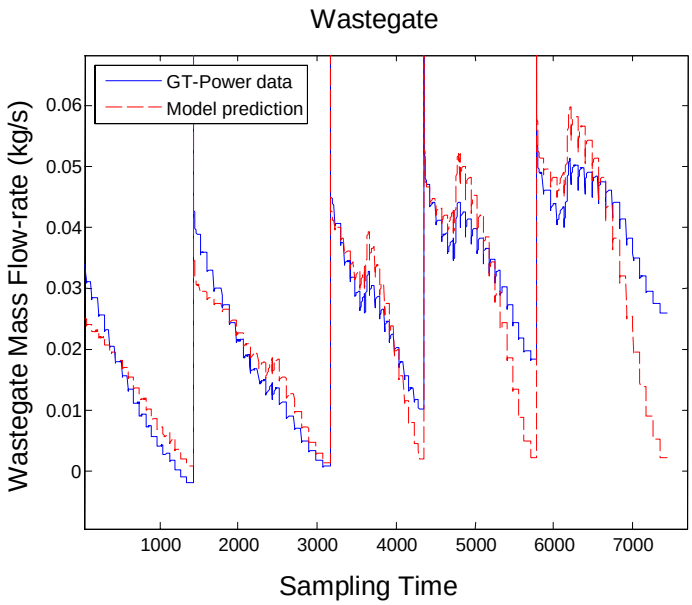

Figure 6.37. Comparison of model prediction and GT-Power data of mass flow rate through wastegate.

6.2.10.3 Turbocharger Dynamic

The Turbocharger dynamics depend on the difference of power consumed by the compressor, P_{comp}, and the power generated by the turbine, P_{turb}.

$$\dot{N}_{tc} = \frac{P_{turb} - P_{comp}}{I_{tc} N_{tc}} \tag{6-27}$$

where I_{tc}, is shaft moment inertia $1.5\times10^{-4}\,\mathrm{kg\cdot m^2}$; the powers are given by

$$\begin{aligned} P_T &= c_{p,c}\dot{m}_c\left(T_{em} - T_t\right) \\ P_C &= c_{p,t}\dot{m}_t\left(T_c - T_{amb}\right) \end{aligned} \tag{6-28}$$

Because the exhaust temperature changes significantly over the engine operating condition,

specific heat needs to be modeled.

$$c_{p,t} = 3.5584 + 4.1684e\text{-}003 \cdot T_{em} + 1.3875e\text{-}006 \cdot T_{em}^2 + 3.0507\text{e-}003 \cdot T_{ex} + 3.0510\text{e-}006 \cdot T_{ex}^2 \quad (6\text{-}29)$$

Figure 6.38 shows the model prediction as a function of inlet and outlet temperature of turbine the compared with the GT-Power data.

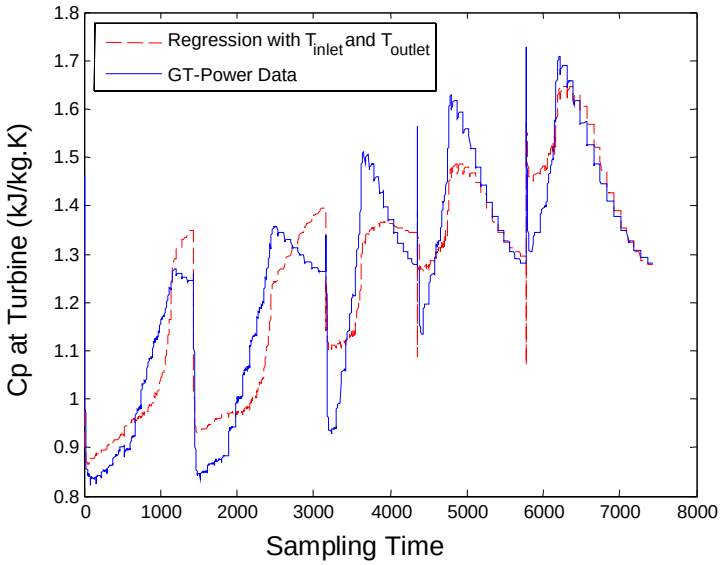

Figure 6.38. Specific heat data and regression at turbine.

Implementation of Turbine power model

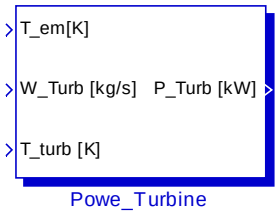

(a) Block module Figure

Figure 6.39. Input and output of turbine model.

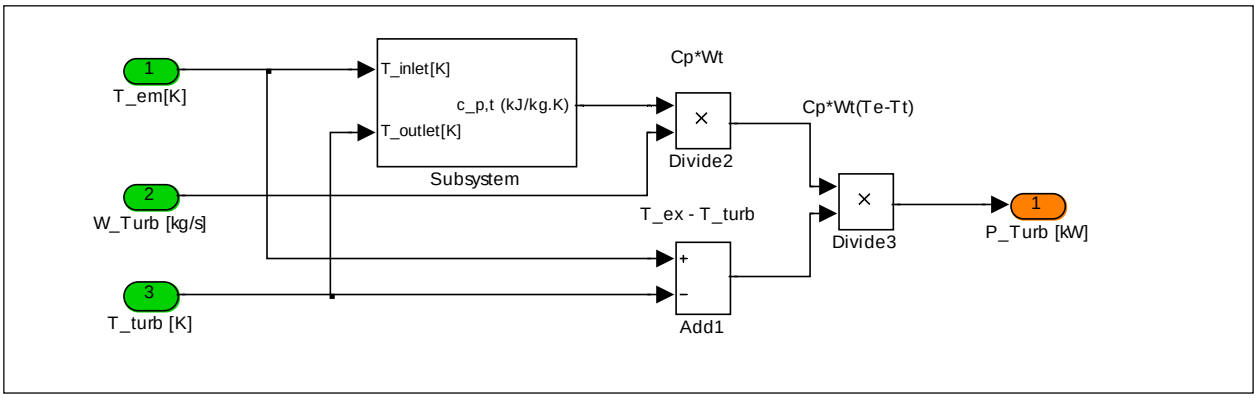

(b) Power sub-model

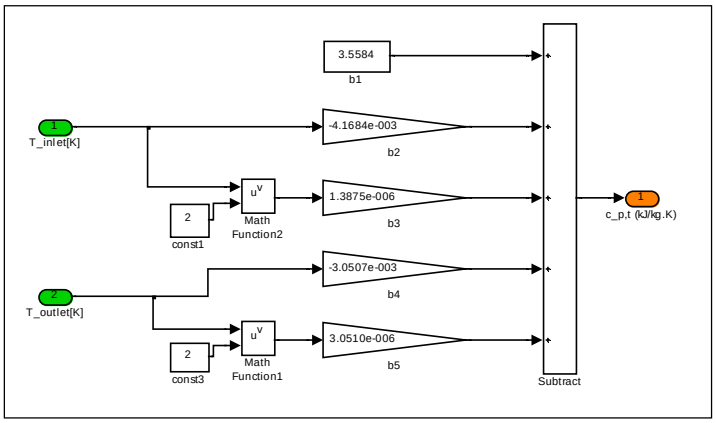

(c) Specific heat model

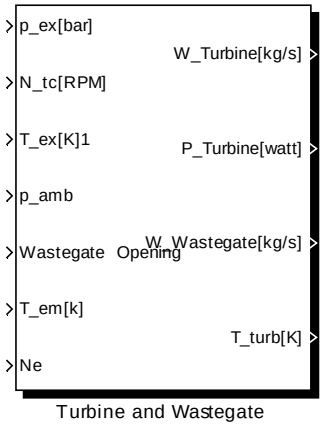

(d) Turbine and Wastegate sub-model

Figure 6.39 (cont.). Input and output of turbine model.

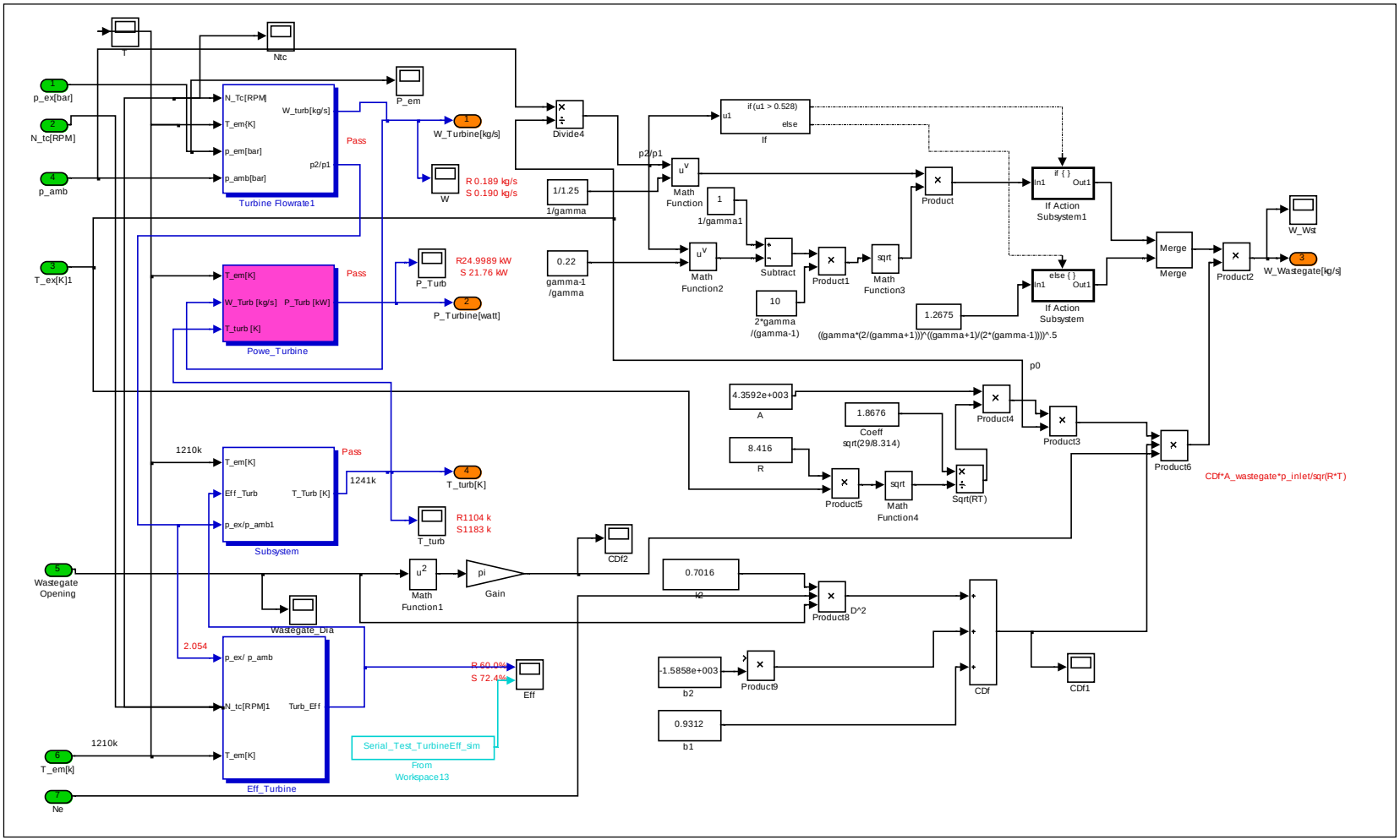

Figure 6.40. Turbine and wastegate subsystem model implementation in Matlab/Simulink.

6.3 MVEM Implementation in Simulink

Each sub-system model was implemented in the Simulink environment. They are integrated as a whole engine to predict engine dynamic for engine system control and power-train control design. The layout of the integrated Simulink model is shown in Figure 6.41. The wastegate opening control and fuel amount control will be designed for engine operation. Further, EGR and vehicle model may be included for after-treatment and power-train system design and simulation.

6.4 MVEM Verification

After the design of mean value engine model, it is necessary to verify the effectiveness of MVEM against the detail engine model data. The verifications are conducted in two steps: (1) Steady-state tests, (2) transient dynamic test.

6.4.1 Unit Verification for Given Input

Each unit is driven with original data from 1D detail model, which are extract from designated simulation runs. The given conditions are list in Table 6.2.

Table 6.2. External conditions for units verification.

Ambient Temperature	298.15(K)
Ambient Pressure	0.965 (bar)
Load Condition	800 (N·m)
Throttle Opening	14.3 (deg)
Wastegate Opening	Closed

For each units, the inputs were driven by the ideal data from detail simulation results, just like the model part was embedded into the detail model. Figure 6.42 shows the compressor verificatoin results. It can be found the mass flow rate through compressor in (a), compressor outlet temperture in (b), and compressor power output in (c), all have good consistence in steady states and transient process. The spines of model curve at about 1s and 3s in three figures may be

caused by the discontinuity of interpolation of the lookup maps. The Intercooler pressure dynamic follows the detail model curve very well, the steady-state is very close to Gt-Power data in Figure 6.43(a). Intercooler temperture doesn't show big fluctuation, model data is closed enough to the ideal data in steady states in Figure 6.43(b). The air flow through the thottle is predicted by orifice model in Figure 6.44 The initail state difference less than 1s can be ignored, the overal prediction is fine. There exist little steady-state error and a drop during transient. For engine model verification, the model simulation results are shown in Figure 6.45(a) to (d). In figure (a), the air charging has good consistence to GT-Power model. Engine exhuat temperture model follows the detail model well, but has little error in steady state. Fuel injection in (d) are fixed with air mass flow rate, and has similar results with (a). Enigne speed is the most concere in all speed governing, it shows satified accuracy corresponse to the GT-Power data. Indicated in Figure 6.46(a) (b), exhaust manifold model results has big error in transient and steady state. It stabilized into close value of 2 bar. But the exhaust temperature follow in good consistence in Figure 6.46 (b). The turbinocharger speed has stable value of 95000 rpm corresponding to 100,000 rpm in Figure 6.47. Shown in Figure 6.48(a), the turbine follow are the combination of air change and fuel injection, the model data are correct follow the GT-Power in transient and steady state. Finaly, the turbine power output, which is important for speed estimation, has good accuracy in steady-state shown in Figure 6.58 (b). The turbine efficiency differenc may be the cause of transient error.

Overall, each engine unit has similar bevior to follow a steady control variable of throttle; they stablize to same or close value in the long run. Next, transient control verification need to further test the MVEM as a whole system.

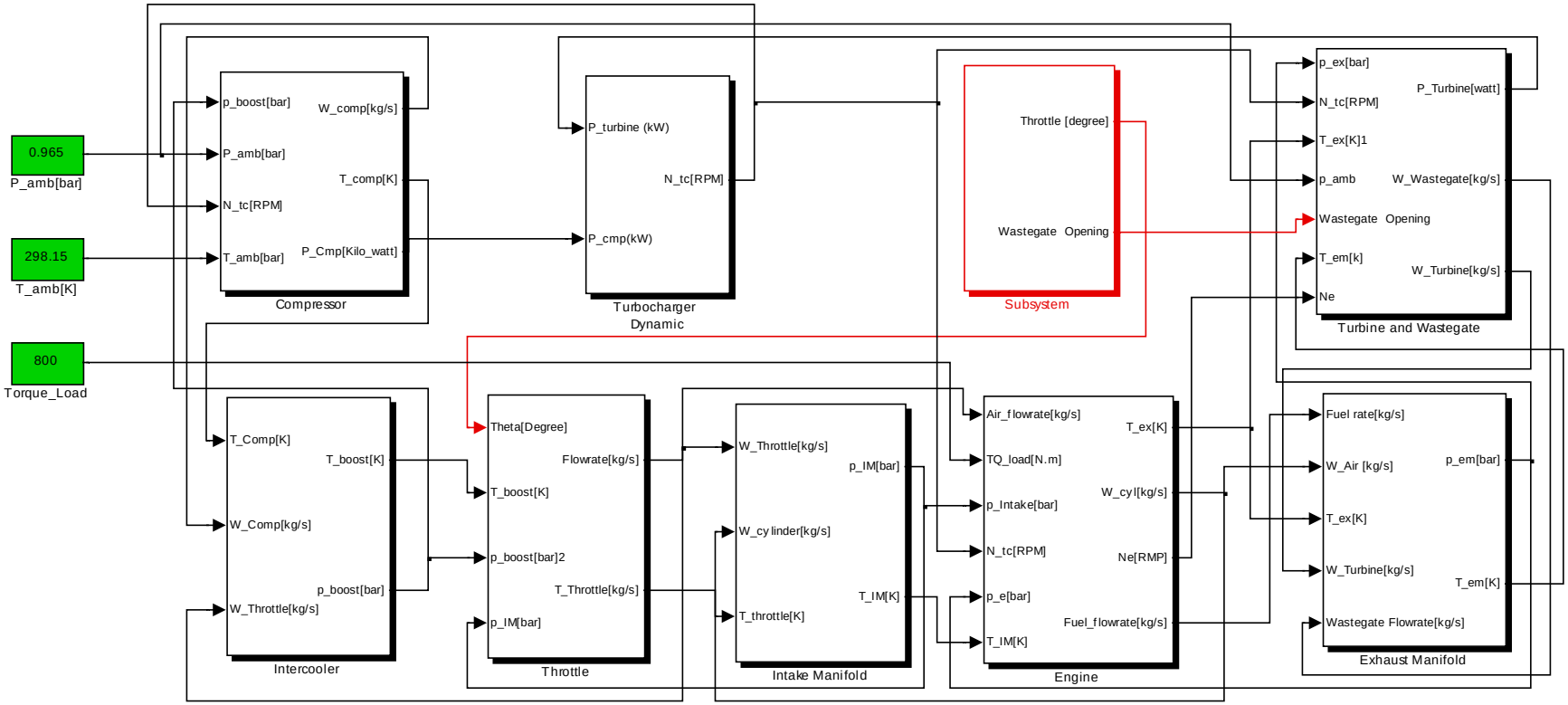

Figure 6.41. MVEM of a diesel engine in Matlab/Simulink.

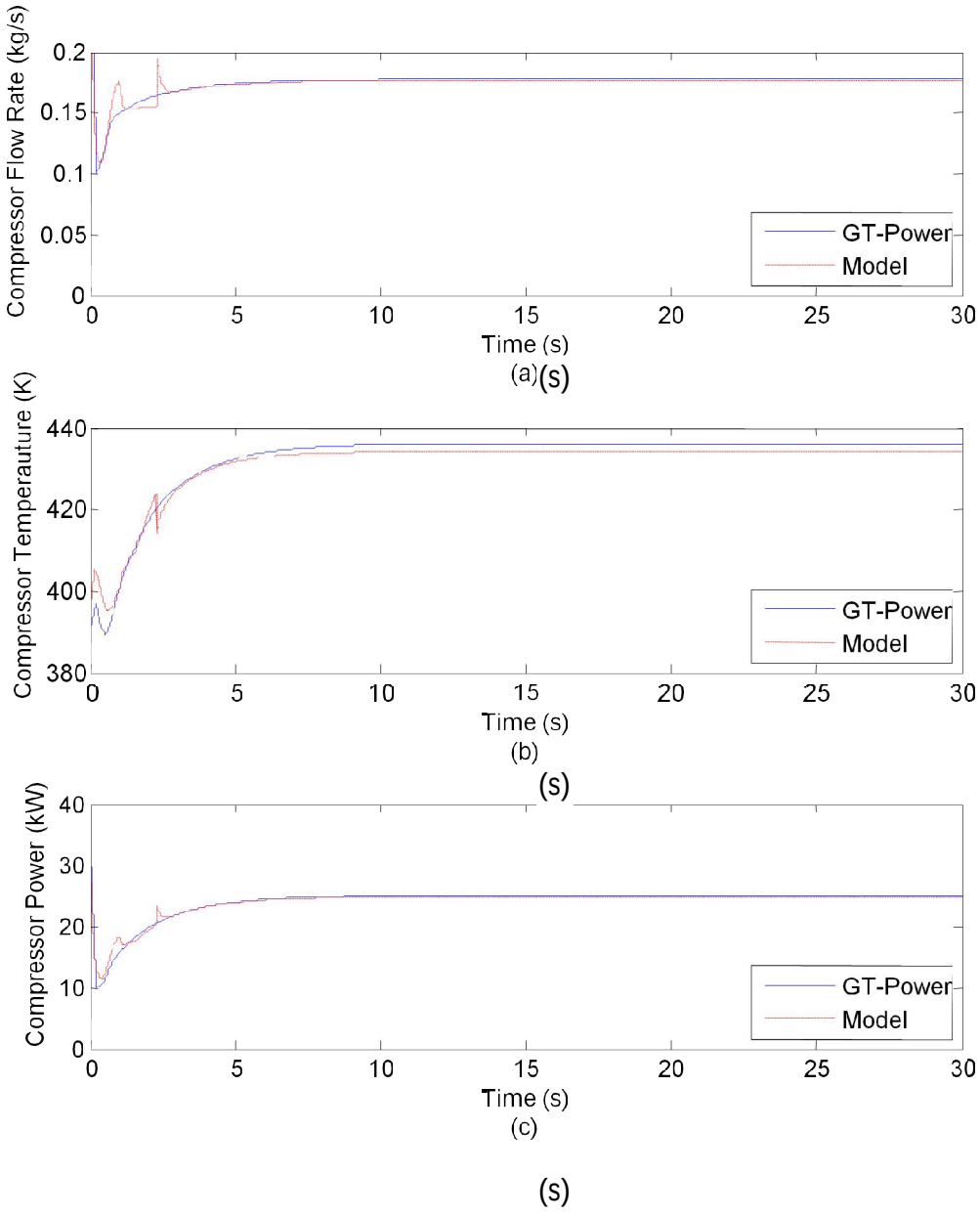

Figure 6.42. Unit verification: (a) compressor mass flow rate, (b) compressor temperature output, (c) compressor power output.

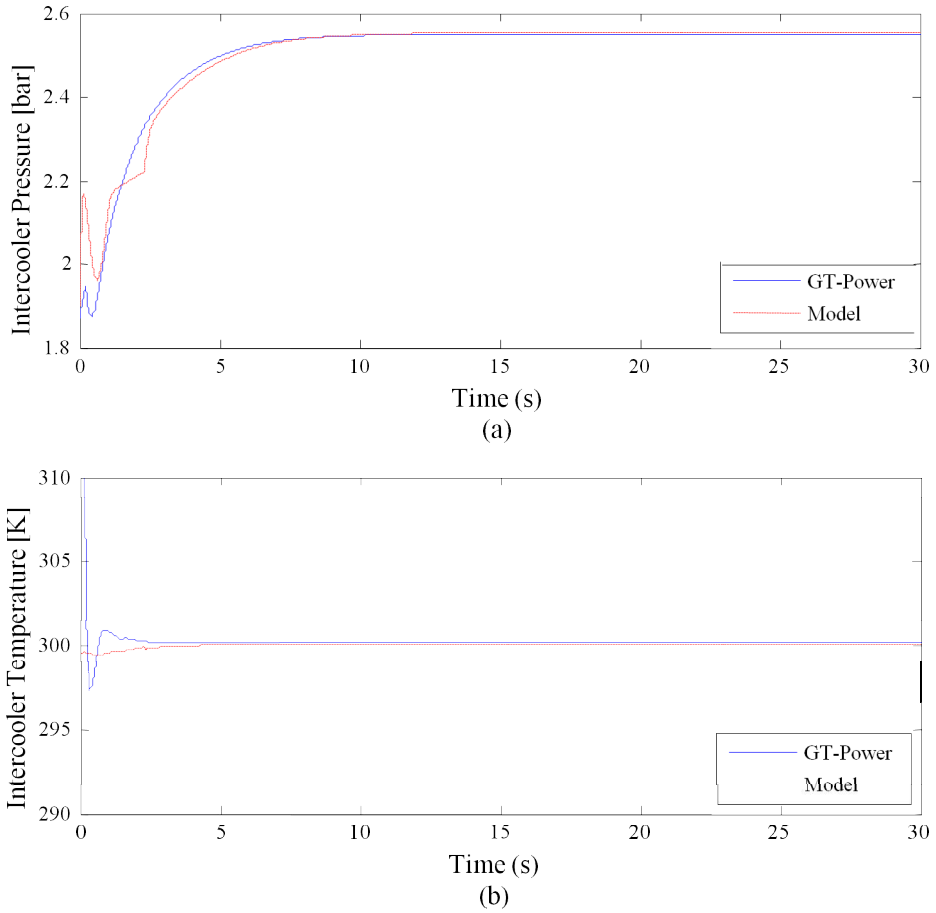

Figure 6.43. Unit verification – intercooler: (a) boost pressure, (b) boost temperature.

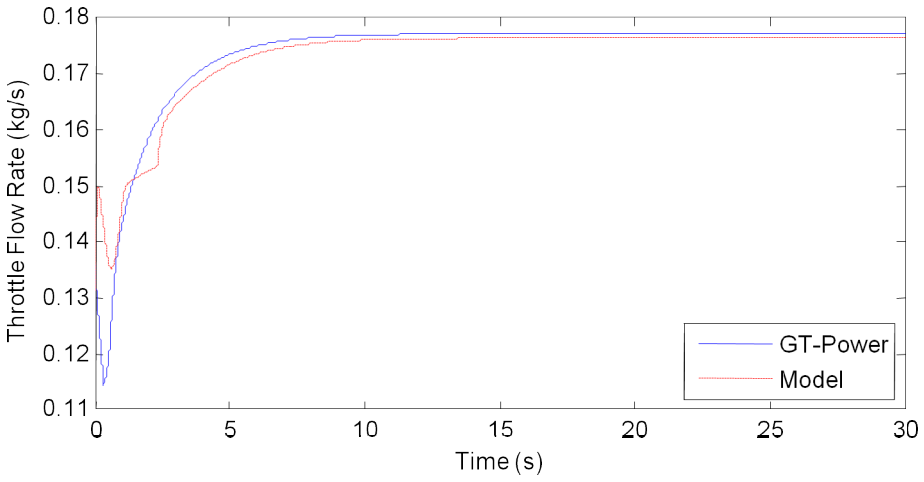

Figure 6.44. Unit verification - throttle flow rate.

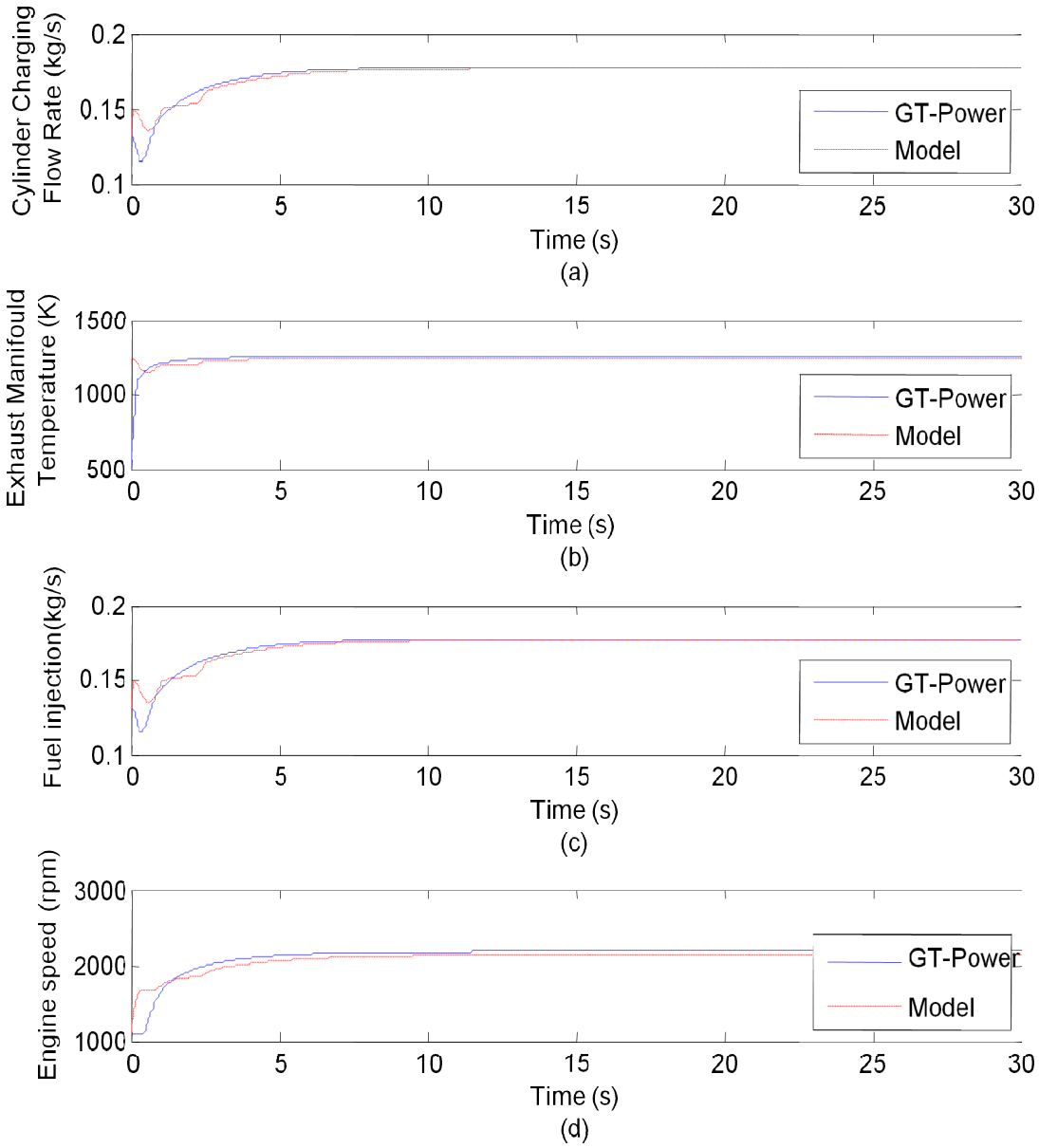

Figure 6.45. Unit verification – engine: (a) cylinder flow rate, (b) exhaust temperature, (c) fuel injection, (d)engine speed.

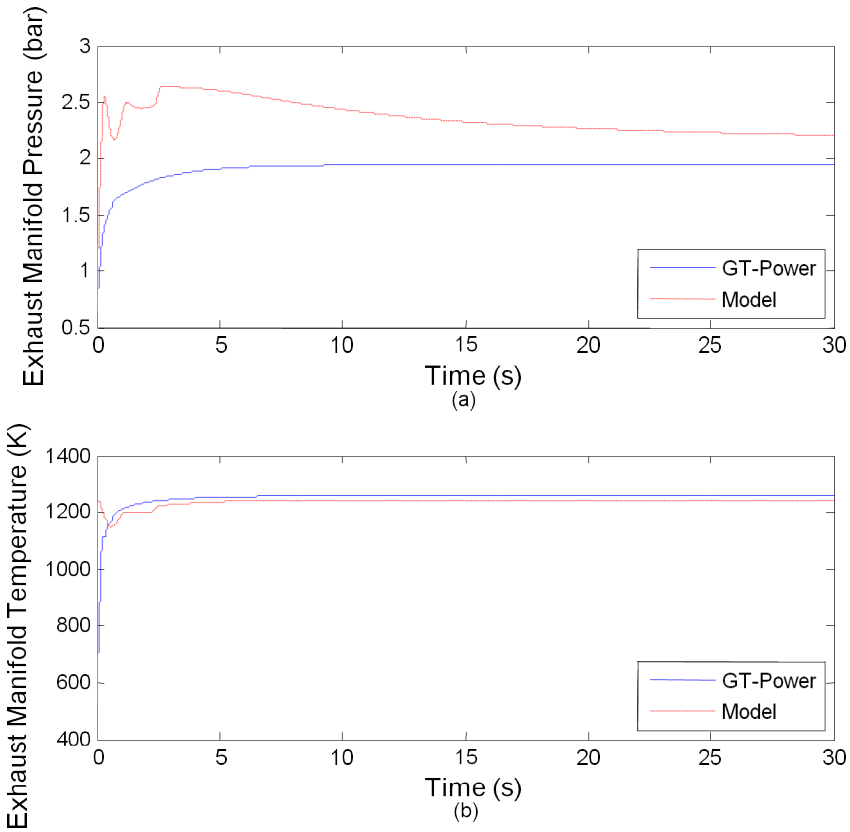

Figure 6.46. Unit verification - exhaust manifold: (a) pressure, (b) exhaust temperature.

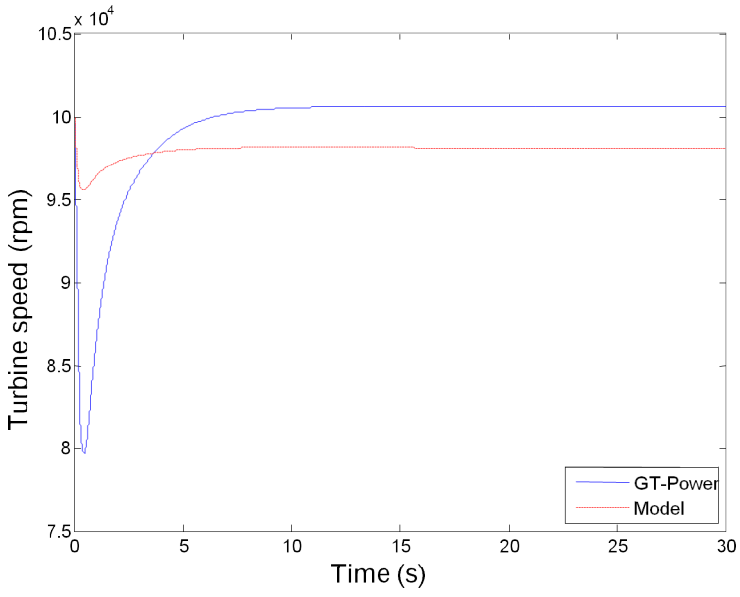

Figure 6.47. Unit verification - turbine speed.

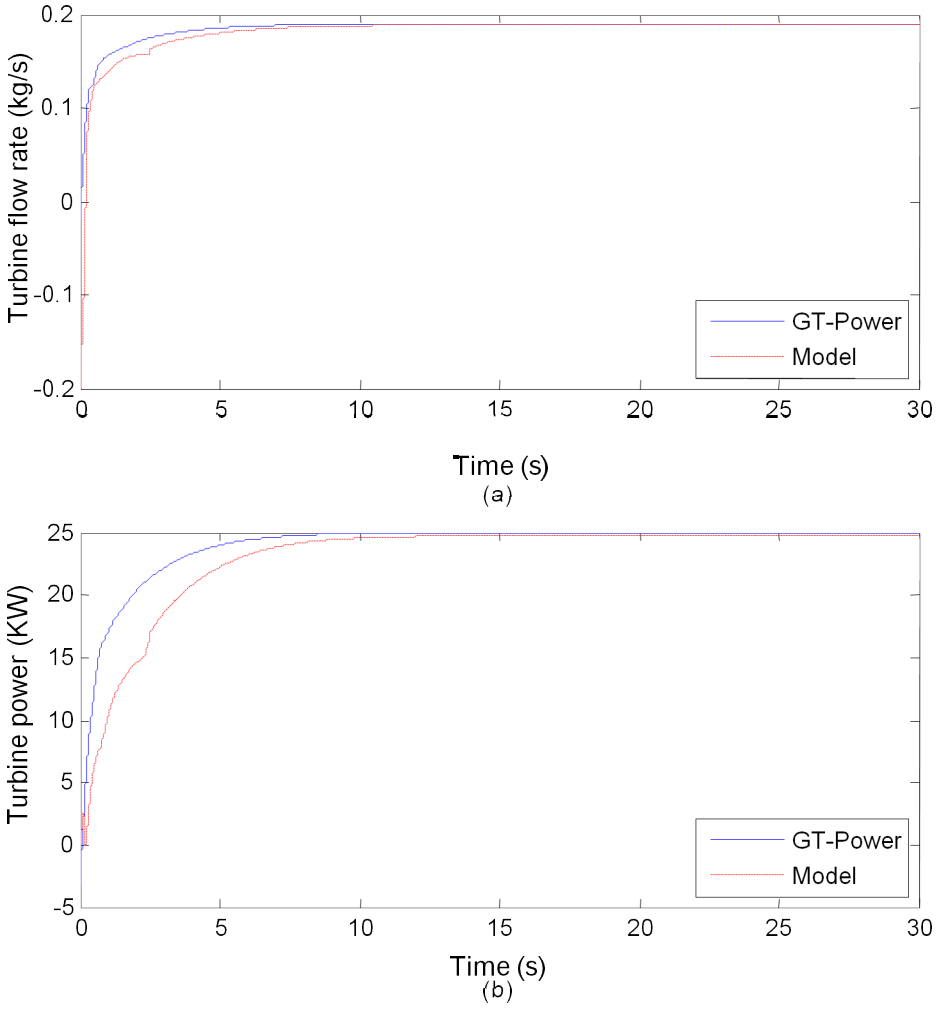

Figure 6.48. Unit verification: (a) turbine flow rate, (b) turbine power.

6.4.2 Transient State Verification

The transient dynamic of the MVEM is critical for the system model verification. Because of the inevitable model error in the unit model, the serial interaction between each part and the feedback effects from the turbocharger loop makes it difficult to test the model for a given input. The verification condition was defined based on the engine speed, which is the most important variable for power-train control. Engine inputs and other internal variables, manifold pressure and flow-rates for instance, were investigated accordingly with the GT-Power model. The

simulation results and comparison with the GT-Power data are listed Figures from Figure 6.49 to Figure 6.58 as follows.

Throttle:

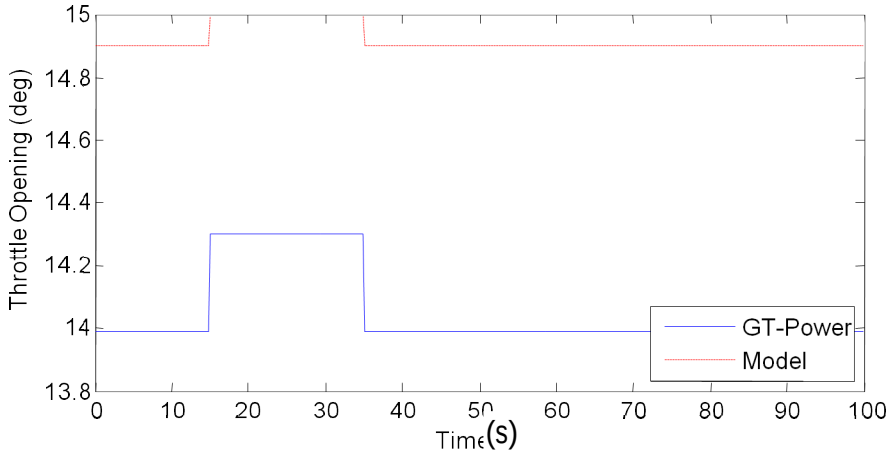

Figure 6.49. Throttle opening for transient verification.

Response in Engine Speed

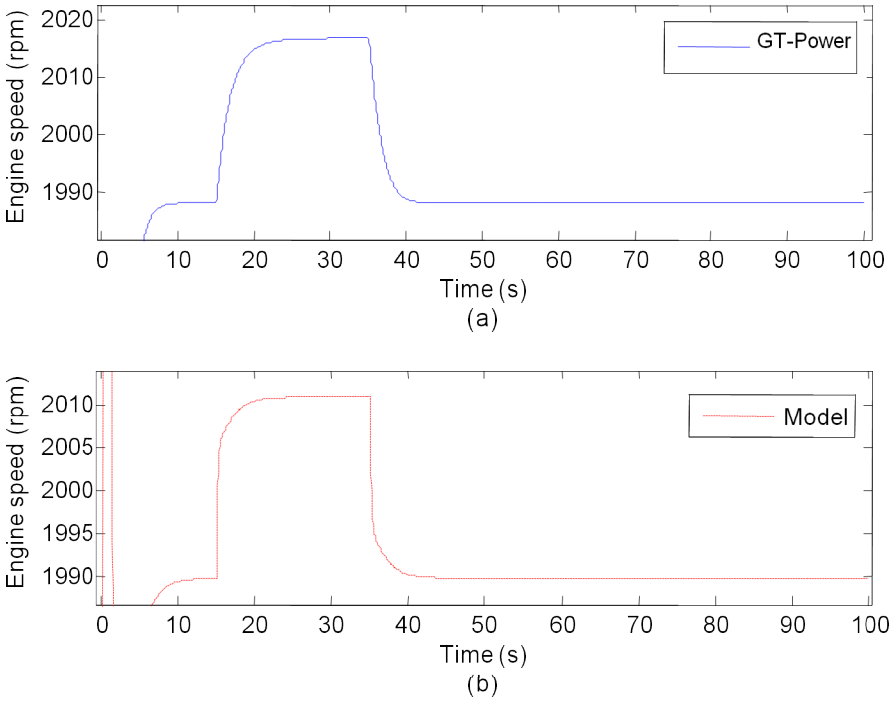

Figure 6.50. Engine speed dynamic: (a) in GT-Power, (b) in model.

Compressor:

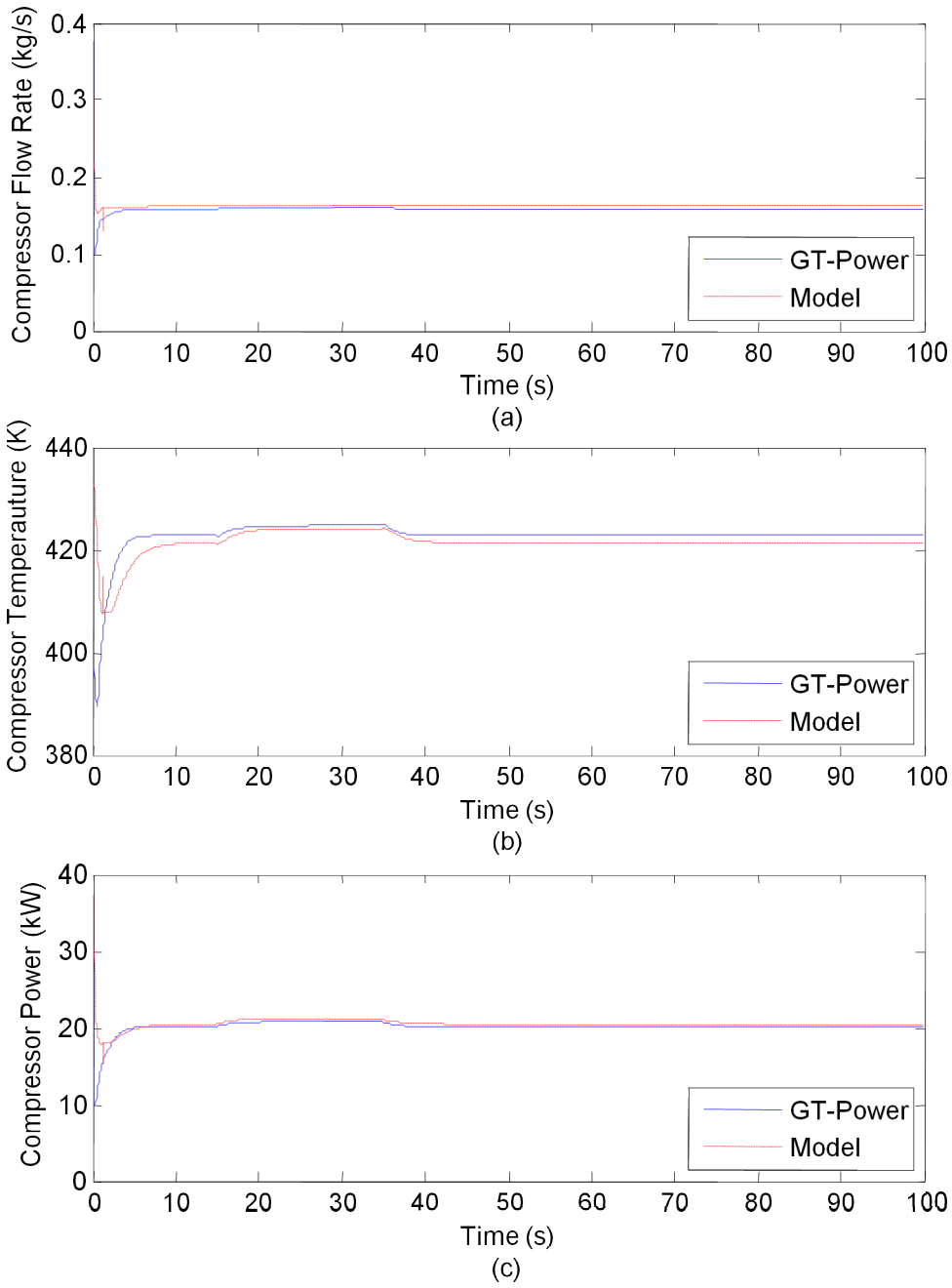

Figure 6.51. Compressor dynamic transients: (a) flow-rate, (b) temperature, (c) compressor power.

Intercooler:

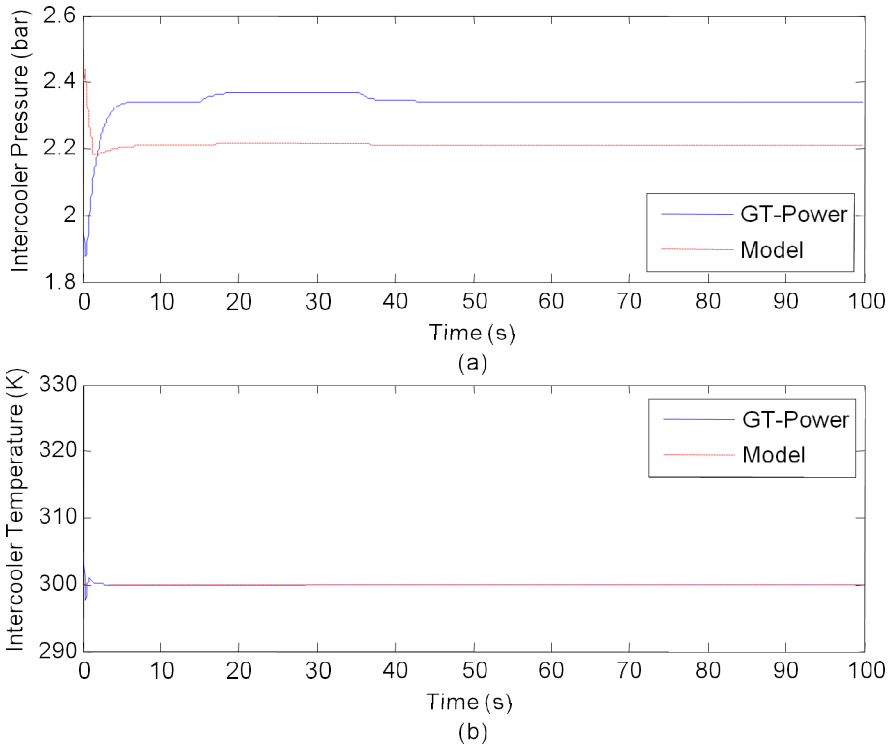

Figure 6.52. Intercooler transients: (a) pressure, (b) temperature.

Throttle:

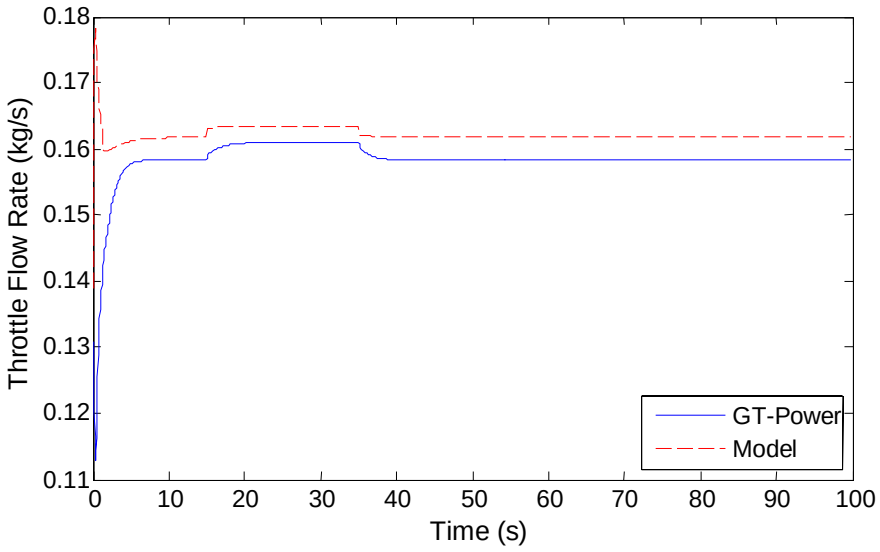

Figure 6.53. Throttle flow rate transient.

Intake Manifold:

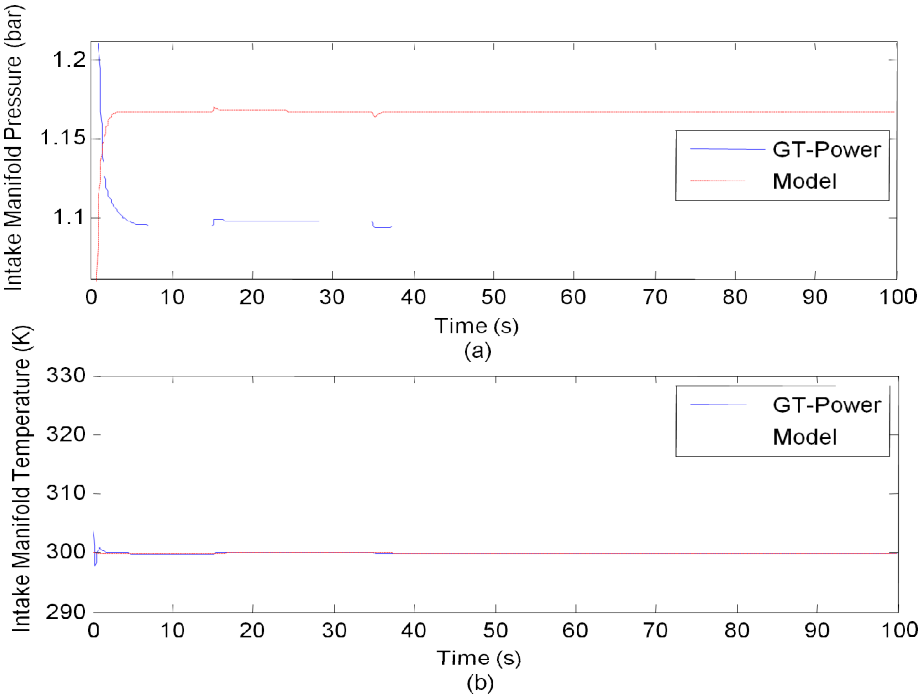

Figure 6.54. Intake manifold transients: (a) pressure, (b) temperature.

Turbine Speed:

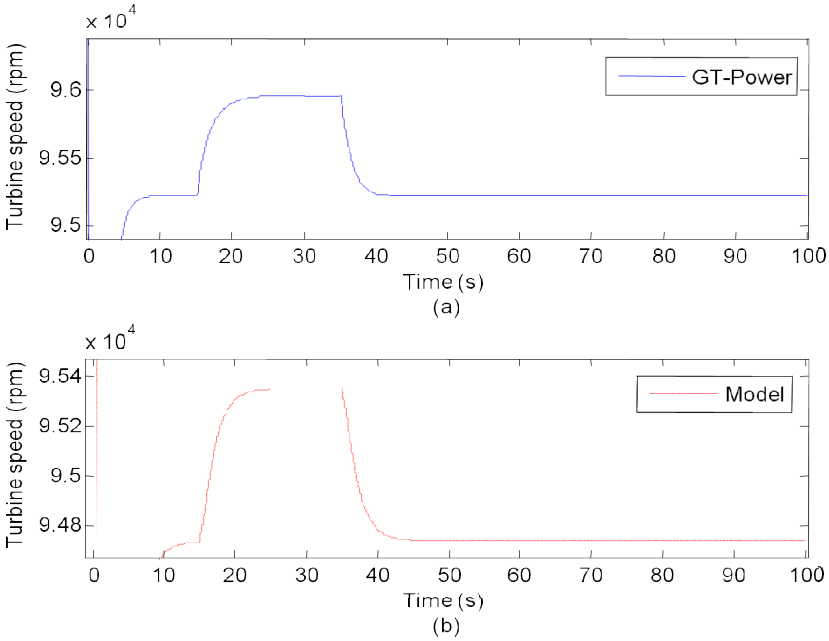

Figure 6.55. Turbine dynamics: (a) in GT-Power, (b) in MVEM.

Engine Cylinder:

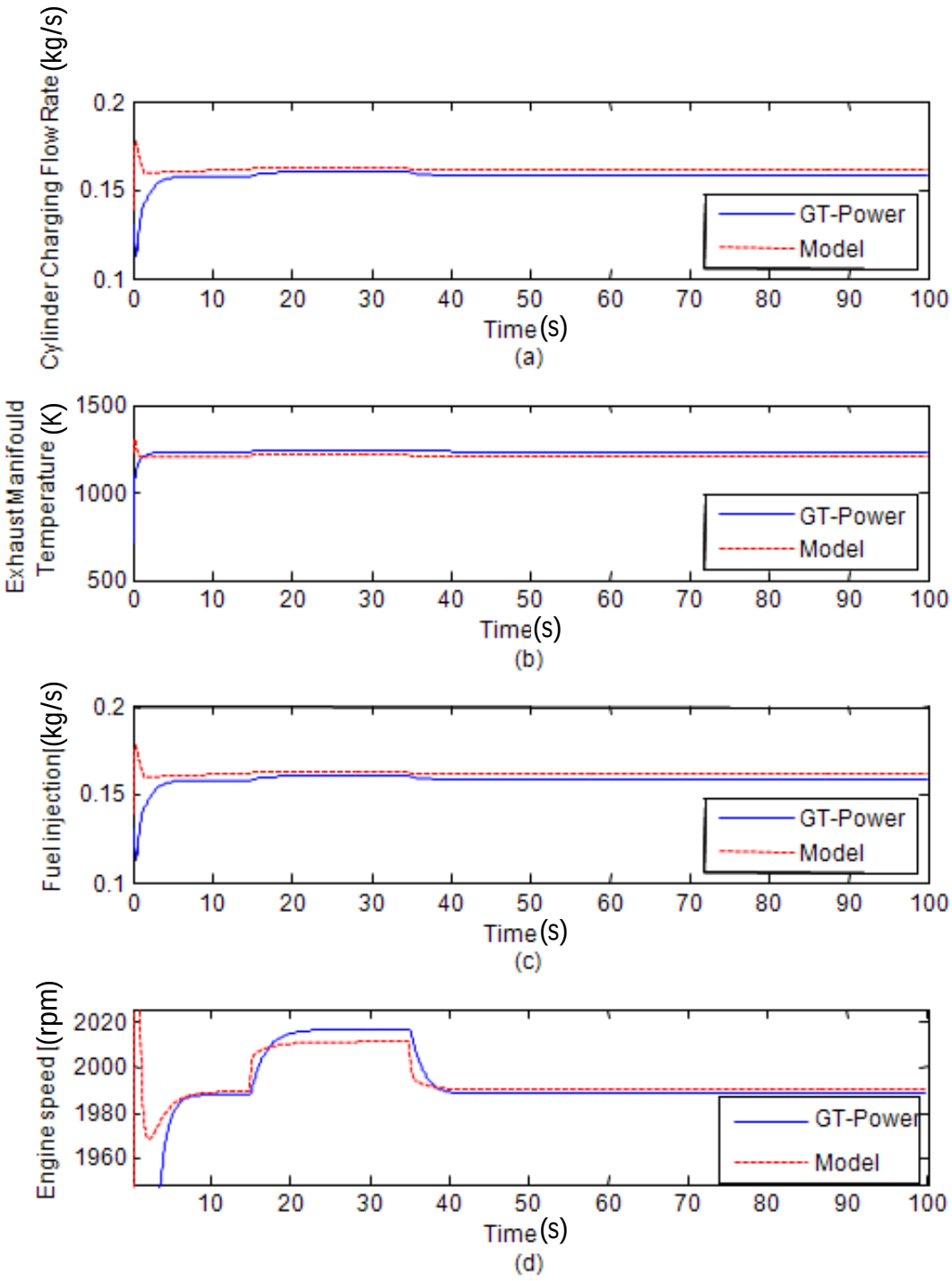

Figure 6.56. Engine cylinder transients: (a) charging flow-rate, (b) exhaust temperature, (c) fuel injection, (d) engine speed.

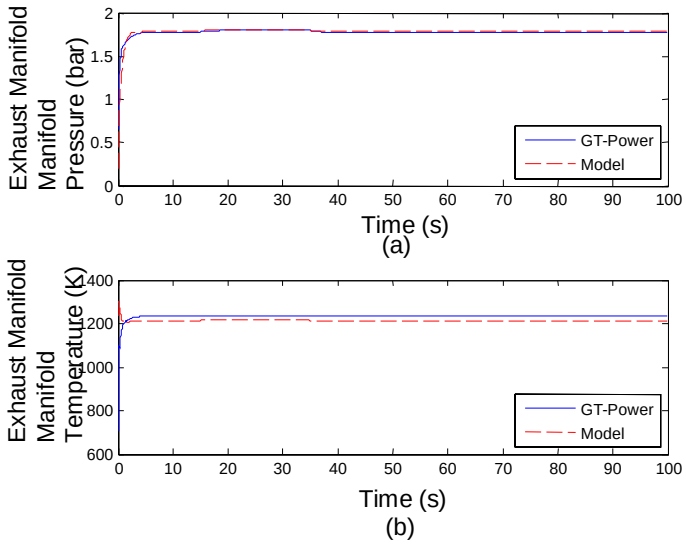

Figure 6.57. Exhaust manifold transients: (a) pressure, (b) temperature.

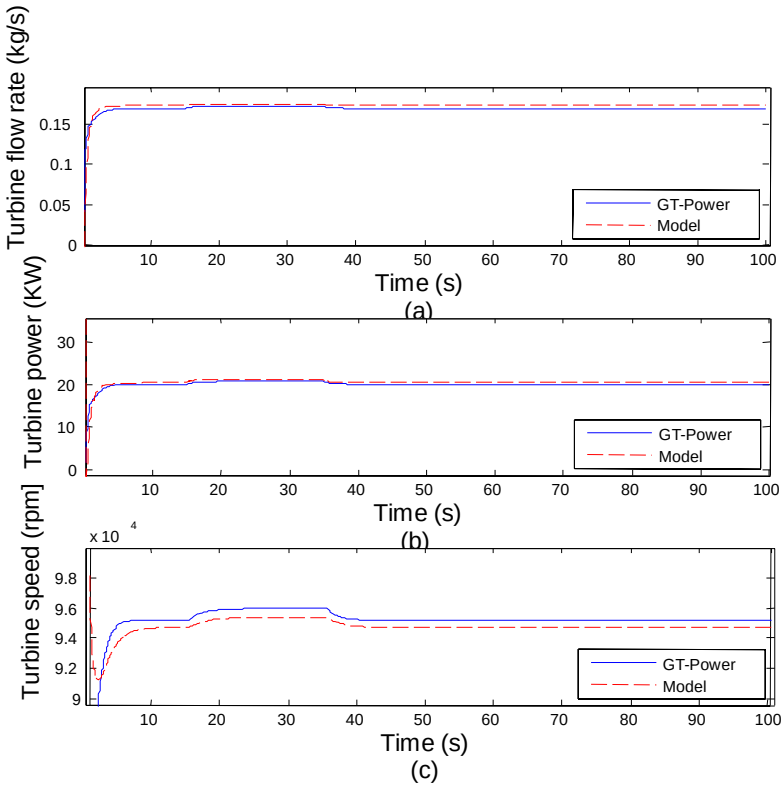

Figure 6.58. Turbine transients: (a) flow-rate, (b) power output, (c) speed.

Because of the steady-state error existing in parts, the throttle opening was chosen to get a similar engine response for the transient verification purpose. The opening in the MVEM steps from 14.9 degree to 15 degree at 15 second, then back to 14.9 degree at 35 second, corresponding to the opening in the GT-Power of 14 degree to 14.3 degree at 15 second, then to 14 degree at 35 second in Figure 6.49. As shown in Figure 6.50 and Figure 6.55, the major concerns in the power-train control are the engine speed and turbine speed. The transient process of the MVEM has a settling time of 10 second in Figure 6.50 (b), compared to the similar settling time of 13 second. At the same time, the turbine dynamic shows a close match in the transient characteristics and value. The steady-state value is not worth comparing so far, because of the steady-state error in parts. But the steady-state error could be eliminated by the compensation in the efficiency parameters, for instance, in the turbine efficiency or volumetric efficiency.

The internal variables of the compressor are shown in Figure 6.51, the flow rate, temperature and power output follows the date from the GT-Power in transient and steady state. The intercooler variable of pressure has an error of 0.1 bar out of 2.2 bar in steady state, but has a similar trend in the transient in Figure 6.52 (a). The intercooler outlet temperature has an identical value with the GT-Power data in Figure 6.52 (b). The throttle flow rate from the MVEM in Figure 6.53 has a difference in steady-state from the GT-Power because of the difference of upstream and downstream pressure from the manifold in Figure 6.54 (a). The cylinder charging in Figure 6.56(a) and fuel injection in Figure 6.56(c) also follow similar transients as they are defined by the throttle flows. As mentioned formerly, the engine speed follows the GT-Power data's transient in time as shown in Figure 6.56(d). The exhaust manifold variables in Figure 6.57 are the key for the turbine control; the turbine speed in Figure 6.58(d) shows the consistency of the MVEM in transient with the 1D detail model.

The consistency of the MEVE in both steady-state and transient state gives it the capability to represent the engine operation for control design. For control design purposes, the state space model can be further extracted by using the Simulink function.

6.5 Conclusions

A control oriented mean value engine modeling process from the 1D detail model is discussed. The goal of this modeling discussion is to demonstrate the feasibility of a new approach for an engine model. The MVEM is established from software simulation data instead of engine test

data, so the cost and time to develop the model is reduced. There is good agreement between the modules and the detail model. The main features of this novel modeling method are summarized as follows.

It is a cost effective modeling method to keep sufficient accuracy while reducing the complexity. For control design application, simplified models are appreciated because large amounts of testing simulations are needed to run during the initial design. Instead of running the engine in a test cell, detailed simulations are conducted to extract the dynamic of each engine sub-system. Risks and accidents could be avoided during the initial engine design process. Some detail modes could be inherited from the former engine. Control development can be conducted with other designs simultaneously.

Computation speed is dramatically increased for the new model. The new model consists of lumped parameters or simple nonlinear polynomials. No iterating computation for a differential equation is needed in the MVEM based simulation. Computation time could substantially be saved by using the MVEM.

Accuracy is slightly compromised due to the neglect of heat losses, approximations of temperature calculation over a wide range of operation points are compared with the detail model. However, the new MVEM still keeps the capability to predict engine behavior for dynamics analysis of the complex engine system. As the parameters go through a wide range of simulation data, all the operating conditions will be covered in the new model too.
Each model of the engine module is reusable for other specific engines. Only the model parameters need to be identified again. They could be extended to a more detail parameter lumped model if a more accurate prediction is necessary.

The new modeling method has a certain commercial value, as it can be included into a commercialized software package to enhance the software function. All the modeling data are already available once the detail model was developed. After the operation parameters are defined, the software could run the sub-routine to extract the MVEM automatically. The trade-off of model accuracy and computation speed was explored and evaluated for the developed mean value model, compared with the 1D detail model.

The feasibility of a new modeling approach was investigated in detail. The control oriented models, like the state space model, the transfer function model can be extracted further. The

Simulink MVEM model can be easily included in the control design environment. Control verification can be conducted with integrated simulation back to the 1D detail model before conducting the HIL and engine testing.

The dynamic term is introduced and included in the volumetric efficiency model. Better transient accuracy is obtained from comparison with the original data.

7 LEAN NO_x TRAP STORAGE MODEL

7.1 Model Development

7.1.1 Description of LNT Operation

The understanding of the characteristics and chemical kinetic processes of LNTs is necessary to implement a practical system model for the purpose of diagnosis and control. The concept of the lean NO_x trap catalyst, also referred to as the NO_x adsorber, has been developed based on acid-based washcoat chemistry. It involves adsorption and storage of NO_x in the catalyst washcoat during lean driving conditions and releasing it under rich operation. The released NO_x is catalytically converted to nitrogen. The NO_x trapping and purging mechanism is illustrated in Figure 7.1. The catalyst washcoat combines three active components: an oxidation catalyst (e.g. Pt), an adsorbent (e.g. barium oxide, BaO), and a reduction catalyst (e.g. Rh).

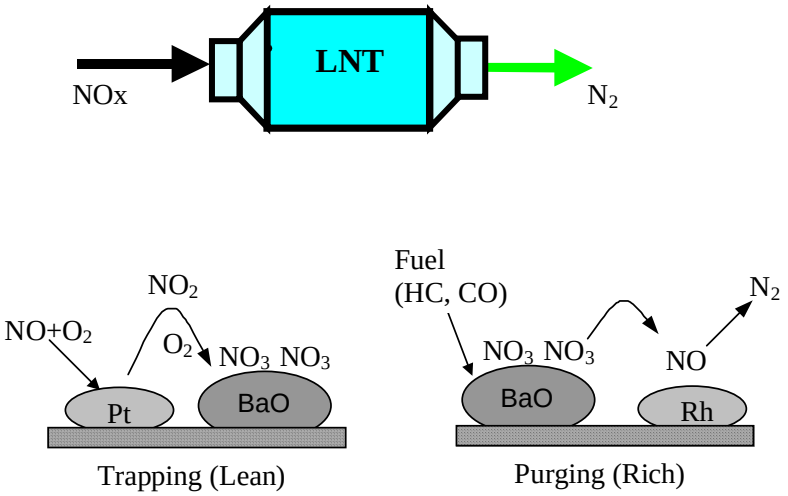

Figure 7.1. LNT NO_x trapping and purging mechanism.

The adsorption process involves two steps, as represented by Eq.(7-1) and Eq.(7-2), which occur during normal lean engine operation. NO_x emissions from the diesel engine are typically composed of 90-95% nitric oxide (NO). In the first step, the nitric oxide reacts with oxygen on active oxidation catalyst sites to form NO_2. The second step involves adsorption of NO_2 by the storage material in the form of an inorganic nitrate (Kabin, et al., 2004). When the engine runs under excessive fuel conditions or at elevated temperatures the nitrate species become thermodynamically unstable and decompose, producing NO or NO_2, according to Eq.(7-3).

Under rich conditions, the released NO_2 is converted to N_2 by the reductant, such as CO, H_2 and HC, over the reduction catalyst (e.g. Rh). The oxygen in NO_x is released in the form of oxygen gas and carbon dioxide. One of the possible reduction paths is shown by Eq.(7-4).

$$NO + 1/2O_2 = NO_2 \tag{7-1}$$

$$BaO + 2NO_2 + 1/2O_2 = Ba(NO_3)_2 \tag{7-2}$$

$$\begin{aligned} Ba(NO_3)_2 &= BaO + 2NO + 3/2O_2 \\ Ba(NO_3)_2 &= BaO + NO_2 + 1/2O_2 \end{aligned} \tag{7-3}$$

$$NO + CO = 1/2N_2 + CO_2 \tag{7-4}$$

This simplified set of reactions allows for an understanding of the basic NO_x adsorber chemistry and abstracting the mathematical model from the basic analysis. The storage phase is more important for lean-rich switch control and diagnosis. Effective control of the NO_x absorption processes allows for the optimization of the storage characteristics of the available capacity of the LNT to avoid NO_x break through at greatest extent and significantly reduce the NO_x emission while improving the fuel efficiency. In this study, only the storage process of LNTs was investigated.

7.1.2 Development of LNT Adsorption Model

NO_x adsorption in LNT during lean operation is a combined physical and chemical process. The NO oxidation rate and the mass transfer rate are the two important factors that affect the storage of NO_x in LNT. The NO_x storage rate is a function of LNT storage capacity, LNT internal brick temperature, exhaust gas mass flow rate (MAF), and inflow NO_x concentrations. How to classify these factors and propose a good model structure is the first step of model design.

7.1.3 The Effect of Temperature on NO Oxidation Rate

The NO oxidation rate is an important factor that affects the storage of NO_x in LNT. As shown in Eq. (7-1), NO is first oxidized over Pt by oxygen to NO_2, which is ready for next step adsorption. In-bed temperature controls the oxidation rate of NO to NO_2. The oxidation rate increases while the temperature increases. When there is enough storage sites in the catalyst

substrate for NO_x, NO_x storage at low temperatures is limited primarily by the low NO oxidation rate. But the oxidation rate decreases when the in-bed temperature goes beyond a certain limit due to reducing equilibrium NO_2/NO ratios. This is because nitrates begin to decompose at higher temperature, even under the lean condition with extra O_2 presented. Once the NO converted to NO_2, the chemical adsorption and reaction kinetics will contribute to the NO_x storage mechanism by forming the chemical bonds between NO_2 and the substrate as shown in Eq. (7-2). The NO_2 storage rate will be controlled by the chemical reaction rate between NO_2 and BaO. Because chemical adsorption is a monolayer adsorption, BaO will no longer be available after it captures two NO_2 molecules. To simplify the model derivation, we define the reaction rate as the change of the number of adsorbent sites that are proportional to the moles of BaO on surface per unit area.

$$r_{ad} = (1/S)(ds/dt) = rate \tag{7-5}$$

where s is the number of adsorbent sites, S is the area of available site for NO_x storage. According to Arrhenius law (Butt, 2000), the LNT in-bed temperature and the concentration of NO_x are the two main factors affecting the reaction rate as in an equation of mass action law (Butt, 2000)

$$r_{Nox} = k(T)(C_{NOx})^n \tag{7-6}$$

where $k(T)$ is the reaction coefficient and is a function of temperature T. C_{NOx} is the concentration of the reactant, that is, NO_2 in this case. The exponent n is the order of the reaction. In this proposed model, the reaction order is assumed as pseudo-first order for simplicity at reasonable accuracy. The temperature dependent reaction coefficient $k(T)$ is given by exponential form called the Arrhenius equation (Butt, 2000):

$$k(T) = k^0 e^{-E/RT} \tag{7-7}$$

where E is the activation energy of the reaction, R is the gas constant, T is the temperature, and k^0 is the pre-exponential factor. The reaction coefficient is the exponential function of temperature as commonly expected.

Based on analysis of chemical adsorption mechanisms and the effect of temperature on the reaction rate and the nitrates decomposition, the NO oxidation rate varies in a mountain shape during the overall span of temperature range. The reaction rate of NO is difficult to measure, but the oxidation rate could be represented by NO_x conversion efficiency when the mass flow rate is kept constant. This analysis can be verified by the experimental results from Dou and Balland's work, as illustrated by an example curve of a characteristic temperature window in Figure 7.2 (Dou and Balland, 2002).

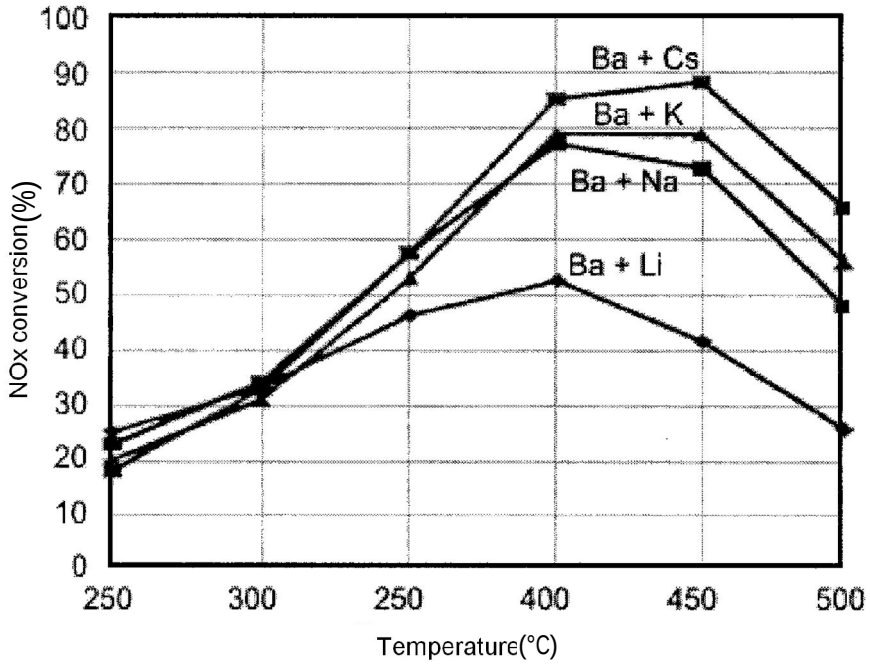

Figure 7.2. NO_x conversion temperature window (Dou and Balland, 2002).

In order to model the NO_x storage rate with this temperature characteristic, we define the NO_x storage capacity function $\Sigma(T)$, which equivalently represents the temperature's effects on the reaction rate under constant concentration. NO_x storage capacity function can be modeled using a Gaussian function of the temperature T in Eq.(7-8), as shown in Figure 7.3.

$$\Sigma(T) = \Sigma_{\max} e^{-\frac{(T-T_m)^2}{2T_w^2}} \tag{7-8}$$

where T_m is the centre temperature of peak value, T_w is the temperature span, and $\Sigma_{\max}(T)$ represents the designed maximum mass of NO_x which could be converted and stored in a given

LNT. Lean NO_x traps exhibit significant conversion efficiencies, in excess of 80-90%, if temperature could be controlled within an optimized range. The maximum storage was achieved at around 300-500^{o}C. At extreme high temperatures, sintering is found to lead to a substantial loss of catalytic activity. Therefore temperature control is critical for adequate utilization of LNT functionality.

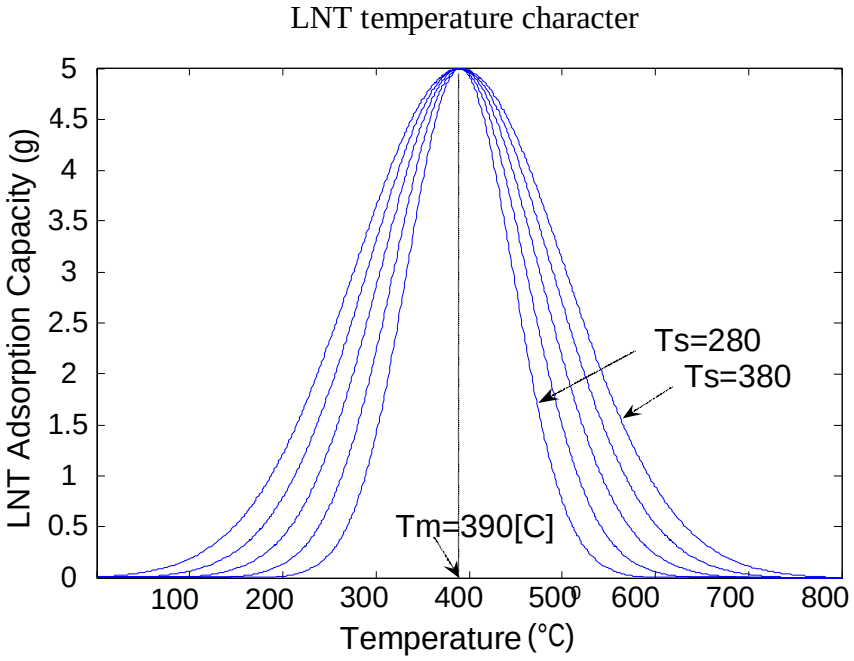

Figure 7.3. Lean NO_x trap storage model parameters (Kim, et al., 2003).

With the ideal maximum reaction rate, the equivalent surface area of the substrate for NO_x storage is written as

$$S(T) = S_{\max} \cdot \left(1 - \frac{x}{\Sigma_{\max} e^{-\frac{(T-T_m)^2}{2T_w^2}}} \right) \tag{7-9}$$

where S_{max} (m^2) is the ideal maximum available substrate area, which represent the corresponding number of BaO sites. x represent the stored mass of NO_x . The term in bracket is the fraction of left area of substrate available for storage. The NO_x storage rate is not only depending on the how much sites available, but also depending on the number of NO_x molecules accessing to the storage sites.

7.1.4 The Effects of Mass Flow Rate on Storage Model

Once NO and NO_2 in the reaction reach equilibrium, the NO_x storage is controlled by the mass transfer processes. The chemical reaction and adsorption happen only on the surface of substrate of the LNT. The physical geometry and the mass transport process of NO_x are two important factors affecting the number of NO_x molecules contacting with the substrate sites. To increase the surface area of the substrate for better adsorption, most catalyst converter use a honeycomb structure as shown Figure 7.5. Theoretically, the smaller the tube size, the better the adsorption efficiency, but will increase the gas flow resistance and backpressure. In order to trap the NO_x, the NO_x molecules must have chance in contact with the substrate. For a NO_x molecule, there is movement in the radial direction due to diffusion when it travels alone the axial direction of each channel. There exists a parabolic profile of velocities for the exhaust air flow to travel alone each channel with maximum velocity at the center and zero at the wall. Hence, an element with radial position near the wall will require a larger amount of time to traverse a given length of tubing than will an element near the center. There will exist a distribution of times required for elements at various positions to traverse the given length. There is a minimum retention time for the NO_x molecules to penetrate to the wall substrate. As a result, when the exhaust mass flow rate increases, some of the NO_x molecules in the center will not have enough time to diffuse to the wall when they left the channels and more NO_x molecules will by-pass the channels without contacting the substrate. When the mass flow rate reaches certain limit, the mass transfer of the NO_x in radial direction reach saturation.

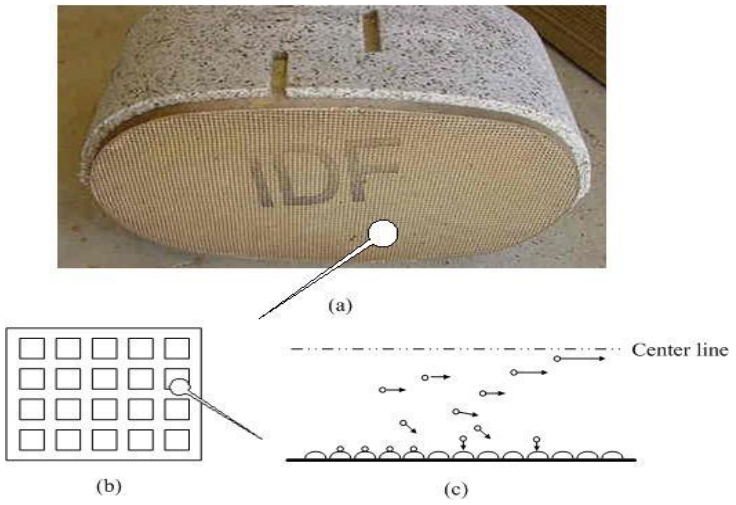

Figure 7.4. Honeycomb catalyst structure and element motion analysis.

The adsorption rate is controlled by the in-bed temperature, the storage rate is also affected by how many NO_x molecules have chance to participate the chemical reaction per unit area.

$$N(t) = \frac{1}{S_{\max}} C_{Nox}(t) M(t) \tag{7-10}$$

where $N(t)$ is the available NO_x molecules close to the substrate surface. $C_{Nox}(t)$ is the concentration of NO_x in exhaust gas. $M(t)$ is the mass flow rate of exhaust gas. Theoretically, the increase of exhaust gas mass flow rate will lead more NO_x molecules available for reaction, then the NO_x storage rate will also increase. As discussed above, there is saturation phenomenon of mass transfer, which is often ignored in some available model. The saturated phenomenon could happen when the exhaust mass flow rate (MAF) exceeds a certain value, which depends on the geometry of the LNT. Some of the NO_x will break through directly without having chance to be captured. To consider this saturation, a mass flow rate filter is designed to limit the mass transport rate as:

$$M' = M_{sat}(1 - e^{-kM(t)}) \tag{7-11}$$

Where $M(t)$ is the real exhaust gas mass flow rate, M_{sat} represents the threshold of mass flow rate and constant *k* could be used to adjust the filter function. The threshold of mass flow rate is the limited flow rate above which extra NO_x in the exhaust gas will break through LNT directly without adsorption. Figure 7.5 shows the response of the filter function to variations in MAF and *k*. After introduction of mass flow rate filter, the available NO_x molecule number on per unit area becomes:

$$N(t) = \frac{1}{S_{\max}} C_{Nox}(t) M_{sat}(1 - e^{-kM(t)}) \tag{7-12}$$

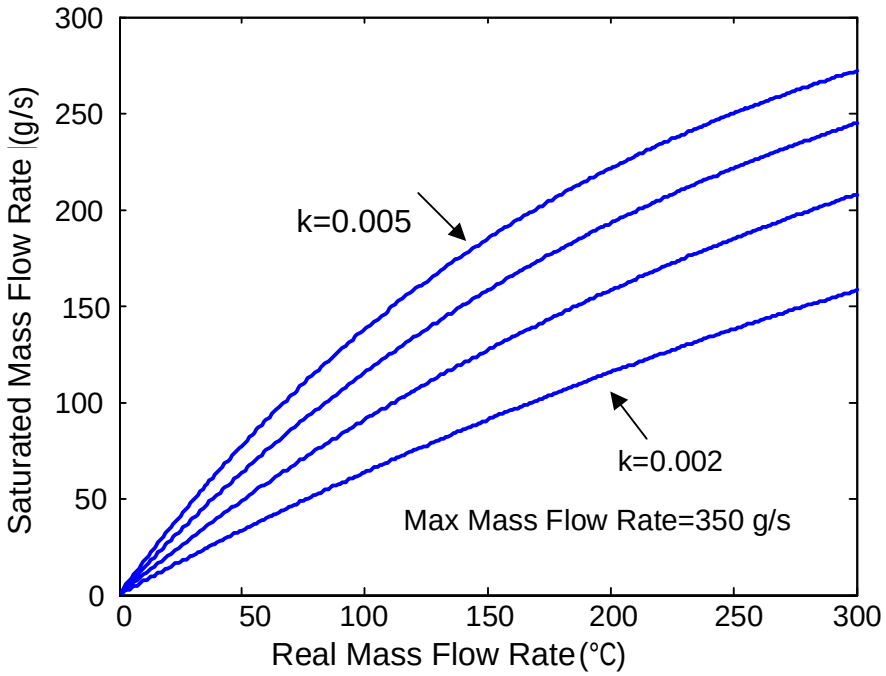

Figure 7.5. Mass flow-rate transfer function.

According to the analysis of the chemical reaction and physical process of NO_x adsorption in the LNT, the NO_x storage rate is the function of the available storage capacity and the available NO_x molecules at substrate site. Based on equations (7-9) and (7-12), a differential equation model is proposed to simulate the NO_x storage rate. Under lean conditions, the NO_x storage rate of the LNT depends on the exhaust gas mass flow rate, the inflow NO_x concentrations, the internal brick temperature of LNT, and the real available capacity of LNT. The system identification model of LNT during lean operation ($\lambda \geq 1$) (λ is the relative air fuel ratio) (Heywood, 1988) can be expressed as:

$$\frac{dx}{dt} = \theta \cdot C_{NOx} M_{sat} (1 - e^{-kM}) \left(1 - \frac{x}{\Sigma_{\max} e^{-\frac{(T - T_m)^2}{2T_w^2}}} \right) \qquad 0 \leq x \leq \Sigma_{\max} \qquad (7\text{-}13)$$

Where:

x is the mass of NO_x stored in the LNT (g)

C_{NOx} is the inflow NO_x concentration (ppm)

M_{sat} is the threshold of the exhaust gas mass flow rate for the LNT (g/s)

M is the exhaust gas mass flow rate (g/s)

κ is a constant

$\Sigma_{\max}$ is the maximum available storage capacity of LNT (g)

T is the internal brick temperature of LNT (ºC)

T_m is the central temperature of LNT adsorption Gaussian function (ºC)

T_w is the temperature span of LNT adsorption Gaussian function (ºC)

θ is the lump parameter of the model

The NO_x adsorption process inside LNT is very complicated and many factors are not practical to be included in the model, such as, non-isothermal condition inside LNT, NO_x concentration gradients in axial and radial direction, et al. The lump parameter θ is an adaptive parameter of the model to count for those factors not included in the model. Otherwise, the model can be very complex if all factors to be included and will be very difficult to be integrated in ECU for control. The lump parameter is very important for the model to be robust and adaptive. For different types of LNT and operating conditions, θ can be identified based on the data. Once the model is developed, for special application, θ can be adjusted online by further adaptive algorithm, which is useful to accurate control and diagnosis of LNT. A good control-oriented model should describe the main character of the system in a simple model structure to afford the real-time computing capacity of embedded control system with adequate accuracy. Another benefit to include the lump parameter in the model is to make this model to be adaptive to engine operating condition changes and unit-to-unit variability.

7.2 Model Validation and Analysis

Six test cycles were designed and run in a transient test dynamometer lab. The test data were collected and provided by a company to develop the proposed model, including exhaust gas mass flow rate, the air fuel ratio, the temperatures at the inlet and outlet of LNT, and the NO_x concentrations at the inlet and outlet of LNT. For confidential concern, this paper did not give much information on the details of test cycles and experimental setup. In addition, the model

validation is not complete because the design information of the LNT in tests, such as: temperature window, catalyst information, and LNT configurations are not provided by the company. The parameters of LNT used in the model are the general information available from the literature. The parameters for this LNT model were selected as: T_w = 190 °C, T_m =390°C, C_{max} = 5g, k= 0.0035, and M_{sat} = 320(g/s). This limits the quantitative comparison between the experimental results and the simulation. However, with limited information available, the model validation discussed here is still useful to show the trends how good the agreement between the model simulation compared with the test data. For the simulations, it was assumed that LNT was completely regenerated during every rich phase, which meant that the initial condition of LNT at each lean phase was clean.

Figure 7.6 shows the comparison of the model simulation and experimental results. The transient change of the major parameters, such as, temperature, the air fuel ratio, and the exhaust gas mass flow rate, are shown in Figure 7.6, too as the test cycle progresses. In general, the model simulation (dotted line) has a good agreement with the experiment data (solid line). However, some lean-rich cycles have bigger errors than others. One possible reason is that the rich modes in or those cycles were not fully executed and the trap was not completed regenerated. This will cause the differences between model simulation and test data.

The error of model simulation is analyzed using the following equations:

$$e(k) = \hat{x}(k) - x(k) \tag{7-14}$$

$$E(e) = \sum_k \frac{e(k)}{n}, \qquad k = 1,2,...,n \tag{7-15}$$

$$P = \sum_k \frac{e(k)}{x(k) \cdot n}, \qquad k = 1,2,...,n \tag{7-16}$$

where

k is the sampling point

n is the total sampling number

$x(k)$ is the NO_x storage in LNT from the experimental measurement

$\tilde{x}(k)$ is the model prediction of NO_x storage

e(k) is the prediction error at sampling point k

$E(e)$ is the overall mean of the error

P is the overall percent error for the cycle

The overall results show close agreement between the real NO_x storage and the model prediction. But there are still some errors during the irregular switch of air fuel ratios (A/F) in lean-rich cycles. At some points the accumulated error can be as high as 87%. At those points, air fuel ratio did not switch as programmed in the Lean and Rich model and caused fluctuation of A/F ratio. These changes will lead the irregular change of exhaust gas composition in LNT. Another error of the model could be caused from inaccurate temperature characteristic of LNT, which significantly affect the oxidation rate of NO during storage phase.

One limitation of the model is not including the effect of potential sulfur poisoning or trap aging. Further experiment investigation and model improvement are needed to make it applicable for transient engine operations in real time with instantaneous changes in exhaust temperature, the air fuel ratio and the exhaust gas mass flow rate.

7.3 Conclusions

A LNT storage model has been developed to predict the NO_x storage in the LNT. The NO_x storage rate in LNT is a function of LNT storage capacity, LNT internal brick temperature, exhaust gas mass flow rate, and inflow NO_x concentrations. The model validation shows close agreement between measurements and the predictions. This model can also be used to predict NO_x out from the LNT during lean operation. The comparison between the model prediction and the sensor measurement during lean combustion periods can be used to detect the failure and malfunction of a NO_x sensor. This system identification model can also be further developed to detect LNT malfunction by utilizing other sensor signals, such as dual oxygen sensors. Further improvement of this model should take into account sulfur poisoning and LNT aging effects, which must be imported into the model for practical applications. Additional data related to sulfur poisoning and aging will be required for model improvement and validation.

Six sets of data are used for statistic analysis of model simulation error, as shown in Table 7.1 The model lump parameter θ is identified at different mode with or without a mass flow rate filter. Based on the analysis of the mean of error and the deviation of error in NO_x storage, the model with filter could reduce the prediction error by 0.32% in the mean of error and by 0.57% in the deviation of error over the whole cycle period. It seems not much for the mean error of a whole cycle, but it is very significant during short periods at high mass flow rate. The saturating filter function and the saturating level can be further improved.

Table 7.1. Statistic analysis of model simulation error.

Lean/Rich Test Cycle No.	1	2	3	4	5	6	Mean Error
Model Lump Parameter θ (without filter)	0.080	0.083	0.081	0.081	0.078	0.082	
Model Lump Parameter θ (with filter)	0.074	0.077	0.076	0.076	0.072	0.076	
Mean of Error (g) (no filter)	0.0682	0.0528	0.0561	0.0572	0.0888	0.1110	1.45%
Deviation of Error (g) (no filter)	0.1131	0.0914	0.0767	0.0937	0.1812	0.1721	2.43%
Mean of Error (g) (filtered)	0.0491	0.0397	0.0452	0.0468	0.0737	0.0840	1.13%
Deviation of Error (g) (filtered)	0.0756	0.0617	0.0546	0.0698	0.1704	0.1261	1.86%

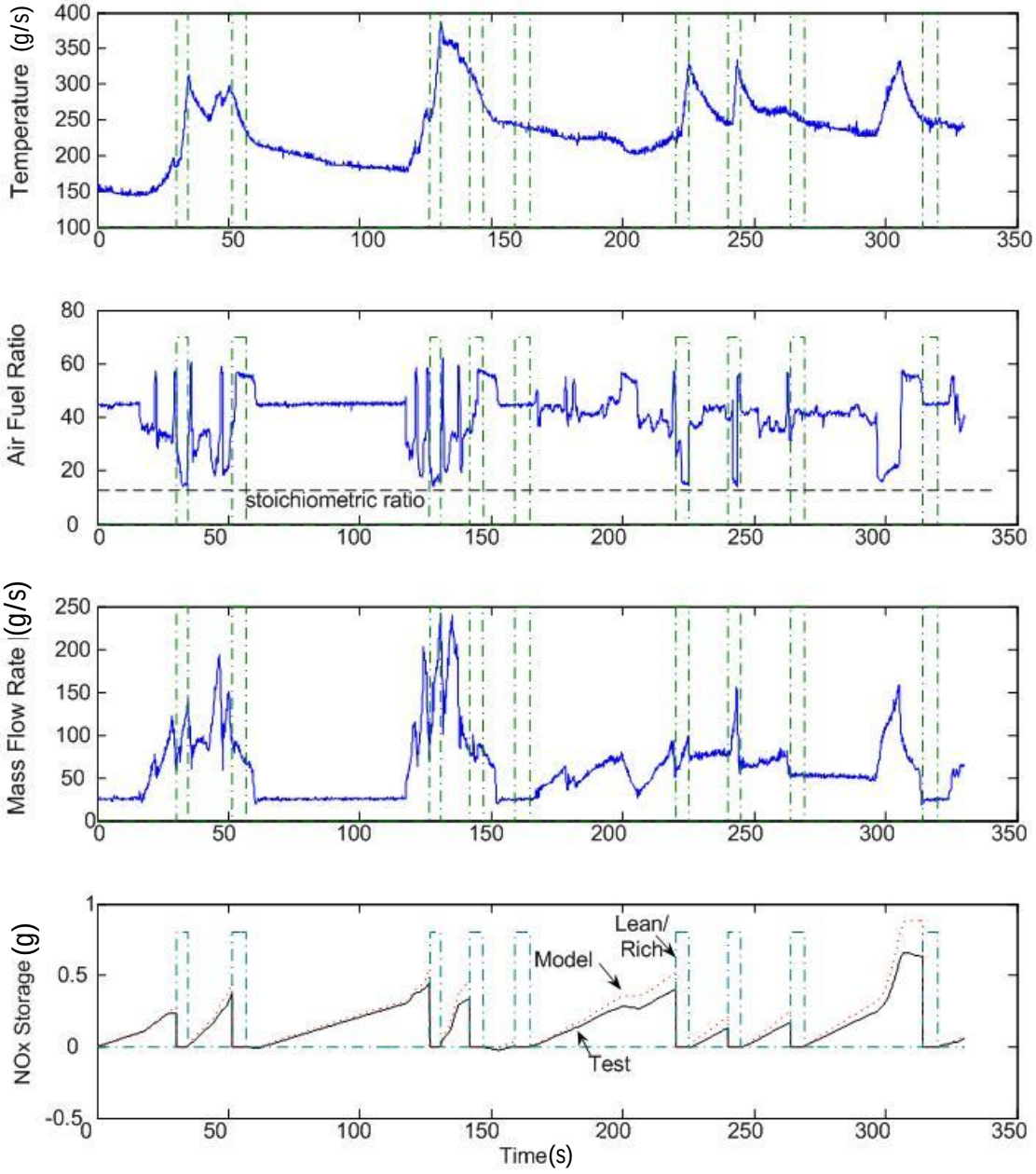

Figure 7.6. Comparison of model simulation and experimental data.

8 Conclusions and Recommendations

A new concept of the Stoichiometric Compression Ignition engine was tested in a new integrated 1D detail model environment with the following controllers designed for SCI engine operation: (1) Air-Fuel-Ratio control for stoichiometry; (2) power limiting for diesel operation; (3) idle speed control with enough robustness for low load disturbance; (4) the challenge of an all speed governing control design was discussed and analyzed for classical control design methods; and (5) a mean value SCI engine model was designed to facilitate model based control analysis and design. The subsystems of SCI-MVEM were verified with 1D detail model data obtained in the integrated simulation environment. The SCI-MVEM was tested against the 1D GT-Power model for steady-state and transient conditions. For the after-treatment system control and optimization, a lean-NO_x trap model was designed to be included into the general engine NO_x emission control, such as LNT operation and fuel efficiency optimization.

The highlights of the contribution and innovative ideas in this research are listed as follows:

1. Proposed that the integrated simulation environment of 1D detail engine model with ECU model
    a. facilitated the engine performance evaluation with control availability, and auto search and auto testing, and
    b. it provided a high fidelity platform for control, diagnosis design and verification.
2. Implemented a SCI engine in an integrated simulation environment.
3. Applied classical control design methods for SCI implementation in ISE, such as AFR, torque limiting, and idle speed control.
4. Introduced the pressure dynamic factor Δp in feed-forward air-fuel ratio control.
5. Developed a mean value engine model for the SCI engine.
6. Developed the lean NO_x trap NO_x adsorption model.
7. Introduced the flow rate saturation factor in the LNT model.

8.1 Conclusions

This research was aimed at investigating the possible techniques and feasible methods of implementations to reduce diesel engine emissions to meet the more stringent Tier 4 standards.

The research was developed around topics of the SCI performance evaluation for a model engine for implementation of such SCI concepts in a designated turbocharged diesel engine. Different modeling methods were discussed for specific control issues. Under the widely accepted accuracy of the 1D detail model, some conclusions are drawn here for discussion.

1 The proposed SCI engine can meet the requirement of production performance.

   a) Turbocharger SCI engine output torque meets designated curves.

   b) Compressor and wastegate bypassed turbine run within maps with reasonable efficiency.

   c) Constant-Speed-Acceptance proved the engine dynamic characters meet the design requirements.

2 The SCI engine is feasible with the addition of some simple controls for basic operation.

   a) Intake manifold pressure based feed-forward control provides feasibility for tight AFR.

   b) Feed-forward control compensates for the time delay of feedback based methods.

   c) All season torque limiting can be implemented in a single PID scheme.

   d) Low idle speed PID controls provide enough robustness for load disturbance.

3 The proposed Integrated Simulation Environment is capable of control design and verification.

   a) The 1D detail model and integrated simulation provides accurate data for control oriented modeling, regression and control strategy verification.

   b) The control module facilitates the performance evaluation with specified algorithm and logic to reduce the human interference.

4 A control oriented model is very useful for advanced engine and after-treatment control.

   a) All speed governing needs model based control for throttle and wastegate coordination and fuel efficiency optimization.

   b) ISE and MVEM are candidates in engine control design for reducing time, cost and risk.

c) Proposed LNT model is verified for engine control for NO_x reduction.

8.2 Recommendations

Engine development is a multi-disciplinary area and has the interaction and cooperation at multiple levels and aspects. This research discusses the co-design and integration of detail modeling and control design. Some proposed methods are not finished and some ideas need further development for verification and application. Following are potential topics:

- Mean Value Model transient verification.
- Control design for throttle and wastegate control.
- Emission model integration with the SCI engine, plus Three-Way Catalyst model verification in the SCI engine.
- Generic Mean Value Model with extension of emission model and after-treatment.
- Integration with combustion model for advanced detail combustion control, such as LTC and HCCI.
- Fault diagnosis design and verification with the Integrated Engine Simulation Model.

9 REFERENCES

Abate, M., and N. Dosio. 1990. Use of Fuzzy Logic for Engine Idle Speed Control. In *SAE Technical Paper Series* 900594. Detroit, Mich.: SAE.

Aswani, D. J., M. J. van Nieuwstadt, J. A. Cook, and J. W. Grizzle. 2005. Control oriented modeling of a diesel active lean NO_x catalyst after-treatment system. *Transaction of the ASME, Journal of Dynamic Systems Measurement and Control* 127(1):1-12.

Bailey, O. H. 1997. DieselNet Technical Report: NO_x Adsorbers for Diesel Applications: General Considerations and Operational Issues. Available at: http://www.dieselnet.com/papers/9712bailey/.

Bengtsson, J., P. Strandh, R. Johansson, P. Tunestal, and B. Johansson. 2007. Hybrid modelling of homogeneous charge compression ignition (HCCI) engine dynamics survey. *International Journal of Control* 80(11):1814 - 1847.

Bolton, B., X. Fan, N. Hakim, K. Sisken, and H. Zhang. 2002. Update on Modeling for Effective Diesel Engine After-treatment Implementation: Master Plan, Status, and Critical Needs. In *8th Diesel Engine Emissions Reduction (DEER) Workshop 2002,*. San Diego, Cal.

Butt, J. B. 2000. *Reaction Kinetics and Reactor Design*. 2nd ed. Marcel Dekker, Inc., New York, NY.

Butts, K., N. Sivashankar, and S. Jing. 1999. Application of l_1 Optimal Control to the Engine Idle Speed Control Problem. *IEEE Transactions on Control Systems Technology,* 7(2):258-270.

Butts, K., N. Sivashankar, and J. Sun. 1995. Feedforward and Feedback Design for Engine Idle Speed Control Using l_1 optimization. In *Proceedings of the American Control Conference, 1995*.

Canova, M., F. Chiara, M. Flory, S. Midlam-Mohler, Y. Guezennec, and G. Rizzoni. 2007. Dynamics and Control of DI and HCCI Combustion in a Multi-cylinder Diesel Engine. In *Fifth IFAC Symposium on Advances in Automotive Control*. Seascape Resort, Cal.: IFAC

Carnevale, C., and A. Moschetti. 1993. Idle Speed Control With H_∞ Technique. In *SAE Technical Paper Series* 930770. Detroit, Mich.: SEA.

Chase, S., R. Nevin, R. Winsor, and K. J. Baumgard. 2007. Stoichiometric Compression Ignition (SCI) Engine. In *SAE Technical Paper Series* 2007-01-4224. Detroit, Mich.: SAE.

Chauvin, J., G. Corde, N. Petit, and P. Rouchon. 2007. Airpath Strategy for Experimental Transient Control of a Diesel HCCI Engine. *Oil & Gas Science and Technology* 62(4):483-491.

Daw, C. S., K. Chakravarthy, and K. E. Lenox. 2003. A Simple Model for Lean NO_x Adsorber Catalysts. In *Proceedings of the Third Joint Meeting of the U.S. Sections of The Combustion Institute*. Chicago, Ills.: University of Illinois at Chicago.

Del Re, L., Frank Allgöwer, Luigi Glielmo, C. Guardiola, and I. Kolmanovsky. 2010. *Automotive Model Predictive Control: Models, Methods and Applications*. Lecture notes in control and information sciences.

Dobner, D. J., and R. D. Fruechte. 1983. An Engine Model for Dynamic Engine Control Development. In *American Control Conference, 1983*. San Francisco, Cal.

Dou, D., and J. Balland. 2002. Impact of Alkali Metals on the Performance and Mechanical Properties of NO_x Adsorber Catalysts. In *SAE Technical Paper Series* 2002-01-0734. Detroit, Mich.: SAE.

Gibson, A., I. Kolmanovsky, and D. Hrovat. 2006. Application of Disturbance Observers to Automotive Engine Idle Speed Control for Fuel Economy Improvement. In *American Control Conference, 2006*. Minneapolis, Mn.: American Automatic Control Council.

He, Y. 2005. Development and Validation of a 1D Model of a Turbocharged V6 Diesel Engine Operating Under Steady-State and Transient Conditions. *SAE Technical Paper Series* 2005-01-3857.

He, Y., and C. C. Lin. 2007. Development and Validation of A Mean Value Engine Model for Integrated Engine and Control System Simulation. In *SAE Technical Paper Series* 2007-01-1304. Detroit, Mich.: SAE.

Hendricks, E. 1997. Engine Modelling for Control Applications: A Critical Survey. Netherlands: Kluwer Academic Publishers.

Hendricks, E., A. Chevaller, M. Jensen, S. C. Sorenson, D. Trumpy, and J. Asik. 1996. Modeling of the Intake Manifold Filling Dynamics. In *SAE Technical Paper* 960037. Detroit Mich.: SAE.

Hendricks, E., and S. Sorenson. 1990. Mean Value SI Engine Model for Control Studies. In *American Control Conference, 1990*. San Diego, Cal.: American Automatic Control Council.

Heywood, J. B. 1988. *Internal Combustion Engines Fundamentals* McGraw-Hill Book Company, Singapore.

Kabin, K. S., R. L. Muncrief, and M. P. Harold. 2004. NO_x Storage and Reduction on a Pt/BaO/alumina Monolithic Storage Catalyst. *Catalysis Today* 96(1-2):79-89.

Kim, J., S. W. Park, M. Andrie, R. D. Reitz, and K. Sung. 2009. Experimental Investigation of Intake Condition and Group-hole Nozzle Effects on Fuel Economy and Combustion Noise for Stoichiometric Diesel Combustion in An HSDI Diesel Engine. In *SAE Technical Paper Series* 2009-01-1123. Detroit, Mich.: SAE.

Kim, Y. W., J. Sun, I. Kolmanovsky, and J. Koncsol. 2003. A Phenomenological Control-oriented Lean NO_x Trap Model. In *SAE Technical Paper Series* 2003-01-1164. Detroit, Mich.: SAE.

Kjergaard, L., S. Nielsen, T. Vesterholm, and E. Hendricks. 1994. Advanced Nonlinear Engine Idle Speed Control Systems. In *SAE Technical Paper Series* 940974. Detroit, Mich.: SAE.

Lee, S., A. Manuel, D. Gonzalez, and R. D. Reitz. 2006. Stoichiometric Combustion in a HSDI Diesel Engine to Allow Use of A Three-way Exhaust Catalyst. In *SAE Technical Paper Series* 2006-01-1148. Detroit, Mich.: SAE.

Li, X., and S. Yurkovich. 1999. IC engine Air/fuel Ratio Prediction and Control Using Discrete-time Nonlinear Adaptive Techniques. In *American Control Conference, 1999. Proceedings of the 1999*.

Li, X., and S. Yurkovich. 2000. Discrete Adaptive Sliding Mode Control for Idle Speed Regulation in IC Engines. In *Proceedings of the 2000 IEEE International Conference on Control Applications*. Anchorage, AK.

Los Alamos National Laboratory. 1989. *KIVA-II: A Computer Program for Chemically Reactive Flows with Sprays.*

Lueders, H., and P. Stommel. 1999. Diesel Exhaust Treatment - New Approaches to Ultra Low Emission Diesel Vehicles. In *SAE Technical Paper Series* 1999-01-0108. Detroit, Mich.

Monk, J., and J. Comfort. 1970. Mathematical Model of An Internal Combustion Engine and Dynamometer Test Rig. *Measurement and Control* 3(6):7.

Moskwa, J. J., and J. K. Hedrick. 1987. Automotive Engine Modeling for Real Time Control Application. In *American Control Conference, 1987*. Minneapolis, MN: American Automatic Control Council.

Nishimura, Y., and K. Ishii. 1986. Engine Idle Stability Analysis and Control. In *SAE Technical Paper Series* 860415. Detroit, Mich.: SAE.

Pettiti, M., L. Pilo, and F. Millo. 2007. Development of A New Mean Value Model for the Analysis of Turbolag Phenomena in Automotive Diesel Engines. In *SAE Technical Paper Series* 2007-01-1301. Detroit, Mich.: SAE.

Powell, B. K. 1979. A Dynamic Model for Automotive Engine Control Analysis. In *18th IEEE Conference on Decision and Control including the Symposium on Adaptive Processes, 1979* Fort Lauderdale, Fl.: IEEE Control Systems Scoiety.

Powell, B. K., and W. F. Powers. 1981. Linear Quadratic Control Design for Nonlinear IC Engine Systems. In *International Symposium on Automotive Technology & Automation*. Stockholm, Swed: Automotive Automation Ltd.

Rausen, D. J., A. G. Stefanopoulou, J. M. Kang, J. A. Eng, and T. W. Kuo. 2005. A Mean-Value Model for Control of Homogeneous Charge Compression Ignition (HCCI) Engines. *Journal of Dynamic Systems, Measurement, and Control* 127(3):355-362.

Schulten, P. J. M., and D. Stapersoma. 2003. Mean Value Modelling of the Gas Exchange of a 4-stroke Diesel Engine for Use in Powertrain Applications. In *SAE Technical Paper Series* 2003-01-0219. Detroit, Mich.: SAE.

Shamim, T., C. S. Daw, and J. C. Conklin. 2002. Mid-year Progress Report NO_x Trap Systems for Diesel and Lean Burn Engine Applications: Modeling and Simulations. Available at: http://www.engin.umd.umich.edu/ ceep/reports/2001/MidYearShamim01.html.

Shu, Y. 2001. Modelling and Control of Advaned Technology Diesel Enigne. Ph.D.: diss. Cleveland, Ohio 44106: Case Western Reserve University.

Stefanopoulou, A. G., I. Kolmanovsky, and J. S. Freudenberg. 2000. Control of Variable Geometry Turbocharged Diesel Engines for Reduced Emissions. *Control Systems Technology, IEEE Transactions on* 8(4):733-745.

U.S. EPA. 2004. Clean air nonroad diesel: Tier 4 Final rule. Washington, D.C.: U.S. Environmental Protection Agency. Available at: www.epa.gov/nonroad-diesel/2004fr.htm.

Wang, L., I. Kolmanovsky, and J. Sun. 2000. On-line Identification and Adaptation of LNT Models for Improved Emission Control in Lean Burn Automotive Engines. In *Proceedings of the 2000 American Control Conference*. Chicago, IL, USA: IEEE.

Wang, Y., S. Raman, and J. W. Grizzle. 1999. Dynamic Modeling of A Lean NO_x Trap for Lean Burn Engine Control. In *Proceedings of the 1999 American Control Conference*. San Diego, Cal.: American Automatic Control Council

APPENDIX A

A.1 Regression Models of Fueling

Method 1: Based on IMP, EMP

$$M_{fuel} = 89.4P_{im} + 18.9P_{em} - 23.6 \tag{A-1}$$

Model 2: Based on IMP, EMP, IMP (transient information)

$$M_{fuel} = 130\,P_{im} - 132\Delta P_{im} - 14P_{em} - 2.2 \tag{A-2}$$

$$\Delta P_{im}(i) = P_{im}(i) - P_{im}(i-1) \tag{A-3}$$

Model 3: IMP, change of IMP, EMP, turbocharger speed

$$M_{fuel} = 116P_{im} - 72\Delta P_{im} - 6P_{em} - 0.0000024N_{tc} - 2.3 \tag{A-4}$$

Model 4: Eliminate EMP for measurement consideration

$$M_{fuel} = 110P_{im} - 61\Delta P_{im} - 6\times10^{-5}N_{tc} - 3.8 \tag{A-5}$$

Model 5: Add N_e to cover different turbocharger speed

$$\begin{aligned} M_{fuel} = {} & 112.96P_{im} - 0.00301P_{im}N_e + 2.993\Delta P_{im} \\ & -0.0000174N_{tc} - 10.87 \end{aligned} \tag{A-6}$$

Model 6: Add *Ne* term on P_{im}, dP_{im}, N_{tc}

$$\begin{aligned} M_{fuel} = {} & 121P_{in} - 0.007P_{in}N_e - 5.6dP_{in} + 0.0055dP_{in}N_e \\ & -0.00017N_{tc} + 0.000000095N_{tc}N_e - 11.68 \end{aligned} \tag{A-7}$$

Model 7: Add N_e term on Model 6

$$\begin{aligned} M_{fuel} = {} & 122P_{im} - 0.007P_{im}N_e - 4.6dP_{im} + 0.0047dP_{im}N_e \\ & -0.00018N_{tc} + 0.000000092N_{tc}N_e - 0.001N_e - 13.41 \end{aligned} \tag{A-8}$$

Model 7^{+}: Add more initial steady-state data

$$\begin{aligned} M_{fuel} = {} & 127.8P_{im} - 0.011P_{im}N_e - 16.1dP_{im} - 0.03dP_{im}N_e \\ & -0.00015N_{tc} + 0.000000065N_{tc}N_e - 0.0014N_e - 25.86 \end{aligned} \tag{A-9}$$

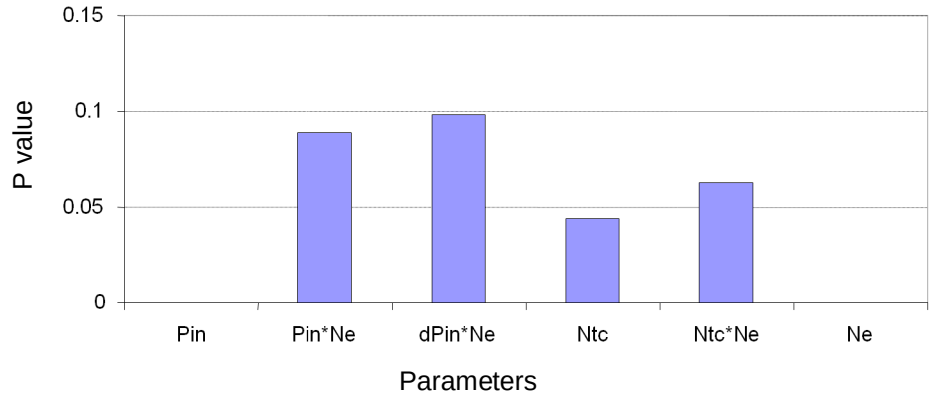

(a)

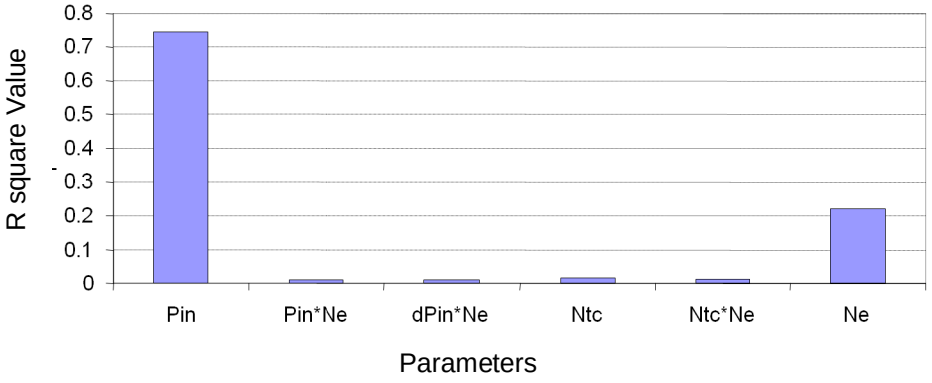

(b)

Figure A.1. Variance analysis of model 8 (a) P value analysis, (b) residues analysis.

APPENDIX B

B.1 Simulation Verification of Fueling Control

Case 1: Wastegate Initially Closed, 50%-100 % Load Simulation

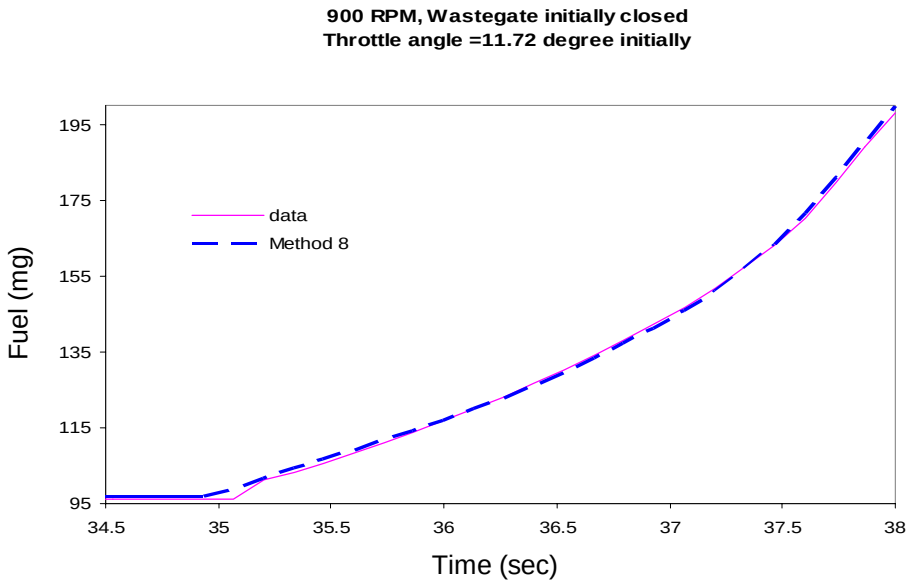

Figure B. 1. Fueling control verification under 900 rpm, wastegate initially closed 50%-100 % load.

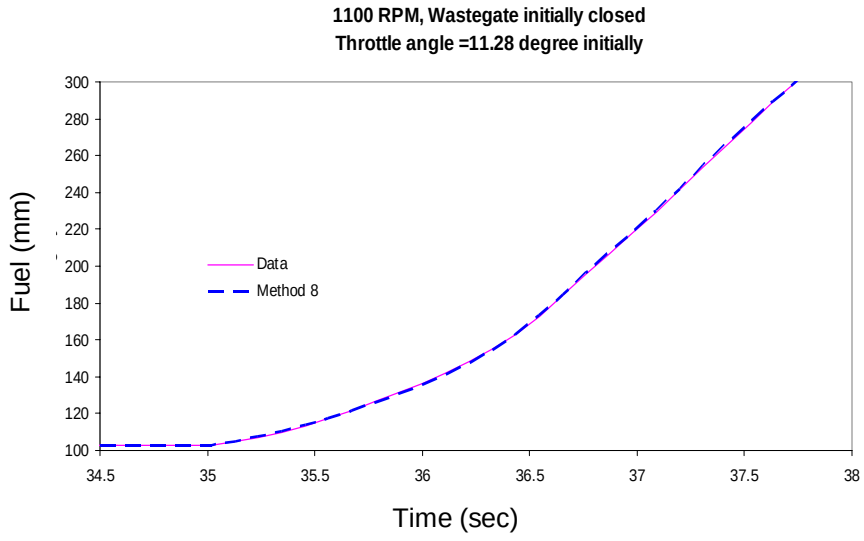

Figure B. 2. Fueling control verification under 1100 rpm, wastegate initially closed 50%-100 % load.

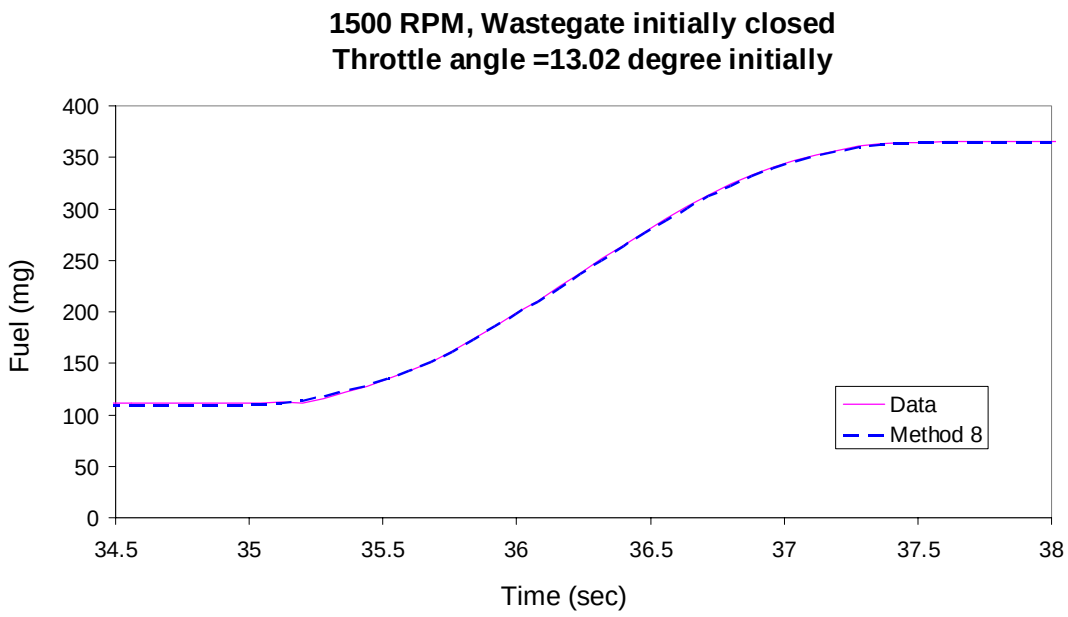

Figure B. 3. Fueling control verification under 1500 rpm, wastegate initially closed 50%-100 % load.

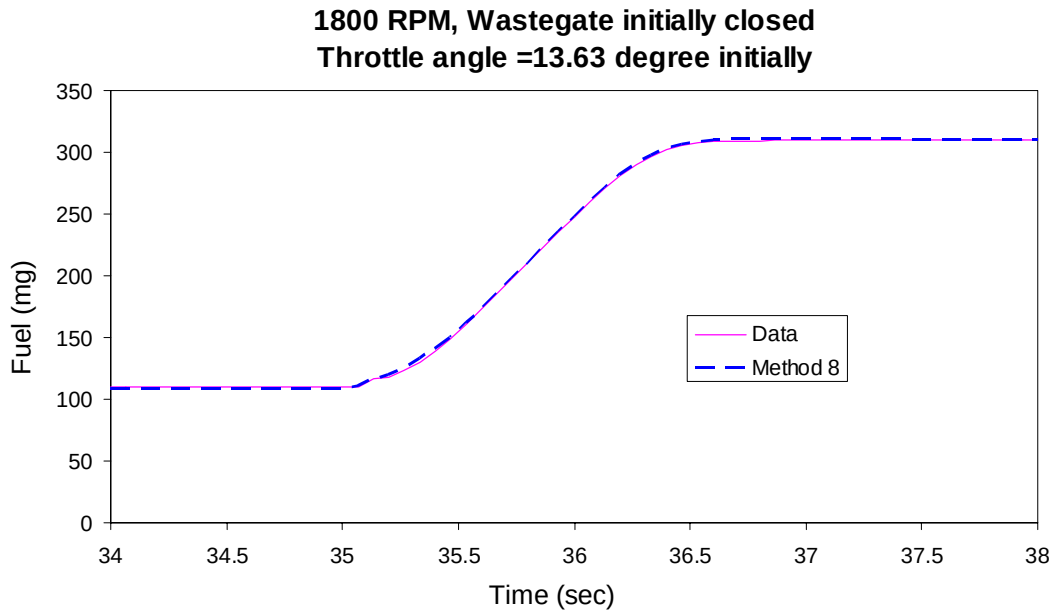

Figure B. 4. Fueling control verification under 1800 rpm, wastegate initially closed 50%-100 % load.

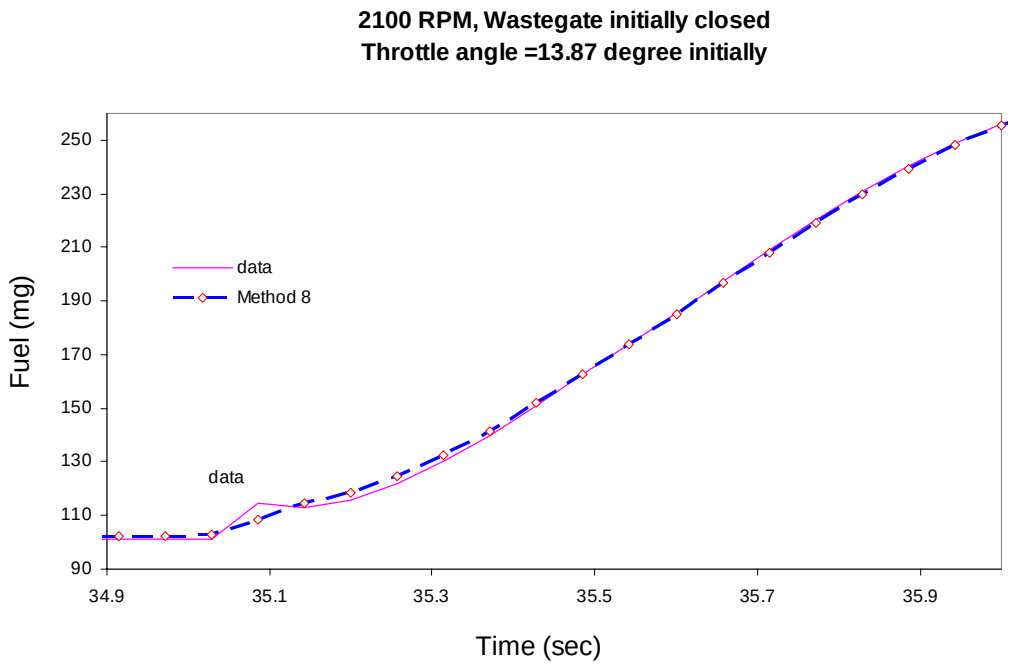

Figure B. 5. Fueling control verification under 2100 rpm, wastegate initially closed 50%-100 % load.

Case 2: Wastegate Initially Closed, 0%-90 % Load Simulation

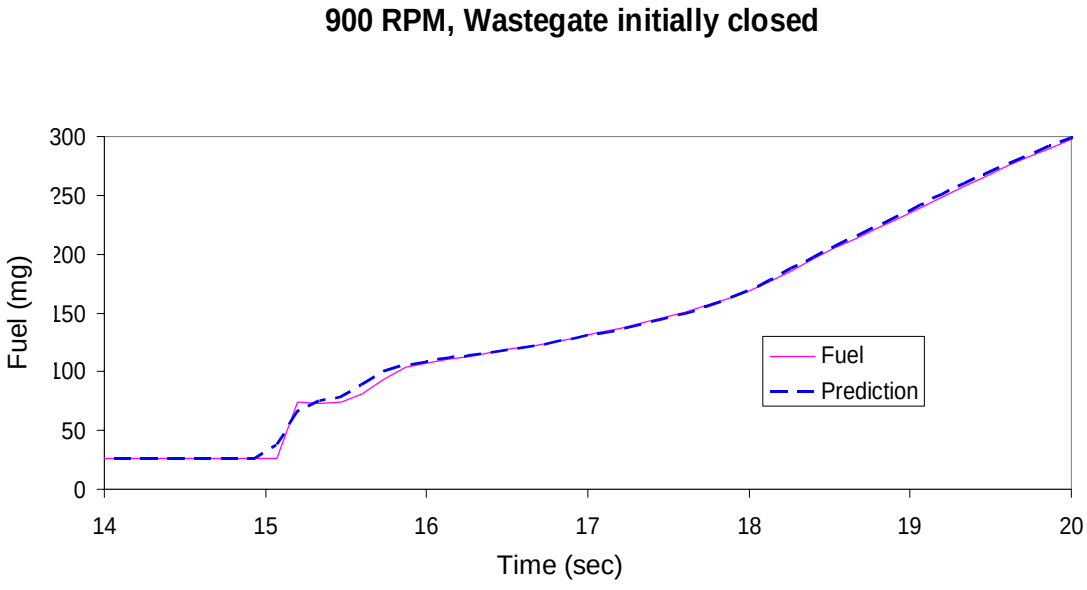

Figure B. 6. Fueling control verification under 900 rpm, wastegate initially closed, 0%-90 % load.

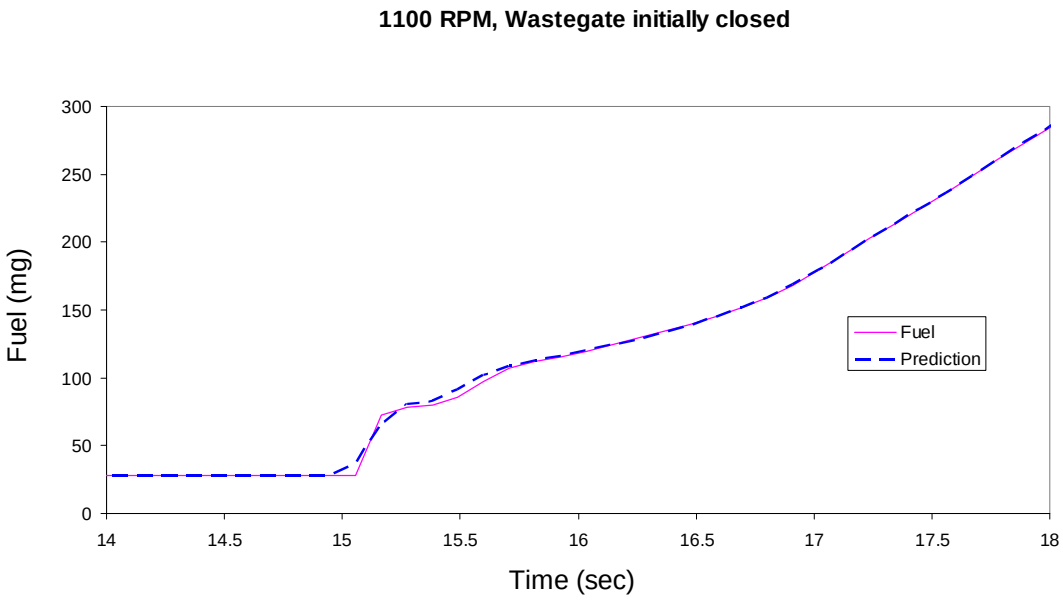

Figure B. 7. Fueling control verification under 1100 rpm, wastegate initially closed, 0%-90 % load.

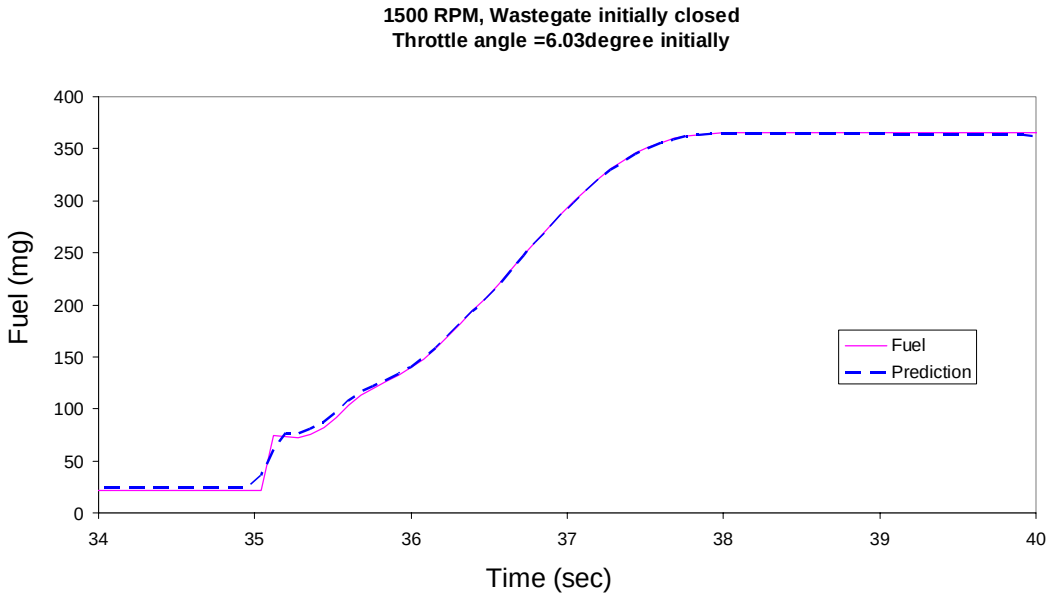

Figure B. 8. Fueling control verification under 1500 rpm, wastegate initially closed, 0%-90 % load.

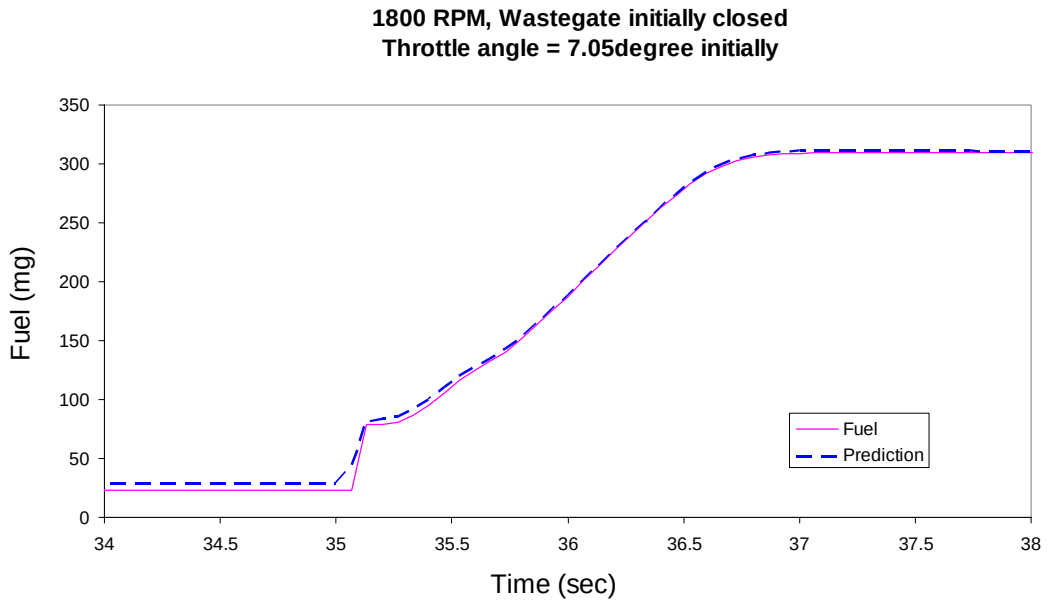

Figure B. 9. Fueling control verification under 1800 rpm, wastegate initially closed, 0%-90 % load.

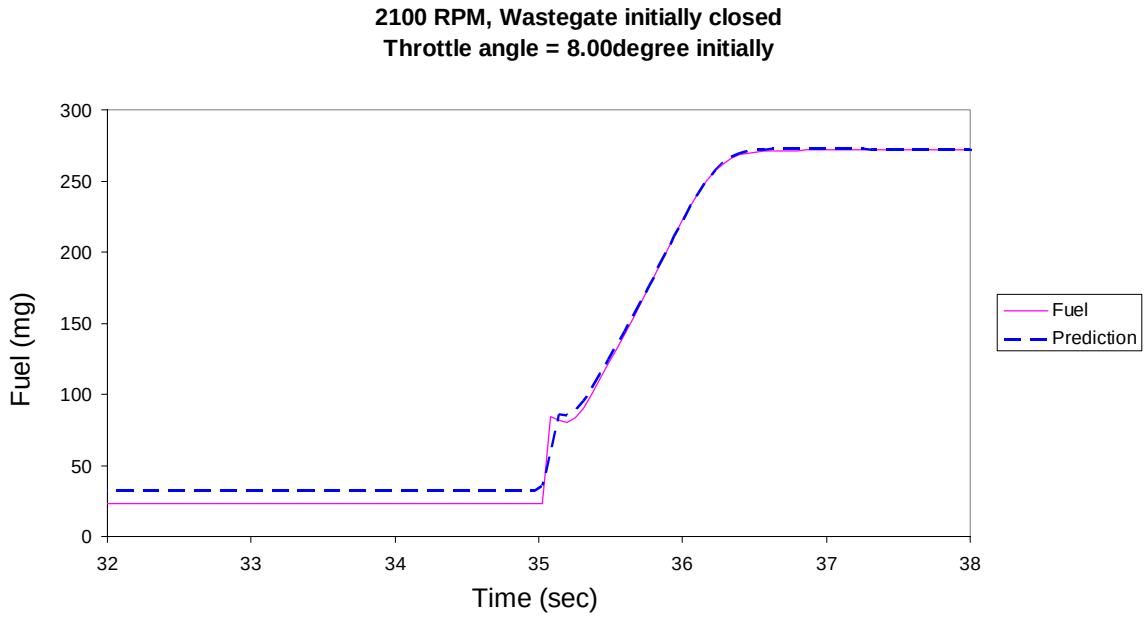

Figure B. 10. Fueling control verification under 2100 rpm, wastegate initially closed, 0%-90 % load.

Case 3: Wastegate Initially Open, 50% -100 % Load Simulation

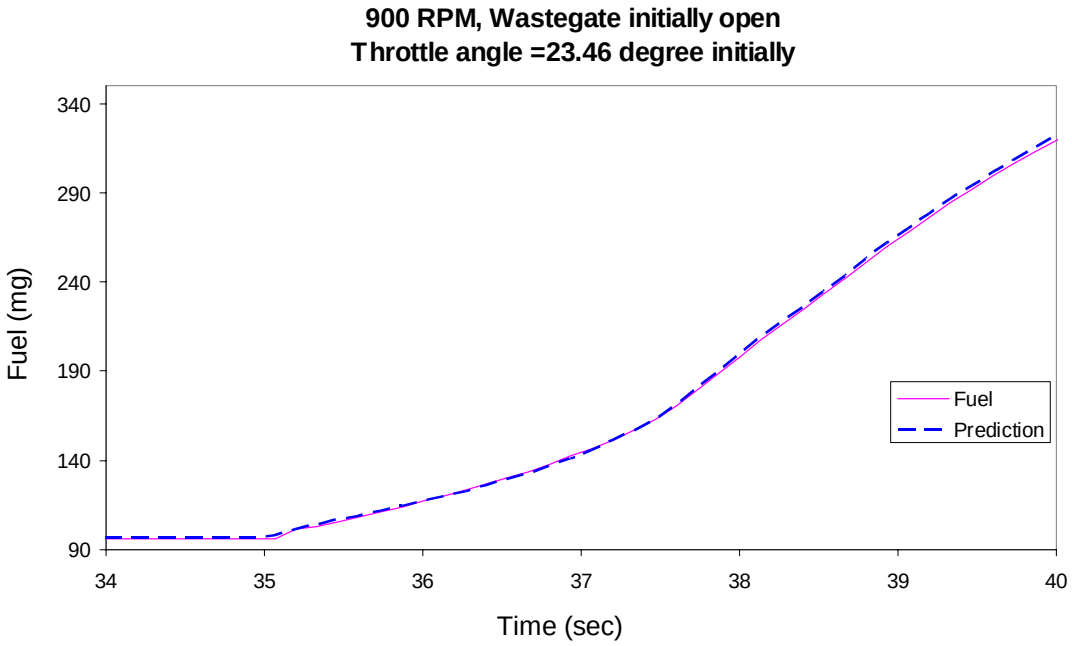

Figure B. 11. Fueling control verification: 900 rpm, wastegate initially open, 50%-100 % load.

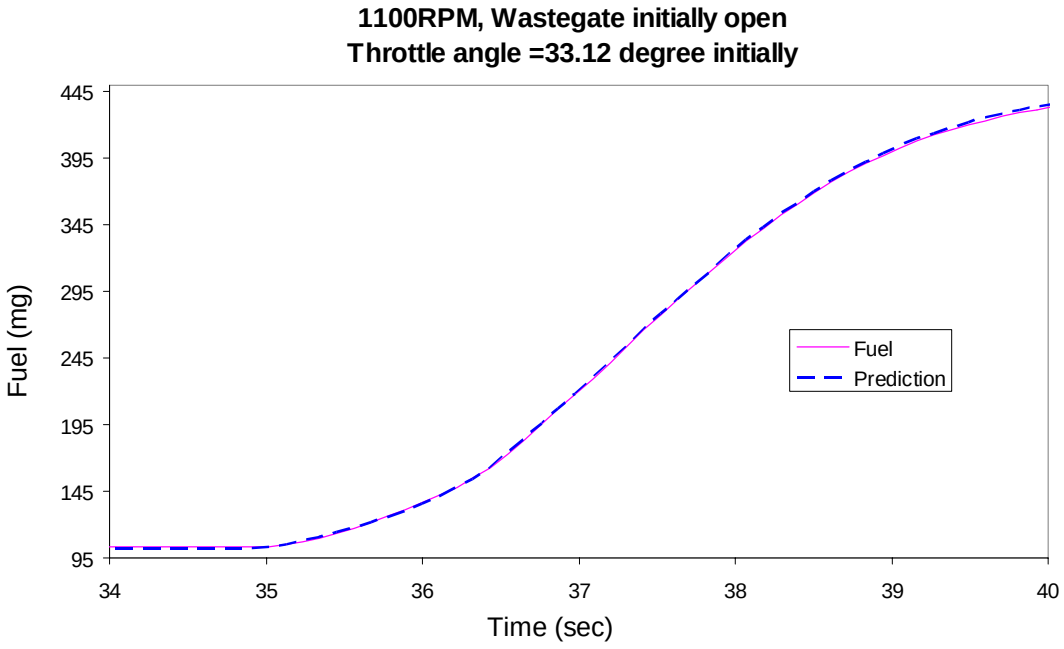

Figure B. 12. Fueling control verification: 1100 rpm, wastegate initially open, 50%-100 % load.

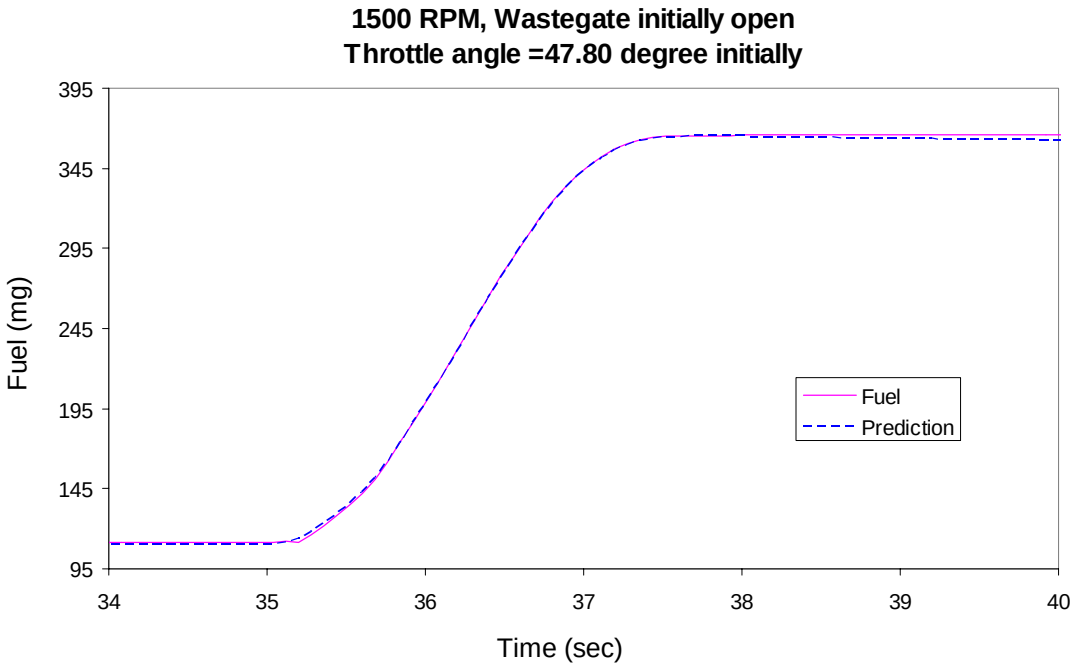

Figure B. 13. Fueling control verification: 1500 rpm, wastegate initially open, 50%-100 % load.

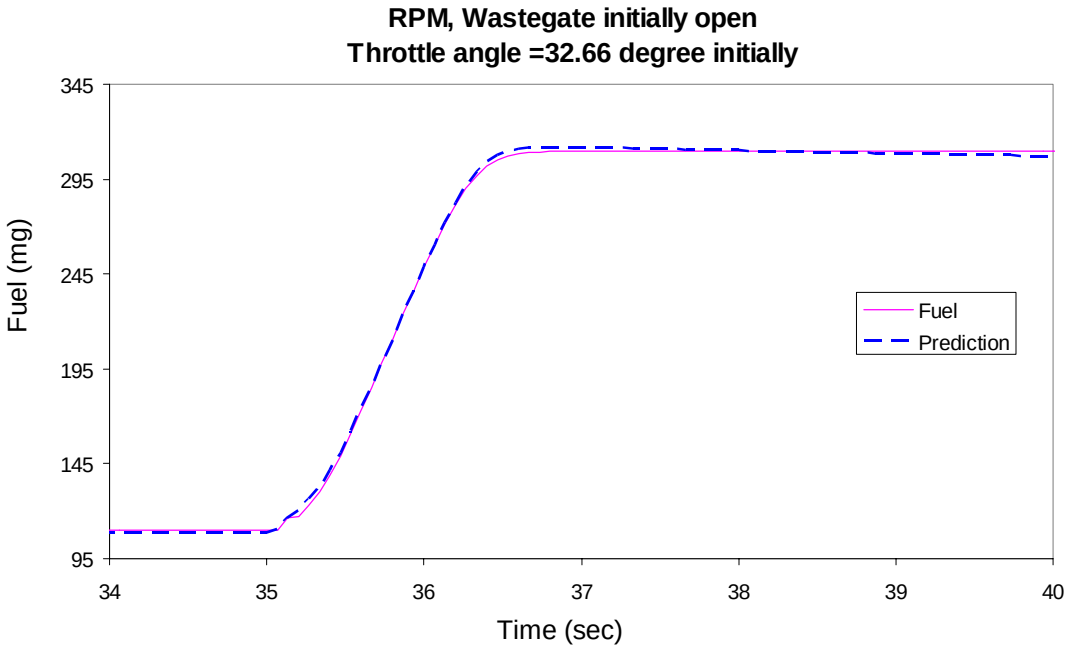

Figure B. 14. Fueling control verification: 1800 rpm, wastegate initially open, 50%-100 % load.

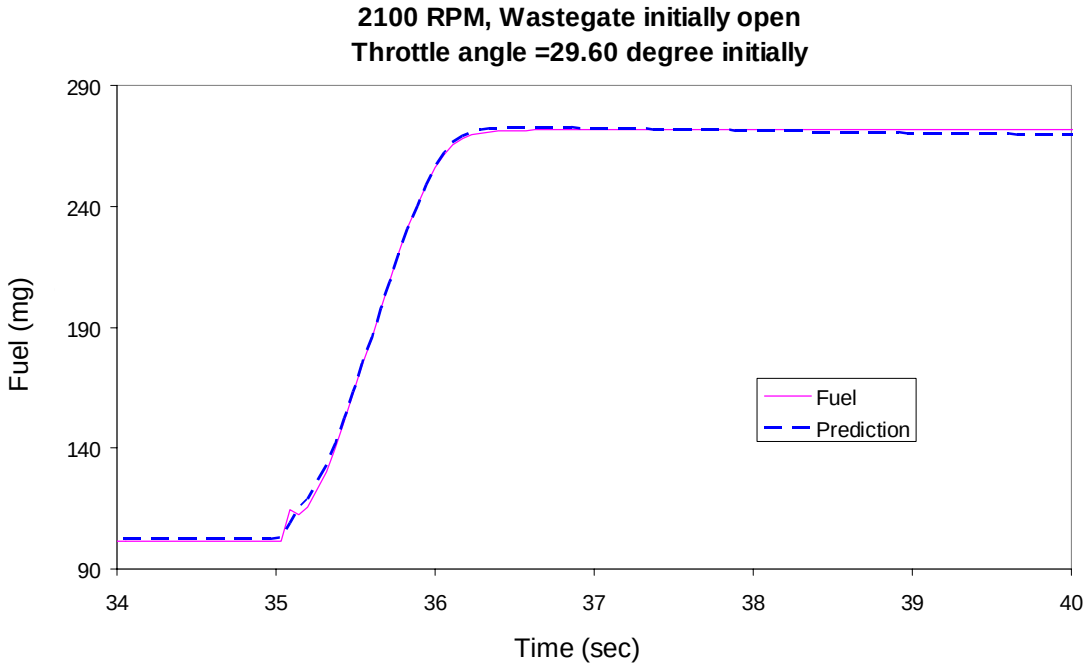

Figure B. 15. Fueling control verification: 2100 rpm, wastegate initially open, 50%-100 % load.

Case 4: Wastegate Initially Open, 0%-90% Load Simulation

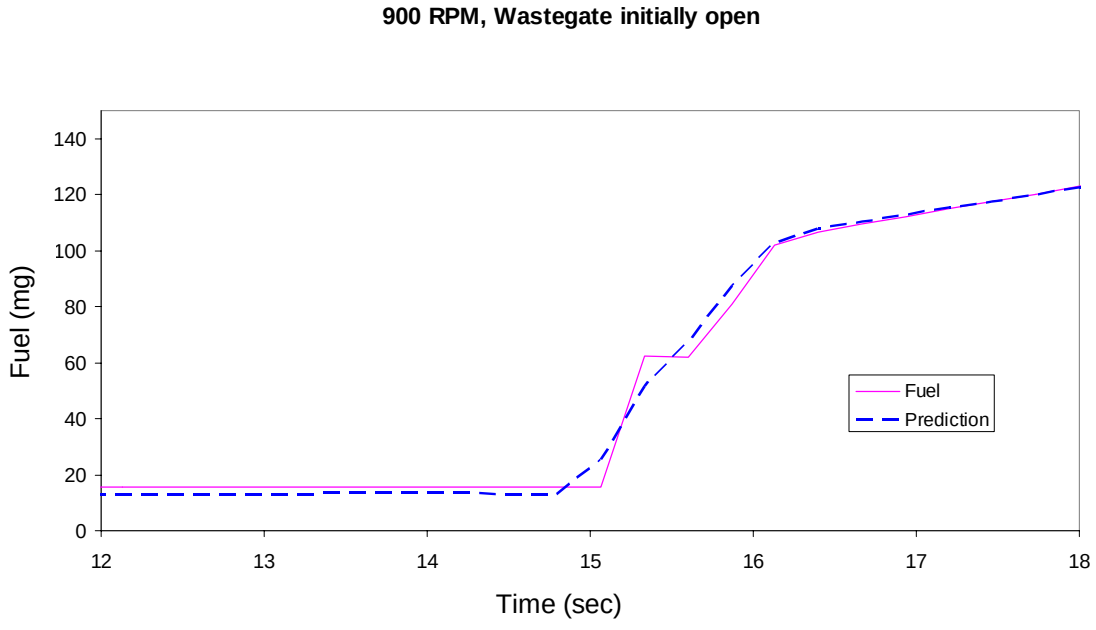

Figure B. 16. Fueling control verification: 900 rpm, wastegate initially open, 0%-90 % load.

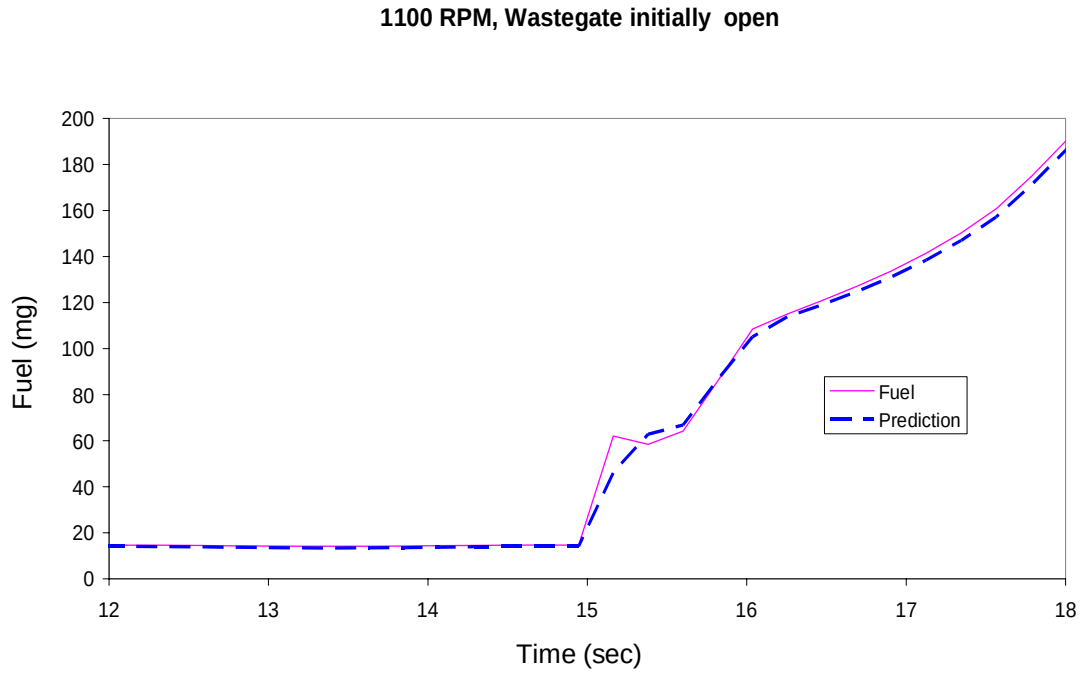

Figure B. 17. Fueling control verification: 1100 rpm, wastegate initially open, 0%-90 % load.

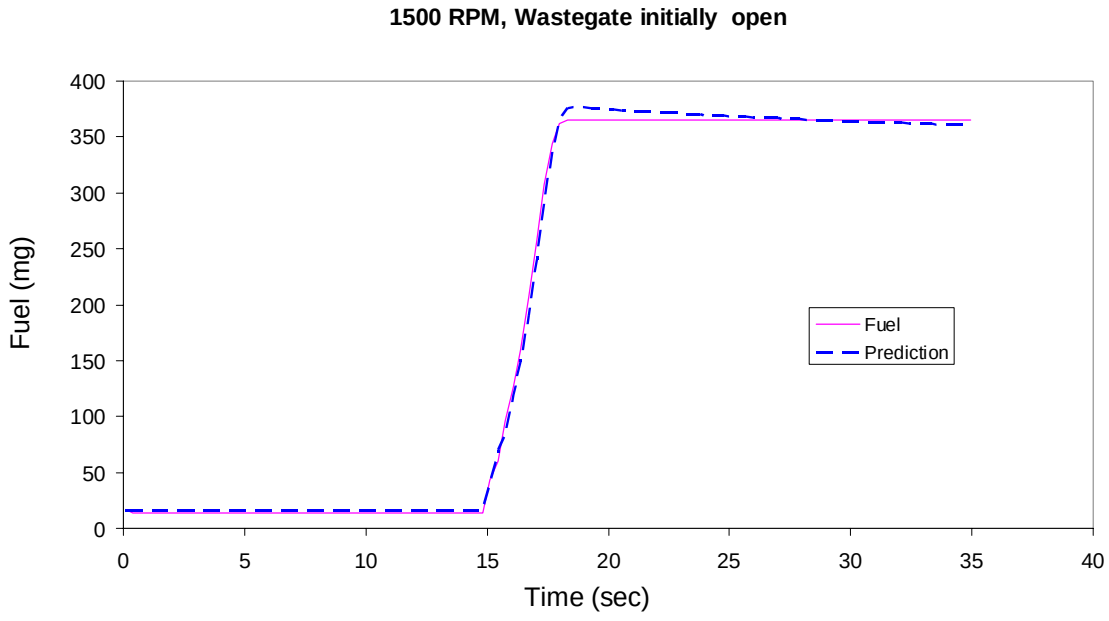

Figure B. 18. Fueling control verification: 1500 rpm, wastegate initially open, 500%-90 % load.

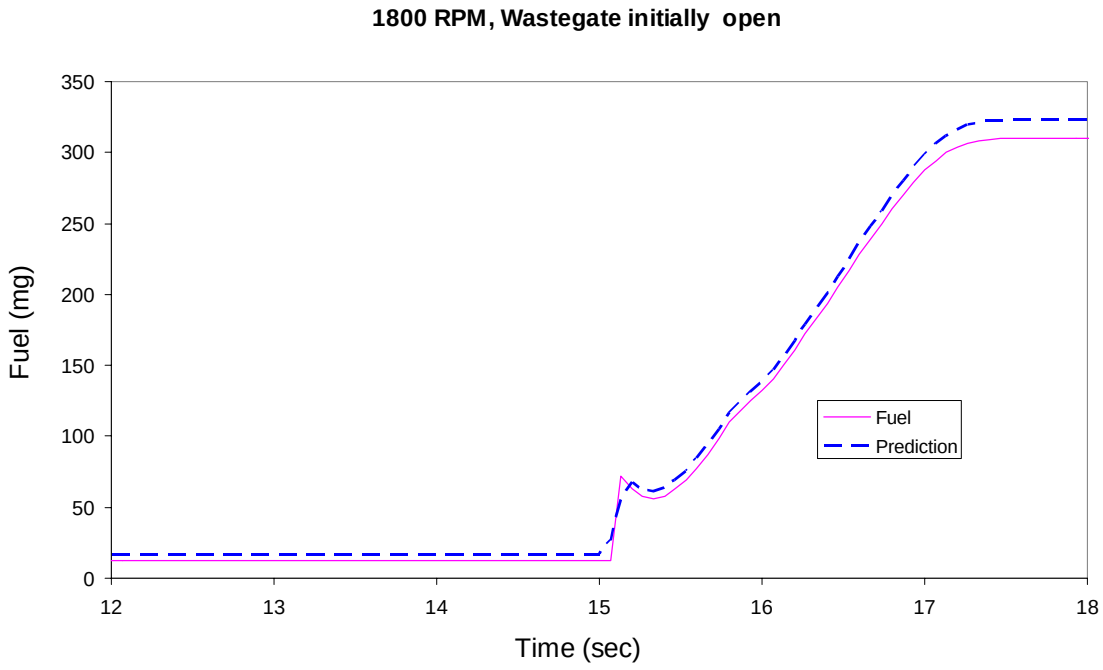

Figure B. 19. Fueling control verification: 1800 rpm, wastegate initially open, 0%-90 % load.

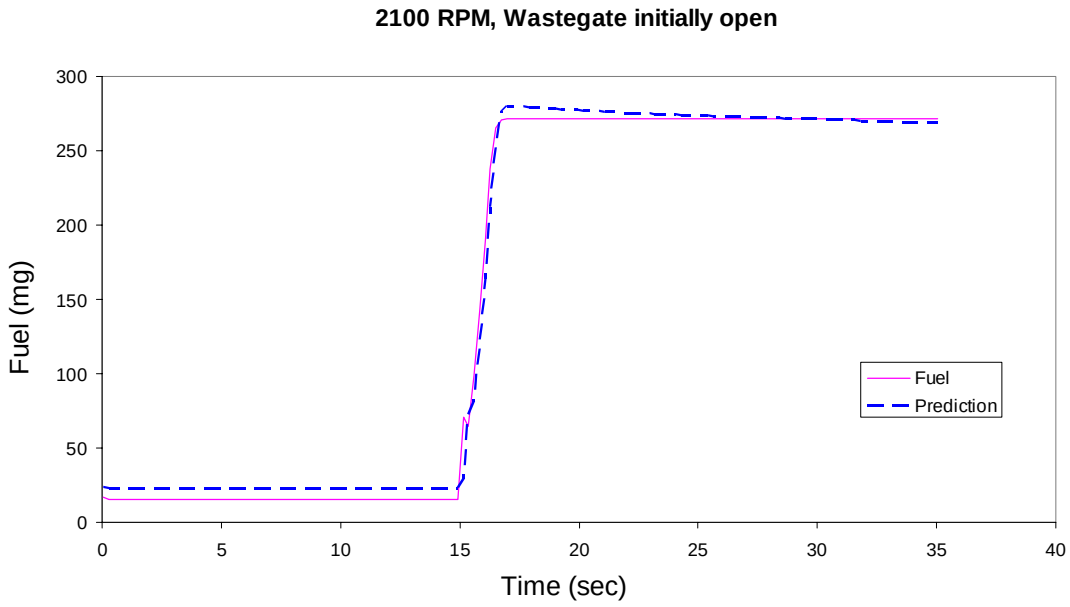

Figure B. 20. Fueling control verification: 2100 rpm, wastegate initially open, 0%-90 % load.

B.2 Simulation Verification of Torque Limiting Control

Torque Limiting PID Control Results

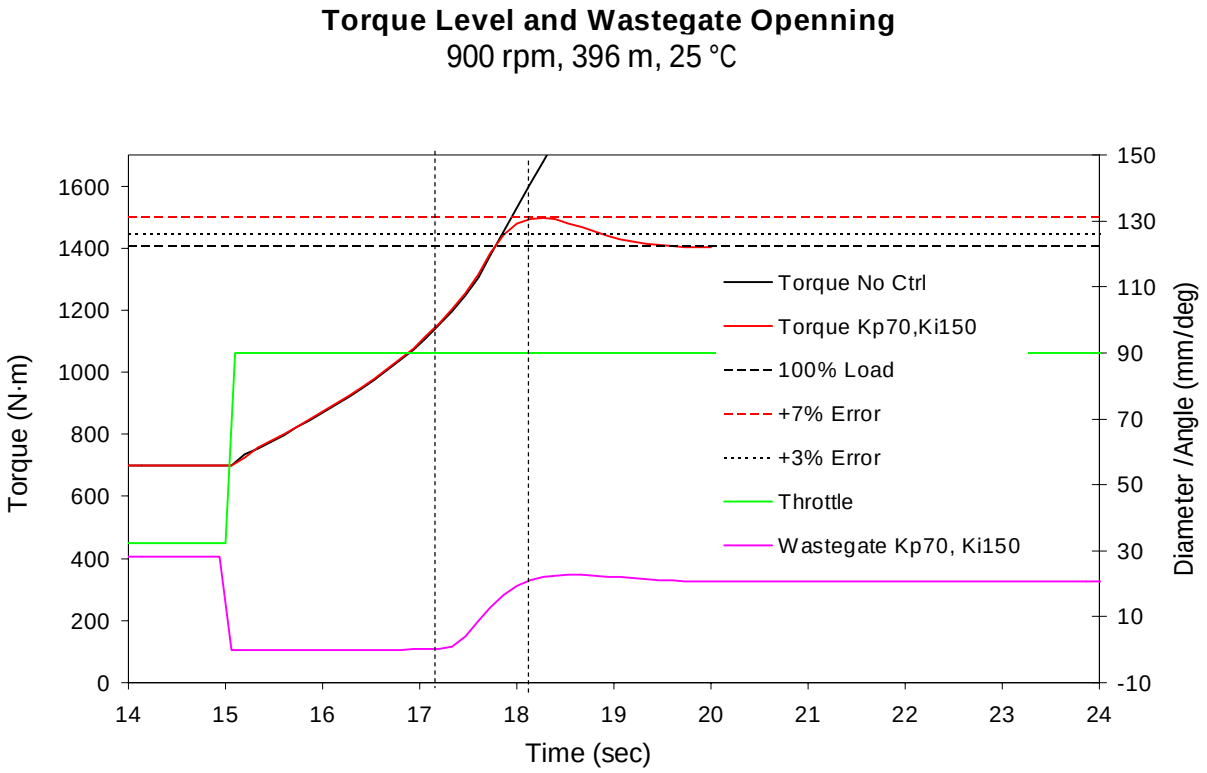

Figure B. 21. Torque limiting control verification of torque: 900 rpm, 396 m, 25˚C.

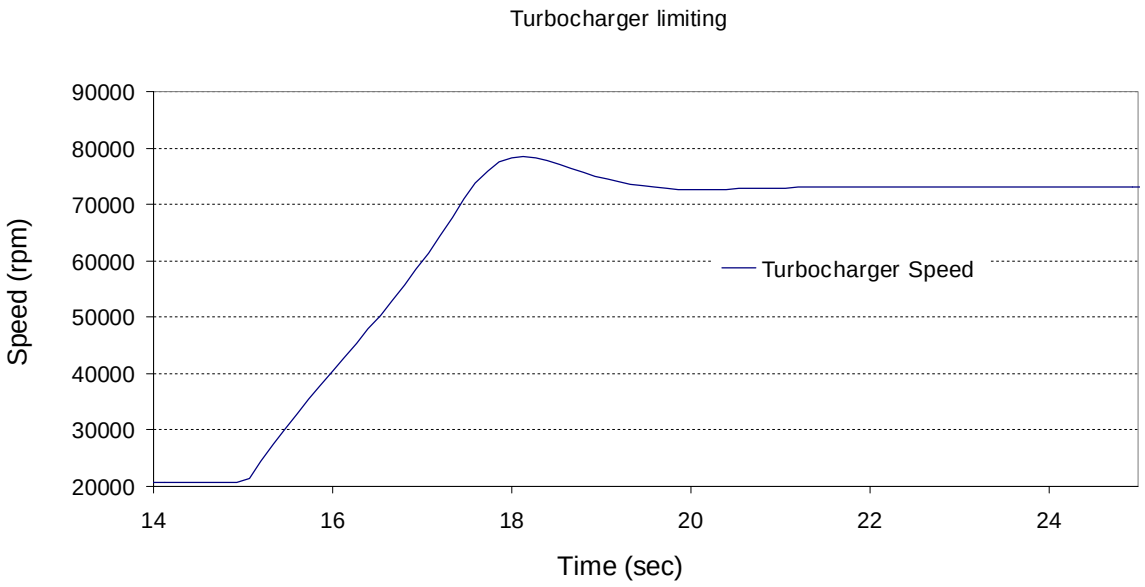

Figure B. 22. Torque limiting control verification of turbine speed: 900 rpm, 396 m, 25˚C.

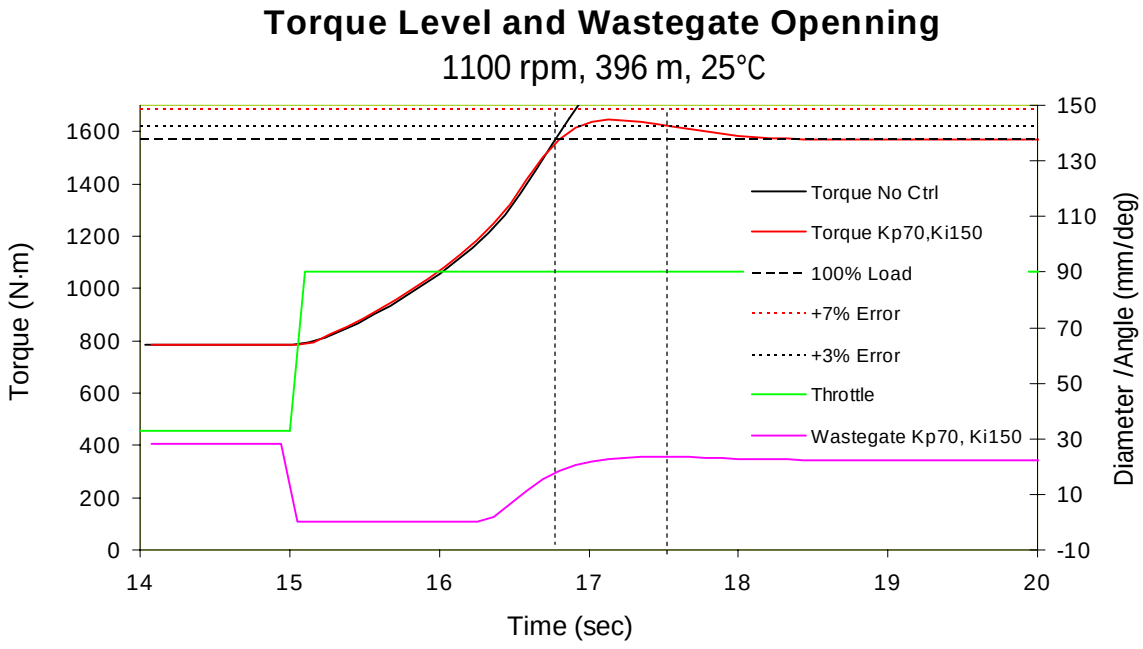

Figure B. 23. Torque limiting control verification of torque: 1100 rpm, 396 m, 25˚C.

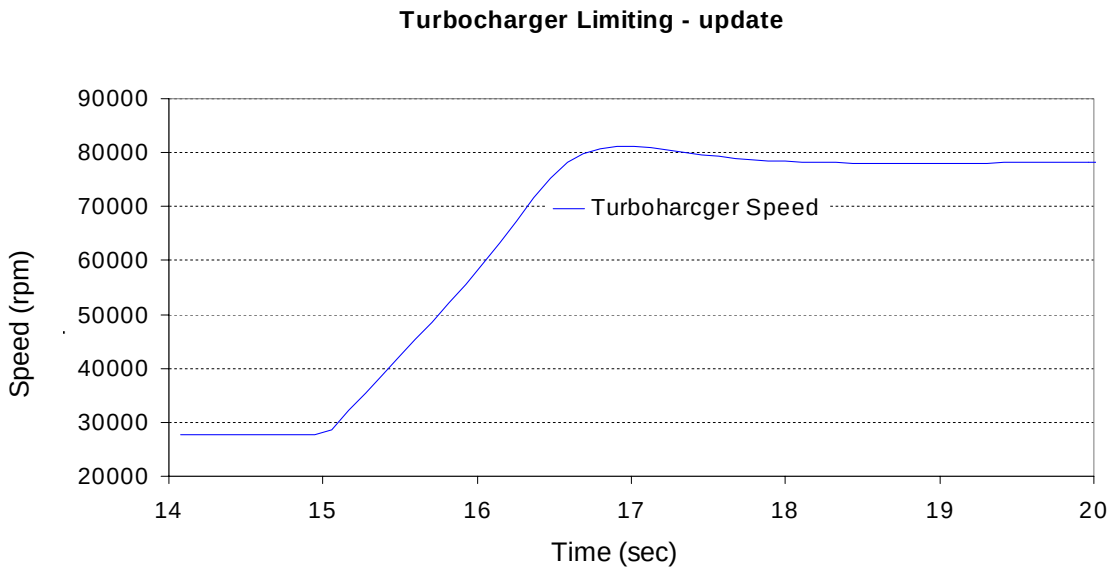

Figure B. 24. Torque limiting control verification of turbine speed: 1100 rpm, 396 m, 25˚C.

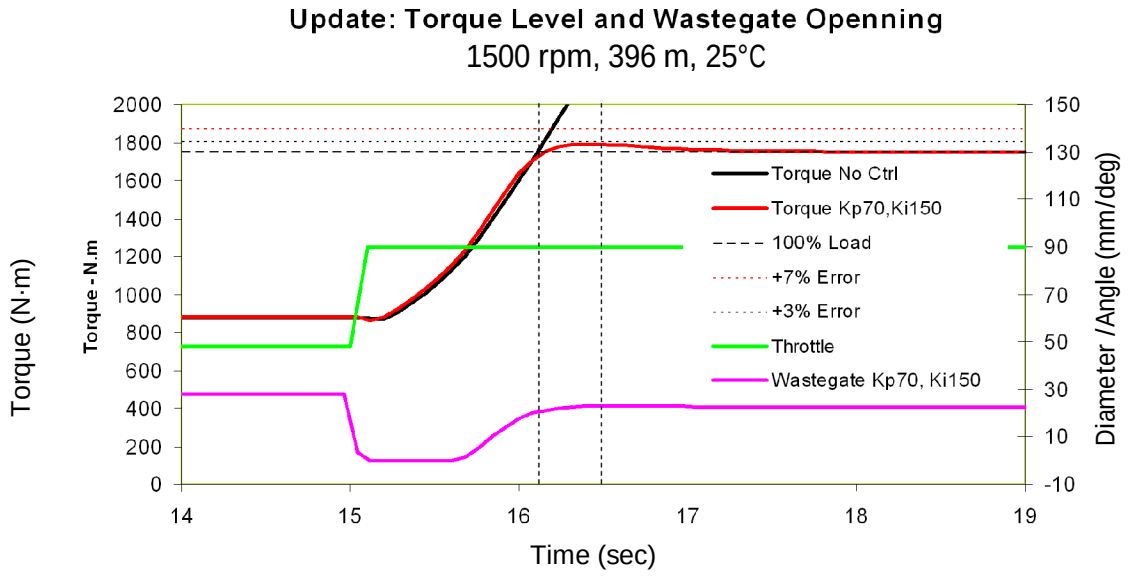

Figure B. 25. Torque limiting control verification of torque: 1500 rpm, 396 m, 25˚C.

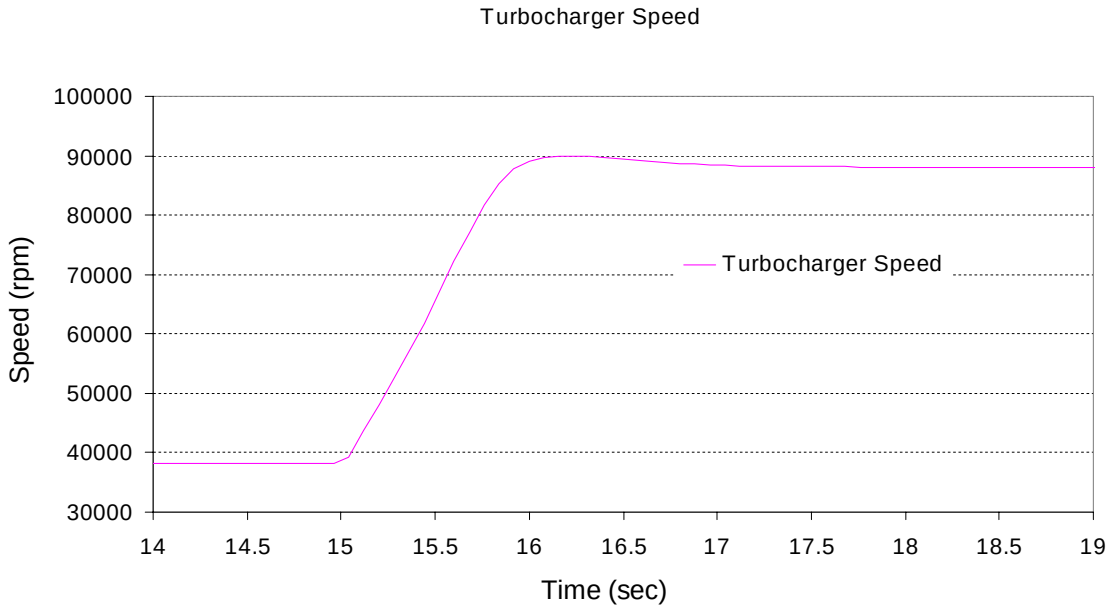

Figure B. 26. Torque limiting control verification of turbine speed: 1500 rpm, 396 m, 25˚C.

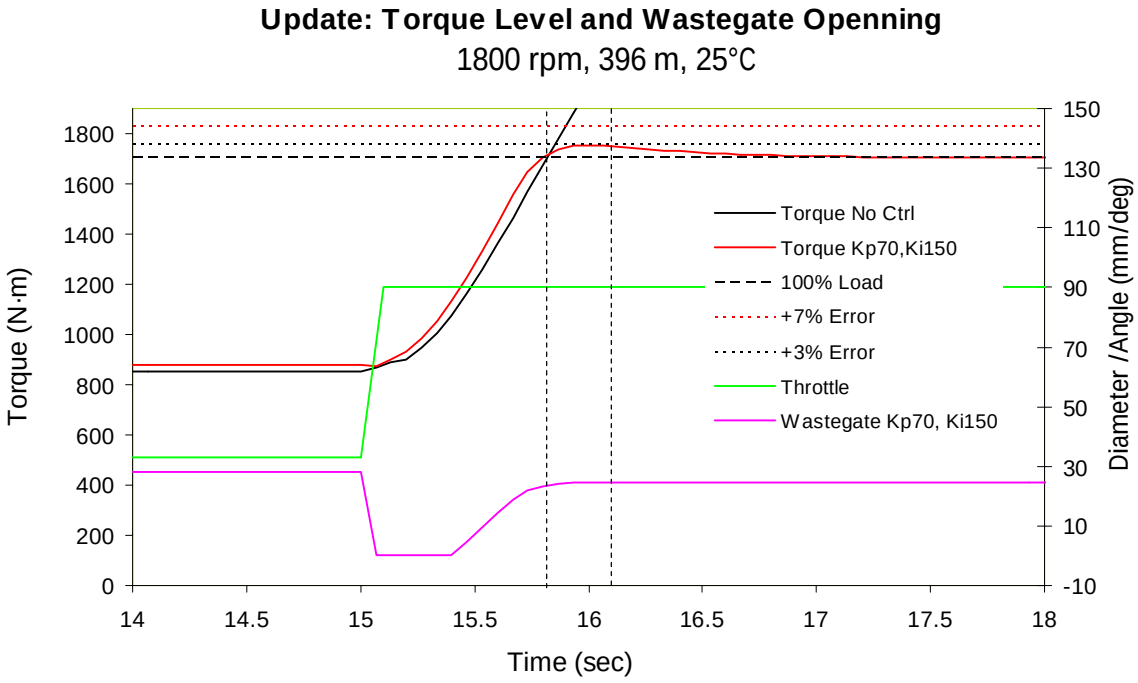

Figure B. 27. Torque limiting control verification of torque: 1800 rpm, 396 m, 25˚C.

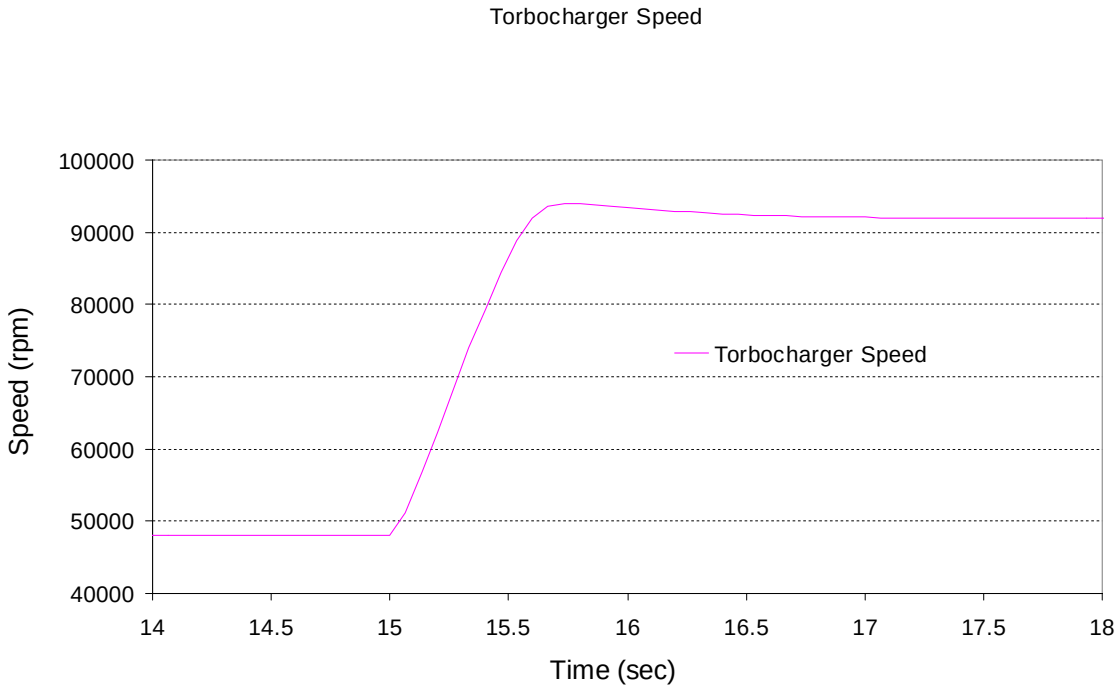

Figure B. 28. Torque limiting control verification of turbine speed: 1800 rpm, 396 m, 25˚C.

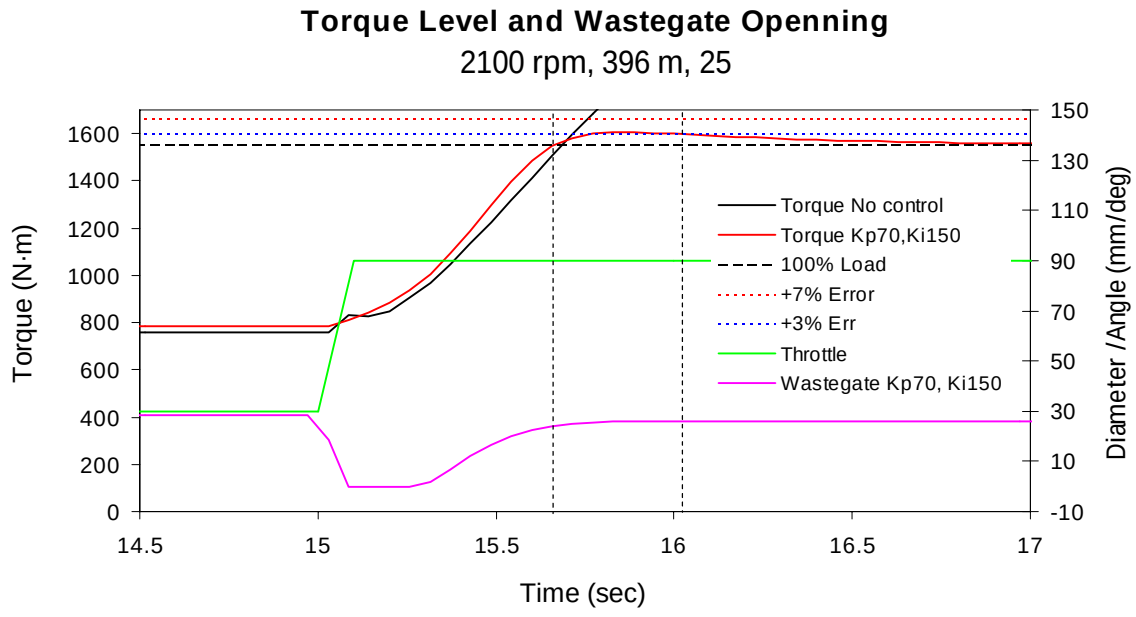

Figure B. 29. Torque limiting control verification of torque: 2100 rpm, 396 m, 25˚C.

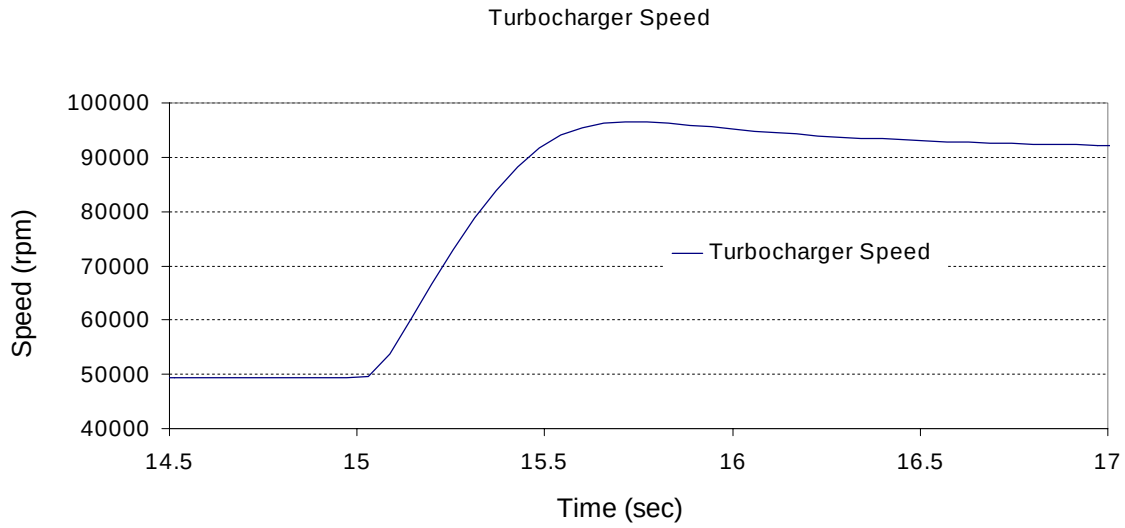

Figure B. 30. Torque limiting control verification of turbine: 2100 rpm, 396 m, 25˚C.

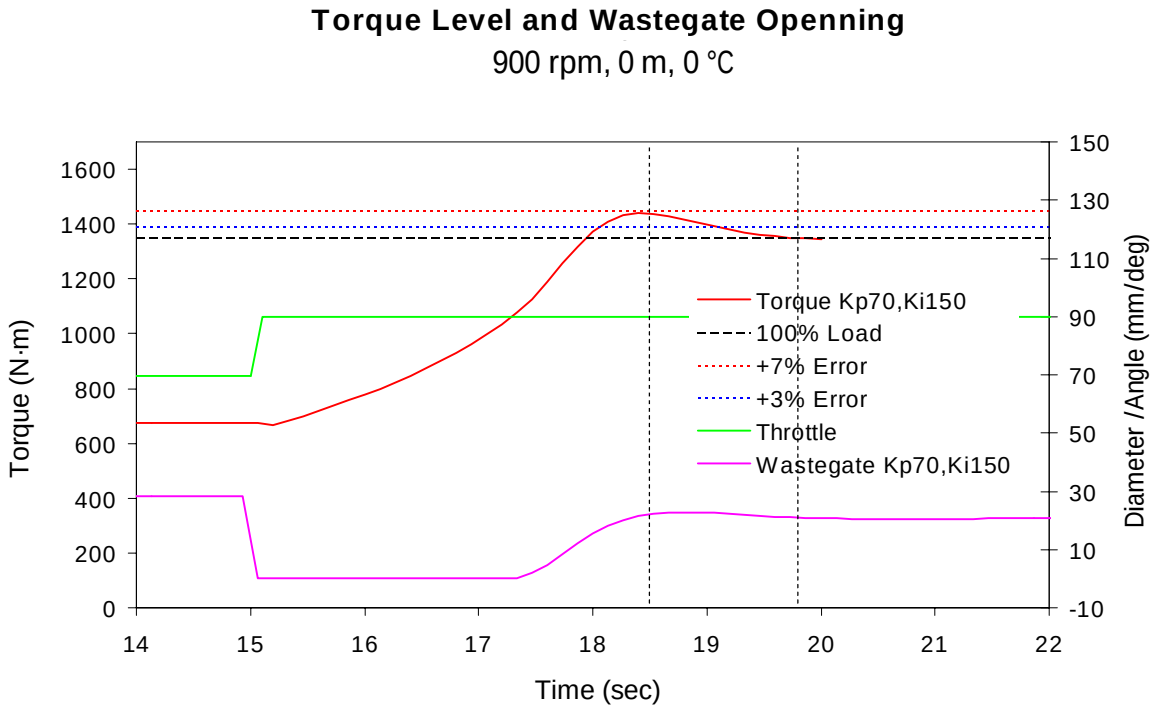

Figure B. 31. Torque limiting control verification of torque: 900 rpm, 0 m, 40˚C.

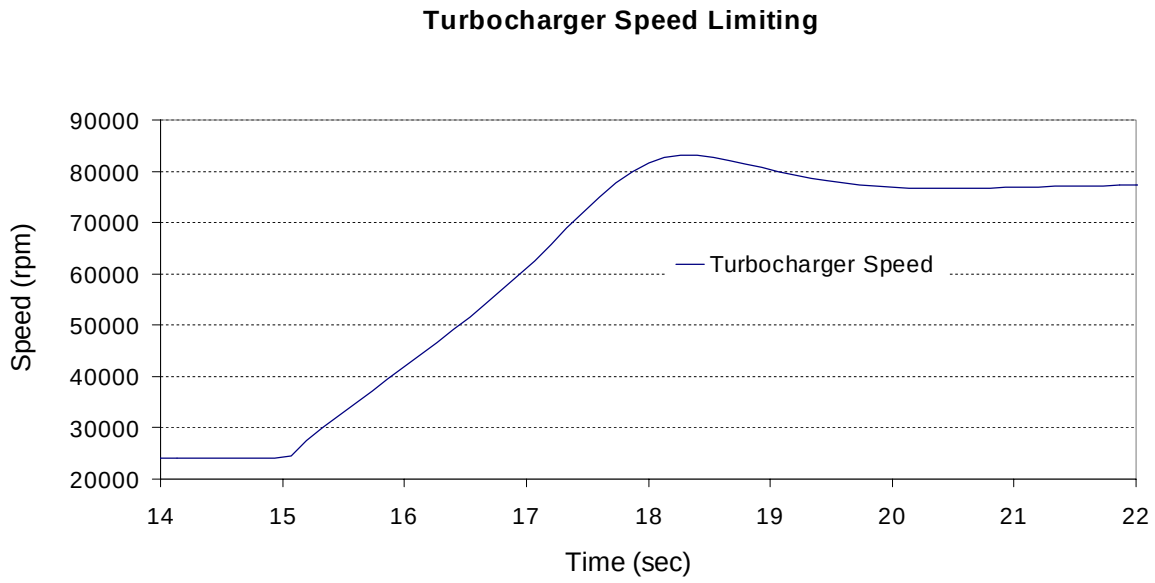

Figure B. 32. Torque limiting control verification of turbine speed: 900 rpm, 0 m, 40˚C.

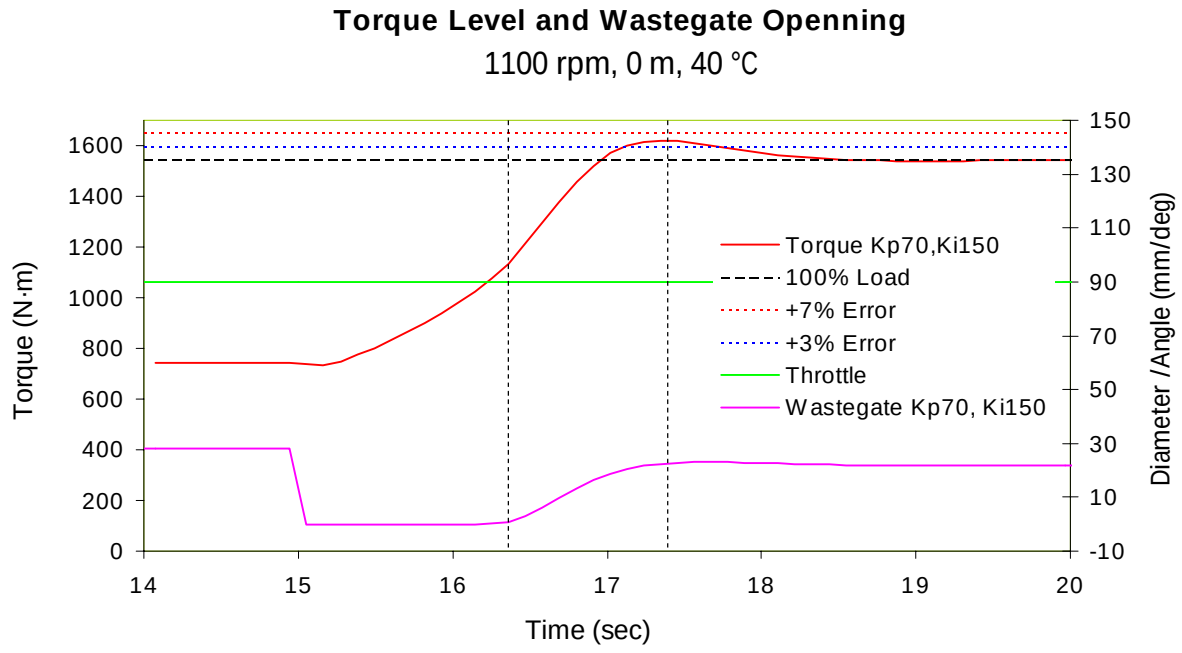

Figure B. 33. Torque limiting control verification of torque: 1100 rpm, 0 m, 40˚C.

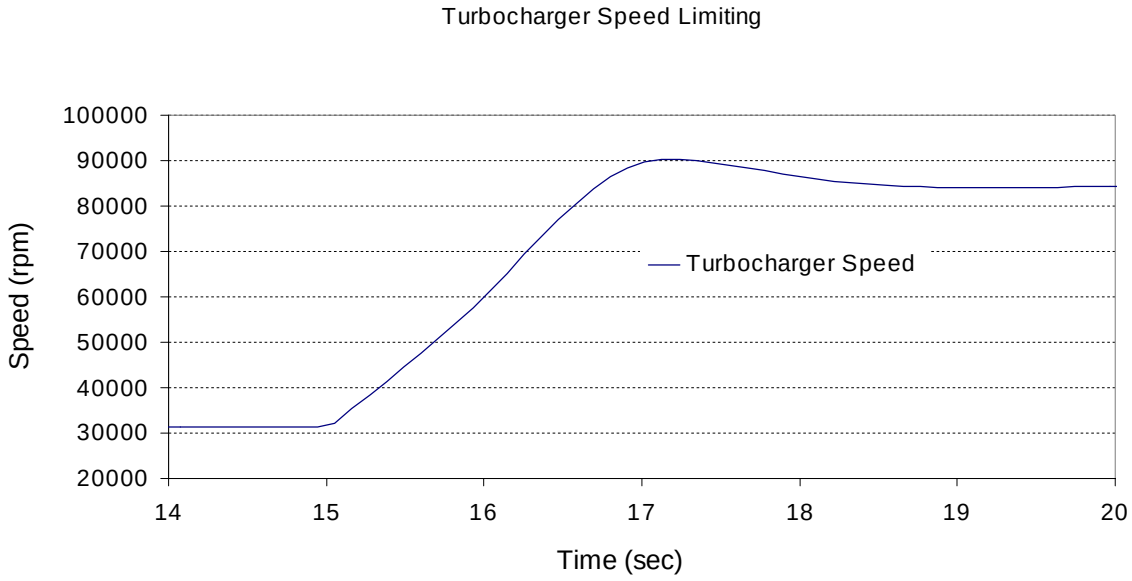

Figure B. 34. Torque limiting control verification of turbine speed: 1100 rpm, 0 m, 40˚C.

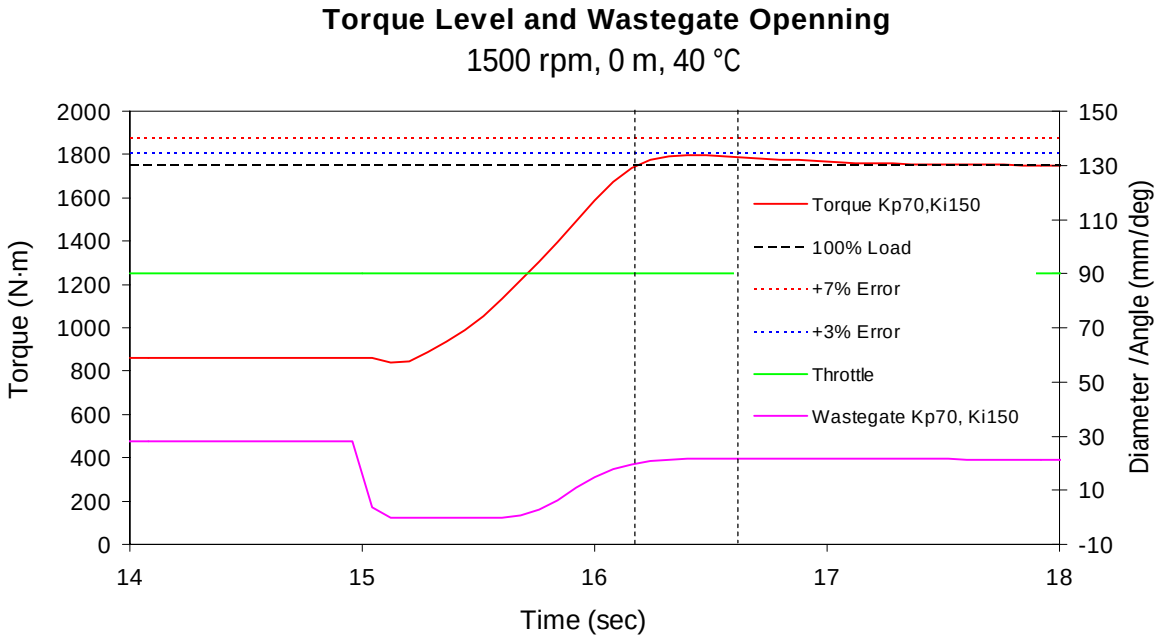

Figure B. 35. Torque limiting control verification of torque: 1500 rpm, 0 m, 40˚C.

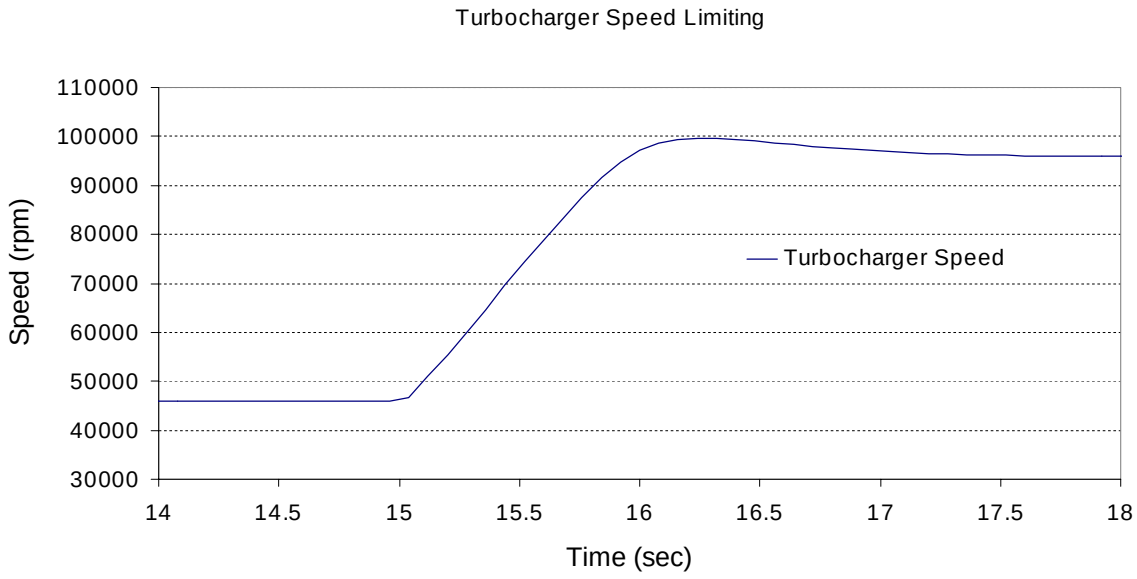

Figure B. 36. Torque limiting control verification of turbine speed: 1500 rpm, 0 m, 40˚C.

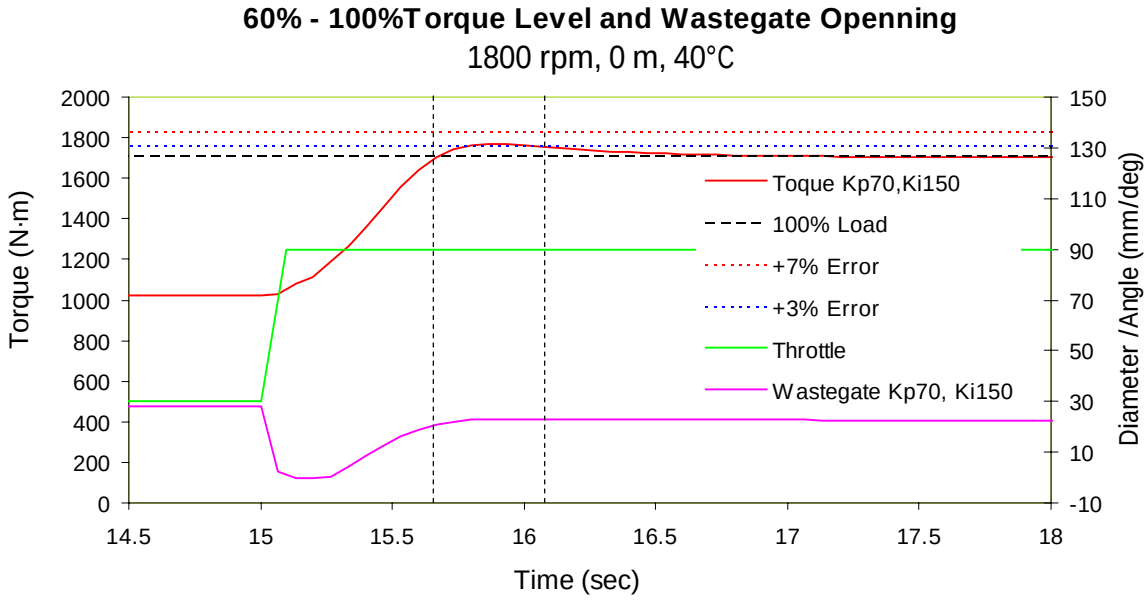

Figure B. 37. Torque limiting control verification of torque: 1800 rpm, 0 m, 40˚C.

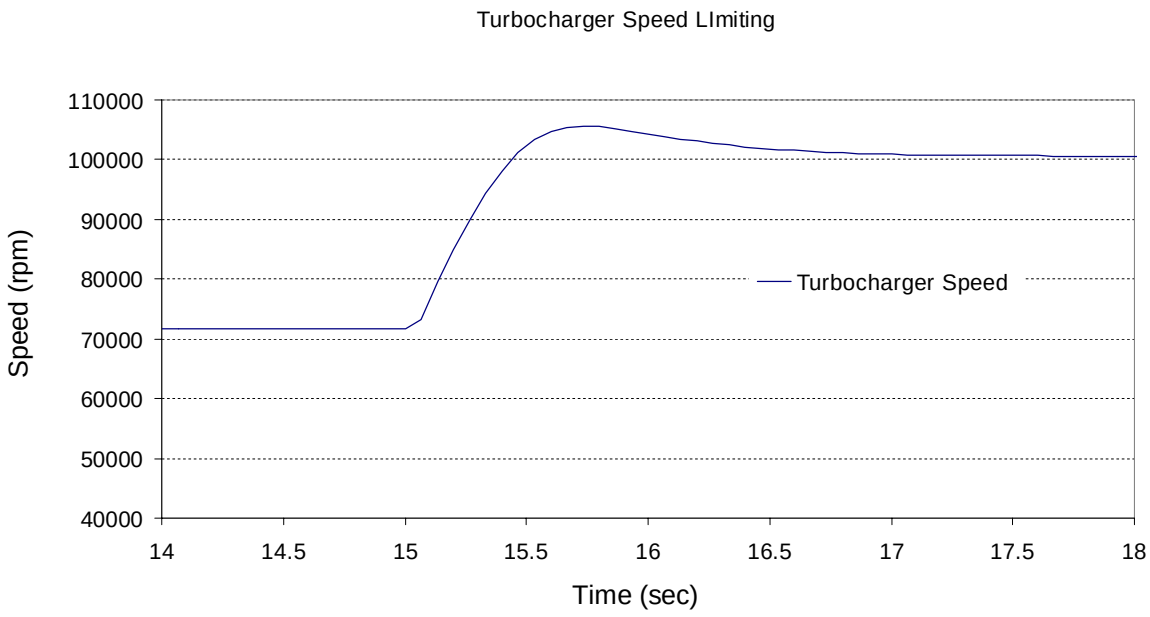

Figure B. 38. Torque limiting control verification of turbine speed: 1800 rpm, 0 m, 40˚C.

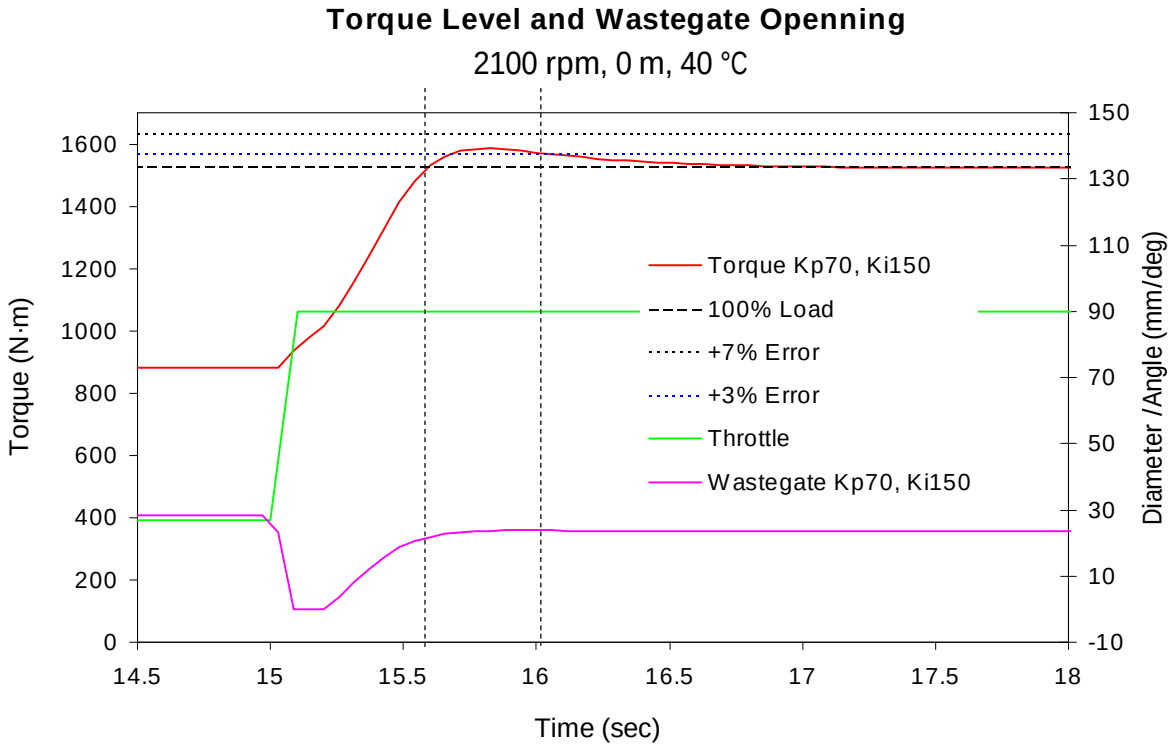

Figure B. 39. Torque limiting control verification of torque: 2100 rpm, 0 m, 40˚C.

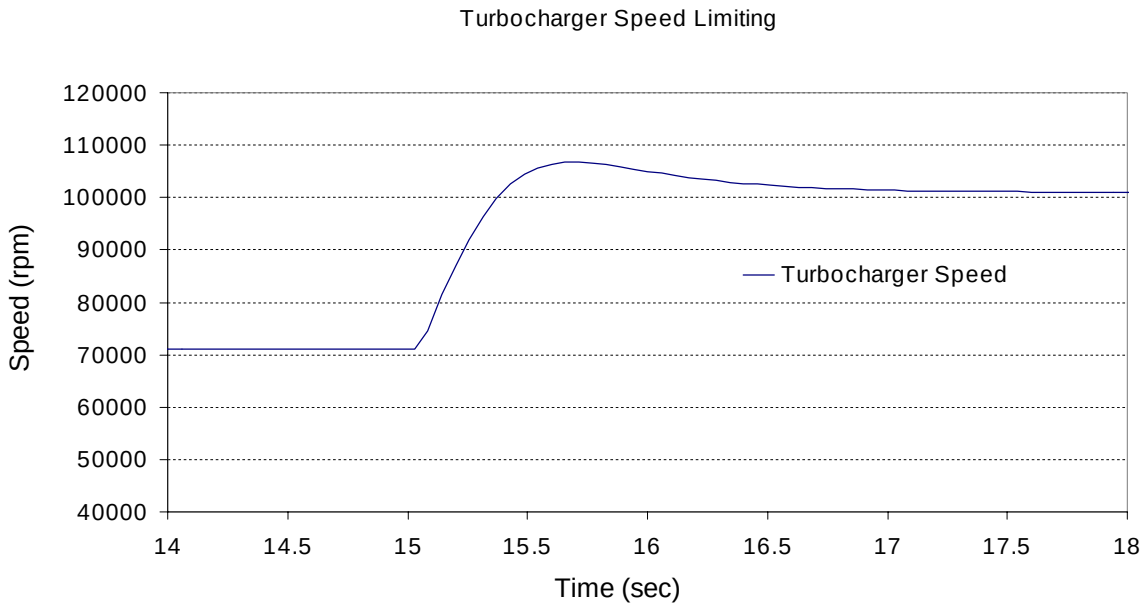

Figure B. 40. Torque limiting control verification of turbine speed: 900 rpm, 0 m, 40˚C.

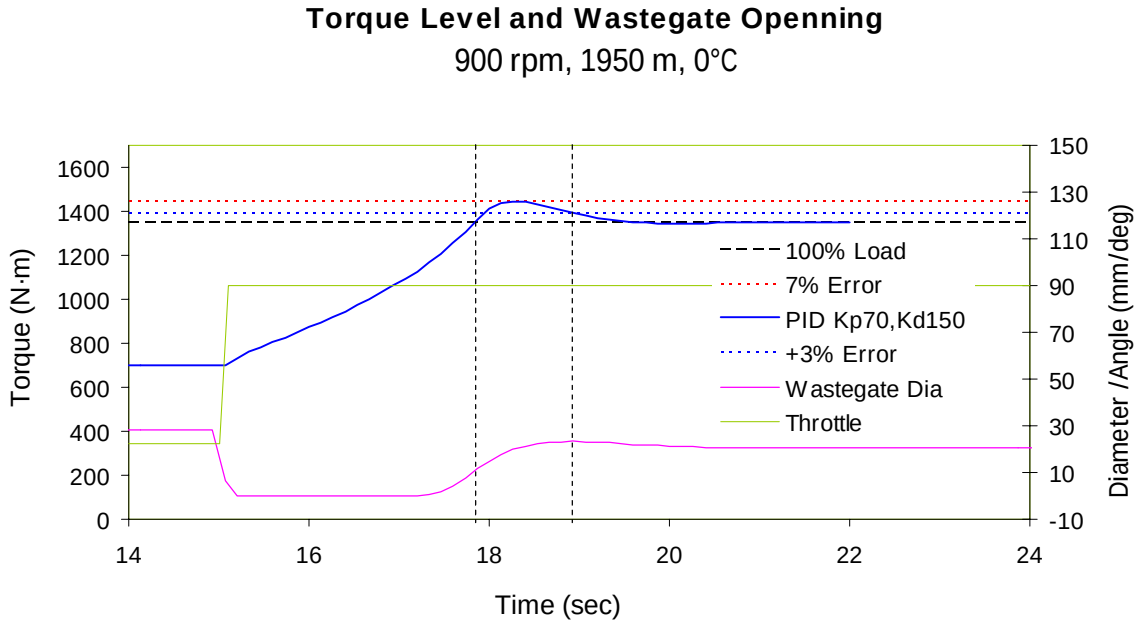

Figure B. 41. Torque limiting control verification of torque: 900 rpm, 1950 m, 0˚C.

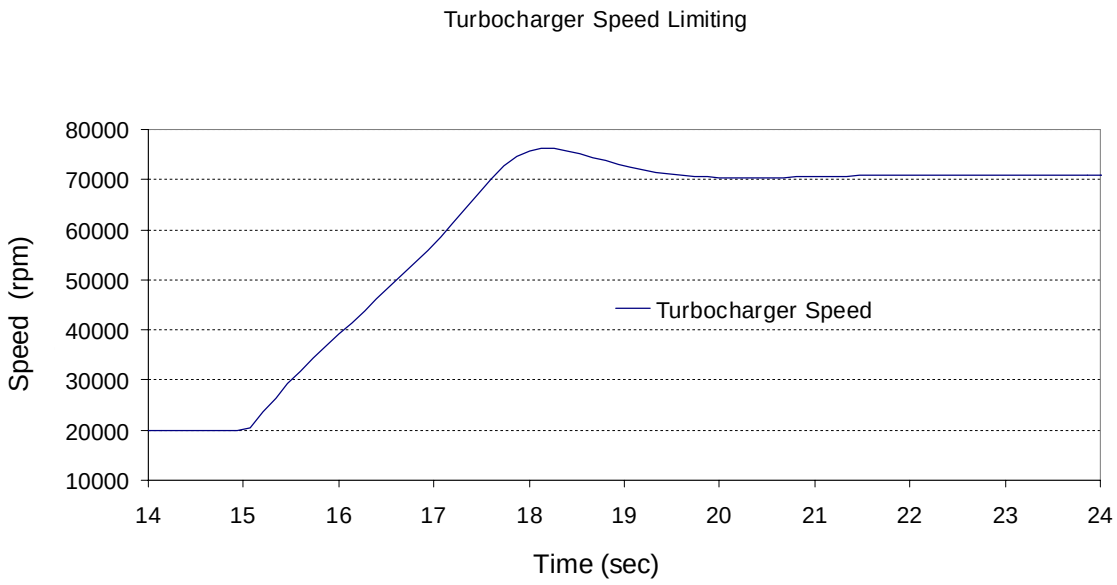

Figure B. 42. Torque limiting control verification of turbine speed: 900 rpm, 1950 m, 0˚C.

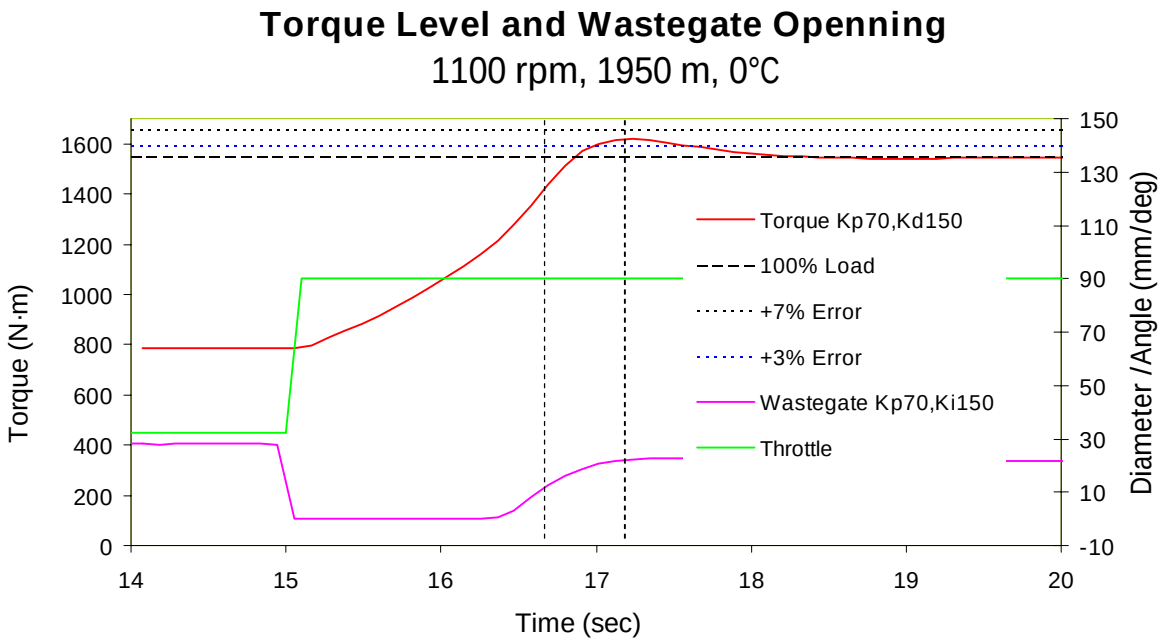

Figure B. 43. Torque limiting control verification of torque: 1100 rpm, 1950 m, 0˚C.

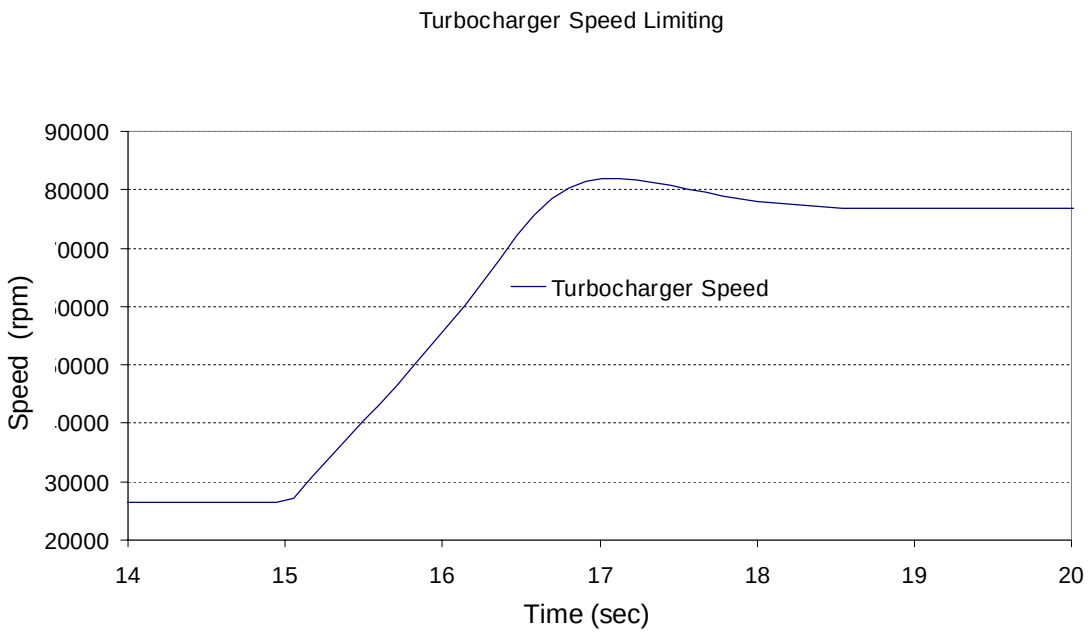

Figure B. 44. Torque limiting control verification of turbine speed: 1100 rpm, 1950 m, 0˚C.

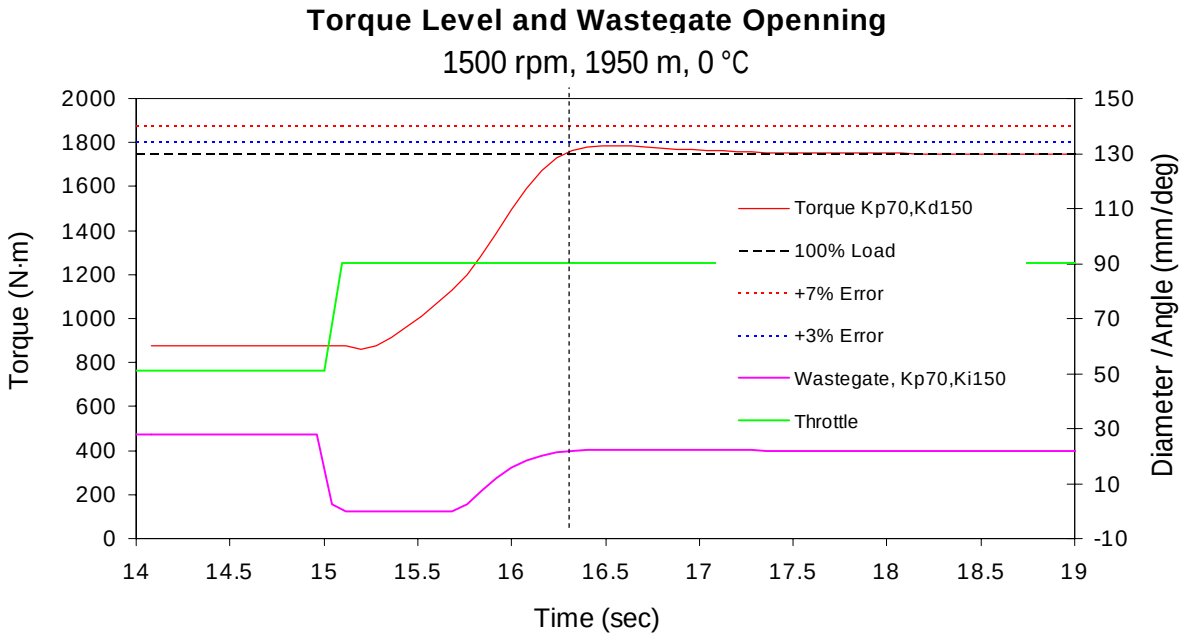

Figure B. 45. Torque limiting control verification of torque: 1500 rpm, 1950 m, 0˚C.

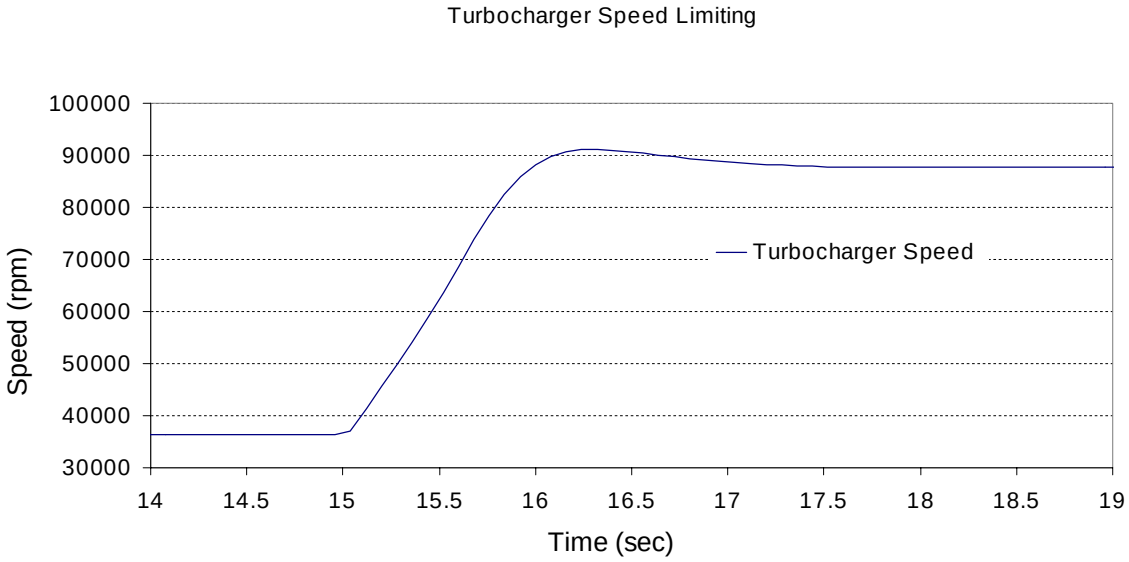

Figure B. 46. Torque limiting control verification of turbine speed: 1500 rpm, 1950 m, 0˚C.

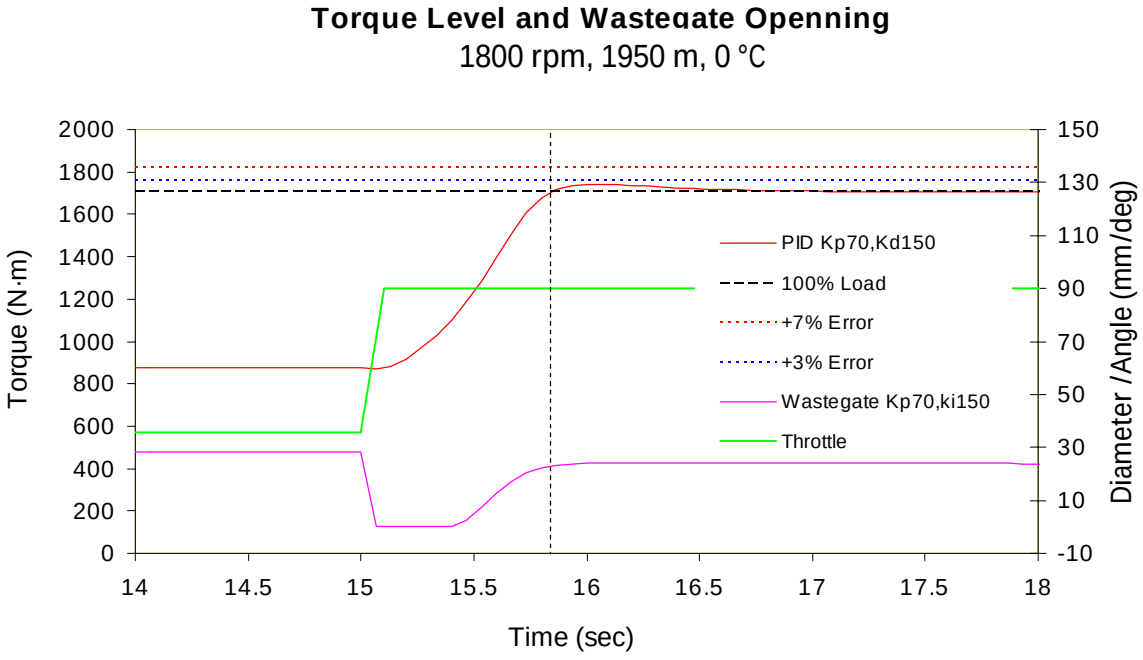

Figure B. 47. Torque limiting control verification of torque: 1800 rpm, 1950 m, 0˚C.

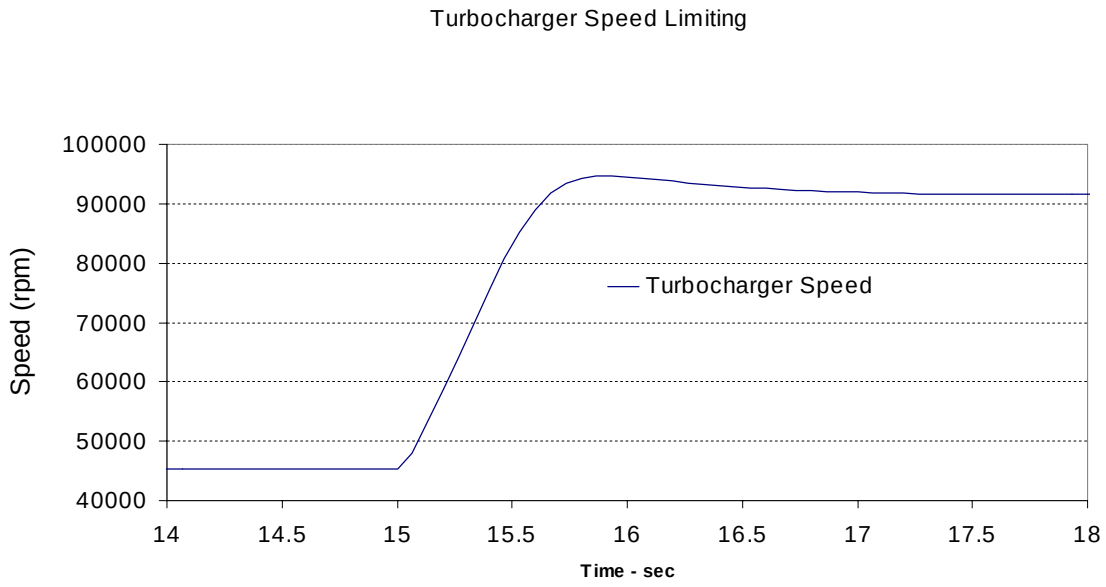

Figure B. 48. Torque limiting control verification of turbine speed: 1800 rpm, 1950 m, 0˚C.

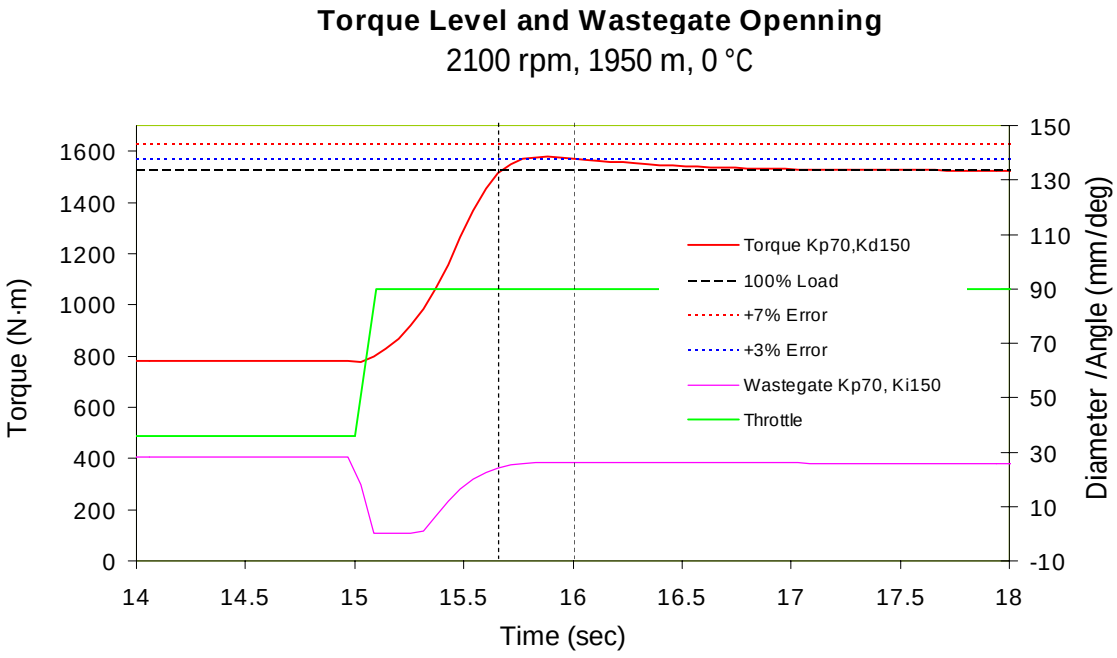

Figure B. 49. Torque limiting control verification of torque: 2100 rpm, 1950 m, 0˚C.

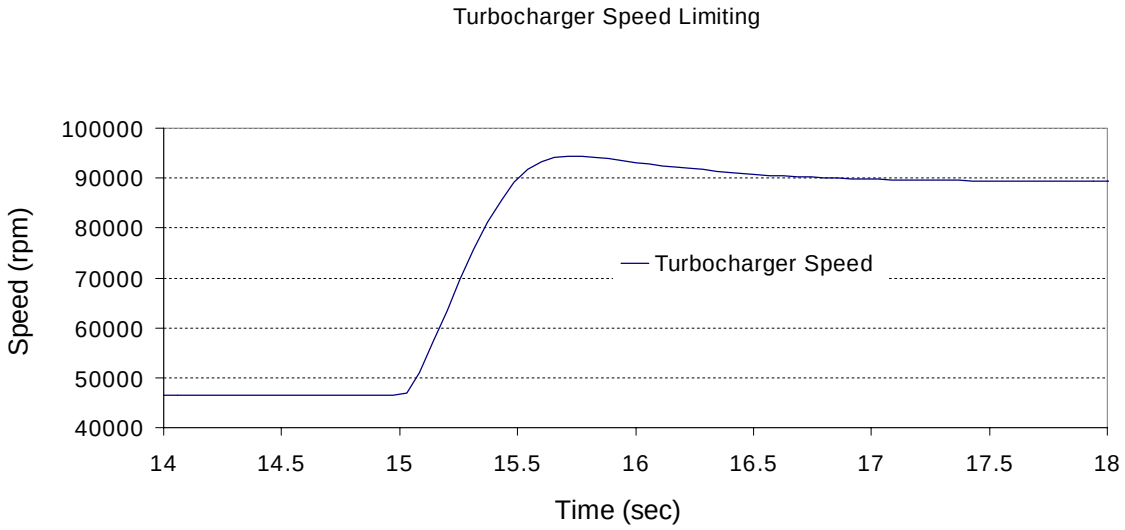

Figure B. 50. Torque limiting control verification of turbine speed: 2100 rpm, 1950 m, 0˚C.

Table B. 1. Altitude and pressure data used in torque limiting.

Altitude Above Sea Level		Absolute Barometer		Absolute Atmospheric Pressure		
(ft)	(m)	(in. Hg)	(mm Hg)	(psi)	($kg/cm^{2)}$	(kPa)
0	0	29.92	760.0	14.696	1.0333	101.33
500	153	29.38	746.3	14.43	1.015	99.49
1,000	305	28.86	733.0	14.16	0.996	97.63
1,500	458	28.33	719.6	13.91	0.978	95.91
2,000	610	27.82	706.6	13.66	0.960	94.19
2,500	763	27.32	693.9	13.41	0.943	92.46
3,000	915	26.82	681.2	13.17	0.926	90.81
3,500	1,068	26.33	668.8	12.93	0.909	89.15
4,000	1,220	25.84	656.3	12.69	0.892	87.49
4,500	1,373	25.37	644.4	12.46	0.876	85.91
5,000	1,526	24.90	632.5	12.23	0.86	84.33
6,000	1,831	23.99	609.3	11.78	0.828	81.22
7,000	2,136	23.10	586.7	11.34	0.797	78.19
8,000	2,441	22.23	564.6	10.91	0.767	75.22
9,000	2,746	21.39	543.3	10.5	0.738	72.40

Date from: Engineering ToolBox at website: http://www.engineeringtoolbox.com/air-altitude-pressure-d_462.html

APPENDIX C

C.1 Engine Geometry

Table C. 1. Engine geometry.

Bore	(mm)	118.4
Stroke	(mm)	136
Rod	(mm)	218
Compression Ratio		16.75
TDC clearance height	(mm)	1
Crankshaft Inertia	$(\mathrm{kg}\cdot\mathrm{m}^2)$	1.6
Throttle diameter	(mm)	74.5
Wastegate diameter	(mm)	28.28

BIOGRAPHY

Hai Wu was born in Liaoning, China in April, 1967. He was admitted to the Air-Force Surface-to-Air Missile Institute, Sanyuan in 1984, and received a bachelor's degree in Electrical Engineering in 1988. He worked in the Air Force Shenyang District for four years before being admitted to the Graduate School at Northeastern University, Shenyang in 1992. He received his master and Ph.D degrees in 1995 and 1999 in electrical engineering. Wu joined Shenyang University of Technology in 2000 and taught classes in control system design. He was a Visiting Scholar at the University of Illinois at Urbana-Champaign from 2003 to 2006, and worked on engine after-treatment systems and digital control design. He joined the PhD program in 2006 and worked as a research assistant and then research associate for the Department of Agricultural and Biological Engineering. During this time, he also worked for the John Deere Technology Innovation Center.

Hai Wu is a member of the Society of Automotive Engineering (SAE) and the American Society of Agricultural and Biological Engineering (ASABE) and in 2008 he was inducted into Alpha Epsilon, the honor society for outstanding biological and agricultural engineers.